STUDIES IN EQUATORIAL AERONOMY

A THESIS
SUBMITTED FOR THE DEGREE OF
DOCTOR OF PHILOSOPHY
OF THE

GUJARAT UNIVERSITY

BY
HAR SURENDRA SAHAI SINHA

NOVEMBER 1976

PHYSICAL RESEARCH LABORATORY
AHMEDABAD 380009
INDIA

DEDICATED

TO

MY PARENTS

CERTIFICATE

I hereby declare that the work presented in this thesis is original and has not formed the basis for award of any degree or diploma by any University or Institution.

H. S. S. Sinha

H. S. S. SINHA
(Author)

Certified

Satya Prakash

SATYA PRAKASH
(Professor-in-charge)

October 26, 1976

STATEMENT

The work presented in the thesis was carried out by the author, at the Physical Research Laboratory, Ahmedabad, under the guidance of Professor Satya Prakash.

The first measurements of electron density irregularities in the equatorial D and E regions were made by Satya Prakash, B.H. Subbaraya and S.P. Gupta from the Thumba Equatorial Rocket Launching Station (TERLS). The work presented here is an extension of the above work and was carried out with the rocket borne Langmuir probe. The author was closely associated with the design and development of Langmuir probe system and with many modifications required for the study of the irregularity parameters. This thesis is based on the results obtained from many rocket launches from Thumba by the

author during the periods of normal as well as counter electrojet.

Ionization irregularities produced due to cross field instability as well as Neutral turbulence mechanism have been studied during different times of the day on many normal electrojet days. Theoretical estimates of growth rates were made, using different atmospheric models, to interpret the irregularity observations. The shapes spectra and prominent scale sizes of the irregularities produced through cross-field instability mechanism in the lower equatorial ionosphere are being reported for the first time. The in-situ measurements of the D region which resulted in the study of the irregularities produced through neutral-turbulence mechanism are also being reported for the first time.

In addition, it has been possible for the first time to make in-situ measurements of irregularities in D and E regions, during periods of counter electrojet. The results obtained from the rocket flights, conducted during counter electrojet periods, show many important features which could not be obtained using any other technique. Some of these are (a) in-situ observations regarding the occurrence of cross-field and neutral turbulence generated irregularities during counter electrojet, (b) the nature of vertical polarization field and (c) the observations of wave like perturbations in a region of very steep upward gradient. These results would also be described for the first time.

In Chapter I the author has made an attempt to review the different models of equatorial electrojet, the phenomenon of counter electrojet, and the observational results of the irregularities produced through cross-field and neutral turbulence mechanisms. Both rocket and VHF backscatter radar results have been reviewed in detail. In chapter II the theories of cross-field instability and neutral turbulence have been reviewed. Both linear and non-linear theories of cross-field instability have been discussed in detail in light of their ability and limitations to explain the experimental observations. The theory of neutral turbulence is also discussed in brief. In chapter III the author has discussed various features of the Langmuir probe which make it capable of resolving the fine structures in the electron density and the data analysis. In chapters IV and V the author has described in detail the results obtained during normal and counter electrojet periods, respectively. A detailed discussion of the experimental results and the important conclusions reached are given in chapter VI. Finally, a list of original papers published in reputed international journals referred in this dissertation, has been included at the end.

ACKNOWLEDGEMENTS

I wish to express with deep gratitude my indebtedness to Professor Satya Prakash who guided me during all the facets of this work. His vast experience, profound knowledge, critical insight and unassuming nature have left a deep impression on me and I consider it a privilege to have worked with him.

I wish to record my gratefulness to Professor B.H. Subbaraya and Dr. S.P. Gupta for their invaluable suggestions, kind advice and pertinent consultations. Many fruitful and stimulating discussions with them are gratefully acknowledged.

Dr. P.K. Chaturvedi merits my special thanks because of many suggestions and improvements he offered and because of the diligence with which he assisted me in the chore of

going through the manuscript. I express my particular appreciation to him for many extended discussions which I had with him on the theoretical aspect of the problem.

Dr. P. Muralikrishna, Messrs T.R. Rao, Y.B. Acharya, Shyam Lal and R. Pandey have been friendly critics and sources of informations for many years, and I would be remiss in not expressing a warm note of thanks for their interest and encouragement of my work.

I am thankful to all members of the erstwhile 'Rocket Borne Aeronomy' group of PRL and especially so to Messrs I.L. Kriplani, K.S. Modh, J.T. Vinchhi and R.I. Patel for their help in fabrication and testing of the payload. The general assistance rendered by Messrs R.S. Patel, I.A. Prajapati, V.R. Choksi and K.S. Patel deserves high appreciation.

It is a pleasure to thank Drs. Dinesh Patel, K.S. Rao and D.R. Kulkarni and Mr. C.S.R. Murthy and their colleagues at PRL Computer Centre, for their kind cooperation in data processing and analysis.

The staff of Library, Workshop and Drafting Section were very cooperative on all occasions; I acknowledge with a deep sense of appreciation their helping and pleasing attitude.

Mr. K. Venugopalan's cheerful deciphering of my handwriting and his immaculate typing are highly appreciated.

I wish to express my sincere thanks to Mr. R. Arvamudan, Head, Thumba Equatorial Rocket Launching Station (TERLS), Mr. V. Sudhakar and their colleagues of TERLS whose enthusiastic cooperation and sense of preparedness made the rocket launchings successful.

The ionograms and the magnetograms used in this study were supplied by Indian Institute of Astrophysics, Kodaikanal and Indian Institute of Geomagnetism, Bombay, respectively. I take this opportunity to thank the Directors of these institutions.

I am grateful to Professor D. Lal, the Director and Professor S.P. Pandya, the Deputy Director, Physical Research Laboratory, for providing all the facilities during the course of this work and for the encouragement they gave me from time to time.

I am very thankful to Professors P.R. Pisharoty, B. Buti, R.K. Varma, P.D. Bhavsar, R.G. Rastogi, R.P. Kane, D.P. Agrawal, K. Gopalan and Drs. Vijay Kumar and G. Subramanian for their helpful attitude, timely encouragement and extremely valuable suggestions.

It is a privilege for me to thank Professor S.P. Venkiteshwaran who introduced me to the field of Space Sciences and has helped me in all circumstances through his kind advice and encouragement.

The preparation of this dissertation could not have been possible without the encouragement, support and inspiration of my elder brother, Shri H.M.S. Sinha and my grandfather Shri T.P. Srivastava. In terms of acknowledgements, a special debt of gratitude is due to them who patiently and uncomplainingly participated in the creation of this thesis.

Finally, my appreciation for the forbearance and understanding of my wife, Aruna, during the preparation of this dissertation cannot be expressed in words. Her quiet and heartful support was a significant factor in the completion of my work.

H.S.S. SINHA

Ahmedabad,
October 26, 1976

C O N T E N T S

CHAPTER - I

INTRODUCTION

Equatorial Aeronomy deals with that region of upper atmosphere over the equator where the processes of dissociation and ionization are important. This region extends from approximately 30 km above the surface of the earth to the outer limit of atmosphere at many earth radii. In this vast domain of aeronomy lies a region of relatively smaller extent known as 'ionosphere'. The term ionosphere is strictly applied to those regions where free electrons exist in such an abundance so as to affect the radio wave propagation significantly. The lower limit of ionosphere is at an altitude of nearly 50 km. The upper boundary of ionosphere is rather less sharp and merges with the magnetosphere. The ionosphere is subdivided into three regions: D-region, below

80 km altitude, E-region, between 80 and 160 km and F-region, above 160 km.

The nature of ionospheric plasma in D, E and F-regions is quite different. In the D region due to large neutral density, the collision frequencies of electrons and ions with neutrals are larger than their respective gyrofrequencies. The electrons and ions are thus controlled entirely by the collisions and for all practical purposes do not see the effect of the magnetic field below 75 km. Beyond 75 km and in the E-region, the collision frequency of electrons is smaller than their gyrofrequency whereas for ions the reverse still holds good. Thus in the E-region electrons are highly magnetised and ions are not. This region, therefore, is succeptible to charge separation. It is in this region of equatorial ionosphere that a strong current known as equatorial electrojet has been observed. This current is generally eastward during the daytime. However, on some special occasions the direction of current becomes westward for a few hours during daytime, the flow of such reversed current is termed as counter electrojet. The direction of current reverses during nighttime and becomes westward.

The present dissertation concerns with the study of ionization irregularities in the D and E-regions of the equatorial ionosphere. The irregularities are defined as spatial and temporal variations in the electron density. The study of ionization irregularities helps, to a very large

extent, in understanding the various plasma processes taking place in these regions. It has become increasingly clear by now that the study of irregularities gives very valuable information about the nature of the electric fields and the electrojet currents in the ionosphere. In addition, since the irregularities can scatter radio waves, their presence has been recently exploited for the communication at VHF frequencies. A knowledge of the properties of these irregularities would thus be very useful in planning high frequency communication links.

The electron density irregularities are produced by a number of causative mechanisms which operate in different regions of the ionosphere. An attempt has been made by the author to study the properties of irregularities produced through two such important mechanisms, viz. the cross field instability and the neutral turbulence. Since the excitation of cross field instability is closely related to the equatorial electrojet, section 1.1 is devoted to the models of equatorial electrojet. Sec. 1.2 deals with the phenomenon of counter electrojet. Observational results of ionization irregularities obtained using ground based and the rocket borne studies would be described in Sec. 1.3.

1.1 Equatorial Electrojet

The history of electrojet dates back as early as 1722 when Graham found that the compass needle executes some regular

oscillations (variations) during the day. The first explanation of these variations was given by Stewart (1882) in terms of an electric current flowing in the upper atmosphere. Stewart suggested that due to sun's heating convective currents of air are produced which can be regarded as conductors moving across magnetic lines of force. This is known as 'Stewart's atmospheric dynamo theory'. This theory got support from Schuster (1889) who proved that the major portion of the magnetic field variations has its source outside the earth. A more detailed theory was developed by him a little later (Schuster, 1908).

In 1922, a new feature of the geomagnetic field variations was brought to light at the geomagnetic observatory, Huancayo, Peru. It was found that unlike the daily ranges of the declination D and the vertical component Z the diurnal range of the horizontal component H was abnormally large. The dynamo theory and the above mentioned observations got a new impetus with the experimental discovery of the ionosphere independently by Appleton and Barnett (1925), and Breit and Tuve (1925,26). The verification of dynamo theory with the new discovery of ionosphere got slightly impeded when Pedersen (1927) pointed out that the conductivity of the ionosphere would be reduced due to the geomagnetic field. Preliminary calculations by Pedersen yielded a value of conductivity which was 5000 times less than the one required by Schuster's theory. The discrepancy in the conductivity values was, however,

reconciled by Cowling (1933) who found that if the medium is polarised the Hall current will be inhibited and, therefore, the conductivity would be highly enhanced. The idea of Martyn (1948) that this enhanced conductivity is good enough for the dynamo theory at all latitudes was modified by Cowling and Borger (1948) who pointed out that the enhancement of the conductivity is possible only at the equator because at other latitudes the polarisation which inhibits the Hall currents, would leak away horizontally.

Consistent with the above ideas were the observations of Egedal (1947,48) who found that the diurnal range of H at six stations, when plotted against dip latitude, exhibited a peak at the dip equator. Such enhanced diurnal variation at the dip equator was attributed by him to the electric currents flowing in a narrow zone near the dip equator. This observation was confirmed afterwards by other workers for many equatorial zones. This current was later named as "Equatorial Electrojet" by Chapman (1951).

1.1.1 Conductivities in the Ionosphere

In the lower region of the ionosphere (below 75 km) the electrical conductivity is very small as the region is characterized by

$$\frac{\Omega_e}{\nu_{en}} \ll 1 \qquad \text{and} \qquad \frac{\Omega_i}{\nu_{in}} \ll 1$$

where Ω_e and Ω_i are electron and ion gyrofrequencies and ν_{en} and ν_{in} are electron-neutral and ion-neutral collision frequen-

In most of the E-region of the ionosphere the electrical conductivities are large because the region is characterized by

$$\frac{\Omega_e}{\nu_{en}} \gg 1 \quad \text{and} \quad \frac{\Omega_i}{\nu_{in}} \ll 1$$

Under these conditions electrons are magnetised whereas the ions are not. The direction of primary electric field at equator is eastward during daytime. This field is generated due to tidal motions in the non-equatorial regions. Due to the presence of magnetic field the conductivity does not remain a scalar quantity and becomes a tensor.

In a weakly ionized plasma such as the E-region plasma, if the electric field is applied in a direction parallel to the magnetic field the resulting conductivity is known as 'direct conductivity' or 'longitudinal conductivity' and is represented by σ_0 where

$$\sigma_0 = Ne^2\left(\frac{1}{m_e \nu_e} + \frac{1}{m_i \nu_i}\right)$$

where N is the electron or ion density both being equal

e is the electronic charge
m_e is the mass of the electron
m_i is the mass of positive ion

The direct conductivity is independent of the magnetic field. If the electric field is applied in a direction perpendicular to the magnetic field, the conductivity in the

direction of the electric field is known as Pedersen conductivity and is represented by σ_1 where

$$\sigma_1 = Ne^2 \left\{ \frac{\nu_e}{m_e(\Omega_e^2 + \nu_e^2)} + \frac{\nu_i}{m_i(\Omega_i^2 + \nu_i^2)} \right\}$$

In the above condition there is also a flow of electric current in the direction $\vec{B} \times \vec{E}$ where $\vec{B}$ is the magnetic flux vector. This current is known as Hall current and the conductivity supporting the current is known as Hall conductivity and is represented by σ_2 where

$$\sigma_2 = Ne^2 \left\{ \frac{\Omega_e}{m_e(\Omega_e^2 + \nu_e^2)} - \frac{\Omega_i}{m_i(\Omega_i^2 + \nu_i^2)} \right\}$$

The general expression of the total current can be obtained if the electric field is resolved into two components viz. E_o and E_1, parallel and perpendicular to the magnetic field respectively. The current density J is given by (Baker and Martyn, 1953).

$$J = \sigma_o \vec{E}_o + \sigma_1 \vec{E}_1 + \sigma_2 (\vec{b} \times \vec{E}) \qquad (1)$$

where $\vec{b} = \frac{\vec{B}}{B}$ is the unit vector in the direction of the magnetic field.

As pointed out earlier the inhibition of Hall current leads to an enhanced conductivity. To obtain the effective conductivity of the medium, Baker and Martyn (1953) considered the ionosphere as an ionized layer. If x and y represent magnetic south and east respectively, the magnetic flux B dips

down at an angle I to the xy plane and the z axis is towards the vertical, then the sheet in the xy plane can be considered to be the ionosphere in the northern hemisphere. With the assumption that the Hall current is inhibited ($j_z=0$) the conductivity in the x-direction due to x component of the electric field is represented by σ_{xx} and is given by

$$\sigma_{xx} = \frac{\sigma_0 \sigma_1}{(\sigma_0 \sin^2 I + \sigma_1 \cos^2 I)} \qquad (2)$$

The conductivity in the x direction due to y component of the electric field is represented by σ_{xy} and is given by

$$\sigma_{xy} = \frac{\sigma_0 \sigma_2 \sin I}{(\sigma_0 \sin^2 I + \sigma_1 \cos^2 I)} \qquad (3)$$

The total conductivity in y direction due to y component of the electric field is represented by σ_{yy} and is given by

$$\sigma_{yy} = \frac{\sigma_0 \sigma_1 \sin^2 I + (\sigma_1^2 + \sigma_2^2) \cos^2 I}{\sigma_0 \sin^2 I + \sigma_1 \cos^2 I} \qquad (4)$$

As I = 0 at the magnetic equator the above equations reduce to $\sigma_{xx} = \sigma_0$, $\sigma_{xy} = 0$ and $\sigma_{yy} = \sigma_1 + \frac{\sigma_2^2}{\sigma_1}$. σ_{yy} is the effective conductivity in the y-direction and is known as Cowling conductivity. Due to the inhibition of the Hall current the effective conductivity in the y-direction i.e. the Cowling conductivity is enhanced. The physical explanation of such an enhancement is simple and can be understood as the following. The primary electric field in conjunction with the N-S magnetic field tries to lift the plasma in upward direction.

But since the positive ions do not see the effect of the magnetic field owing to their large collision frequencies, a vertical polarization field namely the Hall field is created. The Hall field crosses with the magnetic field and makes the electrons drift in eastward direction and thus enhances the conductivity in the E-W direction.

1.1.2 Models of the Equatorial Electrojet

The first attempts for the in-situ measurement of electrojet current were made by Maynard et al. (1965) and Maynard and Cahill (1965b). Four Nike Apache rockets were launched in January, 1964 from Thumba, India by Maynard et al. (1965) under a joint NASA-INCOSPAR programme. The rockets carried the Packard and Varian (1954) type 'Proton Precession Magnetometer'. The measured values of the magnetic field were plotted against altitude. Theoretical estimates of the magnetic field over Thumba were also made using the spherical harmonic analysis of Finch and Leaton (1957). Theoretical values were then subtracted from the actual observed magnetic field in order to get the field due to electrojet current. These results yielded a value of 60-70 gammas for the electrojet field. The peak current was found to be situated around 109 km and a diffuse trail upto 130 km (Maynard and Cahill, 1965a).

A second campaign of similar measurements was started by Maynard and Cahill (1965b) who launched four Nike Apache

rockets from the USNS Croatan during March 1965. The launchings were made off the coast of Peru and were a part of NASA Mobile Launch Expedition. Payloads flown were similar to ones flown in India. The results showed that the departure field or the difference field exhibited a change of slope at 95 km and that maximum departure was about 120 gammas at 108 km. Beyond 108 km the current layer diffused upwards upto 130 km in a manner similar to that observed by them over India.

The two attempts to measure the electrojet currents over India and Peru brought very interesting results. Suguira and Cain (1966) tried to interpret these results by proposing the first model of the equatorial electrojet. Following were the main features of the model:

(a) Vertical currents were neglected ($j_z = 0$)

(b) Electric field in the north-south direction was neglected ($Ex = 0$)

(c) Primary field in the East-west direction was taken to be constant ($Ey = const$) with altitude

(d) Realistic magnetic field values were incorporated

(e) Height profiles of collision frequencies and electron densities were assumed.

The model was developed from the basic equations of current and layer conductivities (Equations 1 to 4). The final expression for the current in the E-W direction was found to be

$$j_y = \sigma_{yy} \cdot E_y \qquad (5)$$

This model, better known as σ_{yy} model qualitatively explains the features of the electrojet. This model, however, gave much smaller width for the equatorial electrojet than later observed by Davis et al (1967). The model was later proved to be self-inconsistent by Untiedt (1967). The actual equations for the current in x and y directions as obtained by them, are

$$j_x = \sigma_{xx} E_x + \sigma_{xy} E_y \qquad (6)$$

$$j_y = -\sigma_{xy} E_x + \sigma_{yy} E_y \qquad (7)$$

The equation (6) shows that if E_x is assumed to be zero the N-S current J_x will be finite. σ_{xy} is dependent of I and, therefore, of x. This suggests a strong divergent current system in the N-S direction which cannot exist in a system like electrojet. In fact a meridional electric field is set up in the XZ plane which according to (7) would contribute to the electrojet currents except at the equator. The meridional field is non-zero and can yield a non-divergent meridional current system, a major part of which is in the vertical direction, therefore the first assumption that $j_z = 0$, everywhere is not valid.

In March 1965 there was another series of rocket launchings by NASA Mobile Launch Expedition. Nine rocket launchings were made by Davis et al. (1967) for the latitudinal survey

of the equatorial electrojet over Peru. Rubidium vapour magnetometers were on board to find out the total field. On one of the flights which was conducted during nighttime a very weak current opposite in direction to the eastward daytime electrojet was detected. The experimental results of Davis et al. (1967) showed that the equatorial electrojet had a lower maximum current density and was much more extended in latitude than indicated by Suguira and Cain (1966). The cross-sectional current density profiles derived by Davis et al. (1967) could not be accounted for by the model. Appreciating the obvious incompatibilities between model and their results, Davis et al (1967) proposed a modified model in which N-S current was completely inhibited in addition to the vertical current i.e. both j_x and j_z were assumed to be zero. Putting $j_x = j_z = 0$ in equation (6) and (7) one gets

$$j_y = \left(\sigma_{yy} + \frac{\sigma_{xy}^2}{\sigma_{xx}}\right) E_y \qquad (8)$$

and equations 2-4 now yield

$$\sigma_{yy} + \frac{\sigma_{xy}^2}{\sigma_{xx}} = \sigma_3 \qquad (9)$$

where $\sigma_3 = \sigma_1 + \frac{\sigma_2^2}{\sigma_1}$ is the Cowling conductivity.
In the model of Davis et al. (1967) σ_3 does not depend upon x hence the assumption $j_x = 0$ does not lead to electrojet. The self inconsistencies of σ_{yy} and Davis et al.'s model led Untiedt (1967) to propose a numerical two dimensional model.

The main features of Untiedt's model were the following:

(a) The vertical currents were not assumed to be zero ($j_z \neq 0$)

(b) A flat earth picture was taken

(c) Similar to σ_{yy} model all quantities were assumed to be dependent of x and z only

(d) The current function ψ was assumed to be non-divergent

(e) Winds were assumed to be stationary so that $\frac{\partial B}{\partial t} = 0$ and the electric field is irrotational.

To solve the resulting equations following simplifying assumptions were made:

(a) E_y was assumed to be constant with the latitude and altitude. A value of 1 mv/meter was used for calculations. In actual case E_y varies with altitude as seen by Subbaraya et al. (1972) who find that the electric field increases with altitude. All currents and magnetic fields of the electrojet system are proportional to Ey hence the model can be scaled to represent different conditions by simply changing E_y.

(b) $\frac{dI}{dx} = 3 \times 10^{-7}$ (1.72 deg/100 km.). This means magnetic inclination depends linearly on x and its dependence on z is neglected. This is justified for the electrojet as it occurs in a narrow region.

(c) σ_1 and σ_2 do not depend on the latitude 'x'.

Under the above assumptions the total current will be non-divergent but not the partial currents due to ions and electrons.

The conductivities used in Untiedt's model were calculated from the height profiles of electron density obtained by Maynard and Cahill (1965a) who used a d.c. Langmuir probe. The results of Untiedt's analysis show that:

(a) A toroidal magnetic field was obtained which points towards magnetic west in the northern hemisphere and towards magnetic east in the Southern hemisphere. In z direction the field was maximum at 125km whereas in x direction the maxima occured at a distance of 325 km.

(b) The meridional currents of 80 amp/km flow towards the equator below 125 km and away from the equator above 125 km. At the equator the direction of current is vertically up with a maxima at 123 km where the current density is 5×10^{-7}

(c) The reduction in electrojet current as one goes away from the equator is much less than predicted by σ_{yy} model. The height of the peak of the electrojet shifts only from 105 km to 100 km as one moves from x = 0 (equator) to x = 500 km. At the equator current densities are slightly more than the ones obtained in σ_{yy} model. A comparison of current and σ_3 profile shows that Cowling conductivity represents the electrojet fairly well in the neighbourhood of the equator.

(d) The H value at the ground due to ionospheric currents is 92.5 γ at the equator. The ratio of H at equator to H outside equatorial zone is 2.4 against a higher value of 3.2 given by σ_{yy} model.

A minor improvement in Untiedt's model (1967) was made by Suguira and Poros (1969). They used a spherical harmonic expansion for the geomagnetic field and have given model electrojet for six different longitudes. This model is different from Untiedt's model in the following ways:

(a) The magnetic field used is more realistic.

(b) Spherical earth geometry and spherical polar coordinates are used.

In this model the ratio of vertical polarization field to the primary electric field was found to be 25 at 100 km altitude. The same ratio was 28 in case of σ_{yy} model. This shows that meridional currents reduce the vertical electric field but only to a very small extent.

Kato (1973) pointed out that the general belief regarding the equatorial electrojet that it is driven entirely by an electrostatic field namely the Hall field may not always be true. In presence of the N-S magnetic field B and an E-W wind W which can be generated due to tidal motions, the dynamo action creates a charge separation. This charge separation is responsible for the polarization, which is such that, the total field $E_{pol} + W \times B \simeq 0$. If the cancellation is complete there is no contribution to the vertical electric field due to the horizontal wind motion and electrojet current does not get affected by winds. Kato (1973) has shown that when more realistic curved field lines are considered (instead of approximate horizontal lines) the effect of horizontal winds is such that the cancellation is not complete and hence there is a net vertical field due to wind motion. Thus the vertical Hall field which drives the electrojet would be modified with this vertical field due to wind motion.

The effect of neutral winds on the equatorial electrojet was considered in detail later by Richmond (1973) who developed a numerical model of equatorial electrojet. In this model the geomagnetic field lines were assumed to be perfect

conductors i.e. σ_0 was assumed to be infinite. The results of currents and the ground level variations (Δ H) of infinite σ_0 model were found to be same as in finite σ_0 model. In addition, the assumption of infinite σ_0 simplifies the computations to a great extent and provides additional conceptual insight into the physical mechanism of electrojet. It was emphasized in the model that the electric field and current at any given point is strongly dependent on the conditions prevailing all along the geomagnetic field line and is almost independent of condition prevailing in the neighbouring field lines. The effect of height varying E-W and N-S winds has also been taken into account in this model. It is found that E-W winds do not affect the electrojet current upto $\pm 1^{o}$. Beyond $\pm 1^{o}$ these E-W winds significantly affect the eastward current and the ground level variations (Δ H). The inclusion of N-S winds did not have much effect on the eastward current but resulted in generation of cross-equatorial currents.

1.2 Counter Electrojet

The history of the counter electrojet dates back to the year 1940 when Bartels and Johnston (1940) while studying the geomagnetic tides in horizontal intensity at Huancayo observed that on some of the magnetically quiet days the variation of H was abnormal and exhibited a large depression during daytime. Bartels and Johnston attributed these depressions to large fluctuations in the lunar component L which they thought

could exceed even the solar quiet day component Sq at the time of such large depressions. The next important observation in the series of counter electrojet phenomenon, as has become evident now, was made by Matsushita (1957) who found that at Huancayo on some days the equatorial E_s or E_{s-q} which was quite normal upto 1330 Hrs (L.T.) suddenly vanished at 1345 Hrs (L.T.) and then reappeared after a gap ranging between half an hour to a few hours. Since the main objective of Matsushita was to study the lunar effects on E_{s-q}, no attempt was made by him to correlate drifts or magnetic field with the observed phenomenon.

Gouin (1962) reported some abnormal behaviour of the horizontal component of the geomagnetic field H, over Addis Ababa which is an equatorial station under the direct influence of the equatorial electrojet. The normal behaviour of H for Addis Ababa or for that matter any other equatorial station is a gradual start with a small dip before sunrise, then a maximum around local noon and thereafter, a steady fall, with slight positive assymetry, to nighttime level. The maximum during noon lies somewhere between 100 and 200 gammas above the nighttime level. Gouin found that on three days in the month of January, 1962 the H curves were very much deviated from the normal one and had large depressions during daytime. These depressions in H were reflected in the vertical component z, and the declination D also. There was, however, no trace of any such depression before and after these three days.

lunar effects alone. While studying the properties of blanketing type of sporadic E over an equatorial station, Kodaikanal (dip 3.4°N), India, Bhargava and Subrahmanyan (1964) found that at the time of appearance of E_{s-q} all geomagnetic and ionospheric features which are observed under the influence of electrojet are suppressed. They found that just before the local noon the horizontal component of geomagnetic field showed a large departure and the E_{s-q} was either absent or was very weak. But in addition to the disappearance of E_{s-q} at the time of depression in H, which was found earlier by Cohen et al. (1962), Bhargava and Subrahmanyan (1964) found that, at the same time, i.e. just before the local noon when depression in H was seen, the height of maximum F-region ionization decreases, the extent of F-region gets reduced, i.e. thinning of the F-layer and, the region becomes denser. Based on all the features such as depression in H and disappearance of E_{s-q} etc., Bhargava and Subrahmanyan (1964) concluded that there should be a westward electric current in the ionosphere at the time when blanketing E_s is observed.

An extensive study of such depressions was later carried out by Gouin and Mayaud (1967) who found that the occurrence of such depressions was more during morning and evening hours and that the occurrence during noon was rare. Since the occurrence was confined to same local time on a number of consecutive days the lunar origin of such depressions was ruled out. Gouin and Mayaud (1967) were convinced that these depressions were limited to equatorial zone only like the equatorial

electrojet' and since the variations in H were not related to S_R, variations in the declination, they christened the phenomenon 'Counter Electrojet'. Later, Hutton and Oyinloye (1970) observed the disappearance of E_{s-q} during the periods of counter electrojet at Nigerian stations Zaria and Ibadan.

Using a VHF backscatter radar Balsley and Woodman (1971) measured the horizontal electron drift in the E-region during the period of counter electrojet. Their results showed that during counter electrojet the drift velocity reduced to zero but did not reverse. On the other hand Rastogi (1971) using three spaced receiver's technique found that horizontal drifts in the E-region, and the vertical drifts in the F-region over Thumba reversed during the period of counter electrojet. Later on it was shown by Rastogi (1973) that even for Huancayo E_{s-q} disappeared when electron drift velocity as measured by VHF doppler spectra indicated very small velocity or even reversed E-region drift and downward F-region drift. If these reversals in the drifts are true the direction of primary electric field and, therefore, the direction of main electrojet must have got reversed during such periods. If the electrojet current gets reversed it should be reflected in the magnetic field above the ionospheric height. Kane (1973a) using the POGO satellite data of Cain and Sweeney (1973) observed one such case where the electrojet signatures (as shown by the magnetic fields in the higher regions) were reversed during a period when counter electrojet was observed at ground

About the extent of the counter electrojet Rastogi (1972) showed that it can be seen at two stations separated by a few hundred Km in the N-S or a few thousand km in the E-W direction. The decreased $h_{max}\ F_2$ which was first observed by Bhargava and Subrahmanyan (1964) during the depression in H was later studied in detail by Rastogi (1974). Rastogi (1974) showed that during the period of counter electrojet the height of maximum ionization in F_2 region, $h_{max}\ F_2$, decreases. A new term 'partial counter electrojet' was introduced by Rastogi (1974) who observed the cases where the depression was seen around afternoon hours but the minimum value of the field was much above the nighttime level.

Osborne (1964) suggested that the strength of the electrojet can be estimated from the difference of H values of an equatorial station and a station just outside the influence of electrojet. On magnetically quiet days the identification of counter electrojet is easy and can be made by locating a depression below the night level in $\triangle (H_{eq.} - H_{low\ lat.})$ curve. This method of defining the strength of electrojet currents would be in error depending upon the relationship between the low latitude Sq variations and equatorial magnetic field variations. Nevertheless this method seems to be quite good in establishing the presence of counter electrojet. On disturbed days, however, the method is not so straightforward and involves the removal of D_{ST} and DS effects completely. Kane (1973b) has defined an index Sd_I to test whether it is a

$$Sd_{I(equator)} = H_{(equator)} - H_{(low\ lat.)} + Sq_{(low\ lat.)}$$

If $Sd_{I(equator)}$ goes below the baseline it is termed as counter electrojet day.

Recently a VHF backscatter radar operating at 54.95 MHz was used to study the irregularities present at Thumba, India during the period of counter electrojet (Muralikrishna 1975). On most of the counter electrojet days the backscatter signal was absent indicating thereby the absence of 3-meter irregularities. On a few occasions, however, weak return echoes were detected. It was found that radar echoes appeared only when the reversed currents had become sufficiently strong and when sufficient time had elapsed after the onset of the reversal. The return echoes lasted for longer periods and were much stronger when observed during decay phase of the counter electrojet currents as compared to these observed during the development phase. A comparative study of number of counter electrojet occurrences with solar A_p index revealed that quiet days were more favourable for the occurrence of counter electrojet.

1.3 D and E-region Irregularities

1.3.1 Observational Results of Ionization Irregularities from Ground Based Studies

1.3.1.1 Studies with Ionosonde

Sir Edward Appleton while studying the ionograms for

in the E-region trace (Appleton, 1930). The occurrence of such abnormalities was so unpredictable that the name 'sporadic E' was attributed to them. The name sporadic E or Es adopted by the international community is a misnomer as these irregularities are more or less a regular feature in different latitudinal zones. At the equator the name 'q-type' or E_{s-q} is used to designate these irregularities.

On an ionogram the E_{s-q} appears either as a dense layer or a patchy structure at E-region heights in 100-120 km region. At times when the layer is so dense that the reflection from the higher regions are not possible, it is known as 'blanketing type' of sporadic E or simply E_{s-b}. The blanketing frequency f_bE_s is the lowest frequency at which echoes from higher layers are received through E_s layer. When there is a complete blanketing the observations of F-region are prevented by this layer but at other times the layer could be partially transmitting over a small frequency range.

An indication whether the layer is thick or thin can be had by observing the retardation near the maximum frequency on the E_s traces. The presence of retardation near the maximum frequency indicates that the layer is thick whereas the thin layers is characterised by no retardation.

The important parameters most frequently used to describe the sporadic E are the critical frequencies of E_s layers, f_oE_s and f_xE_s (both ordinary and extraordinary),

blanketing frequency f_bE_s and the virtual height $h'E_s$. When the usual 'cusp' type reflections are not seen on the ionogram the frequency f_tE_s, which is the top frequency at which the reflections are observed, is used.

1.3.1.2 Studies with VHF Forward and Backscatter Radar

a) Electrojet Irregularities

The studies of ionization irregularities started with the work of Booker and Gordon (1950) who applied the theory of scattering of radiowaves, by turbulent medium, to the tropospheric heights. Bailey et al. (1952) made the calculations of such scattering at higher levels (E-region altitudes) and then performed an experiment to check the validity of the theory. In accordance with their calculations Bailey et al. (1952) were able to receive high frequency signals between two mid-latitude stations separated by about 1245 km. Although the high frequency signals (49.8 MHz) were received irrespective of the time of observation, season and the status of the geomagnetic field their intensity was slightly dependent on these factors. These observations were later interpreted in terms of scattering caused by irregularities in the E-region altitudes.

Bowles and Cohen (1957) operated a chain of 50 MHz VHF forward scatter radars near the magnetic equator in South America. The results of these observations showed that the propagation of VHF signals was associated with sporadic-E and

was well correlated with the time variations and height of the equatorial electrojet. It was later experimentally established by Bowles et al. (1960) that plane wave electron density irregularities were acting as scattering centres for the VHF radar echoes. These plane waves were found to be moving in the general direction of the electron flow which is towards west during daytime. Bowles et al. (1960) predicted that the irregularities should be highly field aligned, i.e. the scale sizes of the irregularities along the field lines must be much larger than across them. This proposed field aligned nature of irregularities was later confirmed by Egan (1960) who used an obliquely looking radar at Huancayo, Peru ($0^{o}31'$ N dip) and found that the echoes were highly aspect sensitive and could only be observed when radar beam was looking at right angles to the magnetic field which is in N-S direction over Huancayo.

Another valuable information regarding the region of generation of these irregularities was presented by Cohen and Bowles (1963) who used the VHF forward scatter radar over a transequatorial path and showed that the irregularities are generated between 95 to 110 km. This range of 95 to 110 km agreed well with the limits of equatorial electrojet given earlier by Singer et al. (1951). In addition to the region of occurrence, Cohen and Bowles (1963) found a positive correlation between the radar echo intensity and the variation

in the horizontal component of the geomagnetic field. Bowles et al. (1963) found that the apparent radar echo cross-section increases with the elevation angle.

As the operating frequency of the radar decides the scale size under study Bowles et al. (1963) used two different frequencies (148 MHz and 50 MHz) to have an idea of the behaviour of two different scale sizes; their results showed that threshold needed at 148 MHz was higher than the one needed at 50 MHz but nevertheless they had similar characteristic spectra. Upto this time the irregularities observed by VHF scatter radar were thought to be generated due to the two stream instability mechanism (Farley, 1963). But around the same time it was pointed out by Bowles et al. (1963) that at times when the threshold of two stream instability is not reached, a vertically pointing radar detects echoes which did not have the above mentioned characteristic spectra. The large scale blobs of irregularities were also found to be moving in westward direction. These observations, however, could not be reconciled with the Farley's two stream instability theory. A detailed study of these irregularities (at 50 MHz) was made by Balsley (1967) who classified the irregularities into two types namely 'type I' and 'type II' and suggested that two separate mechanisms must be operating in the electrojet which give rise to these types of irregularities. Balsley identified the two-stream instability as the generating mechanism for type I echoes. But the rocket studies of Prakash et al. (1971c) show

that the threshold requirement for two stream instability is not met in case of type I echoes. Regarding the generating mechanism of type II echoes it has become clear from the rocket studies (Prakash, et al. 1971c) that these echoes are due to small scale irregularities which are generated through cross-field instability mechanism.

The velocities of both type I and type II irregularities were derived by Balsley (1967) from the doppler shift in the returned radar signal. Using the following simple formula one can compute the velocity of irregularities if the doppler shift is known.

$$\Delta f = \frac{2 V_d f \sin\theta}{C}$$

where f is the transmitter frequency,

Δf is the dopper shift in the received signal,

V_d is the drift velocity of irregularities,

θ is the angle which the direction of antenna beam makes with the vertical, and

C is the velocity of light.

The doppler shift in case of type I irregularities is always around -120 Hz when the radar beam is pointed westwards during daytime. This doppler shift was found to be independent of antenna elevation angle. As the radar beam is pointed westwards during these observations, a negative doppler shift of 120 Hz indicates that the irregularities are moving in westward

direction with a velocity of $\approx$ 360 meters/sec, a velocity which is close to ion-acoustic velocity in that region. Such a fixed doppler shift is usually observed at a time during which the electrojet is supposed to be quite strong.

The doppler shift for type II irregularities is always much smaller than type I indicating that type II are moving with relatively slower speeds. Type II irregularities are usually present at all times except when electron drift velocity may be expected to be near zero. Another important point made by Balsley (1967) was that the power of the return signal was proportional to the square of the drift velocity of irregularities.

In case where both type I and type II echoes are present the individual contribution from two types can be estimated on the basis of signatures of these echoes. This method of spectral decomposition was given by Cohen (1973). Balsley (1967) studied the variation of observed drift velocity with the antenna elevation angle; the results of observed drift velocities showed a very good agreement with the theoretically predicted value of horizontal velocity.

In order to know the lower scale sizes upto which the spectrum of type I and type II irregularities extends Balsley and Farley (1971) made radar studies at three different frequencies viz. 16.25 MHz, 49.92 MHz and 146.25 MHz. These studies showed that at higher radar frequencies the strength of type II echoes decreased much more rapidly than type I; the

decrease being so large that at 146.25 MHz type II signals were not at all observed. The velocities of type I and type II irregularities were found to be independent of radar frequency. It was also pointed out by these studies that the dependence of type I scattering cross-section on electrojet strength was more at higher radar frequencies.

A detailed study of small and large scale structures of the irregularities was carried out later by Farley and Balsley (1973) using the Range Time Intensity (RTI) diagrams. The technique of RTI diagrams has been described by Balsley (1969). Using a vertically pointing radar beam which was 1^{o} wide, Farley and Balsley (1973) could get the spatial resolution of the order of 300 meters. Such observations showed that structures of 300 to 1000 meters scalesize were present and were moving, sometimes, vertically upwards and, sometimes, downwards with a velocity lying between 50-75 m/s. The velocities could not be conclusively determined with RTI diagrams, but their being in the range was indicated by doppler shift radar measurements. At another occasion they used radar of wider beam width ($\sim 30^{o}$) and pointed it towards 45^{o} west. The resolution achieved in this case was about 1.5 to 2.0 km. The results of RTI diagrams showed that irregularities of few km. scale size had life times of the order of 10-30 seconds and were moving in westward direction. Since their pulse width was very small ($=10\mu s$) such features could be seen, otherwise usually when one averages the signal for about a minute or so, or uses wider radar

pulses, the echo would appear to come from all directions. These studies were in agreement with the earlier rocket observations of Prakash et al. (1970) wherein it was found that the irregularities have scalesizes of a few km. in the vertical direction. The region of occurrence, amplitude, shape and spectrum of the irregularities with scalesizes from a few km down to one meter have been given in a comprehensive review by Prakash et al. (1973).

As the radar observations showed that type II irregularities were present even when the drift velocity was less than the ion-acoustic velocity, it was suggested by Farley and Balsley (1973) that small scale irregularities must be generated indirectly through some non-linear processes wherein energy is fed from larger scale sizes to smaller ones. The large scale irregularities, whose presence was first pointed out by Prakash et al. (1970) and later confirmed by RTI diagrams, when grown sufficiently could significantly alter the local conditions so as to make them suitable for invoking the nonlinear feed back of energy to generate smaller scalesize irregularities. Such a mode - mode coupling was proposed by Sudan et al. (1973) and would be described in Chapter II. Balsley and Farley (1973) carried out another set of measurements with improved altitude and time resolution. If the spatial resolution of radar measurements is comparable to the size of large scale structures the turbulent model is expected to yield highly variable Doppler structures. In the earlier measurement of Farley and Balsley (1972) due to poor spatial and temporal

resolution, these features were obscured and spectrum was found to be fairly narrow and symmetrical about zero Doppler shift with practically no structures. With the improved altitude resolution the Doppler shift which represented the vertical velocity was found to vary rapidly with altitude to the extent that the direction could be reversed two times in a bare distance of 5 km. With the improved time resolution it was possible to study the evolution of Doppler shift in time at a given altitude. It was found by Balsley and Farley (1973) that at a given altitude the Doppler shift could be markedly change in about 2.5 seconds and could even reverse sense in about 5 seconds. Although these resolutions were orders of magnitude better than the earlier ones but were certainly not the ones which one would like to have. A new signal processing and data display technique named as the modified range time intensity (MRTI) display was developed by Fejer et al. (1975). With the help of MRTI technique the structures could be studied with a altitude resolution of 1 km, and a large dynamic range of 60 db could be covered. This system was very much suited for nighttime observations. Using this technique Fejer et al. (1975) studied the vertical structure of the VHF backscattering region in the electrojet. During daytime echoes were observed from a region extending from 93 to 113 km, during the evening they were obtained from two split regions around 100 and 120 km whereas during nighttime echoes were obtained from an extended region of 93 to 130 km. The results of Fejer et al. (1975) confirm the earlier rocket results of Prakash et al.

(1971c) that type II irregularities are produced through cross-field instability mechanism . The author also gets similar results from the rocket data at Thumba. The results obtained by the author would be described and discussed in chapter IV and VI respectively.

Using a 54.95 MHz VHF backscatter radar from Thumba, India, Muralikrishna (1975) reported the nature of irregularities around morning and evening reversals of electric field. It was found that just before the morning reversal the observed Doppler shift exhibits a pronounced peak at + 120 Hz which corresponds to a eastward velocity of 360 meters/sec. showing that before morning reversal type I echoes are present. During reversal or transition no radar echo was observed. After the morning reversal type II echoes were observed. In addition, it was found that scattering region was higher during times close to the reversal periods. The observations around the evening reversal showed that just before the reversal spectra are generally broad and also the Doppler shift is such that irregularities are moving with low drift velocities of the order of a few tens of meters per second in the east-west direction. During the reversal there was no radar signal. After the evening reversal also type II irregularities are present but the Doppler shift is negative suggesting that after evening reversal irregularities are moving from west to east.

b) Irregularities due to Neutral Turbulence

The theory of scattering of radiowaves by turbulent medium was propose in 1950 by Booker and Gordon (1950). Bailey et al. (1952) calculated the scattering of 50 MHz signal from E-region altitudes for a path length of a few thousand kilometers on the basis of the theory of Booker and Gordon (1950), and then conducted an experiment to verify the theory. The results were remarkable as the signals were transmitted exactly in the fashion as originally thought of. The fading characteristics of these signals followed a Rayleigh distribution. Some theoretical work on the scattering of radiowaves by turbulent medium was done by Villars and Weisskopf(1955). Gallet (1955) proposed a mechanism by which the neutral turbulence could produce electron density fluctuations. Since the mechanism could produce only very weak irregularities Gallet proposed an amplification mechanism of the weak irregularities. Some of these theoretical ideas would be described in chapter II.

As far as experimental results are concerned, to the best of author's knowledge, there are only two attempts which have been made using VHF backscatter radar. The first one was by Crane (1970) and was limited only to stratospheric heights. Although Crane (1970) used a very powerful radar he was unable to get the return echoes of power greater than noise level. Recently Woodman and Guillen (1974) made the observations of irregularities produced by neutral turbulence mechanism. They

used an antenna which had a collecting area of 8.4×10^4 m^2. The peak power of the radar was 1 MW, pulsewidth was 33 μs and bandwidth was 30 KHz which enabled them to have a height resolution of 5 km. The pulse repitition rate was 700 micro-seconds. Since the operating frequency was 50 MHz, Woodman and Guillen (1974) could have studied only 3 meter irregularities. But from the subsequent analysis of the received signal they derived the information about degree of turbulence at 3 meters as well as about large scale sizes wherein 3 meter fluctuations were used as tracers.

Woodman and Guillen (1974) found that below 85 km. altitude there were two regions from which the echoes of sufficient strength were coming. The first one was the stratosphere with which we are not concerned here. The second one was the mesospheric region of 55-85 km. For the region of 55-85 km. a continuous plot of received power versus time was obtained. The behaviour of 3 meter scalesizes was found to be highly variable and echoes were observed only during daytime and were always absent during nighttime. Although their spatial resolution was only 5 km, they claimed that from their results they had an indication that well defined layers, narrower than 5 km, were present, sometimes, for even several hours together and produced echoes which were 10-15 db stronger than the background.

1.3.2 Observational Results of Ionization Irregularities from Rocket Borne Studies

The study of vertical structure of irregularities and their motion with the ground based backscatter radar, both at Jicamarca and Thumba has given very interesting results. As the generation of irregularities depends on the properties of the ambient medium the ground based techniques cannot be employed to study the properties of the ambient medium. With the advent of rockets and satellites for research investigation a new dimension was added to the scope of these studies and irregularities could be studied directly using the in-situ probes.

The in-situ measurements of ionisation irregularities in the equatorial ionosphere were carried out extensively from Thumba, India using rocket borne Langmuir probes, resonance probes and proton precession magnetometers. All the rocket results which were obtained without the involvement of the author would be discussed in the following. The recent work i.e. from the last five years or so in which the author was fully involved would be described in chapters IV, V and VI. Before describing the rocket results the principle of Resonance probe and Proton precession magnetometer would be briefly discussed.

A novel technique based on the mutual admittance of the two antennas (one of the them as an exciter and the other as a

receiver) was developed by Prakash et al. (1972). This system has many practical advantages over the system earlier flown by Heikkila et al. (1968). In this technique a R.F. signal of varying frequency is applied to the exciter and a part of induction current from it is received by the receiving antenna. As the applied signal is varied in frequency the received signal shows amplitude variations due to varying response of the medium and several plasma resonsnces can be detected. The strongest and most easily recognisable resonance is at the upper hybrid frequency f_T which is given by the relation

$$f_T^2 = f_N^2 + f_H^2$$

where f_N is the plasma frequency and f_H is the gyro-frequency of the electrons in the medium. As the value of f_H is accurately known the value of f_N can be easily determined. The electron density N can be calculated from the relation $N = 1.24 \times 10^4 f_N^2$ where N and f_N are expressed in cm^{-3} and MHz, respectively.

For the experimental set up two stainless steel cylinders concentric with the rocket body and insulated from it were used as exciters. One was placed near the fins of the rocket (far exciter) and the other was placed near the telemetry antenna (near exciter). During alternate cycles a voltage of about 0.7 volts R.M.S. was applied to the far exciter and 0.35 volts to the near exciter. The receiving antenna is the front portion of the nose cone and is used to measure the RF

current flowing into it. This current is estimated by measuring the voltage across a resistance of 1 K. This resistance is much less than the impedance of the medium and the impedance of the stray capacitance of the receiving antenna. A sweep frequency exciter with a frequency sweep from 6.5 MHz to 0.5 MHz in about 1.5 second duration is used alongwith a double conversion type superheterodyne receiver with controlled gain and synchronized with the exciter frequency. The transmitter output is maintained at a constant level by means of an AGC system. The receiver uses two kinds of AGC systems to cover a wide dynamic range. A fast AGC system acts on transient variation, and a slow AGC system acts on average level of the received signal. The R.F. system developed by Prakash et al. (1972) is more suitable for ionospheric studies over the one by Heikkila et al. (1968) in the following sense.

(i) Since no booms are used as exciters the arrangement is simple and takes less space. In an experiment where proton precession magnetometers are flown, the space is so limited that booms cannot be flown.

(ii) The booms will also reduce the reliability and performance of the rocket and also the data of ionization irregularities would be more noisy.

(iii) Since the exciter and the receiving antenna systems are symmetric with respect to the rocket axis, it eliminates any possible spin dependent effects on the resonances.

(iv) The arrangement of sensors and their geometry is such that the induction field from the exciter does not reach the receiver directly but first goes out into the plasma and then comes back to the receiver. The effective distance achieved this way is much larger than that in other systems resulting in very sharp resonances.

The measured electron density represents the actual value in the ambient medium unperturbed by the rocket motion. The point has been confirmed by comparison of the data from the far and near exciter when used on alternate cycles.

The proton-precession magnetometer used for the rocket flight consists of a proton sensor, a programming unit, a polarizing unit and a low noise high gain amplifier (Sastry, 1968). This magnetometer is based on Packard and Varian type flown earlier by Cahill and Van Allen (1956). When the rocket borne magnetometer traverses the electrojet region it measures the resultant of the geomagnetic field and the field due to electrojet currents. A theoretically predicted base value (in absence of electrojet currents) is selected and departure $\triangle F$ of the measured field from this base value is calculated. $\triangle F$ values are plotted against altitude to obtain the 'difference curves'. The current density profiles are derived from the slopes of these difference curves under certain assumptions regarding the nature and extent of electrojet currents. The effect of currents induced in the conducting earth is also taken into account during this conversion (Sastry, 1970).

Using the rocket borne Langmuir probe Prakash et al. (1968) obtained the electron density profile and electron temperatures for evening twilight hours. The presence of E_2 layer was confirmed at 130 and 136 km during the ascent and descent respectively. During this first attempt audio frequency fluctuations in the electron density were recorded in the frequency range of 880 Hz ± 15%. The amplitude of the fluctuations varied with height indicating that the nature of the spectra was changing. These fluctuations were proposed to be generated due to ion acoustic waves which in turn were possibly produced by winds and electric fields. Subbaraya (1968) has reviewed the progress of in-situ measurements till that time. Prakash et al. (1969a) made another rocket launch during the evening twilight of 2nd February 1968. In this flight the fluctuations were measured in a frequency range of 70-1000 Hz and the output was termed 'plasma noise'. In the lower ionosphere the plasma noise was observed between 85 to 105 km whereas in upper part it was observed between 142 and 173 km. In the lower region the fluctuations in the range of 85-92 km were guessed to be due to turbulence whereas the ones between 92-105 km were thought to be generated due to combined effect of turbulence and other nonlocalized forces. The fluctuations in the region of 155-173 km which was around the apogee of the rocket were thought to be produced by the rocket itself when it is subsonic. The fluctuations in the height region of 142-155 km were thought of as the genuine ones and produced by non-localized forces. The nature of observed noise suggested that it could be

The detailed analysis of the evening twilight flight was reported later by Prakash et al. (1969b). The spectral index n was obtained using a power law of the type $E(k) = Ak^n$ where E(k) is the energy contained in the wavenumber k, A is a constant and n is the spectral index. For the evening flight the spectral index value was $\simeq$ -3.5 at lower heights (97-106 km) and was $\simeq$ -2.0 at about 150 km. This increase in n is contrary to what would be expected if irregularities were produced by neutral turbulence mechanism. Such an increased value of n was suggestive of some other agency responsible for the production of the irregularities at higher heights. Below 95 km it was suggested that irregularities are produced by neutral turbulence mechanism whereas between 97-106 two different spectra (one due to neutral turbulence with n = -1.6) are superposed over each other. The possibility of Farley's two stream instability(Farley 1963) was ruled out because the theory needs a threshold of electrojet current strength and the flight under consideration was made during evening twilight when electrojet currents are weak. The Reid's theory (Reid 1968) of cross-field instability was also not considered very seriously as it predicts that for a given value of E field there is a minimum wavelength which one can observe. For all reasonable values of electric fields this limit was much higher than the actual observed scale sizes. It was strongly suggested that electric field plays a very important part in generating the observed irregularities.

A little later on 29th August 1968 at 2300 Hrs. IST, Prakash et al. (1970) launched another Nike Apache rocket which yielded invaluable information about the ionization irregularities in the equatorial ionosphere. Two important points were brought out in that communication; the first one was about the shape of the electron density profile which had electron densities of 10^3 and 10^4 cm^{-3} in the height range of 95-120 km and had a deep valley in 120-140 km region. The electron density in the valley was of the order of few hundred electrons per c.c. Secondly this flight showed the presence of three types of structures.

(i) Large scale structures in the electron density were obtained in 95-120 km region. The vertical scale sizes were about a few km whereas the horizontal extent could be of the order of 50 km. The electron density in these structures varied by a factor lying between 4 and 25.

(ii) The irregularities of scale sizes lying between 30 and 300 meter could be seen directly on the probe current. The results of 30-300 irregularities showed that these irregularities were observed only in regions of negative density gradient (i.e. electron density decreases with increase in height). This gave the first experimental observation about the fact that these irregularities are produced by cross-field instability mechanism. During nighttime the Hall polarisation field is acting vertically downwards and hence over Thumba where magnetic field is in the N-S direction a negative density

gradient would be needed at night to excite the cross-field instability mechanism. These scale sizes could be explained in terms of the available theories of cross-field instability [Reid (1968) Tsuda et al. (1966,69)].

(iii) Small scale irregularities in scalesize range of 1-15 meter were observed to coexist with 30-300 scalesize.

The data of 1-15 meter irregularities was spectrum analysed in the 95-125 km region by passing the output of plasma noise amplifier through six band pass filters. These six outputs represented six different scalesize ranges. By assuming a power law as mentioned earlier the spectral index 'n' was evaluated. The spectral index value for 1-15 meter scalesize range were all lying between -2 and -4 (for regions between 95 and 120 km). Such small scale sizes, could not be explained on the basis of cross-field instability mechanism. It was suggested in this paper that even if a separate mechanism were to be involved the cross-field instability mechanism could still promote or inhibit the production of irregularities because the observation of irregularities largely depends upon the orientation of the electric field and the electron density gradient.

Prakash et al. (1971a) showed on the basis of four rocket flights that the irregularities generated due to cross-field instability mechanism are observed only in positive density gradient regions during daytime and in negative density

gradient regions during nighttime. This was due to the reversal of the direction of vertical Hall field. The amplitude of irregularities in 30-300 meter scale sizes was reported to be between 5 and 20%. Whereas the amplitude of 1-15 meter scale sizes was at best a few percent. An attempt was made to calculate the minimum scale size which can be excited directly by the cross-field instability. The results showed that in order to explain the observed amplitudes of scale sizes between 15 to 30 meter one would need electric fields which are an order of magnitude larger than the estimated fields available at that time. Based on the Gallet's (1955) theory, that neutral turbulence can produce ionization irregularities in presence of electron density gradients, Prakash et al. (1971b) attempted to compare the percentage amplitude of irregularities (obtained during evening and nighttime flights) at E region heights with the theoretically calculated ones. It was found that the amplitude of irregularities around 90 km during evening flights was larger than expected from turbulence and electron density gradients. The amplitudes observed during nighttime flight at 87 km were less than theoretical values indicating that in addition to turbulence there must be some other mechanism operating below 90 km during evening whereas at night, turbulence can account for the observed amplitudes around 90 km. This work has been reviewed by Gupta (1970).

Prakash et al. (1971c) flew two rockets which had Langmuir probe as well as Proton precession magnetometers on

board. The flights were conducted during noon hour which is supposed to be the time when the electrojet currents peak. The electron density was obtained from Langmuir probe and the current was obtained from magnetometer data. Using the relation $J = NeV$ the velocity of streaming electrons was obtained. It was found that the streaming instability which operates at the peak of electrojet ($\simeq$ 105 km) does not need the threshold on the drift velocity of electrons as required by Farley's two stream theory (Farley, 1963). The spectrum of these irregularities was flat. The region of occurrence, spectrum and scalesize range (1-15 m) suggest that the streaming instabilities observed by Prakash et al. were same as type I irregularity observed by Balsley (1967).

Later rocket flights from Thumba have provided more information of the characteristic features of these irregularities. Based on these observations Prakash et al. (1973) have classified the irregularities observed by rockets as following:

1. Type L - Large scalesize irregularities with vertical scalesizes greater than a few km. Generation mechanism: Unknown.

2. Type M_c - Medium scalesize irregularities with vertical scalesizes of 30-300 meters. Generation mechanism: Cross-field instability.

3. Type Mn - Medium scalesize irregularities with vertical scalesizes of 30-300 meters. Generation mechanism : Neutral turbulence.

4. Type Mu - Medium scalesize irregularities with vertical scalesizes between 30 and 300 meters. Generation mechanism : Unknown

5. Type S_c - Small scalesize irregularities with vertical scalesizes between 1 and 15 meters. Generation mechanism: Multi-linear cross-field instability mechanism.

6. Type S_n - Small scalesize irregularities with vertical scalesizes between 1 and 15 meters. Generation mechanism: Neutral turbulence.

7. Type S_s - Small scalesize irregularities with vertical scalesizes between 1 and 15 meters. Generation mechanism: Streaming instability.

8. Type R - Small scalesize irregularities with vertical scalesizes between a few cm and one meter. Generation mechanism : Rocket motion.

CHAPTER - II

GENERATION MECHANISMS OF IRREGULARITIES

The mechanisms of generation of ionization irregularities observed by the author in the D and E-regions of the ionosphere are the cross-field instability and the neutral turbulence. The development of some of these theories which are applicable to the ionospheric case is discussed here.

2.1 Theories of Cross-field Instability

2.1.1 Linear Theories

The first quantitative theory of the cross-field instability was proposed by Simon (1963) for the case of laboratory plasma. Simon considered a slab of weakly ionised plasma with mutually perpendicular electric and magnetic fields and found that if the electric field was greater than

a critical value, in presence of non-uniformities of plasma density, the study state could become unstable. While discussing the Penning discharge at high pressure Hoh (1963) showed independently that a weakly ionized plasma column, in an axial magnetic field and an inward directed radial electric field, is unstable to macroscopic perturbations. It was shown that the instability is caused by the presence of a third fluid, the neutrals in an ion electron plasma. Hoh came out with a critical magnetic field which agreed well with the experimental results.

Meeda et al. (1963) and Knox (1964) were the first to apply the Simon's theory to the case of ionosphere. Meeda et al. while attempting to explain E_{s-q} echoes found that a threshold of primary electric field, in W-E direction, was needed. Knox showed that for electrojet region, where crossed electric and magnetic fields are present, the perturbations of electron density can grow when either electron density or electric field gradients is present. The irregularities were found to be moving with wide range of velocities. Further extensions of Simon's theory were done by Morse (1965) who did two dimensional linear analysis for the equatorial ionosphere, and by Tsuda et al. (1966) to explain the temperate latitude sporadic-E.

All the above mentioned work was limited to the 'bounded case' where the electron density and electric field

perturbations are assumed to be present only between two fixed altitudes. In the 'unbounded case' the ambient electron density as well as the perturbations in it vary exponentially with the height for the same scale height. Reid (1968) studied the case of such an unbounded plasma assuming a realistic electron density profile. The salient features of Reid's theory are the following.

Only those wave numbers which were moving towards magnetic west, represented by $k_{\perp}$ were considered whereas the ones parallel to the magnetic field were neglected. The electric field component parallel to the magnetic field, E_{11} was also neglected. The variation of electron density was assumed to be of an exponential form with a scale height, H, such that

$$\frac{1}{H} = -\frac{1}{n_o}\frac{dn_o}{dn}$$

where n_o is electron density and h is the altitude.

The time and space dependence of the electron density perturbation was assumed to be of the following form.

$$n_1(t,x) = n_1(x) \exp\left\{-i(\omega t - \vec{k}_z z)\right\}$$

and

$$n_1(x) = n_1 \exp\left\{-\frac{x \cos I}{H}\right\}$$

where n_1 is the perturbation in the electron density,

ω is the frequency of the perturbation,
k_z is the wave number in z direction (magnetic west),
x is the direction pointing towards the vertical, and
I is the magnetic dip angle.

The functional form of the electric field perturbation was same as that of electron density perturbation. The space dependence of the perturbation shows that only field aligned irregularities which form a rippled pattern in east-west direction are considered. The functional form of the perturbation assumed by Simon (1963) and Tsuda et. al.(1966) was a simusoidal of half wave length with amplitude vanishing at $x = o$ and $x = L$. The spatial averages of electron density and electric field were taken over the distance L in the further analysis. Reid pointed out that these could be true only for the bounded case and were certainly not applicable to the system like ionosphere, and came out with the above mentioned exponential dependence. The analysis of Reid showed that in the presence of a certain critical electric field, the ionospheric E-region could be unstable to the growth of electron density perturbations of sizes ranging from a few tens of meters to a few kilometers. The electric fields supporting the large scale irregularities are conducted upto high latitude F-region heights along the highly conducting magnetic field lines and there they produce small scale irregularities in presence of density gradients. Cunnold (1969) extended Reid's work by including the effects of finite k_{11}. It was

found that the effect of inclusion of k_{11} is to reduce the growth rate and accelerate the loss rate due to diffusion.

The theories of cross-field instability got a momentum with the work of Rogister and D'Angelo (1970). It was pointed out by them that the neglect of ion inertia, by previous workers, was not justified as it leads to dissipative effects. They developed the theory for 95 km and 110 km regions, separately because the collision frequencies and other scaling factors are quite different in both these altitude regions. Although they did not write the Vlasov equation and considered only the fluid picture for both electrons and ions, the results of Farley-Buneman instability were recovered. The effects of ionization and recombination were neglected because the time constants associated with these processes were of the order of minutes whereas the period of the waves considered was of the order of milliseconds. The ionosphere was assumed to be stratified both in east-west as well as north-south direction. It was further assumed that the presence of waves did not modify the magnetic field itself i.e. the perturbation were electrostatic in nature. k_{11} was assumed to be much smaller than $k_{\perp}$. All the perturbed variables were expanded as a power series in terms of a small parameter ϵ, which was the smallest parameter of the entire system. The density perturbation δn was given by

$$\delta n = \delta n^{(1)} + \epsilon \delta n^{(2)} + \epsilon^2 \delta n^{(3)} + \cdots$$

The time dependence of these perturbations is given by

$$\delta n^{m}(t,x) = \delta n^{m}(x)\ \exp(-i\omega t)$$

where ω is the frequency of the perturbation and is in turn represented by

$$\omega = \omega^{(1)} + \epsilon\,\omega^{(2)} + \epsilon^{2}\,\omega^{(3)} + \cdots$$

The space dependence of the perturbation was described by w.K.B. approximation as follows:

$$\delta n(x) = \tilde{\delta n}(\epsilon x)\ \exp\left\{\frac{i\phi(\epsilon x)}{\epsilon}\right\}$$

where $\tilde{\delta n}$ represents the average value.

Using these generalized dependences Rogister & D'Angelo (1970) derived the expressions for the growth rate for lower as well as the upper region. The expression for the growth rate in the upper region was similar to that of lower region except that it had an additional term which represented the effect of shear of electron flow. The growth rate for the lower region is given by

$$\Gamma^{(1)} = \frac{\vec{K}\cdot\vec{V}_{eo}}{\left(1-\frac{\nu_e\nu_i}{\Omega_e\Omega_i}\right)^{2}}\frac{\nu_e}{\Omega_i}\frac{k_y}{K_\perp^{2}}\frac{1}{n_0}\frac{\partial n_0}{\partial\epsilon\xi_2} - \frac{\nu_e}{\Omega_e}\frac{\left(\omega^{(1)^{2}} - K_\perp^{2}C_s^{2}\right)}{\Omega_i\left(1-\frac{\nu_e\nu_i}{\Omega_e\Omega_i}\right)}$$

The first term on the R.H.S. is the manifestation of the cross-field instability and has to be positive for the growth of perturbation. This term can be positive when either, both $\vec{K}\cdot\vec{V}_{eo}$ and $\frac{1}{n_0}\frac{\partial n_0}{\partial\epsilon\xi_2}$ are positive or, are negative. The first condition is satisfied during daytime when electron

flow ($\vec{K}.\vec{V}_{eo}$) is towards west and the gradients are positive (electron density increasing with altitude) whereas the second condition is satisfied during night time. Rogister and D'Angelo (1970) clearly demonstrated that the cross-field instability would occur for the situation prevailing in equatorial electrojet and further attributed the cause of the type II backscatter echoes to the irregularities generated through this mechanism.

The second term is the manifestation of Farley-Buneman instability. As Ω_e was assumed to be negative, a positive contribution to the growth rate from this term is possible when

$$\omega^{(1)^2} \geq K_\perp^2 C_s^2 \quad \text{or} \quad \vec{K}.\vec{V}_{eo} \geq \left(1 - \frac{\nu_e \nu_i}{\Omega_e \Omega_i}\right) K_\perp C_s$$

This indicates the necessity of a threshold of electron drift velocity for excitation of two stream instability. This instability is generally believed to be responsible for the generation of irregularities that cause type I radar echoes in the equatorial electrojet (Farley 1963). The role of linear cross-field instability in generation of irregularities in the equatorial electrojet has also been discussed by Whitehead (1971).

We note here that none of the above mentioned theories could explain the generation of 3-meter irregularities associated with type II echoes observed when electron drift velocity, V_d is smaller than the ion-acoustic velocity C_s.

The two stream instability occurs when $V_d > C_s$ and, therefore, cannot account for the type II echoes. On the other hand, cross-field instability favours the generation of large scalesizes and, therefore, cannot excite 3-meter irregularities directly (Farley and Balsley, 1973). The smallest scalesize that can be generated by cross-field by cross - field instability is given by Sudan et al (1973) as $\lambda_c \simeq \frac{300}{V_d}$. Thus the radar signals at 3-meter cannot be explained when two-stream threshold is not reached. To resolve this difficulty Sudan et al (1973) have proposed a two step mechanism for the generation of small scale irregularities, which we describe below.

2.1.2 Non-linear Theories

The theory of Sudan et al. (1973) is a multilinear theory in which small scalesizes are generated on the top of large scalesizes due to second stage two-stream and cross-field instabilities. In the first step, long wave lengths are generated through the linear cross-field instability mechanism. It is shown that these irregularities do not steepen appreciably because even though they are non-dispersive waves, the phase velocity of these waves does not significantly depend on local parameters such as density or temperature. Since the waves do not steepen in the direction of propagation they attain large amplitudes. The existence of such large amplitude long wavelengths was experimentally

observed by Prakash et al. (1973). The large amplitudes attained by these waves are of the order of a few per cent and, therefore, the associated gradients and the vertical drifts because of local wave electric fields could be much larger than the original vertical gradients and the westward drifts. These gradients and drifts are responsible for small scale perturbations propagating vertically upwards. The quantitative estimates for the generation of small scalesizes show that the minimum scalesize that can be generated by this mechanism is given by λ_z where,

$$\lambda_z \simeq 8\, A^{-1}\, V_d^{-3/4} \text{ meters}$$

where A is the percentage amplitude of the large scalesize irregularity. For a drift velocity of 100 meters/sec and a percentage amplitude of 4% (A = 0.04) one finds the minimum λ_z to be about 6 to 7 meters.

Several theories have been advanced in the past for the non-linear evolution of the cross-field instability. For the saturation of the instability, these theories consider effects like quasilinear flattening of the density gradient and mode coupling to linearly stable higher wave numbers. Thus in a non-linear theory presented by Rogister (1972) for one dimensional cross-field instability, the energy is transferred by mode coupling from large to small wavelengths, where it is absrrbed by linear diffusion damping. This theory predicts a suprathermal fluctuation level for a range of

linearly stable wavelengths and further the amplitude of the density fluctuations is found to be $\simeq$ 20% of the background density for the modes with maximum linear growth rate.

For the case of laboratory plasmas Kim and Simon (1969) have developed a quasi-linear theory in which the instability is quenched by quasi-linear reduction of externally applied electric field. For the case of reflex arc plasmas Hooper (1970) has shown that a quasi-linear flattening of the density gradient would shut off the cross-field instability.

Sato (1971, 74, 76) has shown that for electrojet situation, quasi-linear shielding of both electric field as well as the density gradient would contribute to the saturation of the instability in a weakly unstable situation. Sato (1971) has also shown that for a strongly unstable system mode-coupling effects become important and the final situation is quite turbulent in which smaller scalesizes are generated by large scalesizes in a kind of cascading down the energy from small k's to large k's. In the latter case it was found that turbulent spectrum approaches K^{-3}. In this work Sato (1971) has shown that a critical electric field E_{c_1} exists in the system such that if the applied external electric field $E_x < E_{c_1}$, then quasi-linear effects saturate the instability whereas if $E_x > E_{c_1}$ the turbulent situation arises.

Sato and his coworkers have also carried out numerical investigations for the non-linear cross-field instability.

Sato and Tsuda (1967), Tsuda and Sato (1968) and Sato et al. (1972) performed numerical analysis of the instability in one dimensional model and in general found that when $E_x < E_{c_1}$ then the evolved waveform has a sawtooth shape and for $E_x < E_{c_1}$ the system becomes strongly turbulent. Later on Sato and Tsuda (1968) and Tsuda et al. (1969) extended the analysis to two dimensional model. These computations showed that the important quenching mechanism was cancellation of the external electric field for smaller E_x. The mode coupling effects leading to this turbulent situation were found to be important again for the high values of E_x such that $E_x > E_{c_1}$. Ogawa (1972) has further shown through his numerical computations for two-dimensional case, that the density flattening is also a competing saturation mechanism for the nonlinear evolution of cross-field instability.

Recently, McDonald et al. (1974, 75) have performed a two-dimensional numerical solution of the basic fluid equations believed to describe the equatorial electrojet situation. In their computer simulation experiment, it is found that long wavelength horizontally propagating gradient drift instabilities excite short wavelength vertically propagating instabilities and the final state is highly turbulent two dimensional state which supports the two step theory of Sudan et al. (1973). It is further found that the density fluctuations' power spectra for short wavelength irregularities go as $k^{-3.5}$.

In an attempt to explain some of the rocket observations of Prakash et al. (1973), a two dimensional non-linear theory of cross-field instability was advanced by Rognlien and Weinstock (1974). It is shown by these workers that the non-linear term $\mathbf{v}_e \cdot \nabla n$ in the electron continuity equation is the most dominant non-linearity for the case of two dimensional perturbations. This is in contrast to earlier theories in which only one dimensional case was considered and wherein this non-linearity almost vanishes. Thus in a realistic calculation two dimensional perturbations should be considered as done by Rognlien and Weinstock (1974). This calculation shows that the linearly unstable mode generates a non-propagating mode in the vertical direction which is damped in the linear analysis. This serves to act as a saturation mechanism for the linear cross-field instability mechanism and these authors have calculated saturated amplitudes and spectra of density and electric field fluctuations in the resulting time steady situation. An agreement between the calculated shapes and spectra for the irregularities with our rocket observations has been claimed by these authors. The form of perturbation considered by Rognlien and Weinstock (1974) is

$$\frac{n_1}{n_o} \propto \text{Ri} \quad i \quad \exp \left[i(kyr - \omega t) \right] \quad \text{Cos } k_x \quad x$$

which is equivalent to superposition of two plane waves propagating at equal but opposite angles to the y-axis i.e. the magnetic east. It has been shown by these authors that for such

a perturbation the non-linear term $\vartheta_{e1} \cdot \nabla (n_1/n_o)$ is the most dominant non-linearity. For a case of single plane wave this term is vanishingly small because the two vectors are nearly perpendicular to each other. To illustrate the basic saturation process of this instability they consider interaction of only two modes. Density perturbation of the above mentioned form is assumed to be excited to a small level with an amplitude of $A_{1,1}(y)$ and this mode can be written as following

$$\left(\frac{n_1}{n_o} \right)_{1,1} = A_{1,1} \text{ Sin } (k_{yr}\, y - \omega t) \text{ Cos } k_x\, x$$

The non-linear interaction of this mode with itself as manifested by the term $\vartheta_{e1} \cdot \nabla (n_1/n_o)$ in the electron continuity equation produces a second mode. This becomes evident when the nonlinear term is written down,

$$\vartheta_{e1} \cdot \nabla (n_1/n_o) = - \frac{\nu_i \omega k_x k_{yr}}{2 \Omega_i k_\perp^2} A_{1,1}^2 \text{ Sin } 2k_x x$$

This non-linearity generates a new mode which is given by

$$\left(\frac{n_1}{n_o} \right)_{2,0} = A_{2,0} \text{ Sin } 2 k_x\, x$$

The subscript 2,0 indicates that this mode varies as second harmonic of k_x in x direction (magnetic North) and as zeroth

harmonic in the y direction (magnetic east) or time. This mode does not propagate and the density structures have variations only in x direction. This mode is damped in the linear analysis. The $A_{2,0}$ mode can couple with the $A_{1,1}$ mode through $\vec{v}_{e1} \cdot \nabla (n_1/n_0)$ term to produce a non-linear flux of electrons that will stabilize $A_{1,1}$ mode. Thus one finds that the stabilization mechanism in this theory is a wave enhanced flux or diffusion of electrons.

Following such an approach the saturated amplitudes of both the modes can be calculated. A rather surprising discovery of this analysis was that during the saturation process the linearly damped mode in the saturated steady state has a larger density amplitude than the linearly unstable mode. However, the electric field amplitude for the linearly damped mode remains smaller than the linearly unstable mode in the saturated steady state.

In order to determine the effect of cascading of energy from small wave numbers to high wave numbers many modes were considered in the analysis by these authors. The resulting coupled non-linear equations thus obtained were then numerically solved and the resulting shapes and spectra of the large scalelength modes were computed.

The above analysis pertains to only nighttime situation. The extension of the analysis for the daytime conditions was done later on (Rognlien and Weinstock, 1975). The daytime

situation in the equatorial electrojet is distinguished from that of nighttime by two factors. First the zero order density gradients are weaker during daytime and the second, owing to the large background density during daytime dissociative recombination becomes dominant linear wave damping mechanism rather than the ampipolar diffusion. It is found that irregularities attain large amplitudes $\sim$ 10% and are found to break up into smaller dominant scalesizes in the horizontal westward direction than in the vertical direction. The density waveform in the horizontal direction shows a pronounced steepening in a direction opposite to zero order density gradient whereas in the horizontal direction no tendency towards wave steepening is observed in their calculations. The spectra and shape of the resulting modes were compared with the rocket observations. The observed saw tooth structure in the vertical direction was reproduced in this analysis. A detailed discussion of this theory in light of our results shall be given in chapter VI.

2.2 Neutral Turbulence

2.2.1 General Nature of the Turbulence

Another cause of generation of plasma irregularities is the neutral turbulence. In the following, an attempt would be made to discuss some basic properties of turbulence and the conditions under which turbulence can generate ionisatio

irregularities. Some of the experimental observations which support the existence of turbulence would also be discussed.

Turbulence is a condition of fluid motion in which properties of the fluid, such as the heat content, water vapour content etc. are diffused at a rate large compared with the rate of diffusion by molecular motions. A fluid is said to be turbulent if (a) each component of the vorticity is distributed irregularly and aperiodically in time and space, if (b) the flow is characterized by transfer of energy from larger to smaller eddies and if (c) the mean separation of neighbouring fluid particles tends to increase with time. The term eddy denotes the volume of the fluid which moves more or less coherently with respect to the mean flow. The eddy motion need not be and usually is not of a rotating character. The term eddy is often replaced by a more familiar expression 'Scale of motion'. Any turbulent region contains eddies of varying sizes. The size of largest eddy is comparable to the boundaries which enclose the turbulent region whereas the size of smallest eddies would be decided by the point at which the turbulent structures are damped due to viscous forces. The size of smallest eddy is known as 'Kolmogorov microscale' and is given by

$$\lambda_K = \left(\frac{k^3}{e} \right)^{\frac{1}{4}}$$

where k is the kinematic viscosity and e is the rate at which energy is fed to large eddies (Batchelor 1956). The

energy is fed to larger eddies through wind shears. These larger eddies produce smaller and smaller eddies through momentum transfer processes. The damping due to viscosity is small for larger eddies and goes on becoming important for smaller eddies. The limit beyond which viscous damping becomes very enhanced is related to the mean free path of neutral particles.

Thus there is a range of scale sizes extending from very large eddies, which contain energy, down to smallest eddies which can remain turbulent. If one considers that large eddies are the structures much larger than Kolmogorov microscale then there exists a wave number range from k_o (corresponding to large eddies) to k_k (corresponding to Kolmogorov microscale). This range is known as 'Inertial subrange'. Wave numbers smaller than k_o fall in energy containing subrange whereas the wavenumbers higher than k_k fall in the viscous dissipation subrange. In the energy containing subrange it is not very clear so as how the energy is transferred from shearing forces. In the inertial subrange the energy transfer processes are independent of energy contained in the very large eddies and the viscous damping. In the inertial subrange the energy transfer depends only on the parameter ϵ namely, the rate at which the energy is fed into very large eddies.

On the basis of dimensional analysis it has been shown

the inertial subrange can be expressed as following (Kolmogorov 1941 and Batchelor 1956)

$$E(k) = \alpha \; e^{2/3} \; k^{-5/3}$$

where $E(k)$ is the energy contained in the wave number k and α is a constant of proportionality and is usually taken as unity. The spectral index is - 5/3 in the inertial subrange. At wave numbers larger than k_k i.e. scalesizes smaller than Kolmogorov's microscale the energy $E(k)$ drops of much rapidly than in inertial subrange because viscous damping goes on increasing with higher k. The spectrum in the viscous dissipation range must, therefore, be steeper than that in the inertial subrange.

The turbulence can be generated when either the amoun of energy fed into larger eddies is large or when the amount of energy extracted by viscous damping is very small. When the effect of wind shears is large in dumping energy to larger eddies one can use Richardson's criterion for knowing whether turbulence would occur or not. In cases where viscou damping is too small one can use Raynold's criterion to know the same.

Richardson's Criterion

If ω_g denotes the angular frequency of oscillation of an adiabatically displaced fluid element and if ω_s repres the vertical gradient of the horisontal wind, these quantitie

the inertial subrange can be expressed as following (Kolmogorov 1941 and Batchelor 1956)

$$E(k) = \alpha \; e^{2/3} \; k^{-5/3}$$

where $E(k)$ is the energy contained in the wave number k and α is a constant of proportionality and is usually taken as unity. The spectral index is - 5/3 in the inertial subrange. At wave numbers larger than k_k i.e. scalesizes smaller than Kolmogorov's microscale the energy $E(k)$ drops of much rapidly than in inertial subrange because viscous damping goes on increasing with higher k. The spectrum in the viscous dissipation range must, therefore, be steeper than that in the inertial subrange.

The turbulence can be generated when either the amount of energy fed into larger eddies is large or when the amount of energy extracted by viscous damping is very small. When the effect of wind shears is large in dumping energy to larger eddies one can use Richardson's criterion for knowing whether turbulence would occur or not. In cases where viscous damping is too small one can use Raynold's criterion to know the same.

Richardson's Criterion

If ω_q denotes the angular frequency of oscillation of an adiabatically displaced fluid element and if ω_s represents the vertical gradient of the horisontal wind, these quantities

can be represented mathematically as following:

$$\omega_g = \sqrt{\frac{g}{T}\left(\frac{\partial T}{\partial z} + \frac{g}{C_p}\right)}$$

and

$$\omega_s = \left(\frac{\partial V_h}{\partial z}\right)$$

where g is the acceleration due to gravity,

T is the temperature

V_h horizontal wind speed

Z is the displacement in the vertical direction and

C_p is the specific heat at constant pressure.

The Richardson number Ri is defined as the square of the ratio of ω_g and ω_s

$$R_i = \left(\frac{\omega_g}{\omega_s}\right)^2 = \frac{g\left(\frac{\partial T}{\partial z} + \frac{g}{C_p}\right)}{T\left(\frac{\partial V_h}{\partial z}\right)^2}$$

Richardson's criterion tells that a medium is locally stable against the onset of the turbulence as long as Ri exceeds a certain critical value, Ric. There are many numbers suggested for Ric from different workers such as

Ric = 1 (Richardson and Prandt)

= 1/12 (Townscend)

= 1/25 (David Layzer)

If Ri $<$ Ric medium would be turbulent otherwise it would be stable.

Reynold's Criterion

This criterion was obtained by Osborne Reynold on the basis of his experiments on imcompressible viscous fluids. According to this criterion for incompressible fluids, if a dimensionless quantity R_e (known as Reynolds number) exceeds a critical value the turbulence would be observed. The Reynolds number is given by

$$R_e = \frac{L V}{\nu}$$

where L is the typical scale length of the system; in case of a bounded system L is the diameter of the pipe in which the fluid flows, whereas in unbounded system, it is the scale height, V is the mean velocity of the fluids and ν is the kinematic viscosity.

The Reynolds number is in essence the ratio of inertial terms to the viscous terms in the Eulerian equations of fluid motio

2.2.2 Regions of Turbulence in the Ionosphere

Regarding the existence of turbulence in the atmosphere it was theoretically predicted by de Jager (1952) and Steward (1959) that beyond 100 km altitude there should be no turbulence. In accordance with the theoretical prediction

the existence of neutral turbulence in the atmosphere upto about 100 km height has been confirmed experimentally by many workers (Greenhow and Neufeld, 1959, Blamont and de Jager 1962). Some of the ionospheric phenomena such as D-region scatter propagation have been explained on the basis of neutral turbulence.

If the electron-neutral and ion-neutral collision frequencies are greater than their respective gyrofrequencies the movement of neutral can be transmitted to the electrons, because the effect of magnetic field becomes unimportant and collisions play the major role. In the ionosphere as far as the ions are concerned the ion-neutral collision frequency is much higher than ion-gyrofrequency. But in case of electrons it can be seen from the collision frequency values obtained by Thrane and Piggott (1966) that upto about 75 km the electron-neutral collision frequency is greater than electron gyrofrequency. Thus in the region below 75 km or so the collisional effects dominate over magnetic field effects both for electrons and ions. It has been shown by Villars and Weisskopf (1955) that neutral turbulence can produce fluctuations in the electron density in the 80-90 km region. There are essentially two mechanisms which produce fluctuations in the electron density. The first one is due to fluctuations in the density of the carrier medium i.e. the neutrals. The second one is due to turbulent mixing which implies inhomogeneous average electron density, i.e. the presence of electr density gradient.

2.2.3 Electron Density Fluctuations Due to Fluctuations in the Neutral Density

For an eddy of scalesize L one can define an associated eddy velocity Δv_L as a fluctuation that extends over a distance L. If $\langle v \rangle_L$ is defined as velocity averaged over a spatial region of size L^3 the perturbed velocity can be defined as

$$\left(\Delta v_L\right)^2 = \left\langle \left(v - \langle v \rangle_L \right)^2 \right\rangle_L \qquad (1)$$

where v is the magnitude of velocity change over a distances of L. Similarly the perturbed pressure, due to perturbation in velocity, can be defined as Δp_L. The generation of pressure fluctuations due to velocity fluctuations is given by Bernouilli theorem.

$$p + \tfrac{1}{2} \rho v^2 = \text{constant} \qquad (2)$$

where ρ is the density

from equation (2) it can be easily seen that

$$|\Delta p_L| \simeq \rho \left(\Delta v_L\right)^2 \qquad (3)$$

since the gas has to satisfy the equation of state, in presence of density fluctuations eqn. (3) will become

$$\Delta \rho_L = \gamma \frac{\rho}{p} \Delta p_L \simeq \frac{\rho \, \Delta v_L^2}{v_M^2} \qquad (4)$$

where γ is the adiabatic exponent and v_M^2 is the mean square velocity.

If one writes the perturbed velocity in terms of initial power supply, So, the following expression is obtained

$$\Delta V_L = \left(\frac{SoL}{\rho}\right)^{1/3} \tag{5}$$

By eliminating ΔV_L from equations (4) and (5) one gets

$$(\Delta \rho_L)^2 = \rho^2 \left(\frac{So}{\rho}\right)^{4/3} \cdot \frac{L^{4/3}}{v_M^4} \tag{6}$$

If the scalesize of the eddy is greater than Kolmogrov micro-scale the density fluctuations are so rapid that there is no substantial electron diffusion. These fluctuations would then be transmitted to electron density N which will have a fluctuation δN given by

$$\delta N = \frac{N}{\rho} \delta \rho \tag{7}$$

Substituting the value of N in equation (6) one gets

$$\Delta N_L^2 = N^2 \left(\frac{So}{\rho}\right)^{4/3} \frac{L^{4/3}}{v_M^4} \tag{8}$$

2.2.4 Electron Density Fluctuations Due to Turbulent Mixing

This particular mode considered by Villars and Weisskopf (1955) is more applicable for present studies as in this case an average electron density gradient has been

assumed. In earlier case the density was assumed to be homogeneous one. If the medium is collisional and eddies of scale length L are present the fluctuations in the electron density would be produced and would be given by

$$\Delta N_L \sim \left(\frac{dN}{dh}\right) L$$

The fluctuations in the electron density would be produced only if the life time of the eddy is much shorter than the time scales of the phenomena which tend to change the density. Some of these phenomena are recombination and attachment of electrons. But as the fluctuations are produced the effect of turbulence would be to smear out the gradients in electron density. In the inertial subrange the amplitude of fluctuations depends only on the density gradient and not on the intensity of excitation of turbulence.

Gallet (1955) has shown that in presence of electron density gradient, turbulence can give rise to fluctuations in electron density. He suggested that in presence of electron density gradient an upward moving air blob would carry electrons with it thus causing enhancement in the higher density region and a depletion in low density region. Thus the fluctuations in electron density are created. But since these fluctuations were an order of magnitude less than experimentally observed values, Gallet (1955) suggested an amplification mechanism for the fluctuations in neutral density. In

collision dominated regime these amplified neutral density fluctuations would be transmitted to electron density fluctuations. The amplification mechanism suggested by Gallet (1955) was the following. In presence of a positive background temperature gradient an air blob if displaced upwards loses energy adiabatically and its temperature decreases. As the air blob rises its potential energy increases and the kinetic energy decreases with the result that the temperature decreases. This results in temperature fluctuations and consequently in the neutral density fluctuations. Thus the large neutral density fluctuations are passed on to the electron density which then exhibits enhanced fluctuations.

Dungey (1959) has shown that in presence of a magnetic field a shear flow in neutral air can generate the irregularities in the electron density. He had used equations of motion for each constituent of the gas. As suggested by Dungey the neutral air tries to carry the ionized gas with its motion but the magnetic field resists the motion of the ionized gas across the lines of force. In presence of solenoidal velocity of neutrals he shows that irregularities can be generated.

Thus the existence of turbulence in D-region was theoretically predicted and was confirmed experimentally also. It has also been shown that the fluctuations in neutral density can be transmitted to electron densities when the collisional effects dominate over the magnetic field effects.

CHAPTER - III

LANGMUIR PROBE, INSTRUMENTATION AND DATA ANALYSIS

3.1 Basic Principle of Langmuir Probe Technique

The basic principle of the Langmuir probe technique which was enunciated by Mottsmith and Langmuir (1926), is to measure the current, which an electrode draws from the plasma, as a function of the electrode potential. In case of Langmuir probes flown on rockets the sensor potential is measured with reference to the rocket body potential. Different domains of the current voltage characteristics can be used to study different parameters, viz. electron density, ion density and electron temperature. Therefore, the voltage applied to the sensor depends on the parameter one wants to study.

3.1.1 Behaviour of Probe at Different Potentials

If a metallic probe whose size is small compared to the mean free path of electrons is inserted into plasma and the current drawn by the probe is plotted against the voltage applied to the probe the resulting curve is known as Langmuir probe characteristics. The current reaches a saturation value J_+ at sufficiently large negative potential V_-. With increasing V high energy electrons also start collecting with the result that net ion current gets reduced. On further increasing the potential of the probe a value V_f is reached where the net current to the probe is zero. V_f is known as 'floating potential' because it is the potential which the probe would assume if allowed to float in the plasma. Further increase in the probe potential leads to rapid rise in electronic current until a value V_s is reached. V_s is known as 'Space Potential' at the location of the probe. Beyond V_s the increase in the current is much slower and there is negligibly small collection of positive ions owing to their small energy spread and the repulsive potential of the probe towards them.

Probe in Strongly Retarded Regime

In this regime only positive ions are collected and the region is known as ion saturation region. In the vicinity of the probe only positive ions contribute to the space charge and the potential is a steep function of position, this region

is called as 'plasma sheath'. At larger distances from the probe both electrons and positive ions contribute to the space charge with the result that at large distances electric fields are small. The thickness of plasma sheath depends on the electron density, electron temperature, probe voltage and the size of the probe. A rough idea of sheath can be had from the basic plasma parameter, the Debye shielding distance λ_D which is given by:

$$\lambda_D = \sqrt{\frac{K T_e}{4\pi n_e e^2}} \approx 6.9\sqrt{\frac{T_e}{n_e}} \qquad \text{C.G.S. Unit}$$

where K is the Boltzman's constant, Te is the electron temperature, n_e is the electron density and e is the electronic charge.

Probe in Slightly Retarded Potential Regime

At small negative voltages the probe current is made up of two parts; first one is space charge limited positive ion current and the second one is the current due to electrons which overcome the repelling field of the probe. The electron current density j in this regime is given by

$$j = j_o \exp\left(\frac{eV}{kTe}\right)$$

where V is the retarding potential and j_o is the electron random current density. If one plots log j versus V the resulting curve would be straight line with a slope of $\frac{e}{kTe}$.

From this slope electron temperature can be determined. This is known as 'd.c. technique' of temperature determination. The semilog plot would yield a straight line only if the electrons have Maxwellian distribution of energy. If the energy distribution is non-Maxwellian still the current voltage curve may be analysed. Druyvesteyn (1930) gave the expression of electron energy distribution function F(Ve) by using the second derivative $\frac{d^2i}{dV^2}$. F(Ve) expressed in terms of electron energy in volts, is given by

$$F(Ve) = \sqrt{\frac{8\ mV}{e^3}} \cdot \frac{d^2i}{dV^2}$$

where m is the mass of the electron.

The second derivative $\frac{d^2i}{dV^2}$ can be determined by using a variety of methods which include a simple one given by Takayama et al. (1960), wherein a small a.c. signal is superimposed on the sweep voltage. If i_o is the current into the probe at a given retarding potential V_o then the addition of an a.c. signal $V \cos \omega t$ (where $|V| < |V_o|$) increases the current from i_o to a new value i given by

$$i = i_o J_o (ieV/kTe)$$

where $J_o(ieV/kTe)$ is the zeroth order Bessel function for a pure imaginary argument. A measurement of the ratio of the current with and without a.c. signal yields the value of $J_o(ieV/kTe)$ and since V is known, the temperature can be found out. The frequency of the a.c. signal may be in the

audio or radio frequency range but in any case should be no greater than 10% of the plasma frequency in order to avoid resonance effects.

Probe at Plasma Potential

At the plasma potential the current collected by the probe is entirely due to thermal motion of charged particles. Since the average electron velocity is much larger than the average ion velocity, the probe current can be considered entirely due to electrons. According to the kinetic theory the average number of particles colliding against a unit area of surface exposed to a gas in unit time is $\frac{n_e \bar{v}}{4}$. Therefore, the probe current at plasma potential is given by

$$J = J_o A = \frac{n_e \bar{v}}{4} \cdot e \cdot A$$

where A is the surface area of the probe, J_o is the electron random current density and $\bar{v}$ is the average electron velocity.

Probe in Accelerating Potential Regime

In this regime positive ions are repelled and electrons are attracted towards the probe. Even a small positive voltage is sufficient to make the positive ion component of the probe current negligible as compared to the electron component. In this regime determination of electron current is complicated by consideration of both the size and the shape of the probe. The size of the probe should be smaller than the mean free path

of electrons otherwise the probe would collect more electron than what can be made up by diffusion thereby causing depletion around the probe.

For writing down the expressions for current the usual way is to write down the Poisson's equation and solve it. Mottsmith and Langmuir (1926) have obtained such expressions for spherical, planar and cylindrical geometries. Following are the exact expression for the probes whose dimensions are either very large or very small as compared to the Debye shielding distance.

For Small Sphere $\quad j = j_o \left(1 + \frac{eV}{kTe} \right)$

For Large Plane $\quad j = j_o$

Large compared to the thickness of the plane and the sheath. Here the probe current is determined by the surface area of the probe and plasma parameters.

For Long Thin Cylinder $\quad$ Length $>>$ radius

$$j = j_o \left\{ \frac{2}{\sqrt{\pi}} \sqrt{\frac{eV}{kTe}} + \exp\left(\frac{eV}{kTe}\right) \; p \sqrt{\frac{eV}{kTe}} \right\}$$

where $p\sqrt{\frac{eV}{kTe}}$ is an error function.

There have been many developments in the theory of Langmuir probe in different regions by a number of workers (Schulz and Brown (1955), Allen et al. (1957), Su and Lam (1963), Cicerone and Bowhill (1967), Cohen (1963) and Wesserstrom et al

(1965)). As the author has used the Langmuir probe for ionospheric study it would be relevant to mention different versions of Langmuir probes used for such study.

3.1.2 Different Versions of Langmuir Probe Used by Various Workers

The first attempt to use Langmuir probe technique for ionospheric study was made by Hok et al. (1953) at the University of Michigan, U.S.A. Although the results obtained by Hok et al. were not very promising the potential of Langmuir probe as a diagnostic technique was immediately realised. Spencer et al. (1962) used a bipolar probe which consists of two symmetrical spherical probes between which a fixed or variable voltage is applied. Later Spencer et al. (1962) used cylindrical geometries also. McNamara (1965) used the Langmuir probe with planar and spherical electrodes. Meshed spherical probes wherein the effect of photoelectrons is reduced were used by Aono et al. (1963). In order to quantitatively estimate the contribution by electronic current many workers have introduced an additional grid between the probe and the ambient plasma; this enables one to measure ion current separately which can be subtracted to arrive at the electron energy distribution.

The Langmuir probe system, a modified version of which the author has used, was originally conceived of by L.G. Smith of Geophysical Corporation of America who got the ingenius idea

of using the part of the nose tip itself as the sensor. A conical shaped sensor which fits in at the nose tip was used by him (Smith 1967) in earlier flights. It was observed that the probe current exhibits marked aspect dependence. Later, Smith (1969) found that if one used an ogive shaped electrode the aspect dependence is almost removed. A Langmuir probe system which was functionally similar to the one used by Smith was developed at the Physical Research Laboratory, Ahmedabad, India, by Prakash and Subbaraya (1967). This system has many advantages over the system used by Smith (1967). Different versions of Langmuir probe systems developed by Prakash and Subbaraya (1967) were used on many occasions and some of these were discussed by Gupta (1970). The author has used the above system with necessary modifications and improvements. The advantages of the present system over the Smith's system are following:

(i) Since it operates on a single battery and since the sensor is directly connected to the input of the amplifier the leakage currents are brought down to an irreducible minimum.

(ii) The guard electrode can be fed without additional electronics. The point B in fig. 3.2 follows closely the sensor potential and can be directly connected to the guard.

(iii) As in the present system internal leakages and capacitance leakages are reduced to irreducible minimum the system has many practical advantages. The frequency response of the system is limited by the frequency response of the electrometer amplifier if the sensor is directly connected to the amplifier. Since electrometer amplifier with frequency response from 0 to 10 KHz can be made the system can be used to study audio frequency fluctuations in the ambient ionized medium.

In this system probe electronics can be located anywhere within the nosecone of the rocket and a cable used to connect the sensor to the amplifier. When the sensor is connected through a cable the effective distributed capacity in the cable is reduced to c/g where c is cable capacity and g is the gain of the amplifier.

(iv) As thorough testing of the probe electronics is required just before the launch all the test points are brought out of the rocket through a main connector called umbilical connector. Any lead connected to the sensor cannot be brought to the connector since it will not only produce leakage but also act as an additional sensor during the flight and affect the sensor current in a complicated manner. Therefore in any ordinary Langmuir probe system no test point is brought out from the sweep generator and it is not possible to ensure a completely satisfactory performance of the electronics before launching. In the present system the reference

point which follows the sensor potential can be brought out and hence the performance of the sweep electronics can be checked prior to launching.

3.1.3 Region of the Applicability of Rocket Borne Langmuir Probe

As far as the measurements of absolute value of electron density and temperature are concerned the Langmuir probe can be used safely between 85 to 1000 km. The lower limit of 85 km is set because below 85 km the electron mean free path is much smaller as compared to the Debye shielding distance and also because below 85 km negative ions are present in significant number with their densities comparable to that of electrons (Sagalyn and Smiddy, 1964). The upper limit of 1000 km is due to photoelectric effect. Due to unattenuated solar radiation the photoelectric yield of a metal such as tungsten is about 4 nA/cm^2 (Hinteregger et al. 1959 and Bourdeau et al. 1961). So long as this photoelectric current remains as a perturbation over the electronic current drawn from the plasma the probe can be used safely. In the ionosphere at about 1000 km the electron random current density equals the photoelectric current due unattenuated solar radiation. Hence for the absolute measurements the probe should be use d between 85 and 1000 km.

3.1.4 Sensor of the Langmuir Probe

Langmuir probe sensors of many different shapes such as planar, spherical cylindrical etc. have been used by various workers. But the most suitable shape for rocket borne probe, as suggested by Smith (1967), is an ogive shape. In this particular shape the vehicle aspect effects are removed to a very large extent. This is due to the fact that an ogive shaped sensor offers same area of cross-section if viewed from any direction and hence the collection does not depend on the aspect of the vehicle.

For the present studies we have adopted the use of ogive shape sensor. The sensor shown in fig. 3.1 is made of stainless steel. The material of the probe was so chosen that it can stand the heating caused due to aerodynamic effects. The guard is made of stainless steel of about 1/8" thickness. The job of the guard is to electrically insulate the stainless steel electrodes from the rest of the system. The use of guard electrode renders the electric field near the sensor normal to its surface, eliminates end effects and enhances the value of the insulator. However, in the present case the guard electrode was used to avoid large depletion of plasma and hence the guard does not serve its purpose completely. Two insulators are provided, one between the guard and the sensor and the other between the guard and the rocket body. The latter piece of insulator is having threads so that it can be fitted to the

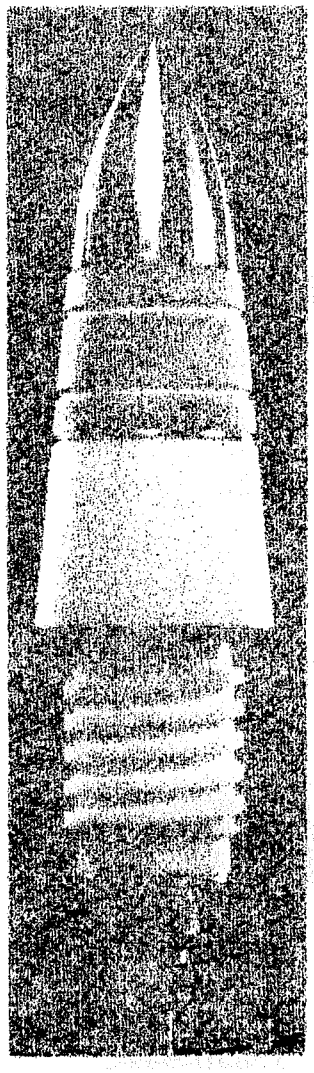

Fig.3.1: The Langmuir probe sensor.

nose cone of the rocket. The construction is easy because both the stainless steel and the teflon can be machined earily.

3.1.5 Reference Electrode

In rocket borne Langmuir probe a potential is applied between two electrodes which are moving in the ambient plasma. Theoretical treatment of such a system is given by Johnson and Malter (1950). When two identical probes are used it becomes necessary to monitor their potentials. But usually a small electrode is used as a sensor and a much larger electrode is used as a reference electrode. Since the area of the reference electrode is much larger than the area of the sensor the potential of the reference electrode can be assumed to remain constant as sensor voltage is varied. In order that the potential of the reference electrode does not vary it should have very large area, because if the probe is collecting charges of one sign the reference electrode should be able to collect equal number of charges of opposite sign. Thus when probe is collecting positive ions the above condition is easily satisfied. But when the probe collects electrons the reference electrode can collect equal number of positive ions only when its area is larger than the ratio of velocity of electrons to that of positive ions. The ratio is about 170 in most of the regions of interest in the ionosphere and Smith (1967) has shown that in such a medium the Langmuir probe system can be treated as a single probe system. If one uses a two stage

rocket like Nike Apache the area which would be available for the reference electrode would be on an average, about 3×10^4 cm^2. Hence the surface area of the probe should not exceed 10-15 cm^2.

3.1.6 Floating Potential

If an electrode is exposed to plasma it acquires an equilibrium potential known as 'floating potential', V_f. At this potential the total probe current due to electron and positive ion fluxes is zero. For an electrode at rest this potential is given by

$$V_f = - (k\,Te/e)\ \log_e (j_o/j_+)$$

where j_+ is the random positive ion current density. For typical ionospheric parameters the floating potential is expected to vary between -0.2 and -1.0 volt. But when the electrode is on board the rocket there are many spurious effects such as rocket motion, solar radiation, presence of fields on moving rocket, the earth's magnetic field and contact potential difference due to dissimilar work functions of different parts of the vehicle. Due to these effects the vehicle potential is different from true floating potential. Sebru (1963) and Smith (1964) found that the probe current becomes zero only when the probe voltage is positive. Vehicle potentials of more than +1 volt with respect to plasma potential were explained by Smith (1964) by taking into consideration both

resonance rectification by antenna voltages and contact potentials. Contact potentials were thought to be responsible for the observed effects. Results from Langmuir probe flights from Thumba also show similar results and have been discussed in detail by Subbaraya (1968).

3.2 Proportionality Between the Probe Current and Electron Density

For a Langmuir probe operating in accelerating regime, it has been shown by Smith (1967, 1969) that, the profile of the probe current is substantially independent of electron temperature variations and represents over a wide range of altitudes the electron density profile in the medium. This allows one to use a conversion factor to get the electron density. The factor remains constant over an extended altitude range and can be evaluated by comparisons with ionosondes (Smith, 1969). In case the Langmuir probe is flown with propagation type of experiments or R.F. Resonance probe, the conversion factor can be evaluated by comparison with the densities obtained by these experiments.

The use of Langmuir probe in the D-region for the measurement of absolute densities is not very sound on theoretical grounds because electrons as well as ions have very small mean free paths in this region. It has been shown by Sonin (1967) that in such a situation the probe current would depend

not only on the electron density but also on the mobility of charged particles. But it was pointed out by Smith (1969) that the treatment of Sonin (1967) is in contrast to the experimental observations which suggest that even in the D-region the proportionality between the probe current and the electron density is maintained (Mechtly et al. 1967).

The proportionality between the probe current and the electron density varies with altitude because of temperature variation. For a spherical electrode operating in highly accelerated regime the dependence of probe current goes as $T^{-\frac{1}{2}}$ (Smith, 1969). For a case of cylindrical electrode it has been shown by Spencer et al. (1962) that in the accelerating region the probe current is directly proportional to electron density and is independent of electron temperature.

Based on the experimental observations it can be inferred that the proportionality factor remains fairly constant above D-region altitudes ($>$ 85 km) upto about 180 km or so. In D-region also the factor can be assumed to be constant but it should be noted that this region should be exploited more for the study of ionization irregularities and the absolute value of the electron density should not be taken very seriously.

For the present study the probe current on many occasions was calibrated with the help of onboard RF resonance

probe and on the other occasions with the ground based ionosondes. On the basis of some 1½ dozen flights it was found that on the average 1 μA of current corresponds to 7.15×10^3 electrons/cm^3. We have adopted the above conversion factor for all the rocket flights.

3.3 Irregularity Measurements with Langmuir Probe

In a conventional Langmuir probe where a sweep voltage is applied to the probing electrode one gets only one value of electron density and one value of electron temperature. An alternate method was proposed by Smith (1964) wherein the sweep voltage stays for one to two seconds when it reaches an accelerating potential of +2.7 volts or more. In such a situation the probe current during the constant potential period would be directly proportional to the electron density provided the electron temperature does not charge during this period. Since the current during saturation period is proportional to velocity of electrons a $T^{-\frac{1}{2}}$ dependence of the current would be existing. In the ionosphere except for a small fraction of high energy electrons rest are in thermal equilibrium with each other. The rocket studies at Thumba have shown that the Langmuir probe is well suited for the study of ionospheric irregularities.

The spatial resolution of rocket borne Langmuir probe depends on two parameter (a) the rocket velocity and

(b) bandwidth of the system. If one assumes a vehicle velocity of 1 km/sec and a system bandwidth (including telemetry also) of 1 kHz the probe can be used to study irregularities of 1 meter scale size.

3.4 Instrumentation

Fig. 3.2 illustrates the basic principle of current measurement using a Langmuir probe and the waveform of the sweep voltage which is applied to the sensor with respect to the rocket body. As shown in the figure the electrometer amplifier is connected directly to the sensor by means of a cable. Since the potential difference between points A and B is much less than 10 millivolts it can be assumed that the sensor potential varies in accordance with the output of the sweep generator. The guard electrode is also fed the same voltage which goes to the terminal B of the electrometer amplifier. The guard electrode ensures that the leakage between the sensor and the rocket body is greatly reduced.

Some of the basic blocks of the Langmuir probe and the actual sweep waveform which was applied on many occasions are shown in fig. 3.3. For the first 0.5 seconds the sensor stays at -2 volts and then rises sharply upto a certain level beyond which the the rise is much slower. The level beyond which the sweep is slow is decided by the output of the electrometer amplifier and would be elaborated during the

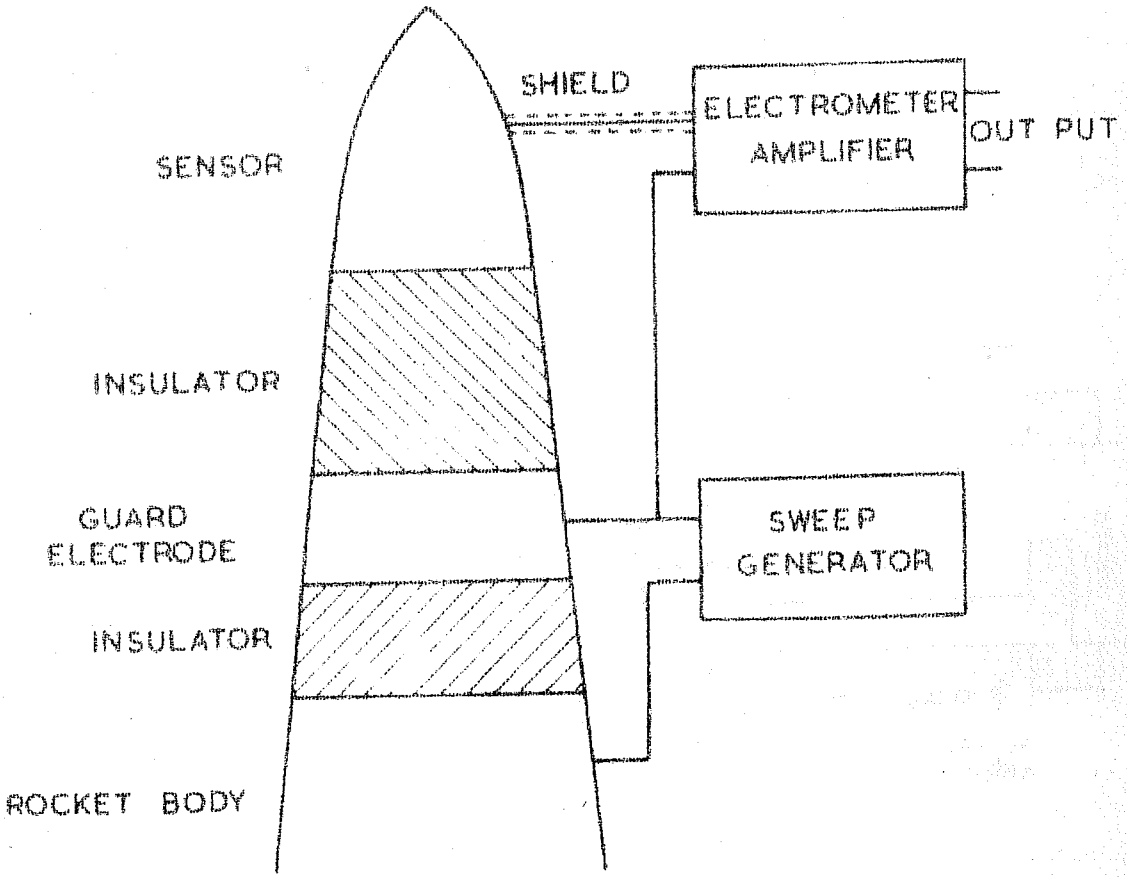

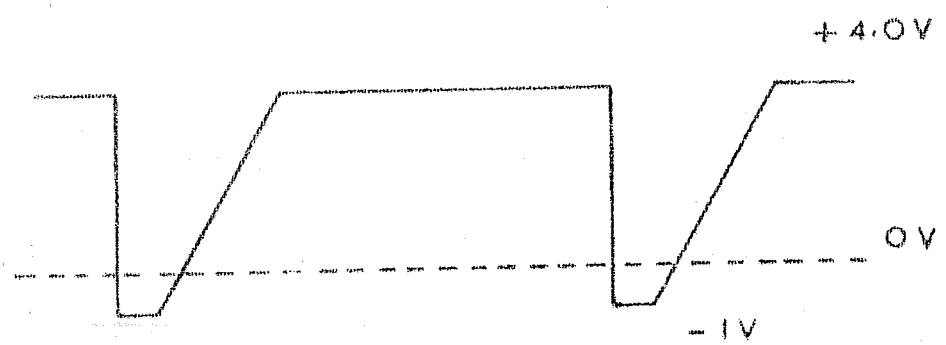

SWEEP WAVEFORM

Fig. 3.2 Schematic of the Langmuir probe system (a) illustrates the principle of the system and (b) shows the program of the sweep voltage.

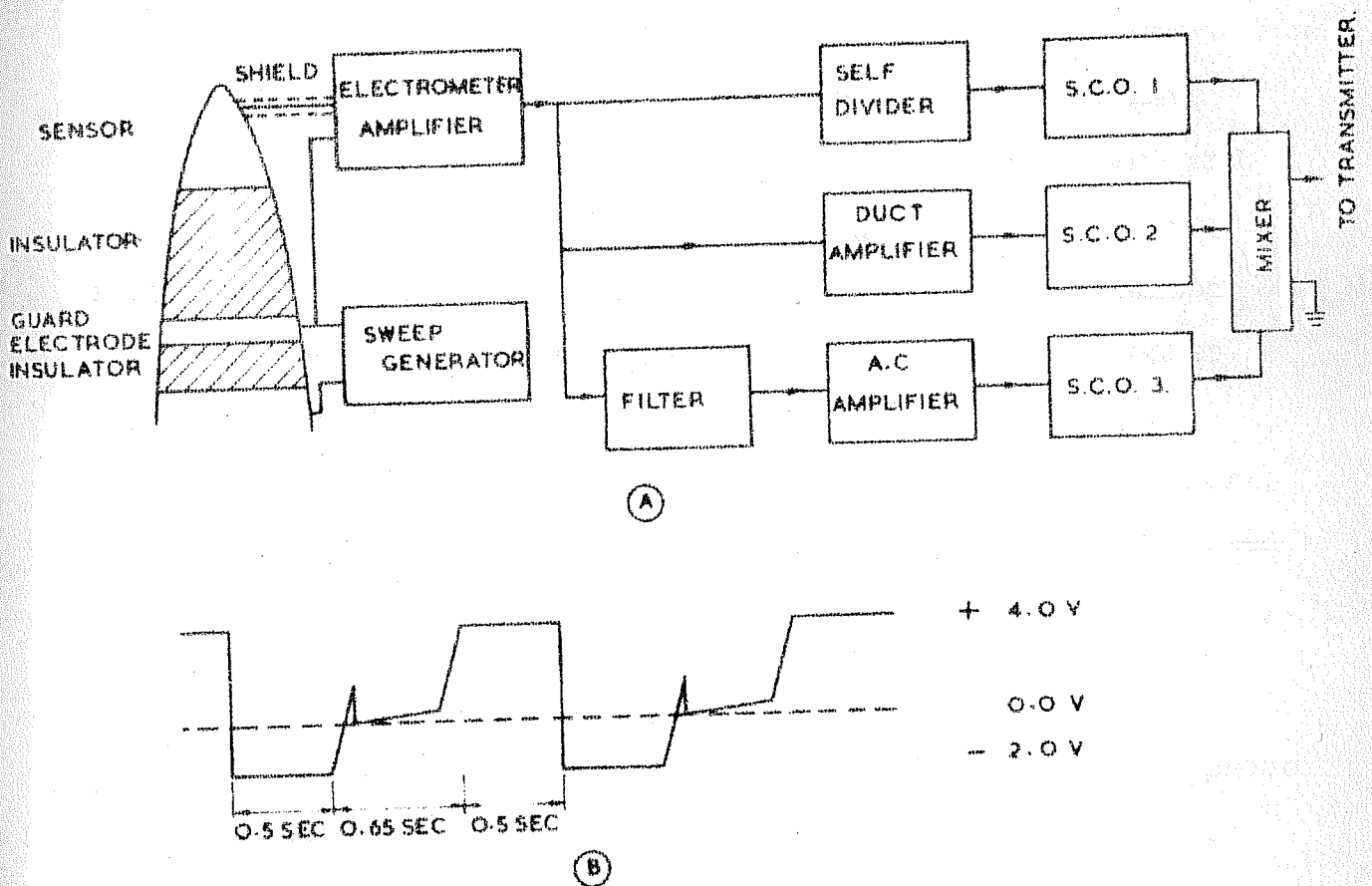

Fig. 3.3 Schematic of the Langmuir probe system **A** illustrates the principle of the system and **B** shows the programme of the sweep voltage.

description of sweep circuit. The incorporation of slow and fast sweep helps in determination of electron temperature. After the sweep portion is over the voltage stays at +4 volts for 0.5 sec.

There are two Langmuir probe systems which we have used. The first one is termed as 'Ground Supply System' and the other as 'Floating Supply System'. In the grounded supply system the sensor can be held only at a fixed predetermined potential (+4 volts in our case) with respect to the rocket body. In the floating system the sensor potential can be varied in accordance with the programme of the sweep waveform. It may, however, be mentioned again that in our system we need to generate an inverted sweep waveform (Prakash and Subbaraya, 1967).

Fig. 3.4 shows the block diagrams of the Langmuir probe with grounded supply. As shown in the fig. the regulator is fed +28 volts and -15 volts with respect to the rocket ground. The regulator generates three voltages +18 M, OM and -9M; it is important to remember that sensor operates nearly at OM. The difference in OM and OV (which is rocket ground) is 4 volts. All the blocks except the regulator operates on +18M, OM and -9M, i.e. +22 V, +4 V and -5 V. Electrometer amplifier converts the input current into analog voltage. This voltage is processed for low frequency component (through duct amplifier) and high frequency component (through 70-1000 Hz Noise amplifier).

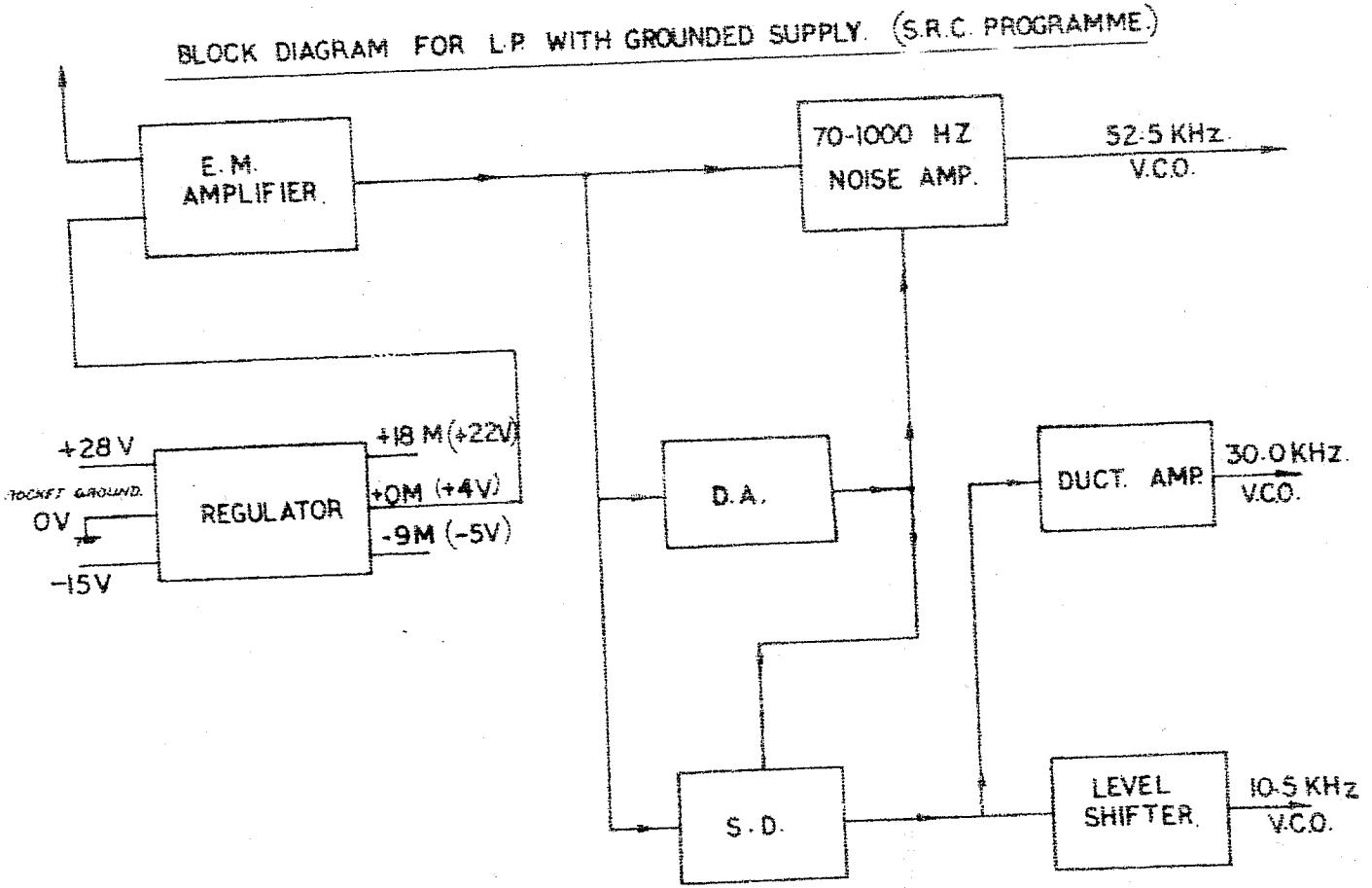

Fig. 3.4 Block diagram of Langmuir probe system using grounded supply

D.A. is a difference amplifier which gives a pulse when the output of the electrometer exceeds 10.5 volts. S.D. is the self divider which divides the signal by a factor of 4.5 when the E.M. amplifier output exceeds 10.5 volts by getting a trigger from D.A. The gain of the Noise amplifier is switched to a lower value so long as the D.A. pulse is present. The noise amplifier does the additional job of level shifting to make its output compatible with the V.C.O. input. The self divided signal which is within the limits of V.C.O. requirements except for its d.c. level, is given to the duct amplifier. The duct amplifier maintains its output d.c. level compatible with V.C.O. input. The self divided signal is also given to V.C.O. through a level shifter; this output is referred to as main channel output.

Fig. 3.5 shows the block diagram of Langmuir probe system with floating supply. The regulator works on unregulated 32 and converts it into three desired regulated voltage viz. +18 M, OM, and -9 M for the entire circuitry. The sweep circuit generates a voltage sweep mirror image of which is shown in fig. 3.3. The output of sweep generator is connected to rocket body. In this case the sensor stays at voltage OM + V volts ($V \lesssim 10$ mV) and, therefore, with respect to rocket body the sensor sees a voltage sweep as shown in fig. 3.3.

When the sensor stays at -2 volts with respect to rocket body only ions can be collected by the sensor, and as the

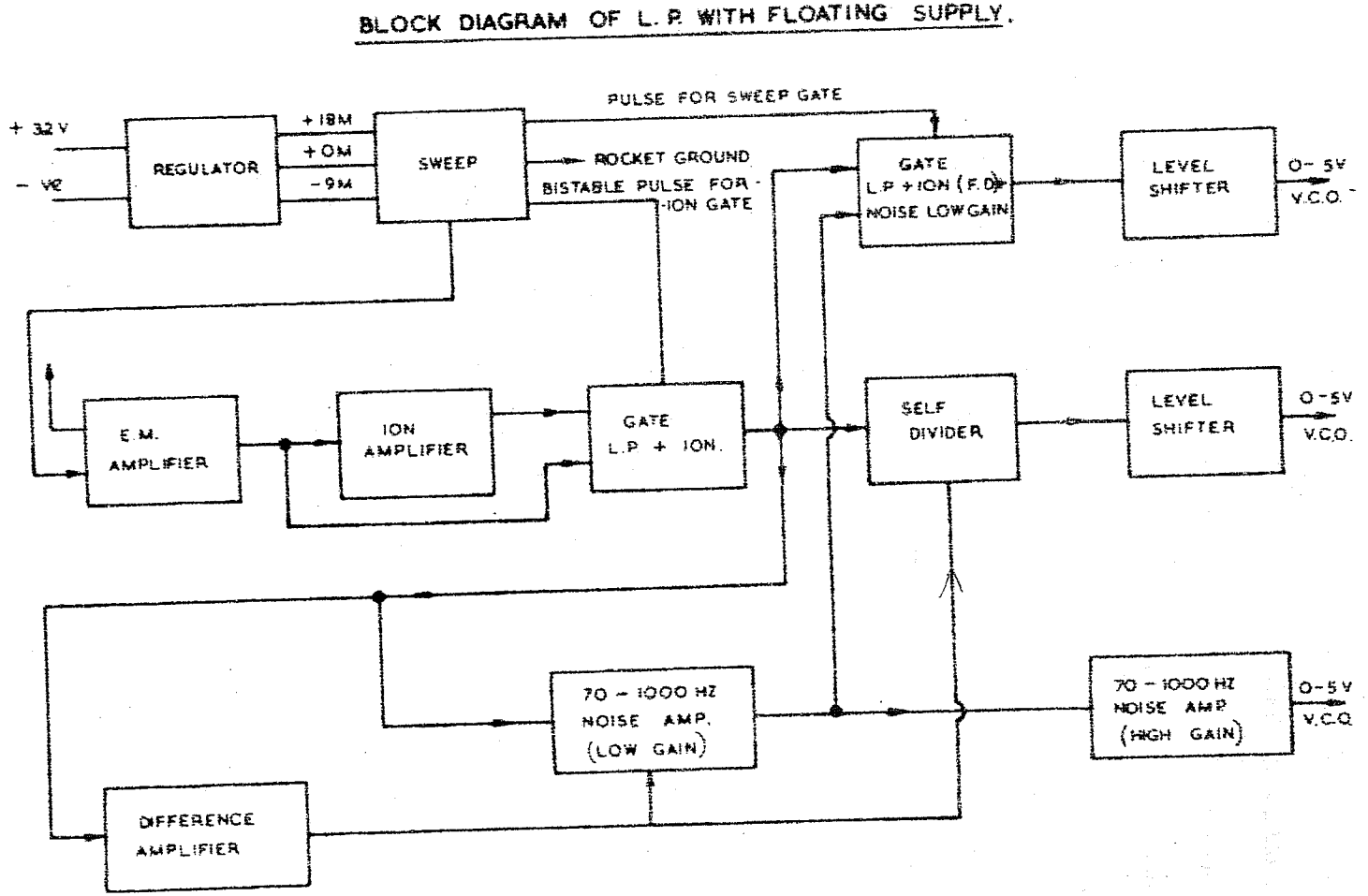

Fig. 3.5 Block diagram of Langmuir probe system using floating supply

ion current is less than the electron current a additional gain of 3 is provided in the ion amplifier. The ion amplifier changes the phase of the signal also so that positive voltages are available both for electrons and ions. The outputs of the ion and the electrometer amplifier are gated together and the gated signal is given to the self divider (which is functionally similar to what was stated earlier) and then to the V.C.O. through a level shifter. In the level shifter sweep is subtracted so that the resulting signal can be used with respect to rocket ground. The L.P. + ION signal is given to 70-1000 Hz noise amplifier which is having low as well as gain stages. The output of the low gain stage is gated with the fixed divided L.P. + ION signal and the gated output is fed to the V.C.O. through a level shifter. The difference amplifier gives a pulse whenever L.P. + ION output exceeds a certain voltage and thereby changes the gain of low gain noise amplifier by a fixed ratio. The high gain noise amplifier amplifies the output of low gain stage and also does the additional job of level shifting to make its output compatible with the V.C.O. input. Both the gates which are shown in the figure work on the pulses which are derived from sweep circuit.

3.4.1 Power Supply Regulators

The two different types of power supply regulators which we have used are shown in fig. 3.6. The system with grounded supply is used when the L.P. sensor is kept at a fixed

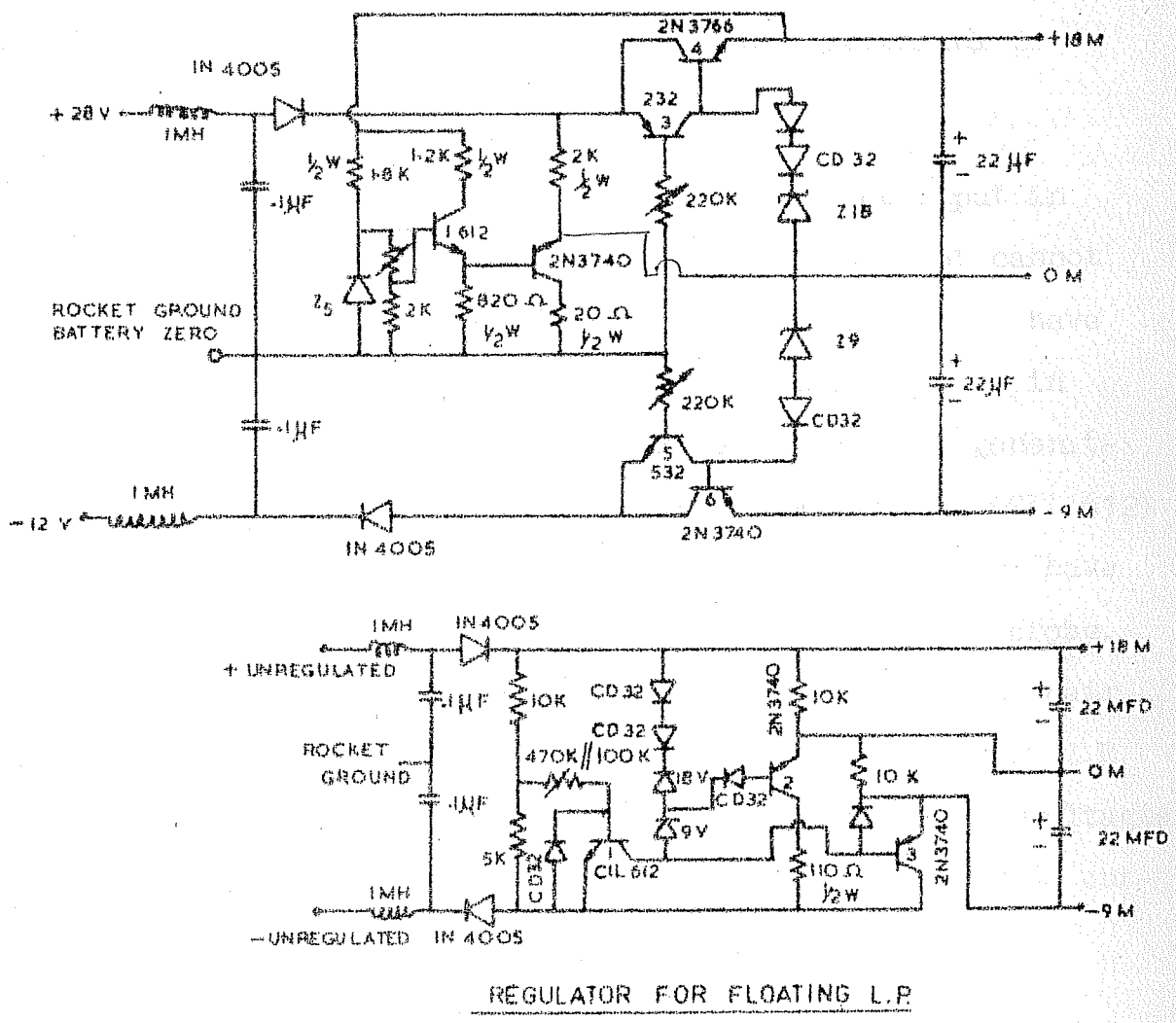

Fig. 3.6 Circuit diagram of power supply regulators used in grounded and floating systems

potential with respect to the rocket body whereas the system with floating supply is used when the sensor potential is swept.

In the grounded system two diodes have been put in series with the +ve and -ve lines so that the current cannot flow in the reverse direction. Two separate regulators have been used for +18 and -9 M supplies. Two zener diodes in series with forward biased diodes have been used for generating reference voltages. Zener diode Z5, transister 1 (CIL 612) and 2N3740 in conjunction with the appropriate resistors have been used to generate the +4 volt bias voltage for the probe. This voltage is taken out from the emitter of 2N3740. A pair of L section filters comprising of 1 mH inductors and 0.1 μ F capacitors have been used to filter the incoming supply voltages. Tantalum capacitors of 22 μ F (30 V) have been used at the output of both the supply lines.

The second regulator used for the floating L.P. also uses series regulator. But this supply is run from a floating battery. Both the incoming powerlines are bypassed to the rocket ground using 1 mH series inductors and 0.1 μ F capacitors. Since + 18 M and -9 M supplies are required for running the payload electronics the division is achieved by transistor 2N3740 (TR2), 18V Zener diode and two forward bias diodes.

3.4.2 Electrometer Amplifier

For the measurement of low currents, a current to voltage converter incorporating a high gain d.c. amplifier is used. Fig. 3.7 shows the schematic of the electrometer amplifier, with a 100% negative feedback, used to convert the input current to a voltage output suitable for further processing of the data. If gain of the operational amplifier is A, feedback resistance is R_f, I is the input current, Z_i is the input impedance of the amplifier and $\triangle I$ is the bias current which is much smaller than I, the output voltage E_o can be evaluated by following simple equations.

$$V_i = E_o + (I - \triangle I)\ R_f$$

where V_i and E_o are given by

$$V_i = Z_i\ \triangle I \qquad \text{and} \qquad E_o = -A\ Z_i\ \triangle I$$

$$Z_i\ \triangle I = -A\ Z_i \triangle I + (I - \triangle I)\ R_f$$

$$\text{or} \quad I\ R_f = (\ Z_i + A\ Z_i + R_f\ )\ \triangle I$$

$$= \triangle I\ Z_i\ (\ 1 + A + R_f / Z_i\ )$$

$$= -E_o\ (\ 1 + 1/A + R_f / A\ Z_i\ )$$

For a typical circuit comprising of a high gain operational amplifier ($A = 10^5$) the above equation reduces to

$$E_o \simeq -I\ R_f \quad \text{or} \quad I \simeq -E_o / R_f$$

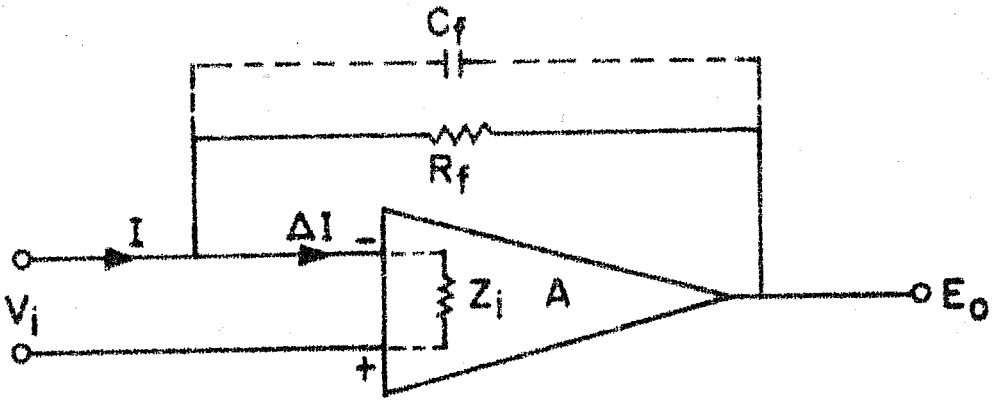

Fig. 3.7: Schematic of electrometer amplifier

This shows that output voltage is independent of amplifier characteristics and depends only on the input current and the feedback resistance. According to Miller's theorem the input impedance of an amplifier is given by R_f/A. If $R_f = 10^8$ Ohms and $A = 10^5$ the input impedance is of the order of kilo Ohms which is much less than Z_i.

Fig. 3.8 shows the block diagrams of the electrometer amplifier (or the L.P. amplifier) along with the switching scheme. A is the main amplifier which converts the input current into an analog voltage. To increase the dynamic range of the current amplifier, three feedback resistances are used which are switched one after another depending upon the input current. An electrometer tube Raytheon CK587 or 5886 which has a maximum leakage current of 10^{-13} amp is provided at the input stage of the amplifier. RF_1, RF_2 and RF_3 are feedback resistances and R_1, R_2 and R_3 are three relays. To start with RF_1 is connected and all the relays are off. As the input current increases the amplifier output increases and as soon as it exceeds 10.5 volts the difference amplifier gives a positive which triggers the flip flop No.1. The positive pulse from flip flop No.1 is applied to relay R1 which now becomes ON and RF_2 gets connected in parallel with RF_1. Thus the amplifier output drops down. If the input current exceeds further such that output voltage is again more than 10.5 volts the difference amplifier gives a pulse and at that instant both inputs to the AND gate (i.e. output of 1st FF and the delayed

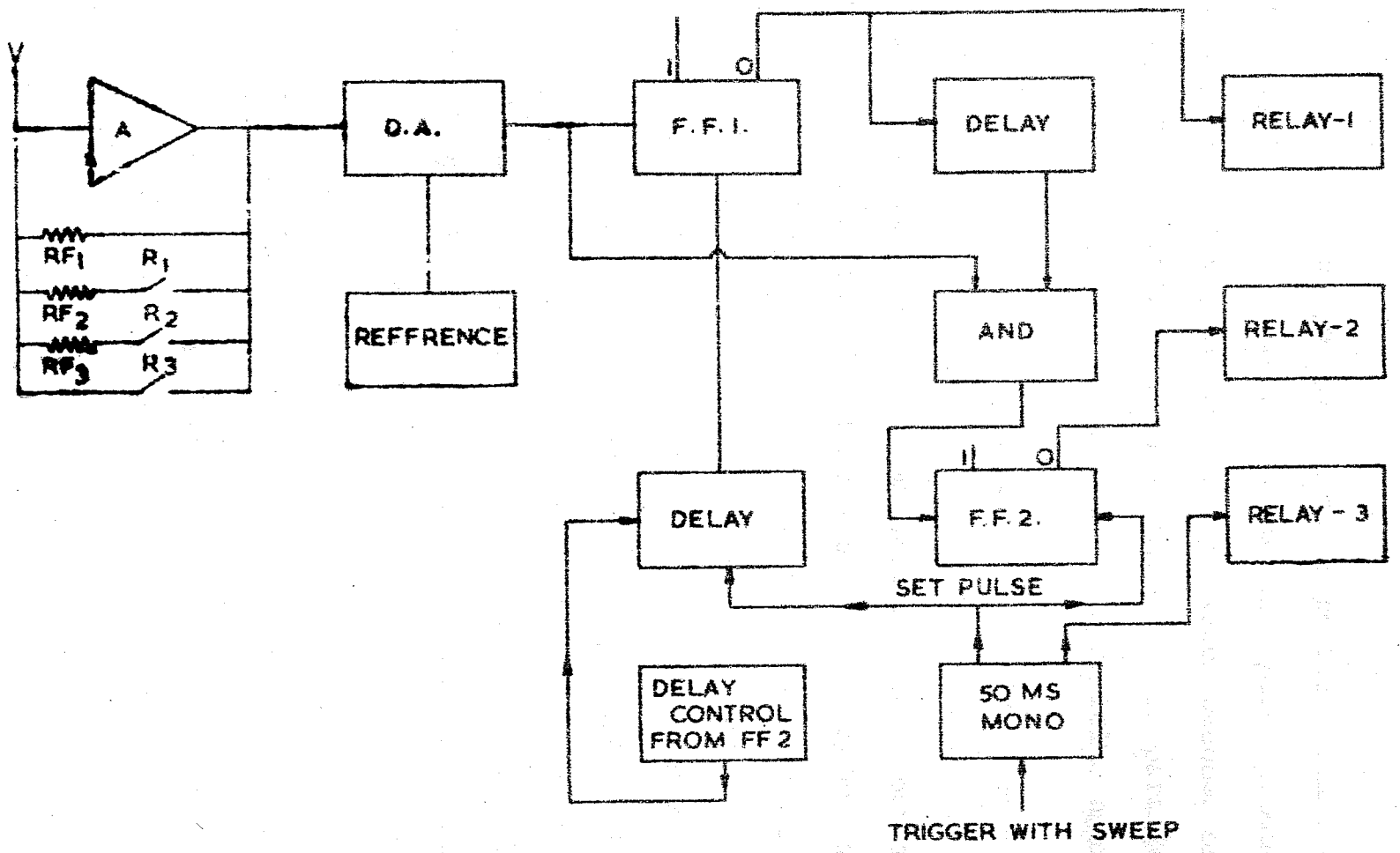

Fig. 3.8 Schematic of electrometer amplifier and the associated switching network.

signal) are present and the gate gives a positive pulse which triggers flip flop No. 2 also. The positive pulse produced by this flip flop is applied to relay R_2 which becomes on and consequently resistance RF_3 gets connected in parallel with RF_1 and RF_2 and thus the amplifier output falls again.

At the end of every sweep cycle 50 ms mono pulse is given to relay R_3 which shorts the input for 50 ms. Thus at the end of every sweep cycle a 50 ms zero marker is obtained. Depending on whether both FF1 and FF2 are off, only FF1 is on or both FF1 and FF2 are on, the pulse width of mono is varied to 50, 75 and 100 ms respectively. Thus at the end of every sweep cycle a zero marker of any of three lengths would be observed; the length of zero marker on the telemetry chart serves to identify which feedback resistance is connected. Also the 50 millisecond mono is used to reset the flip flop 2 if both flip flops are on and flip flop 1 if only flip flop 1 is on. This means in one cycle only one gain is reset; this scheme was conceived of because in the ionosphere the density is not to change drastically in very short times.

Fig. 3.9 shows the circuit diagram of the switching network. The electrometer amplifier output is fed to a difference amplifier (TR2) through an emitter follower (TR1). If the electrometer amplifier output exceeds 10.5 volts the collector of TR2 gives a positive pulse which triggers the flip flop 1 (TR4 and TR5). The output of flip flop 1 is given to

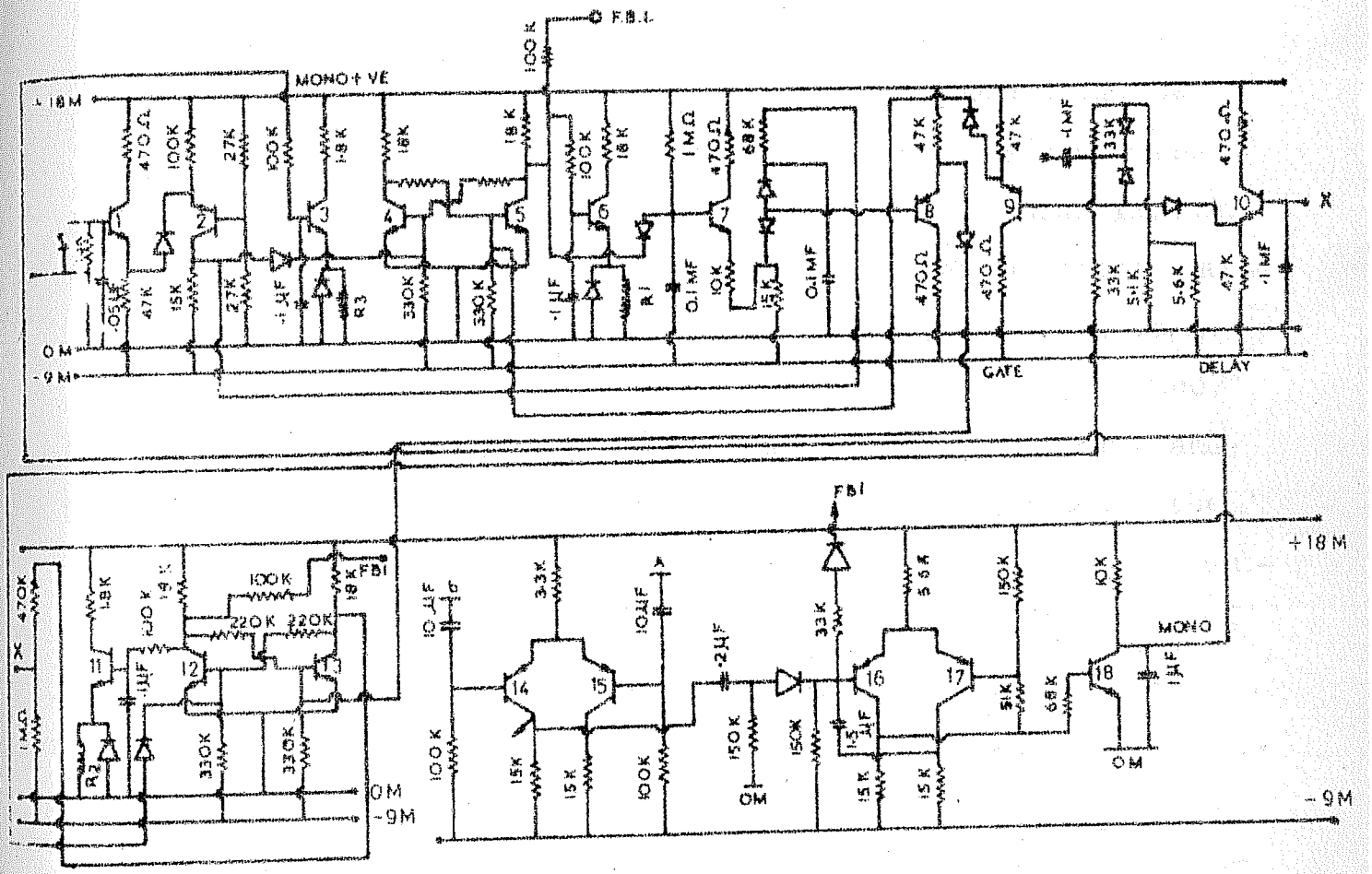

Fig. 3.9 Circuit diagram of the switching network

a relay R_1 through a driving circuitry (TR6). When the relay operates the feedback resistance R_{F2} gets connected parallel with R_{F1}. As soon as R_{F2} is connected the output of electrometer amplifier drops down. If the input current increases further such that the electrometer amplifier output exceeds 10.5 volts the difference amplifier (TR2) gives a positive pulse. This pulse and the delayed output of the first flip flop are gated together. 1 MΩ resistance and 0.1 μF capacitors provided at the base of TR7 produce the necessary delay. Since both the signals are present the output of the gate is also positive which triggers the flip flop 2 (TR12 and TR13). The output of flip flop 2 is given to another relay R_2 through similar driving circuitry (TR11). When the relay R_2 operates the feedback resistance RF_3 gets connected to RF_1 and RF_2 and thus the output of the electrometer amplifier drops down further. TR14 and TR15 form a astable multivibrator of repetition time 1.6 sec. The output of astable multivibrator is differentiated and used to trigger the 50 ms monoshot which is used to set one of the multivibrators and give a zeromark at the end of 1.6 sec. This astable multivibrator is used only when a fixed voltage is applied to the sensor and no sweep is used. However when a voltage sweep is used at the end of every sweep cycle one pulse is derived from the sweep circuit and is used to trigger the monoshot (TR 16,17).

Fig. 3.10 shows electrometer amplifier, self divider and ion amplifier. In the electrometer amplifier a 9 volt zener is used at the base of transistor No.1 to provide the filament current to the tube. The operational amplifier is an integrated circuit chip SSD 741. The output of the electrometer amplifier is given to the switching circuit (Fig. 3.9) to the self divider and to the ion amplifier.

Self divider is a simple three transistor circuit. As soon as the output of electrometer amplifier exceeds 2.5 volts the difference amplifier (shown as 2 V DA on 70-1000 Hz noise diagram, Fig. 3.12) gives a pulse which shorts the transister 13 with the result that the signal fed to the base of T2 gets divided in ratio of 10 K to 2.7 K. By providing three gain switchings and a self dividing arrangement a large dynamic range of more than four orders of magnitude is obtained which is sufficient for measurement of electron densities in the region of interest in the ionosphere.

Shown in the same figure is the ion amplifier which is a single I.C. inverter with a gain of three. The output of ion amplifier is taken from terminal No.6 of the I.C. In addition, the output of the ion amplifier is given to the mono shot (TR1 & TR2) to get a pulse which is used in sweep circuit.

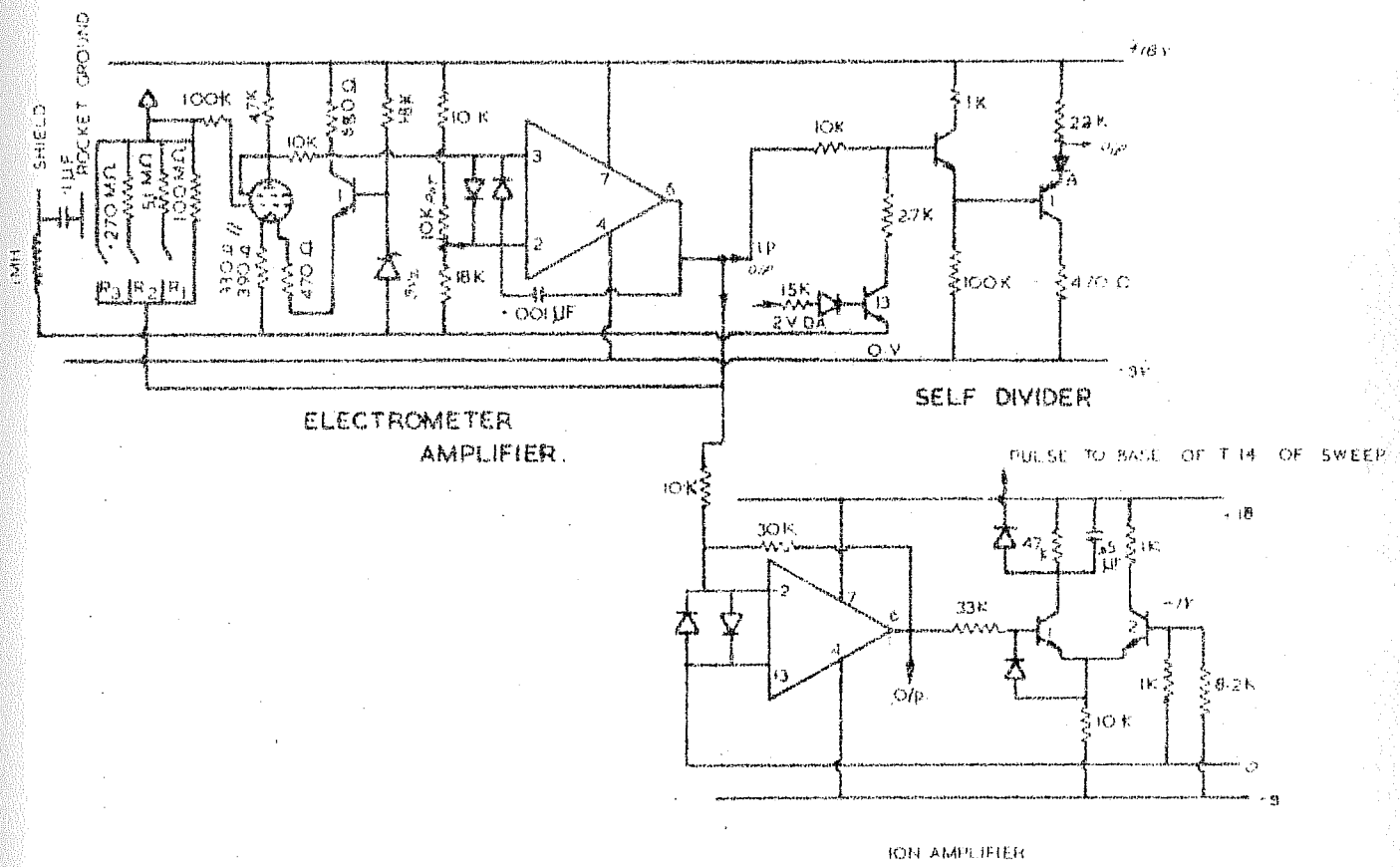

Fig. 3.10 Circuit diagram of electrometer amplifier, self divider and ion amplifier.

3.4.3 Sweep Circuit

There are a number of methods by which a linear voltage sweep can be obtained. They are such as exponential charging, constant current charging, the Miller circuit and boot strap etc. The Miller sweep circuit is used as an operational integrator as illustrated in the following diagram (unnumbered)

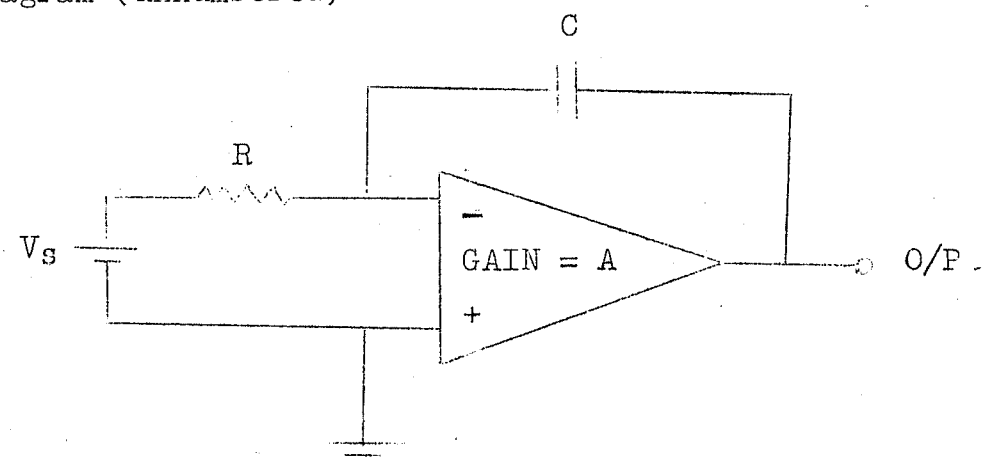

The operational amplifier shown in the diagram is having a high gain A, high input impedance and a low output impedance. The resistance R and the capacitance C form the integrating network. As the voltage at the point B increases, because of constant charging of the condenser, the output voltage of the amplifier falls with the result that a negative going sweep appears at the output. Suppose the decrement in the output voltage in time $\triangle t$ is $\triangle V$, then the increment in voltage at point B would be $\triangle V/A$ where A is the gain of the amplifier. Thus the charging current of the condenser can be equated as $C \frac{\triangle V}{\triangle t} (1 + A)$. This current would be the same as the one

flowing through the resister R because there is no current flowing into the amplifier except the bias current which is assumed to be very small due to high input impedances of the amplifier. The current through the resoster R can be equated to $(V_s - \Delta V/A) / R$. Equating both the currents one arrives at

$$C \frac{\Delta V}{\Delta t} \cdot (1 + A) = (V_s - \frac{\Delta V}{A}) / R$$

$$\frac{\Delta V}{\Delta t} = \frac{V_s}{RC} \left[1 - \left(\frac{1}{A} + \frac{V}{A.V_s} \right) \right]$$

The above equation tells that the output voltage will vary linearly with the time as long as

$$\frac{1}{A} \left(1 + \frac{V}{V_s} \right) \ll 1$$

Following experimental values have been chosen for the sweep circuit.

$$A = 100, \quad \Delta V = 4 \text{ volts} \quad \text{and} \quad V_s = 18 \text{ volts}$$

$$\therefore \frac{1}{A} \left(1 + \frac{\Delta V}{V_s} \right) \simeq 1.2 \times 10^{-2}$$

Hence the linearity of the sweep would be within 1.2%.

Fig. 3.11 shows the circuit diagram of the sweep generator. The resister and capacitor connected at the collector of TR1 form the charging network. Thus the collector of TR1

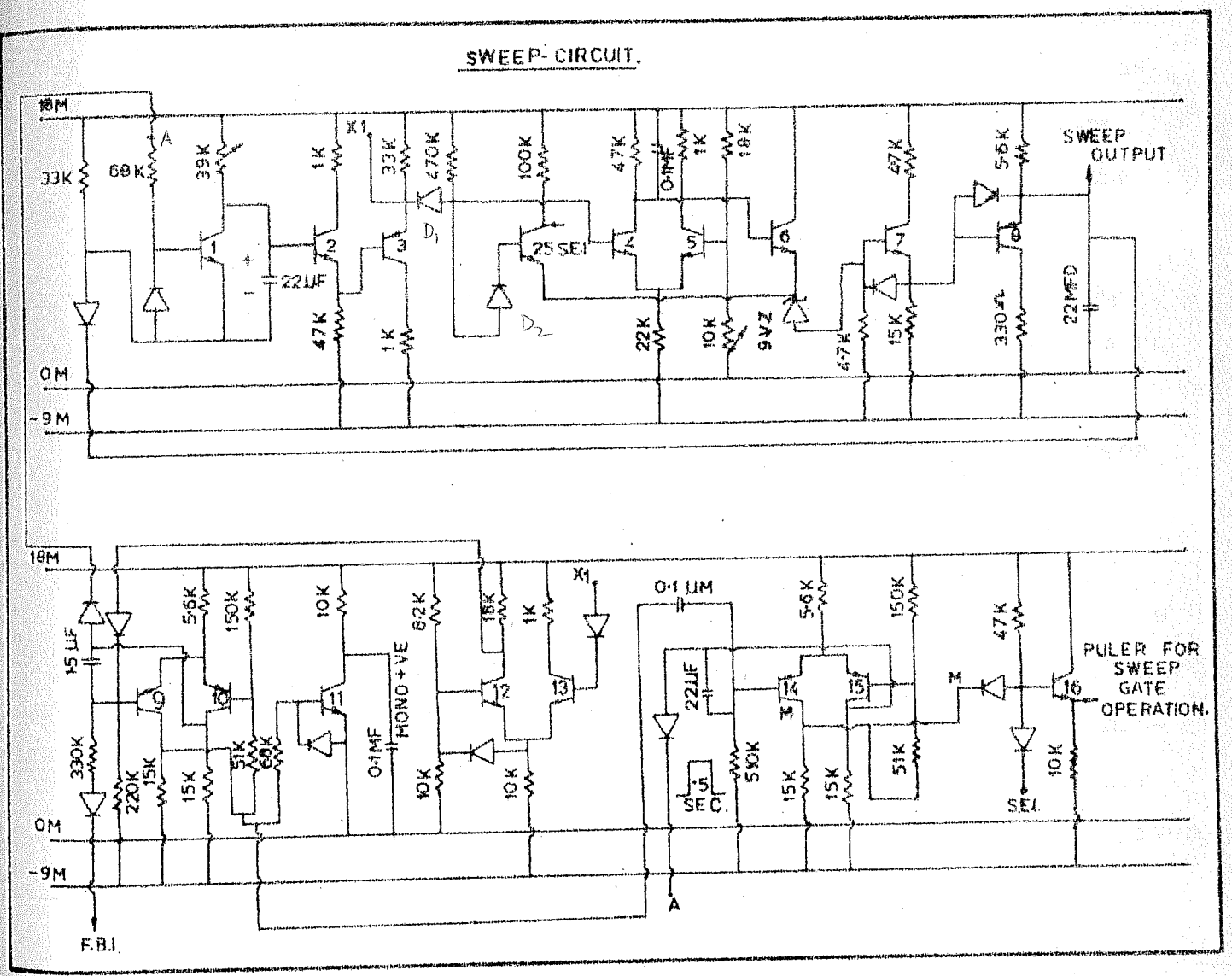

Fig. 3.11 Circuit diagram of the sweep generator

corresponds to point B of the diagram shown on the last page (unnumbered). This point is connected to the input of the amplifier (TR4 and TR5) through proper buffers (TR2, TR3 and TR25). Diodes D_1 and D_2 form the selective network. As long as the voltage at the emitter of TR3 is less than the voltage at the emitter of TR6 the diode D_1 conducts and the output voltage at emitter of TR6 falls. Since the diode D_1 is conducting the voltage at the base of TR4 is increasing. As a result, when the voltage at the base of TR4 becomes more than the voltage at the emitter of TR6 (i.e. at the base of TR25) the diode D_2 starts conducting and D_1 becomes reversed biased. Since the diode D_1 is non-conducting the output no longer follows the voltage at the emitter of TR3. Thus the output of the amplifier remains constant although the voltage at the emitter of TR3 is increasing. The increase in voltage at the emitter of TR3 is monitored at x_1 and is fed to a difference amplifier (TR12 and TR13). The difference amplifier gives a positive pulse when the voltage at x_1 exceeds the given bias of the difference amplifier. By adjusting the bias one can adjust the time for which the output remains constant at the lower voltage level. The pulse given by the difference amplifier (at Collector of T12) is given to 50 ms monoshot (TR9 and TR10). The output pulse of the 50 ms monoshot taken from the collector of TR10 is given to the base of TR1 through a 68 k resister. This pulse shorts the TR1 and hence the voltage at collecter of TR1 as well as at the point x_1 would drop

down and diode D_1 would again start conducting with the result that the output would increase. The trailing edge of the 50 ms monoshot pulse is used to trigger another monoshot of 0.5 sec. duration. The positive pulse of 0.5 sec. is available at the collector of TR15 and is given at point A. Thus the output remains fixed at higher level for 0.5 sec. Once the 0.5 sec. duration is over the voltage at point x_1 would increase and the negative going sweep would again appear at the output.

There is a provision for variation of sweep rate by connecting a resistance in parallel to 39 k (at the collector of TR1). The arrangement has not been shown in the diagram. In addition some other pulses are generated for example sweep end indicator (S.E.I.)and pulse for sweep gate operation. These pulses are used for gating purposes.

3.4.4 High Frequency Noise Amplifier

For studying the small scale irregularities the signal of the Langmuir probe is amplified in the frequency range of 70-1000 Hz with the help of an amplifier which is named as high frequency noise amplifier. Fig. 3.12 shows the circuit diagram of such an amplifier alongwith a 2.4 volt difference amplifier, and a gate with fixed divider. All the three I.C.s shown in the fig. are SSD 741.

First I.C. is used as a difference amplifier which gives a positive pulse at terminal No. 6 when the input voltage

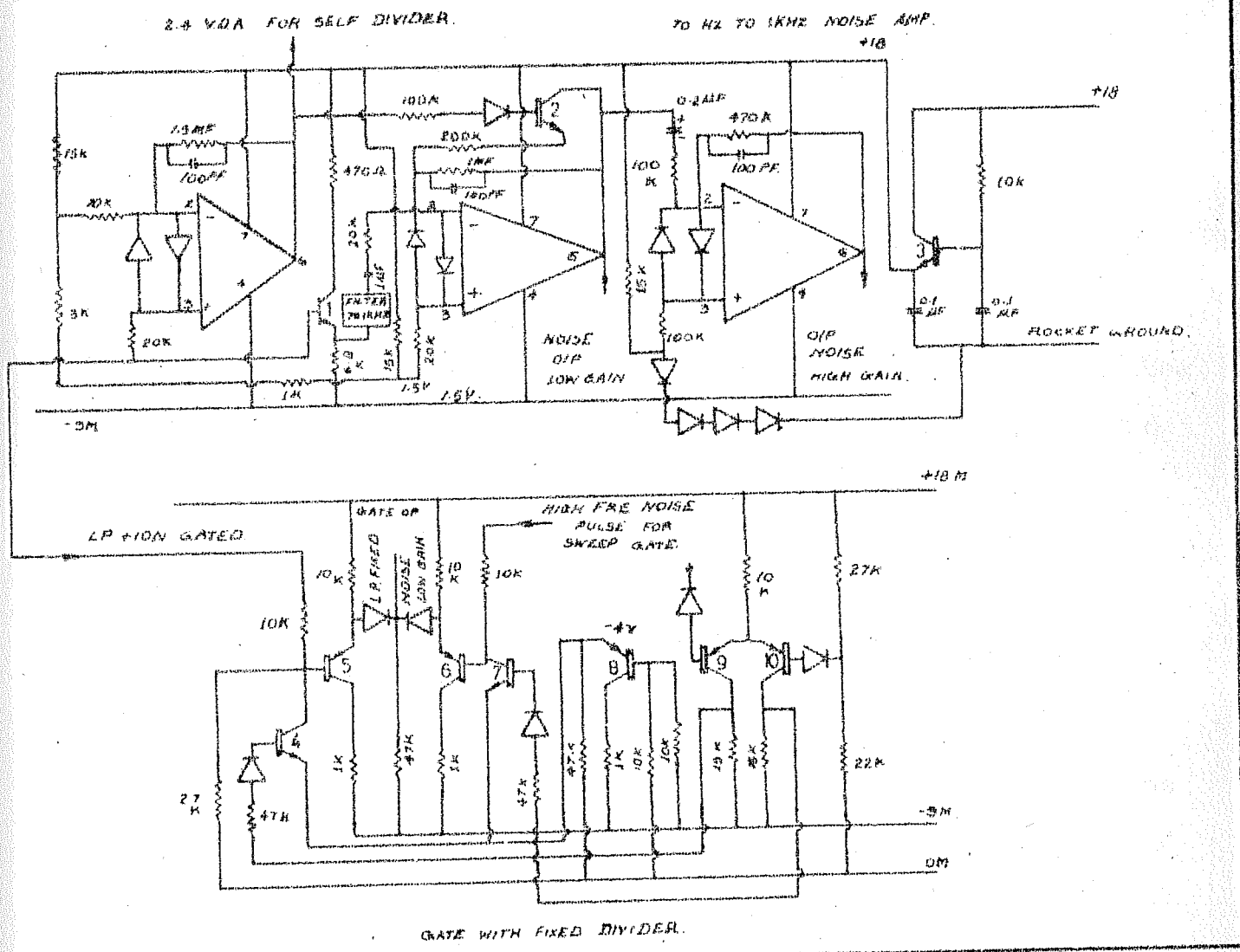

Fig. 3.12 Circuit diagrams of 70-1000 Hz noise amplifier, difference amplifier for self divider circuit and the gates with fixed divider.

exceeds 2.4 volts. This pulse is used for self dividing the Langmuir probe output and for reducing the gain of the first stage of the high frequency noise amplifier in case the Langmuir probe output exceeds 2.4 volts.

The Langmuir probe output is fed at the base of TR1 which acts as a buffer. At the emitter of TR1 a 70-1000 Hz passive filter is connected. The filter output is connected to a two stage a.c. amplifier. As shown in the figure the low and high gain signal can be taken from terminal Nos. 6 of the second and third I.C.s respectively.

The circuit shown in the lower part of the figure is a simple gate with a provision for fixed division. The signal of L.P. and Ion is gated with the low gain high frequency signal. This is a sort of redundency in the system and is very useful in case the high gain signal gets saturated. The pulse which is required to open and close the gate is derived from TR16 emitter of the sweep circuit (fig. 3.11) and is fed through a 10 K resister at the base of TR6 (fig. 3.12).

3.4.5 Duct Amplifier

A duct amplifier was developed to study the low frequency component of the Langmuir probe output specially when the amplitude of irregularities is fairly weakly and cannot be studied through main channel data. The need to develop such an amplifier arose because the amplitude of fluctuations

is very small compared to the change in d.c. level of the signal because of large dynamic range of electron density in the regions of interest in the ionosphere. In the duct amplifier the d.c. level of the output stays at a prefixed value whereas the a.c. level of the output varies in accordance with the fluctuations in the input (whose d.c. level is slowly rising to very large values). The amplifier amplifies the signals in a duct and hence named as a duct amplifier. Thus the use of such an amplifier enables one to see even the weak fluctuations on the telemetry chart.

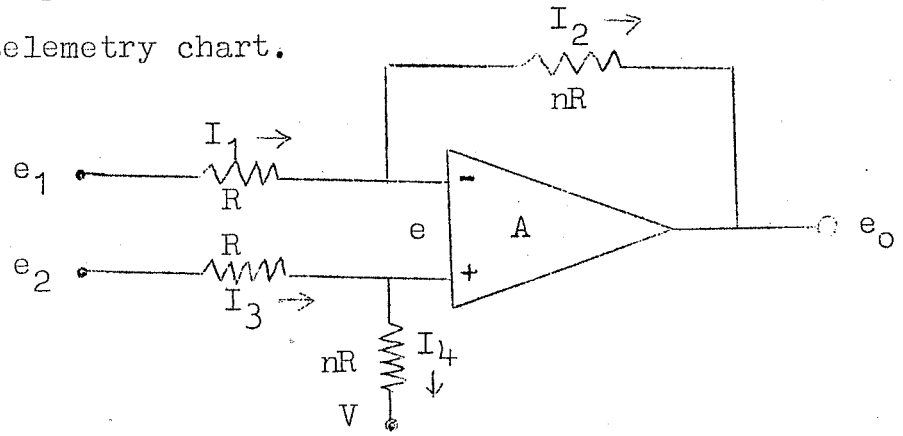

The above circuit is shown to illustrate the d.c. conditions of the duct amplifier. A is an operation amplifier with high input impedance. In a d.c. analysis, following relation would hold good.

$$I_1 \simeq I_2 \qquad \text{and} \qquad I_3 \simeq I_4$$

The slight inequality appears in the equations because of the fact that even though the amplifier A is a high input impedance device it does draw a small current for its operation. Neglecting the small current drawn by the amplifier the currents

can be balanced in terms of voltages appearing at different points.

$$(e_1 - e)/R = (e - e_o)/nR$$

and

$$(e_2 - e)/R = (e-V)/nR$$

From these equations if one eliminates e, the following expression would be obtained.

$$e_1 n + e_o = e_2 n + V$$

But when $e_1 = e_2$ i.e., the same signal is fed, it turns out that $e_o = V$. This shows that the output d.c. level remains constant at V and is independent of input d.c. level.

Fig. 3.13 shows the circuit diagram of the duct amplifier. The self divided L.P. signal is given to the amplifier through a buffer (TR1). The time constant of the circuit is decided by a resistance (22 K across which a FET is connected) and a capacitor (22μF). The time constant in the present case is 0.48 sec. enabling one to go at frequencies beyond 2 Hz or so. Terminals 2 and 3 are almost at same potential, the difference being much less than 10 mV. Terminal No.3 is connected to a fixed 2.5 volts through a 510 K resister. Reference voltage of 2.5 volts is generated by adding four diodes in series. The a.c. gain of the amplifier is nearly 5. During the rising portion of the voltage sweep which is

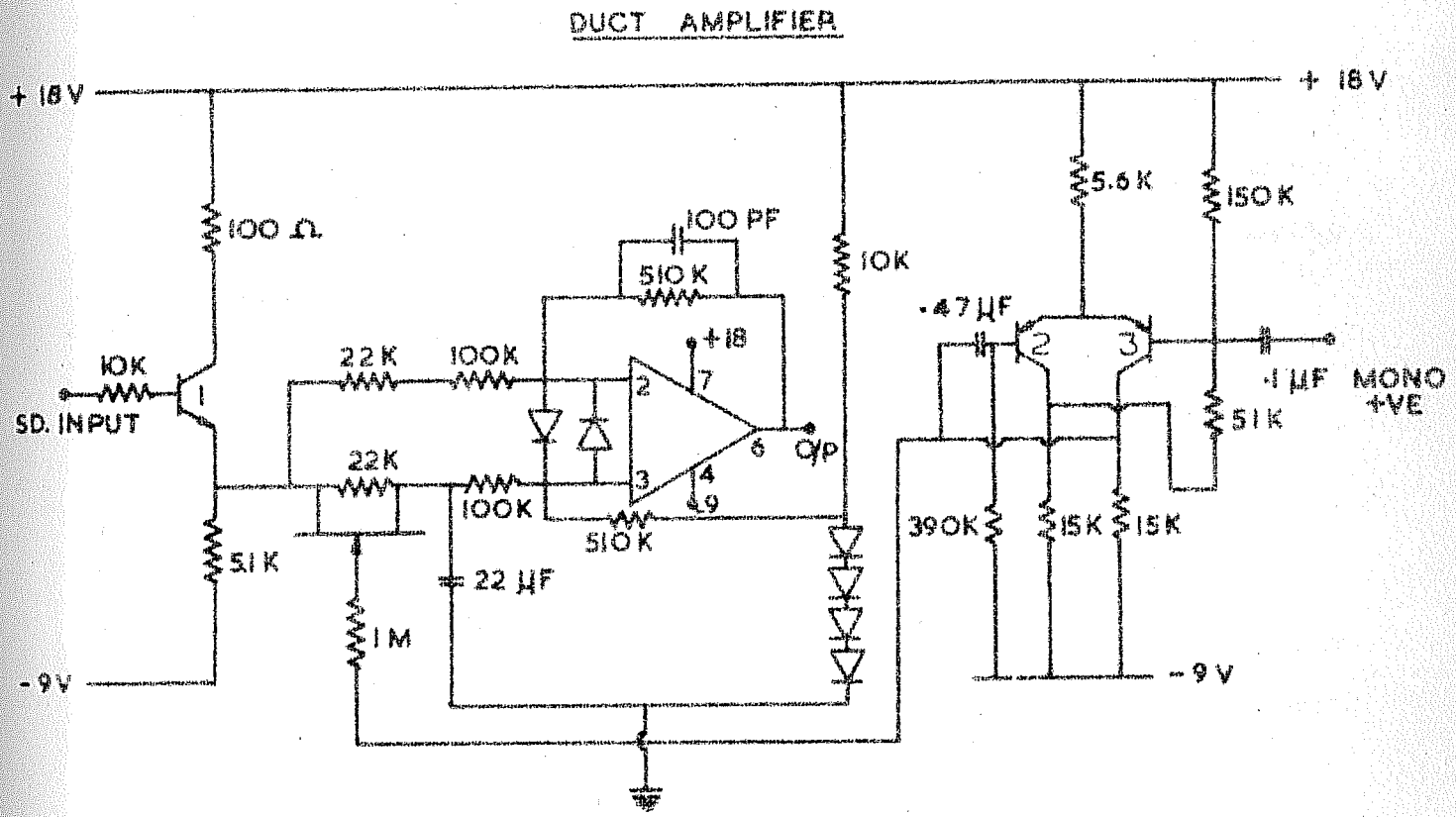

Fig. 3.13 Circuit diagram of the duct amplifier

applied to the sensor, the input to the duct amplifier contains very sharp pulses due to different resistance switchings. In presence of such sharp pulses the output d.c. level would shift. To avoid this shift, the time constant of RC network is made extremely small during the rising portion of the sweep. The 22 K resister is shorted through a field effect transister which gets a pulse of desired duration from a monoshot (TR2 and 3). For driving the monoshot a pulse from sweep circuit is taken.

3.5 Data Analysis

The probe data is transmitted on three V.C.O. channels of 14.5, 30 and 70 kHz. The intelligence bandwidths of these channels are 220, 450 and 1050 Hz respectively. Usually there are some other experiments also onboard the rocket and hence their data are also transmitted on other V.C.O. channels. There are, therefore, 8 to 10 data channels for all the experiments. The output of all these data channels is recorded on a photographic chart moving at a speed of 10"/sec. In addition the data of all channels is recorded on a magnetic tape also so that it can be used later for recordings on paper charts at desired speeds. Before starting the recording on the paper chart, known voltages are fed to obtain the calibration marks for all the channels.

The probe current is transmitted on 14.5 kHz channel. This channel contains information about the electron density,

medium scalesize electron density irregularities and electron temperature. In this thesis we are concerned with the measurement of electron density and irregularities only. The information about these two parameters is contained in the current drawn by the probe when a fixed voltage +4 volts is applied to the sensor. The information about the electron temperature is contained in the probe current when the sensor potential is swept from -2 to +4 volts; a retarding potential analysis yields one value of electron temperature during each sweep cycle. The author has made electron temperature measurements (Subbaraya et al. 1974) also but the results are not being reported here.

The second output is termed as duct channel and is transmitted usually on 30 KHz channel. This channel is used to study medium scale irregularities when their amplitude is very weak. When the amplitude of medium scalesize irregularities is large they can be studied from main channel data and at that time the duct amplifier would be saturated. But when the amplitudes are small the irregularities cannot be seen by main channel and one has to study them through duct channel.

The third output is termed as the high frequency channel and is transmitted on 70 KHz channel. This channel is used to study the nature of small scale irregularities (1-15 meters). The output of the channel shows the composite amplitude in a band of 70-1000 Hz.

3.5.1 Determination of Electron Density

For determination of the electron density first of all the probe current is to be found out. For this the self divided or non self divided L.P. output voltage is to be determined. The usual conversion factor for vertical scale is that 50 mms on the chart correspond to 5 volts. In cases where different displacement is kept the proper ratio has to be used. At the beginning of the sweep cycle a zero marker is obtained whose length is dependent on the feedback resistance which is connected at that instant. From the length of zero marker and switchings on the output the exact factor needed for conversion of output voltage to input current, can be determined. Thus at any instant the probe current values can be evaluated.

The values of probe current thus obtained are multiplied by a proportionality constant to get the electron densities. As mentioned in section 3.2 we have adopted the proportionality factor such that one microampere of current corresponds to an electron density of 7.15×10^3 cm^{-3}.

The smallest current which can be read is limited by the feedback resistance and the smallest displacement which one can read on the y-axis of the telemetry chart. Keeping in view the thickness of the trace it is felt that a displacement of 3 mm above the zero line can be correctly read. This displacement would correspond to about 0.3 volts. Since we

are using a resistance of 100 M Ω, the smallest current which can be read in 3×10^{-9} Amp. The maximum current would be obtained when the self divided output stays at 5 volts with the smallest feedback resister i.e. 0.270 M Ω. Since the self divider divides the voltage by a factor of 4.5 the maximum current which can be measured would be $(5.0 \times 4.5)/(0.270 \times 10^{6})$ amp i.e. 8.0×10^{-5} Amp.

Thus the smallest and highest densities which one can measure with this system are 2.1×10^{1} cm^{-3} and 5.7×10^{5} cm^{-3}, respectively.

The measurement of electron density can be carried out only for 0.5 sec during a sweep cycle because the sensor is kept on +4 volts for only this much time. However, we had a couple of flights in which sweep was not there and sensor was kept at +4 volts for the period of 1.8 sec or so. In such cases the entire data is useful for the electron density evaluation. The electron density values are computed for every half an inch which for a chart running at 10"/sec means an interval of about 0.05 sec. In 0.05 sec the rocket, on an average, traverses about 75 meters or so. Thus electron density values at the interval of 75 meters are available. For determination of altitude, the trajectory provided by the TERLS Control Centre has been used.

3.5.2 Analysis of 30-300 Meter Scalesizes

The analysis of 30-300 meter scalesizes is carried out on the data obtained from the main as well as the duct channel. In order to read the data more accurately and closely, re-recordings were made for the selected intervals. During such recordings the chartspeed was increased to 16"/sec. and large displacement in y-direction was provided. For the study of spectrum of 30-300 meter irregularities, data were taken only from those flights where there is no sweep voltage but the sensor is kept at +4 volts. On an average data of about 1.2 sec is obtained every 1.5 sec. Since the smallest interval at which readings can be taken manually is 1 mm there are nearly 500 points available during each cycle. Thus the data of 1.2 sec is read at about 500 points and is subjected to spectrum analysis. But whenever smaller number of points are available (due to intermediate switchings) the largest scale-size studied was commensurate with the data length. All the spectra which have been presented in chapters IV and V have been evaluated using the data obtained as mentioned above.

a) Fourier Transform Technique

For the estimation of power associated with any frequency the technique of Fourier Transform has been used. In this technique first of all the autocovariance function has to be determined and then it is to be Fourier transformed

to get the power. The exact procedure of analysis, typical values used and standard formulae are given below.

No. of points = 501 $\therefore$ n = 500

τ = 1 mm on the chart = 0.002461 seconds

Record length T_n = 500 x 0.002461 $\simeq$ 1.2 sec.

Maximum lag $T_m = T_n/10$ = 0.12 sec.

No. of lags m = T_m/τ = 0.12/0.002461 $\simeq$ 49

Since the No. of lags m is 49 autocovariance function C has to be determined at m + 1 i.e. 50 points.

$$C(r) = \frac{1}{(n-r)} \sum_{q=r}^{m} x_q \cdot x_{q-r}$$

$$C(0) = \frac{1}{500}\left(x_0^2 + x_1^2 + x_2^2 + \cdots + x_{500}^2 \right)$$

$$C(1) = \frac{1}{499}\left(x_1 x_0 + x_2 x_1 + x_3 x_2 + \cdots x_{500} x_{451} \right)$$

$$\vdots$$

$$C(49) = \frac{1}{451}\left(x_{49} x_0 + x_{50} x_1 + x_{51} x_2 + \cdots x_{500} x_{451} \right)$$

Fourier transform of autocovariance contains real and imaginary parts and is given by

$$J(f) = \sum_{t=0}^{49\tau} C(t)\, e^{-i 2\pi f t} \cdot \tau$$

$$= A + iB$$

$$\therefore P(f) = |A|^2 + |B|^2$$

Thus power at any frequency f can be evaluated. The units of this power are variance/wave number/meter. The power in different waves can be expressed both in time and space domain. The Fourier transform of the autocorrelation function gives the power spectral density. The units are variance/wave number/meter. This means the power at a wave number is expressed as variance per unit wave number per meter of chart. The power is expressed in time domain as variance/unit bandwidth/sec. This means the power at some frequency per unit bandwidth (Hz) per second.

Since $\tau = 0.002461$ sec the Nyquist frequency is given by $f_N = 1/2\tau \approx 200$ Hz

This is the maximum frequency upto which the estimates of power can be made. The smallest frequency upto which the estimates should be made is limited by the record length. Since the record length is 1.2 sec. the Minimum frequency which can be safely studied may be taken as

$$f_{min} = 4/T_n \approx 4/1.2 \text{ sec} \approx 3 \text{ Hz}$$

Thus the scalesizes which one can study with the present data are limited by these two frequencies, viz. f_N and f_{min}. Assuming that the velocity of irregularities is much smaller than the velocity of the rocket (~ 1.5 km/sec) the fluctuations represent the vertical wavelength of the irregularities in the medium. The scalesize of irregularities can be calculated

from the relation $\lambda_{irr} = V_R/f_{irr}$ where V_R is the rocket velocity and f_{irr} is the observed frequency of irregularities. Gupta (1970) has discussed the effect of rocket and irregularity orientations and velocities on the estimate of scalesize. Assuming a rocket velocity of 1.5 km/sec, the scalesize range which can be studied is from 7.5 to 500 meters. But in order to be well within the range we have chosen the scalesize range of 30-300 meters.

In order to estimate the errors involved in the power values thus obtained one has to find the degrees of freedom K where K is defined as $K = 2\ n/m$. In our case $n \simeq 500$, $m \simeq 50$ hence $K \simeq 20$. The upper and lower limits of power estimates for 20 degrees of freedom with 95% level of confidence can be read from the standard tables (Blackman and Tukey, 1959). Thus for $K = 20$ the power estimates have to be multiplied by 1.51 and 0.54 for getting the upper and lower limits respectively.

b) Zero Crossing Technique for Most Prominent Scalesize

The estimate of most prominent scalesize at any given altitude can be made using this simple method. As mentioned in the last section, the data of electron density is available at 500 points during 1.2 sec interval. Thus the total data length is about 1.8 km. These data are subjected to moving

average analysis wherein the moving average is taken over 50, 100, 150, 200, 250 and 300 meters. Once the moving average is taken over a certain displacement there are lesser number of data points available after the averaging. For example if there are 500 points available from x_1, x_2 ..... x_{500} points and one takes moving average over 21 points then the averaged data would be available for points x'_{11}, x'_{12}.... x'_{490}. Now if one subtracts the moving averaged value from the original values at each point one would get values like $(x_{11} - x'_{11})$, $(x_{12} - x'_{12})$ ..... $(x_{490} - x'_{490})$. These values would be positive as well as negative and hence one can count the number of zero crossings. Suppose the number of zero crossings is N then the most prominent scalesize λ_P is given by

$$\lambda_P = \frac{\text{Record Length}}{2\ N}$$

The recordlength in the case of above example would be $V_R/490 \times 0.002461$

where V_R is the rocket velocity.

As one takes the moving average for higher and higher data lengths the final data length goes on decreasing and hence it becomes necessary to normalize the number of zero crossings to a standard length. In our case we have normalized the number of zero crossings to a data length corresponding

to 400 points. Thus at any given altitude region the number of zero crossings has been determined which can be used to compute the most prominent scalesize at that altitude. It may be mentioned here that this information is not obtained from our Fourier Transform technique because the information of phase is lost while evaluating the power.

3.5.3 Analysis of 1-15 Meters Irregularities

The study of 1-15 meter irregularities is carried out with the output of the high frequency noise amplifier. This output after proper amplification is telemetered on IRIG channel 18 (70 KHz $\pm$ 7.5%) which has an intelligence bandwidth of 1.05 KHz and can be used to study fluctuations with scalesizes down to one meter. The telemetered signal recorded on a magnetic tape after passing through a suitable descriminator is recorded on a photographic paper chart moving with a speed of 10"/sec. This record gives the amplitude of fluctuations in the composite band of 70-1000 Hz (1-15 meters scalesize). For determining the spectrum, this frequency range (70-1000 Hz) is subdivided into a number of sub-branches and the composite signal is passed through a bank of band pass filters. The characteristics of the filters which have been used are listed in table III.1.

The centre frequency of 8^{th} filter fell beyond the intelligence bandwidth of 70 KHz channel and hence the data

TABLE III.1

Filter No.	1	2	3	4	5	6	7	8
Frequency f (Hz)	86	122	172	254	356	509	720	1036
Bandwidth $\triangle$f (Hz)	11	17	31	30	50	70	100	130
$\triangle f/f$	7.81	7.17	5.55	8.40	7.12	7.27	7.20	7.97
Corresponding scalesize (mts)	17.4	12.3	8.7	5.9	4.2	2.9	2.1	1.4

from this filter was not used. The output of each filter is further amplified and is recorded on the photographic paper moving at 10"/sec. The signal in each channel of the paper-chart represents the amplitude of fluctuations within the scalesize range corresponding to the centre frequency and bandwidth of a particular filter. Assuming that the velocity of irregularities is much smaller than the velocity of the rocket ($\sim$ 1.5 km/sec) the fluctuations represent the vertical wavelength of the irregularities in the medium. The scale-size of the irregularities λ_{irr} can be calculated from the relation $\lambda_{irr} = V_R/f_{irr}$ where V_R is the rocket velocity and f_{irr} is the observed frequency of the irregularities. These scalesizes are listed in table III.1. This analysis is known as A.C. analysis and the resulting filter outputs on the paper charts are very useful for seeing the change in spectrum.

For the purpose of determination of spectral index each filter output was rectified and averaged for 0.2 sec and was then recorded on the photographic chart moving at same usual speed of 10"/sec. This record we term as D.C. record. Before the actual recording, this system is calibrated by feeding a fixed A.C. signal and noting down the d.c. output. For evaluating the spectral index at any given time the d.c. output of each channel is noted and is converted into peak to peak A.C. value, A_{pp}. If the calibration factor and the bandwidth of that particular channel are represented by C and Δf respectively, then the power associated with the centre frequency in a bandwidth of Δf is given by

$$P = \left(\frac{App.C}{2.828} \right)^2 \frac{1}{\Delta f}$$

The unit of power is variance/unit bandwidth/sec. Unfortunately during the recording of the spectrum the amplification provided at the output stage of 70 KHz channel could not be known properly. Therefore, the results of one flight are not comparable to the other. But for the individual flight all the values are comparable because the amplification is provided to the composite signal. Therefore, all the power estimates have been expressed in arbitrary units.

CHAPTER - IV

RESULTS DURING PERIODS OF NORMAL ELECTROJET

The days on which the electrojet current remains eastward during daytime are termed as 'normal electrojet days'. On some of the days the direction of electrojet current reverses for a few hours in daytime (mostly during afternoon); such days are termed as 'counter electrojet days'. This chapter is devoted to the results obtained from a number of rocket flights made during normal electrojet. The results of ionization irregularities in medium (30-300 meters) and small (1-15 meters) scale-size ranges generated through cross-field and neutral turbulence mechanisms are presented here. The analysis of irregularity data of a large number of flights shows that the behaviour of irregularities is quite systematic. In the following, therefore, only those results are presented which are most typical representations of the irregularities.

4.1 General Nature of the Electron Density Profile During Different Times of the Day

Fig. 4.1 shows the electron density profiles at 0559 and 0745 hrs IST on 9th February 1975 and 12th August 1972 respectively. On the early morning flight namely P158 the Langmuir probe sensor was housed inside the rocket nosecone and since the nosecone was ejected around 85 km altitude the data below that altitude could not be obtained. Around 92 km the density sharply increases from 2×10^2 to 6×10^3 cm^{-3} in just about a kilometer or so and thereafter, the density decreases very slowly upto 110 km after which it exhibits two very prominent structures. The density around 118 km or so falls down by an order of magnitude from its peak value. Since the time of launch for this flight was 0559 hrs the profile exhibits both daytime as well as nighttime features. The reminiscence of the typical 'valley of ionization' can be seen in the profile around 120 km. The region lying below 105 km altitude exhibits an almost constant density upto about 92 km. The densities in this flight which is an early morning flight are much smaller as compared to the late morning flight viz. Co5.14. For flight Co5.14 the density is 3×10^1 cm^{-3} at 63 km and increases upto 75 km or so attaining a value of 6×10^2, thereafter, it decreases during next five kms. Beyond 80 km the density increases very rapidly upto 92 km or so and after that it attains nearly a steady value of $1 \times 10^5 cm^{-3}$.

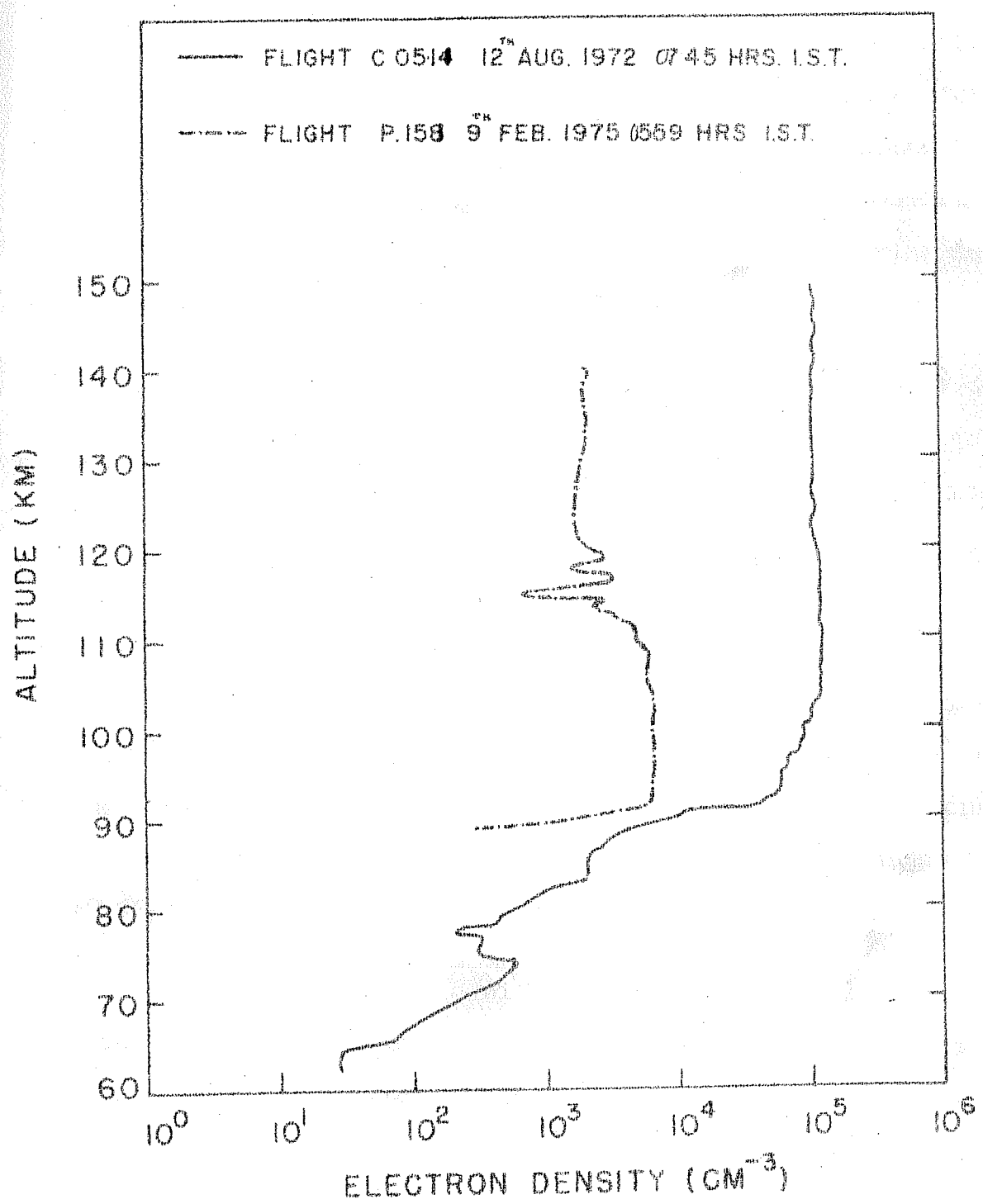

Fig. 4.1 : Electron density profiles during morning time

Fig. 4.2 and 4.3 show the electron density profiles during five daytime flights. The general nature of profiles is: a rapid increase in density upto 75-76 km followed by a slow increase upto 85 km or so which again is acompanied by rapid increase upto 100 km or so beyond which the density remains practically constant. The peak density during daytime is typically of the order of 2×10^5 cm^{-3}.

Fig. 4.4 shows two evening time profiles. The densities below 80 km were too small to be measured by Langmuir probe. Both the profiles show a sharp layer of ionization around 90 km. above which the density increases slowly upto 110 km or so. Above 110 km both the profiles show the valley of ionization which, as would be seen later, becomes more prominent during nighttime. Beyond 140 km the density increases slowly and ultimately assumes a value of 2×10^4 cm^{-3}. The profile of flight 10.11 shows large scale fluctuations beyond 130 km. Although these structures are present in 10.13 profile also, they are not as prominent as in 10.11.

Fig. 4.5 shows a nighttime profile. Both ascent and descent data of the probe current are plotted. The conversion factor needed for getting the density values is also given in the diagram. Like daytime profiles, the nighttime profile also shows a sharp layer around 90 km wherein the density increases by a few order of magnitudes. Beyond 90 km the day and nighttime profiles are very much different. During

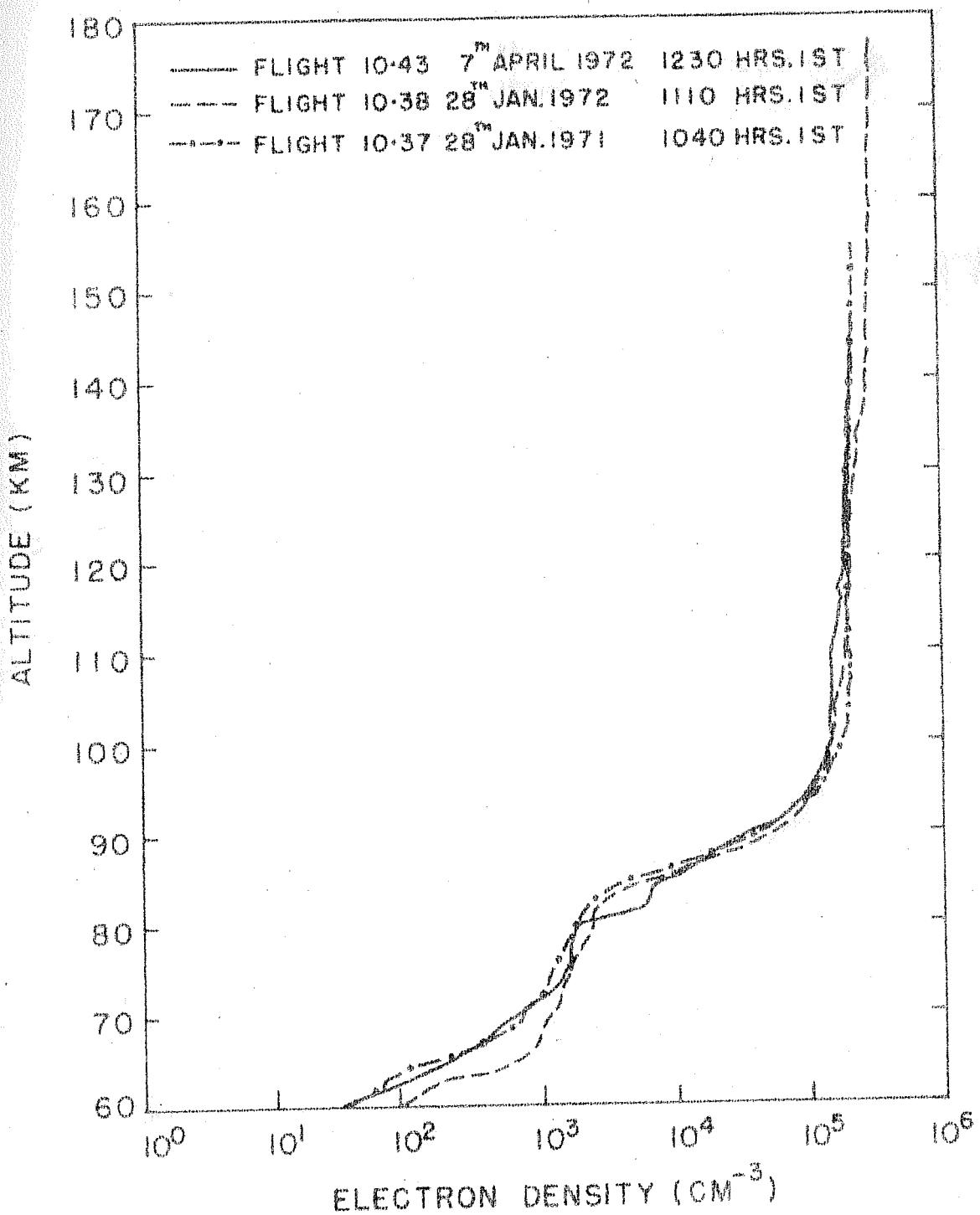

Fig. 4.2 Electron density profiles during noon time

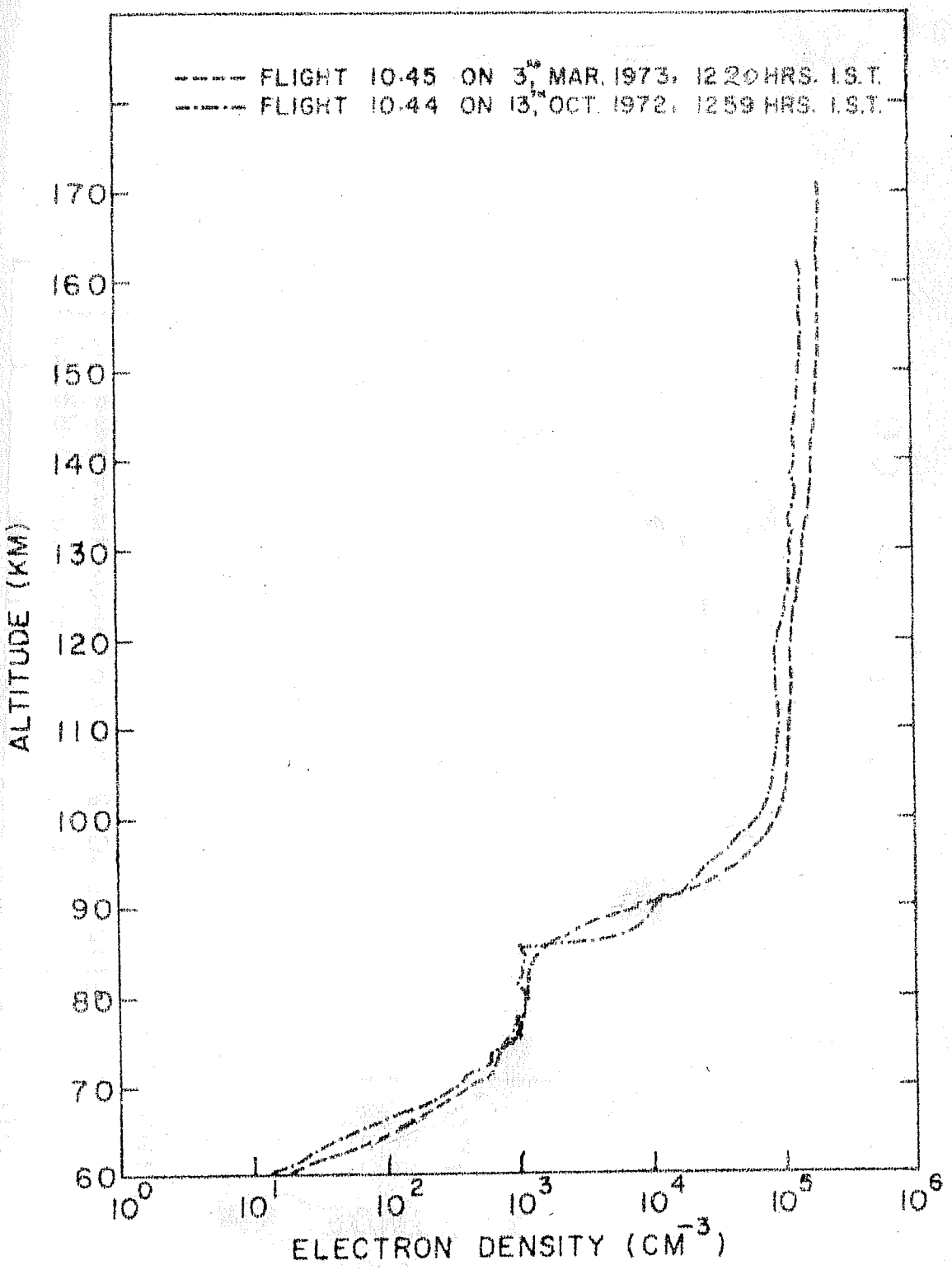

Fig. 4.3 : Electron density profile during noon time

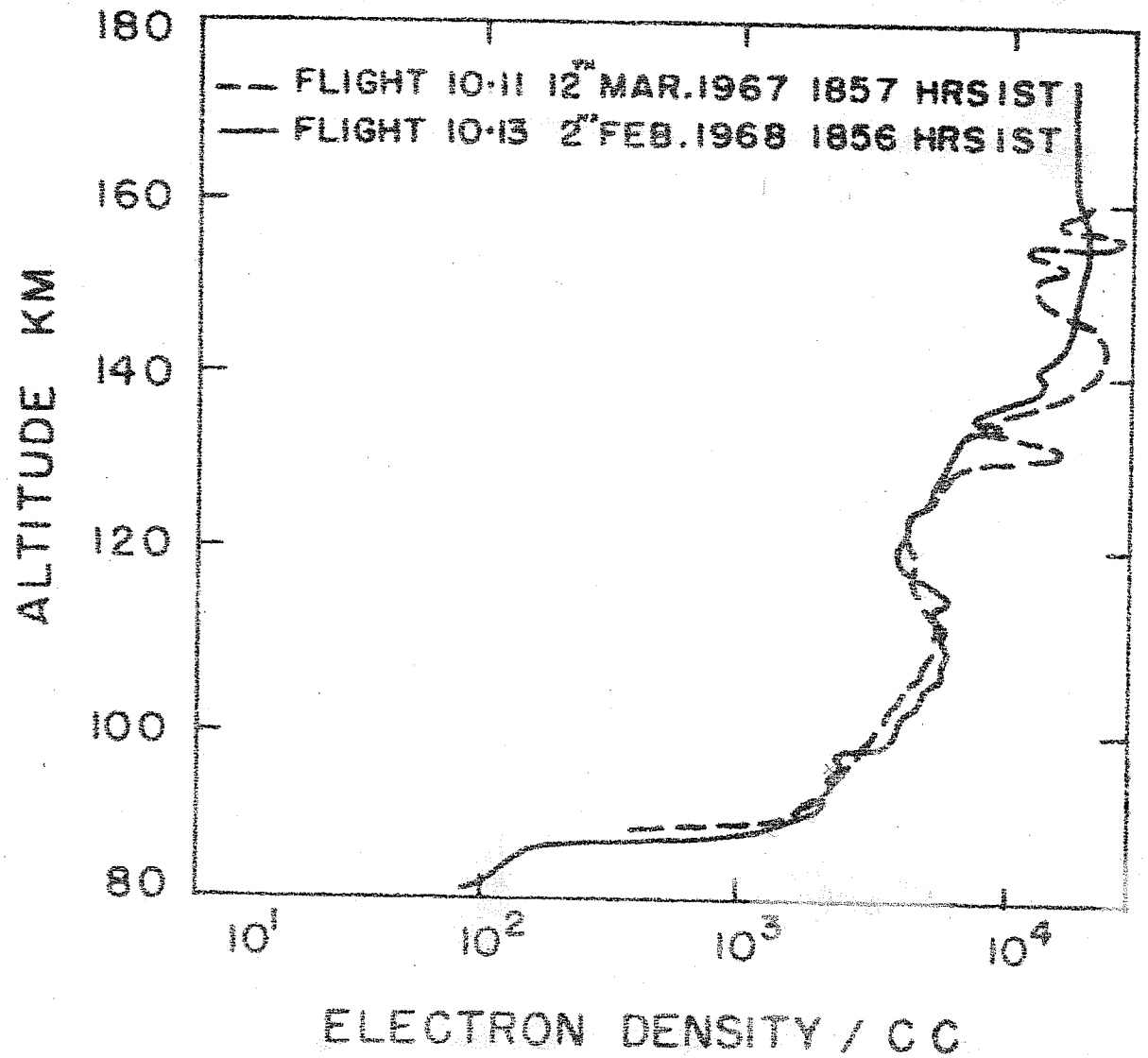

Fig. 4.4 Electron density profile during evening time

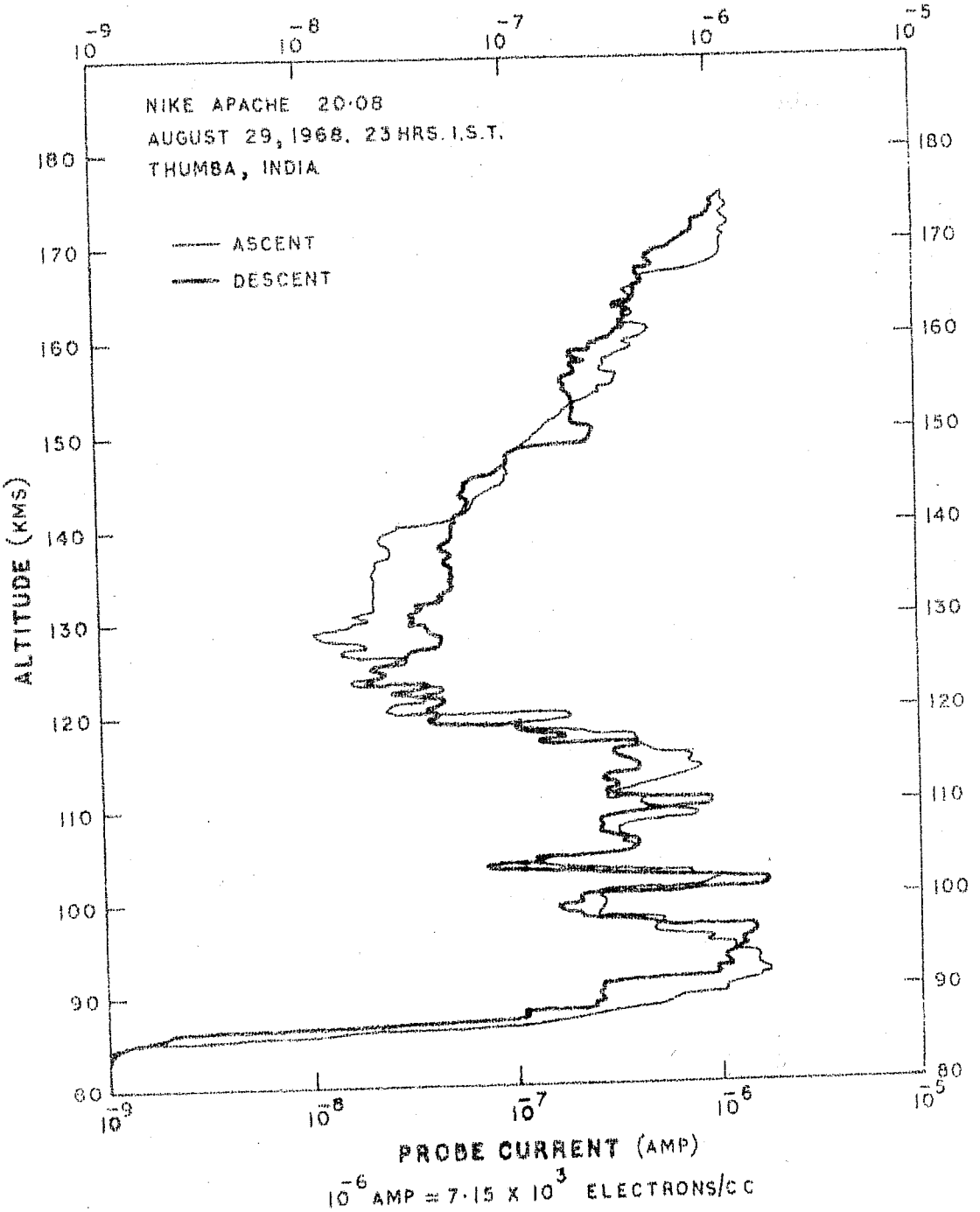

Fig. 4.5 Probe current profile at night during ascent and descent of the rocket.

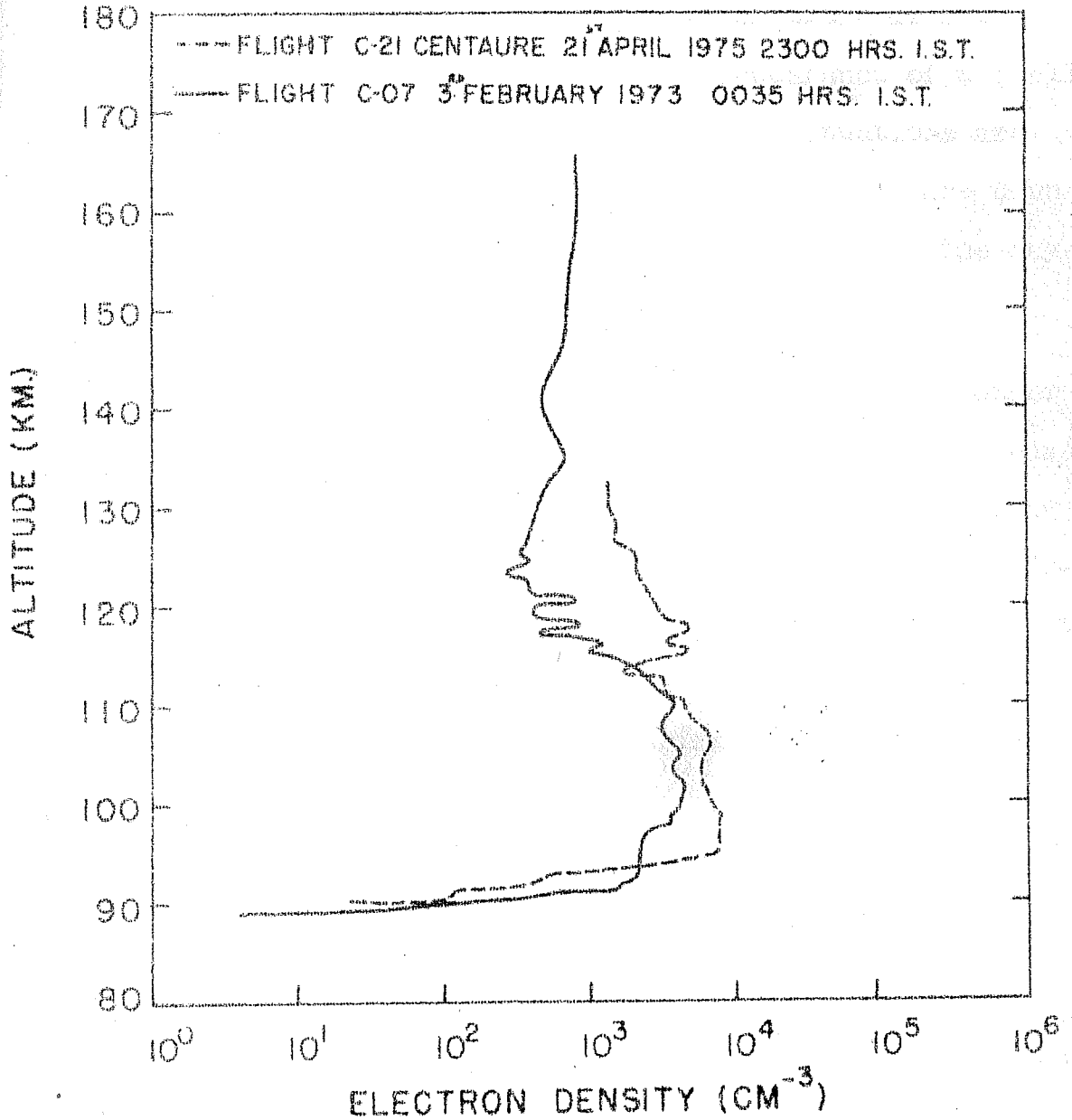

Fig. 4.6 : Electron density profiles during night time

nighttime the density profile exhibits a lot of layered structures upto about 110 km after which there is a bite up of the ionization which gives it the appearance of a 'valley'. Even in the valley portion small scale fluctuations are present in the profile. The nighttime densities are down by more than an order of magnitude as compared to the daytime values.

Fig. 4.6 shows the density profiles of two other nighttime flights. Both the flights show a large increase around 90-92 km after which the density shows large scale fluctuations. The density during C07 shows an overall decreasing trend upto 125 km beyond which it increases and then attains a nearly constant value of 10^3 cm^{-3}. The valley of ionization is very clearly seen during C07 and a similar trend is found in C-21.

4.2 General Nature of Electron Density Gradients During Different Times of the Day

The electron density gradient is usually represented in the literature by a parameter 'L' which denotes the density gradient scale length and is defined as following.

$$\frac{1}{L} = \frac{1}{n} \frac{dn}{dh}$$

where n is the ambient density and h is the height. Larger is the parameter L weaker is the gradient. We have chosen

to show the variation of parameter $\frac{1}{L}$ with altitude for showing the nature of the gradients. In order to show both the negative and the positive gradients on the same plot a linear scale was selected. Occasionally, the gradients are very strong and the value of the parameter $\frac{1}{L}$ shoots up beyond the scale; in such cases value of $\frac{1}{L}$ is written on the plot. For example the value of $\frac{1}{L}$ at 86 km during the ascent of flight 20.08 is 4.6 km^{-1} (see fig. No.4.10).

For determining the gradient at any point all the points lying 500 meters above and below the point were taken and a second degree polynomial fit was obtained; this new curve was then differentiated at that point to get the gradient. Such gradients were obtained at each kilometer from 80 km to 130 km.

Fig. 4.7 shows the nature of gradients during an early morning flight, P-158 and a late morning flight, C05.14. During flight P-158 positive gradients are present around 88 and 114 km and negative gradients are present at 112 and 118 km altitude. In other regions very weak gradients of both signs are present. During flight C05.14 gradients are only positive and there is one major peak at 91 km where $\frac{1}{L}$ value is as high as 2.48. This is a secondary peak at 83 km also.

Fig. 4.8 shows the variation of $\frac{1}{L}$ for six daytime flights. All the profiles show a large positive gradient

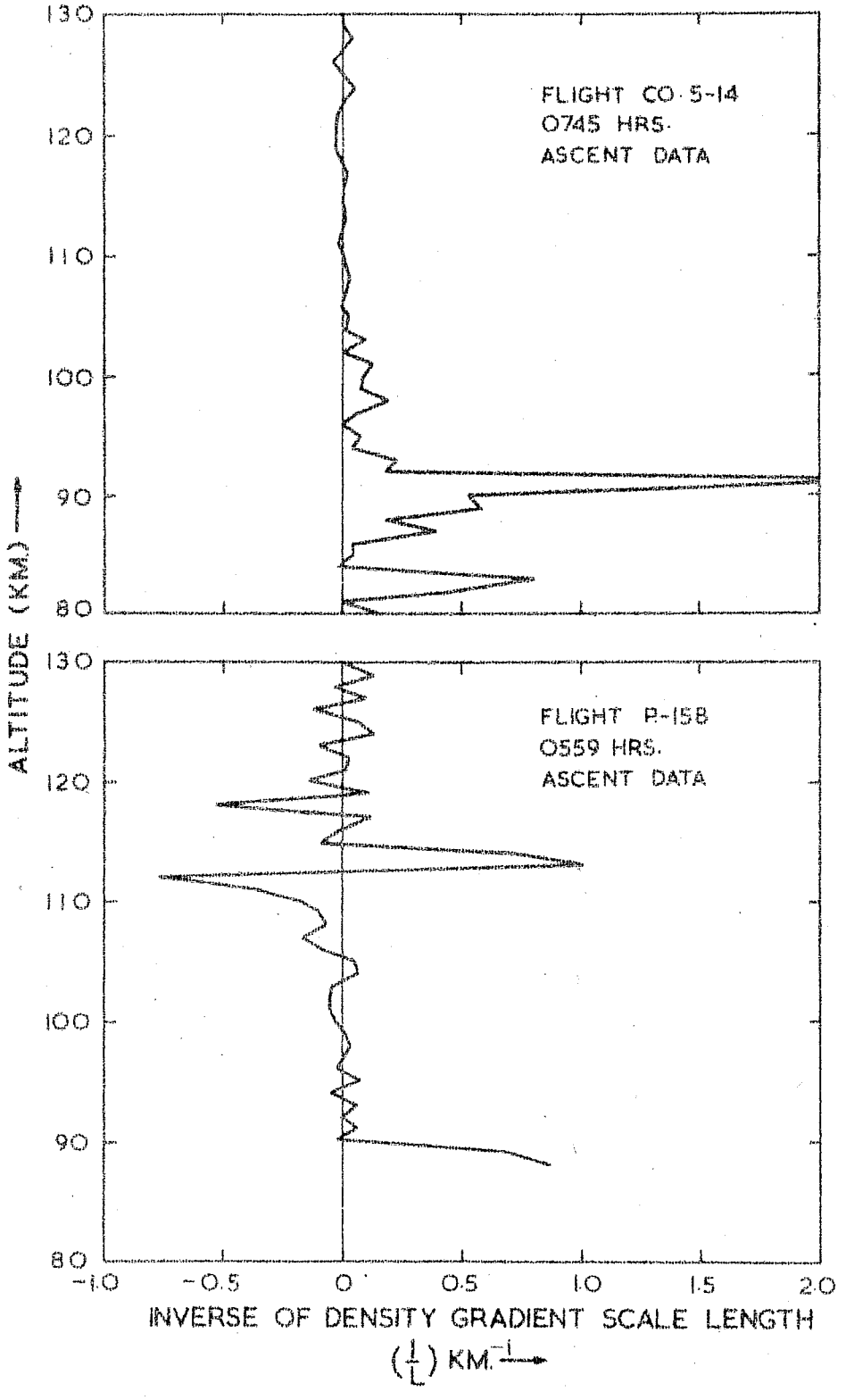

Fig. 4.7 Variation of electron density gradient with altitude for two morning time flights.

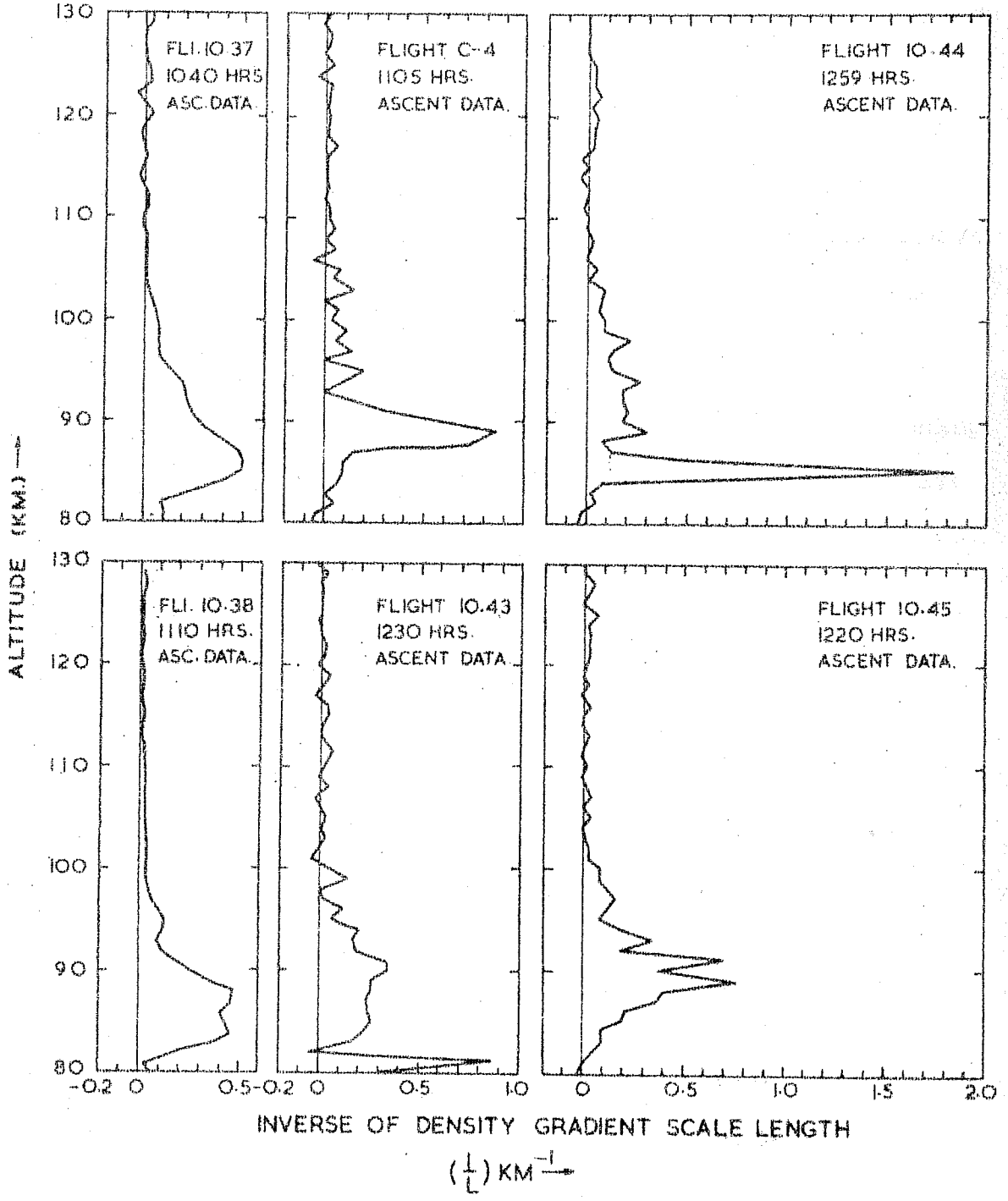

Fig. 4.8 Variation of electron density gradient with altitude for six noon time flights.

around 88-90 km. The behaviour of flight 10.43 is slightly unusual as it shows very strong gradient around 81 km. The region of large gradient is, however, confined only to one km or so. In general, there are no negative gradients present during daytime and especially so below 100 km altitude. Above 100 km the density assumes nearly a constant value and gradients, if present, are very weak.

Fig. 4.9 shows the nature of gradients during evening hours. It can be seen from the figure that a strong positive gradient exists around 80 and 87 km. Above 100 km, gradients of both signs are present with slightly strong positive gradients around 133 and 137 km. In the region above 100 km, the fluctuations in the gradient are more pronounced as compared to daytime value. Fig. 4.10 shows the nature of gradients during nighttime as observed during the ascent and descent of the rocket. The gradients are very strong and show, qualitatively, same behaviour during ascent and descent. Comparing these gradients with daytime gradients it can be readily seen that during nighttime both positive as well as negative gradients are much stronger as compared to daytime. Similar features are shown in fig. 4.11 for yet another nighttime flight.

The overall picture of gradients during different times of the day is as following. During early morning hours both the positive and the negative gradients are present indicating the reminiscence of nighttime features. By 0745 Hrs

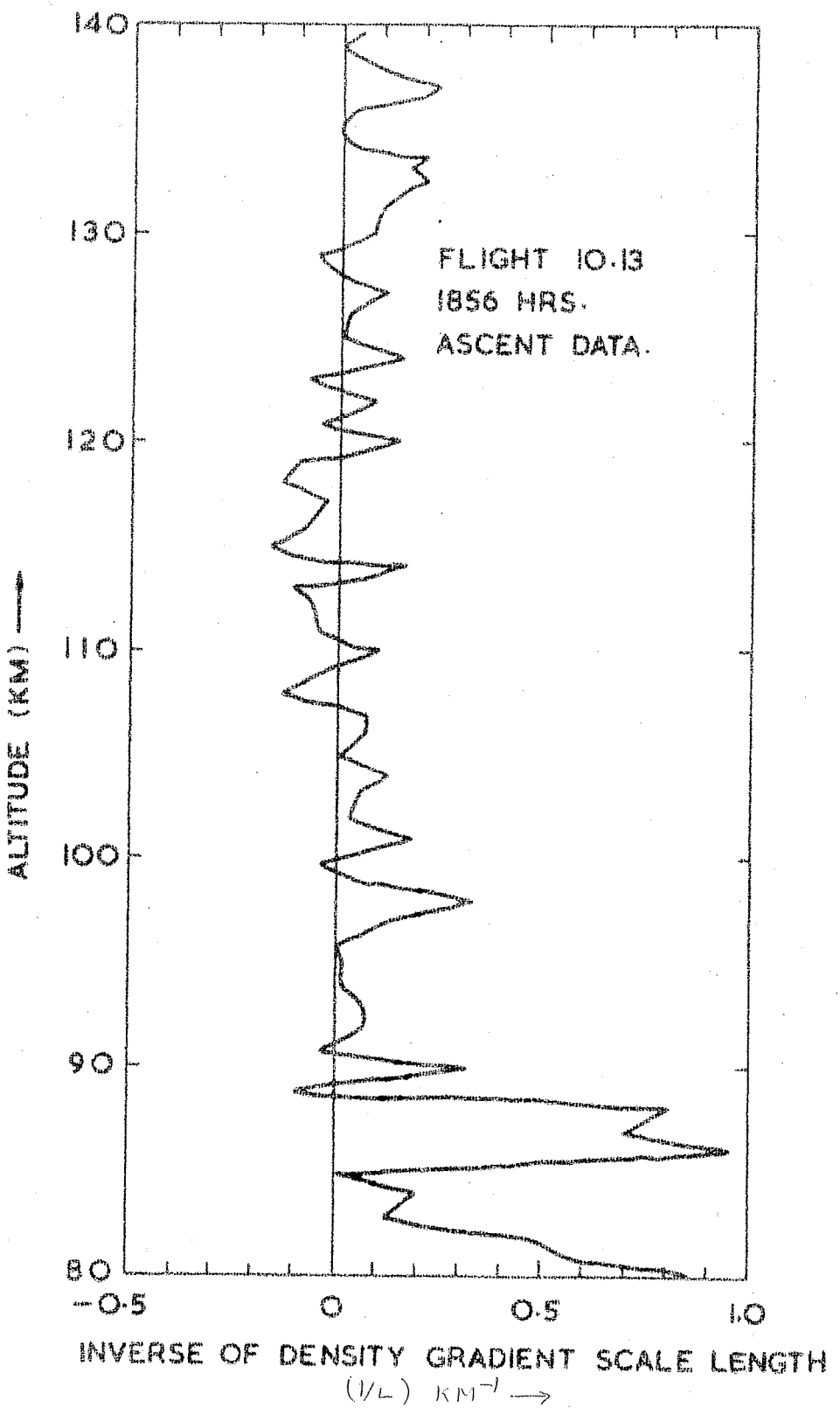

Fig. 4.9 Variation of electron density gradient with altitude for an evening time flight.

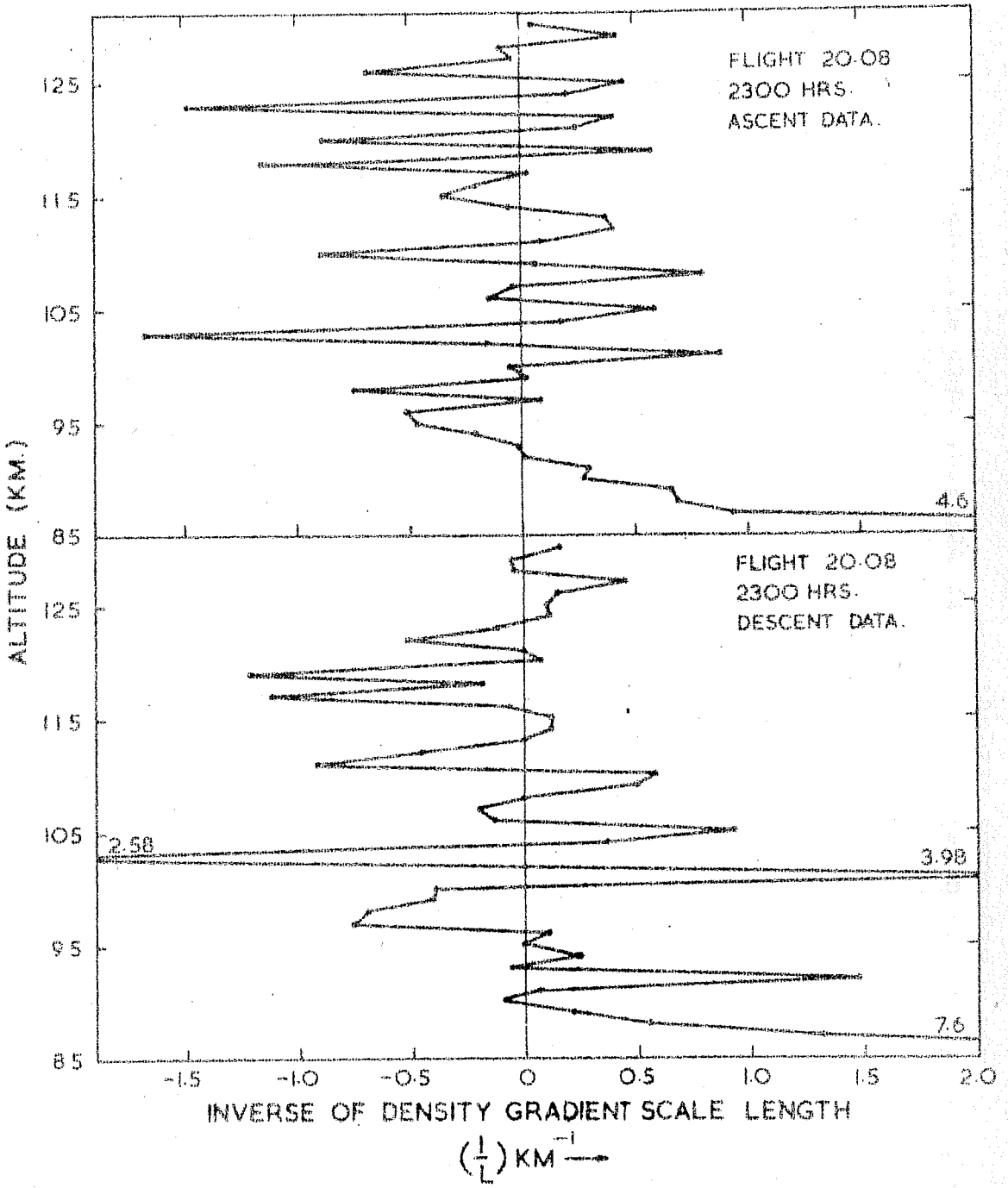

Fig. 4.10 Variation of electron density gradient at night during the ascent and the descent of the rocket.

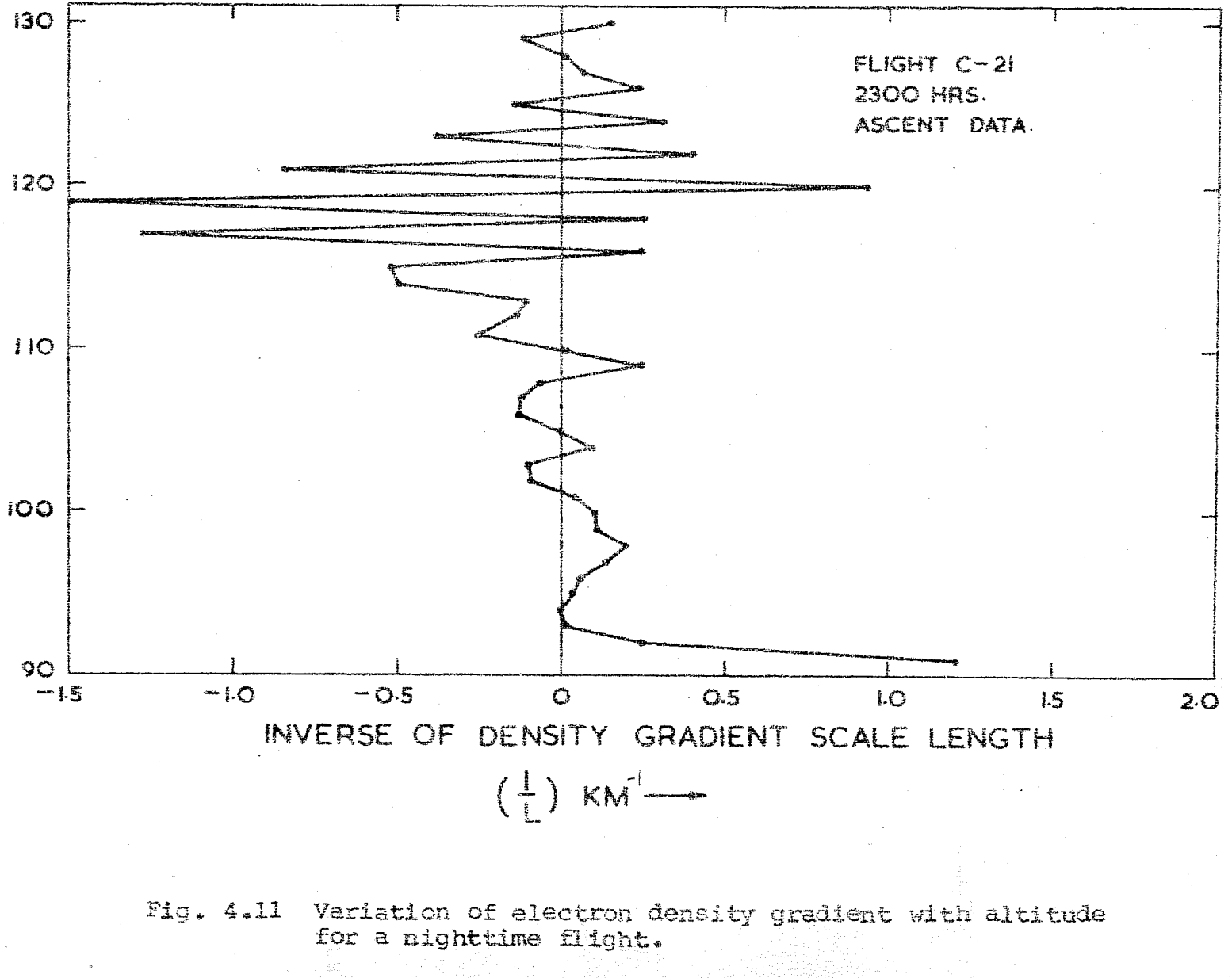

Fig. 4.11 Variation of electron density gradient with altitude for a nighttime flight.

the regions of negative gradients vanish . and the profile exhibits positive gradients only. During noon time strong positive gradients exist around 88-90 km and there are no negative gradients. The evening time results show a sort of transition from daytime to nighttime conditions where both positive as well as negative gradients are present. During nighttime both positive as well as negative gradients are present and they are much stronger than gradients observed at any other time of the day.

4.3 Ionization Irregularities Produced Through Cross-field Instability Mechanism

The rocket data show the presence of ionization irregularities in a large scalesize range from few hundred meters down to one meter. For convenience the data are divided in two scalesize ranges namely 30-300 meters and 1-15 meter and the irregularities in these ranges are termed as type M_c and S_c respectively (see classification in chapter I). The results of both these types are presented here.

4.3.1 Irregularities in 30-300 meter Scalesize Range (Medium Scale Cross-field-type M_c)

a) Regions of Occurrence

These irregularities were observed in different regions during different times of the day. Table IV.1 shows the regions

of occurrence of type M_c during seven rocket flights which typically represent early morning, morning, noon, evening and nighttime periods.

It can be seen from table IV.1 that during morning and noon hours the irregularities are observed continuously between 87 and 110 km altitude. At other times the irregularities are observed in isolated regions. The extent of these isolated regions varies from 110 to 118.5 km during early morning hours, 86 to 100 km during evening hours and 94 to 122 km during nighttime.

Table IV.1

Observed Regions of Occurrence of Type M_c

Period of Observation	Altitudes of Observation km.
Early morning Flight No. P 158	110-112, 115-116, 117.2-118.5
Morning Flight No. C05.14	87 - 93 (Continuously)
Noon Flight No. 10.44	88.5 - 96.6 (Continuously)
Noon Flight No. 10.45	87.5 - 110 (Continuously)
Evening Flight No. 10.13	86.5-88, 89.8-90.7, 92.2-93.2, 96.5-98.8
Night Flight No. 20.08	94-96.5, 97.5-98.8, 109.2-110.5, 117.4-118.4, 119.2-120.2, 121.2-121.9
Night Flight No. C-21	102-103.2, 105.7-107.7, 111.3-115

b) Shape of Irregularities

As seen on the telemetry chart medium scalesize CF irregularities have very typical shapes. On the telemetry record during ascent the positive x-direction represents increasing altitude of the rocket while during descent it represents decreasing altitude of the rocket. In each of the figures 4.12 to 4.15 which are the typical telemetry records the arrow gives the direction in which the density is increasing.

Fig. 4.12 shows the telemetry records of two daytime flights at two different altitudes during the ascent of the rocket. It can be clearly seen from the records at 87.2, 90.5 and 89.4 km that as one moves along the density gradient the rise in electron density is much sharper than the fall. The rises and falls in the density can be seen as sawtooth type structures. At 91.5 km during flight 10.38 the shapes look like distorted sawtooth structures.

Fig. 4.13 shows the telemetry records of flight 10.45 during ascent of the rocket. It can be seen that the irregularities at 87.5 and 90 km have distinct sawtooth type shape. In the next three records at 93.6, 95.5 and 97.5 km the amplitudes have become very small and the structures are not very clear.

Fig. 4.14 shows the telemetry records of flight 10.44 during ascent as well descent of the rocket. During the

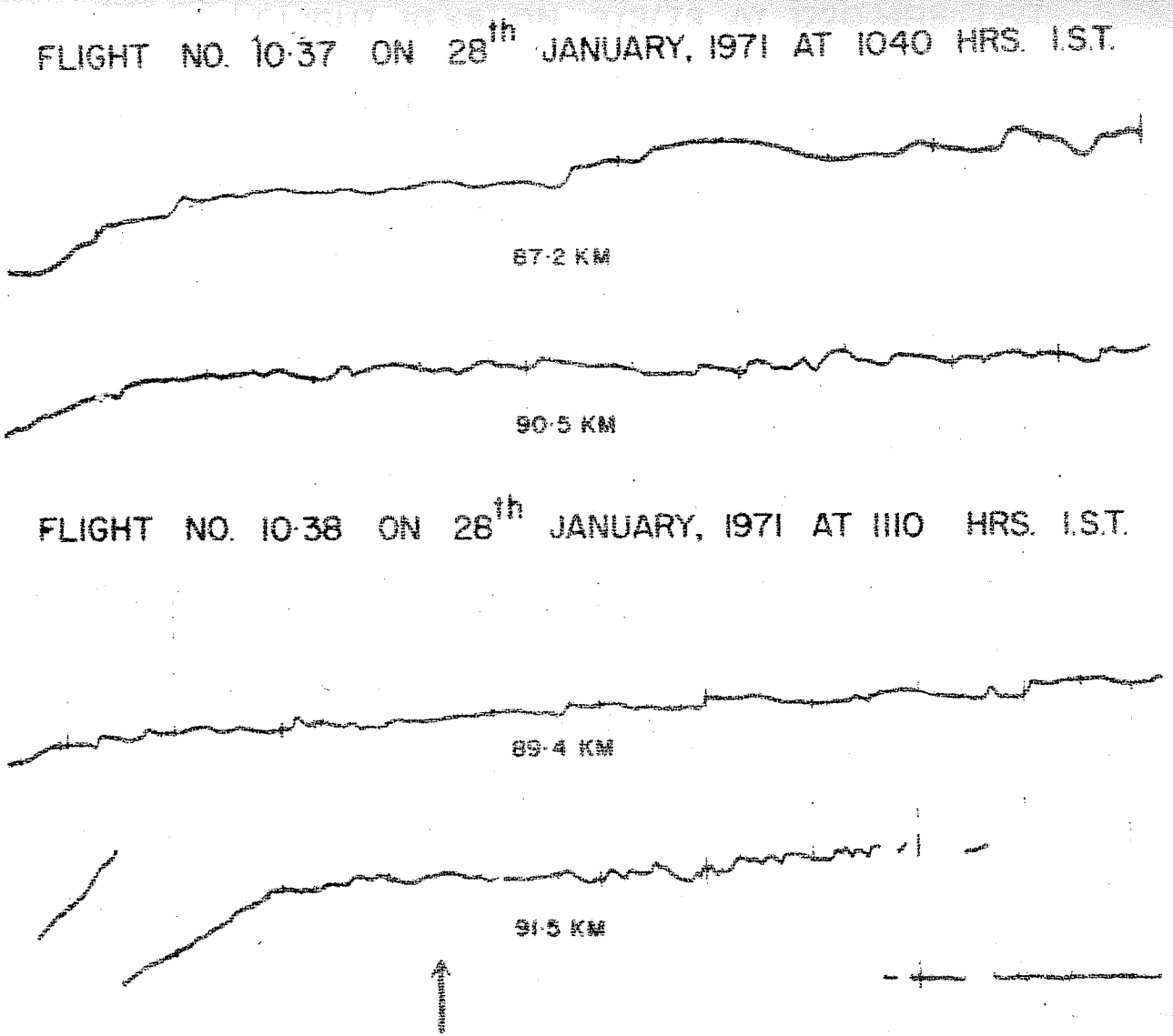

Fig. 442 Telemetry data of flights 10.37 and 10.38 (during ascent) showing the shape of the medium scale size CF irregularities. The arrow points towards the direction in which the density is increasing.

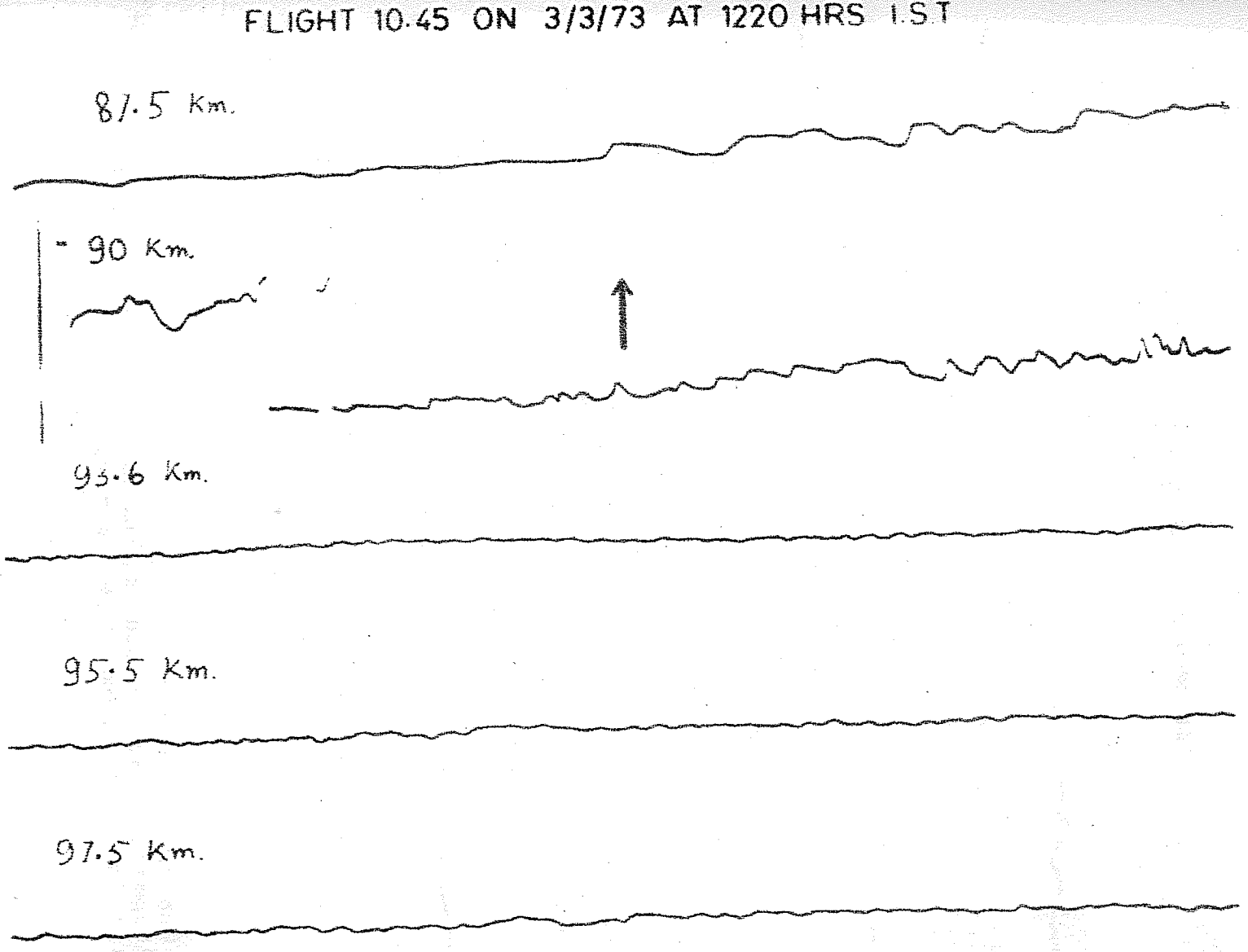

Fig. 4.13 Telemetry data of flight 10.45 (during ascent) at five different altitudes showing the shape of the medium scale size CF irregularities. The arrow points towards the direction in which the density is increasing.

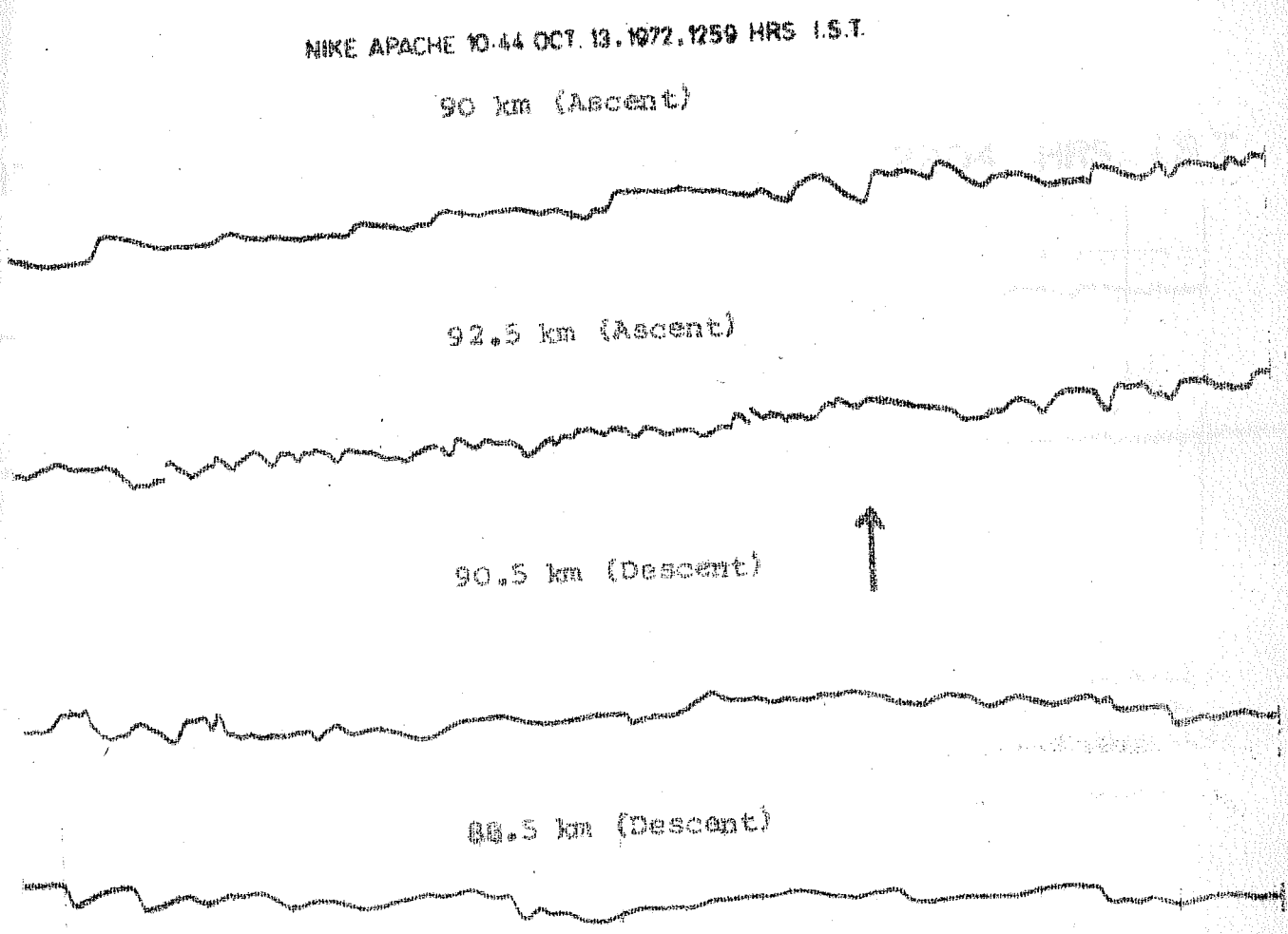

Fig. 4.14 Telemetry record of flight 10.44 during ascent and descent showing the shapes of medium scale size CF irregularities. The arrow points towards the direction in which the density is increasing.

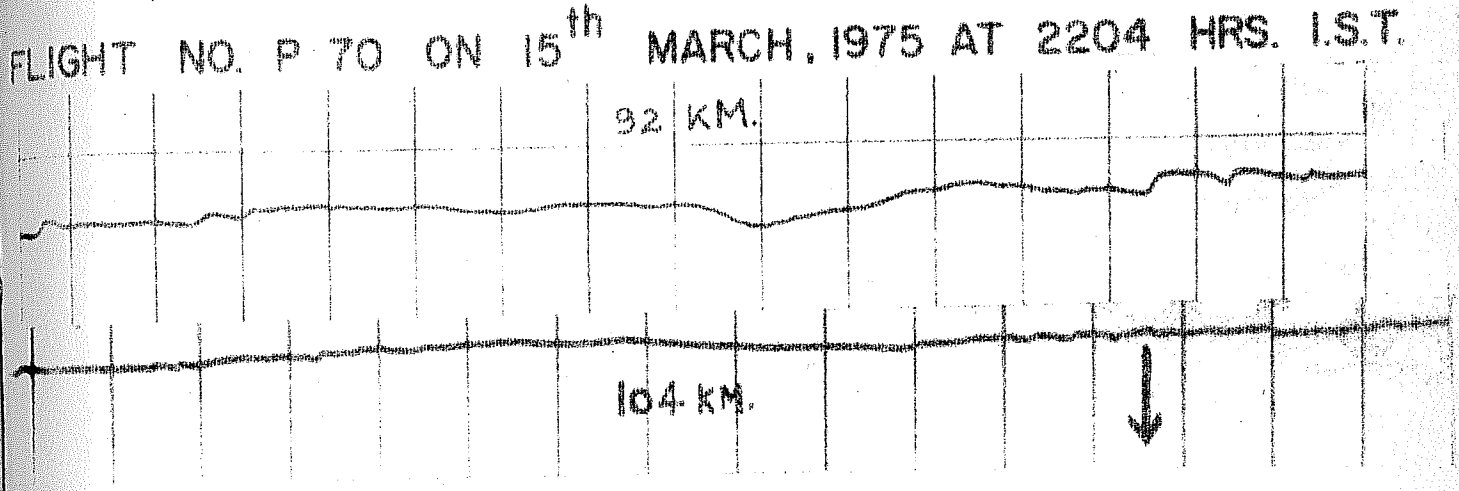

Fig. 4.15 Telemetry record of a nighttime flight P70 (during ascent) showing the shapes of medium scale size CF irregularities. The arrow points towards the direction in which the density is increasing.

ascent records at 90 and 92.5 km the rise in electron density is much sharper than the fall. It may be noted here that during the descent records at 90.5 and 88.5 km the fall in the electron density is much sharper than the rise.

Fig. 4.15 shows the telemetry records of a nighttime flight during the ascent of the rocket. Since the density is increasing in negative y-direction in both the records the orientations of the structures are such that the fall in the electron density is sharper than the rise.

c) Spectrum of Irregularities

For studying the spectra of irregularities power spectral density has to be estimated at different wave numbers. The procedure adopted for calculating the power spectral density from the main and duct channels has already been described in chapter III. It may be recalled that whenever the fluctuations in probe current were larger than about 10% the main channel data were used and in cases where fluctuations were smaller, duct data were used. For determination of spectral index, a power law of following type has been assumed

$$P(k) = C\, k^{n}$$

where $P(k)$ is the power contained in a wavenumber k, n is the spectral index and C is a constant.

The results of spectrum analysis from the main channel data of three different flight are shown in figs. 4.16 to

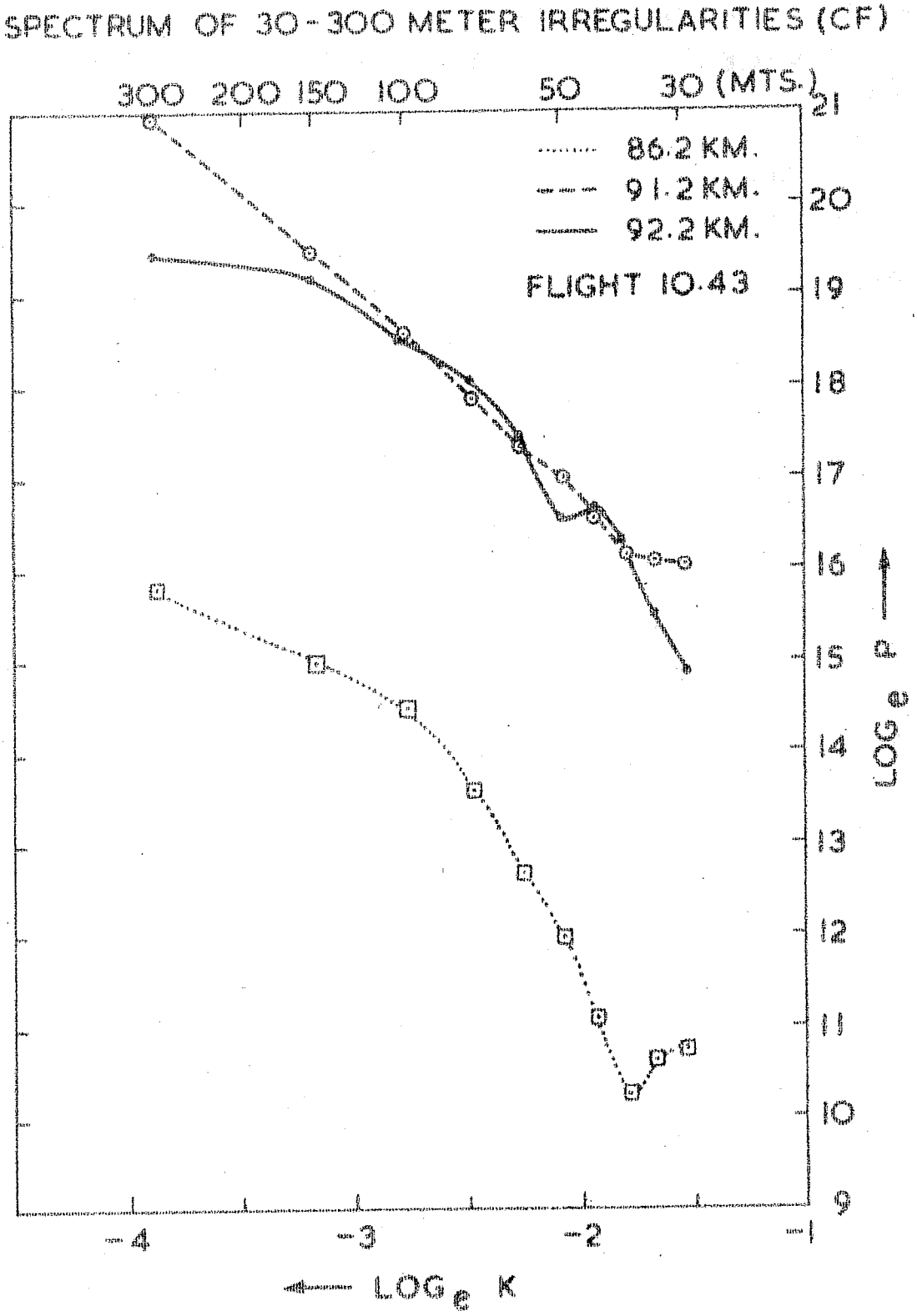

Fig. 4.16 Spectrum of type Mc at three different altitudes obtained from the main channel data of flight 10.43.

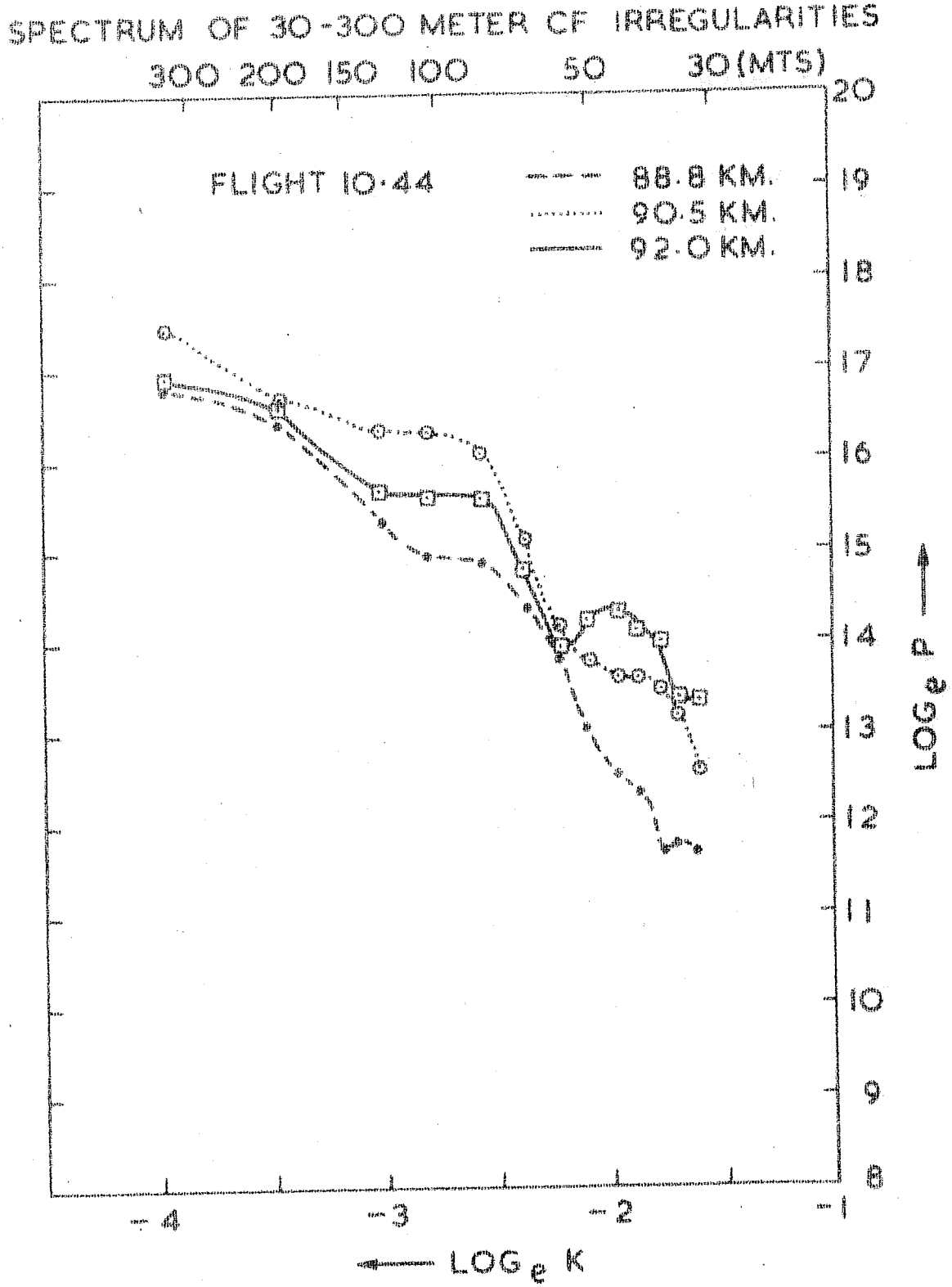

Fig. 4.17 Spectrum of type Mc at three different altitudes obtained from the main channel data of the flight 10.44.

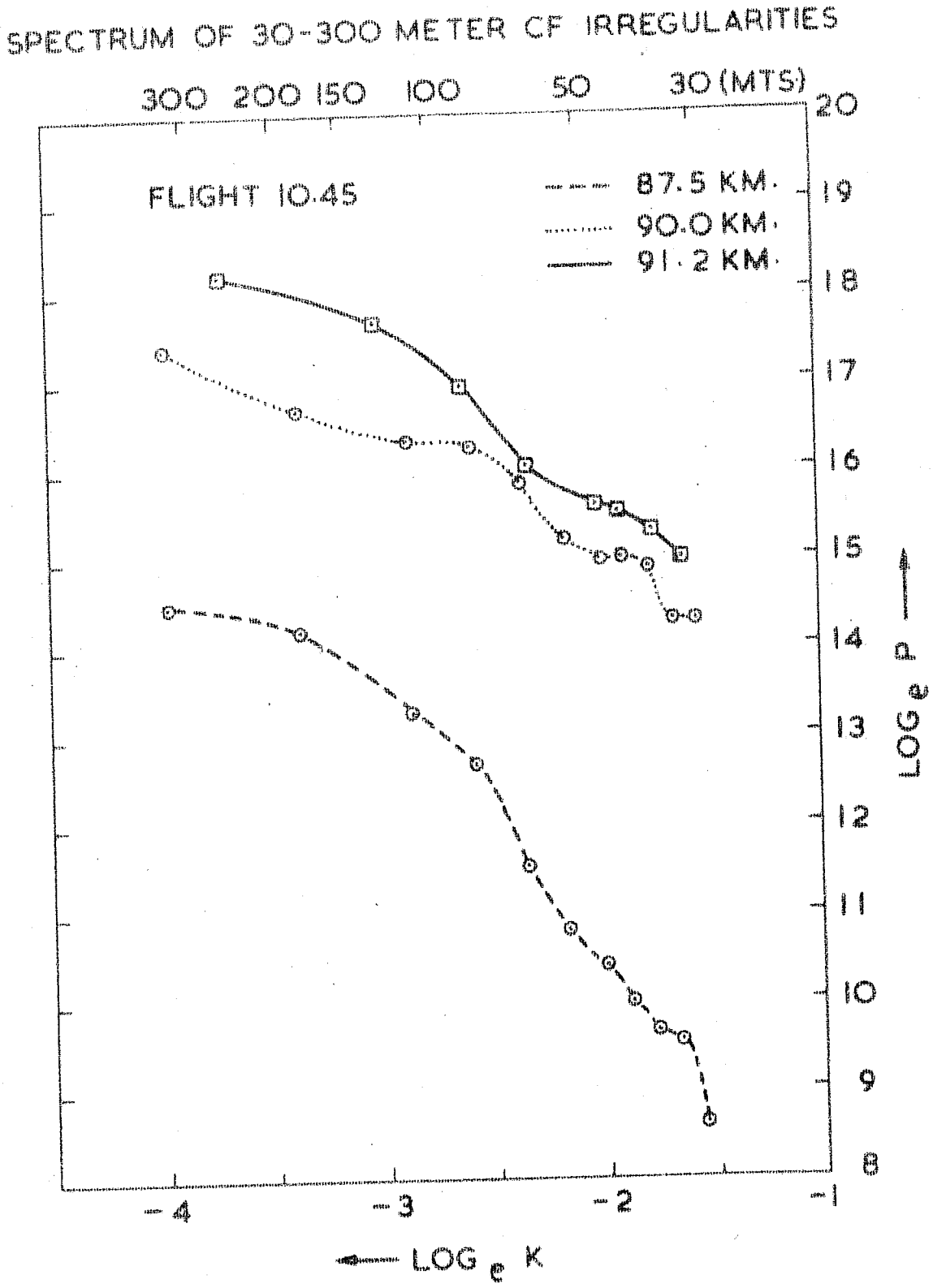

Fig. 4.18 Spectrum of type Mc at three different altitudes obtained from the main channel data of the first 10.45.

4.18. Natural logarithms of RMS power and wave number k have been plotted so that the slope of the spectrum can be seen directly on the plots. As seen from the figures there are two important points to be noted for the type M_c irregularities : (i) the power associated with all scalesizes is maximum around 90-91 km for all the three flights, (ii) with increasing altitude the spectrum becomes flatter. The only exception to the second point is the spectrum at 91.2 km during flight 10.45 which is slightly steeper as compared to the spectrum at 90.0. The flattening of spectrum is more clearly brought out in table IV.2.

Table IV.2

Spectral Index 'n' for Type M_c

Flight No. 10.43		Flight No. 10.44		Flight No. 10.45	
Altitude (km)	'n'	Altitude (km)	'n'	Altitude (km)	'n'
86.2	-2.64	88.8	-2.40	87.5	-2.60
91.2	-2.22	90.5	-2.11	90.0	-1.37
92.2	-2.00	92.0	-1.54	91.2	-1.65

As seen from the table the average spectral index for type M_c is -2.0 ± 0.7. The spectral results presented above were obtained from the main channel data. Now the results obtained from the duct channel data, which was available for flight 10.45, would be presented. Fig.4.19 to 4.21 show the spectrum of type M_c from 93.5 to 109 km.

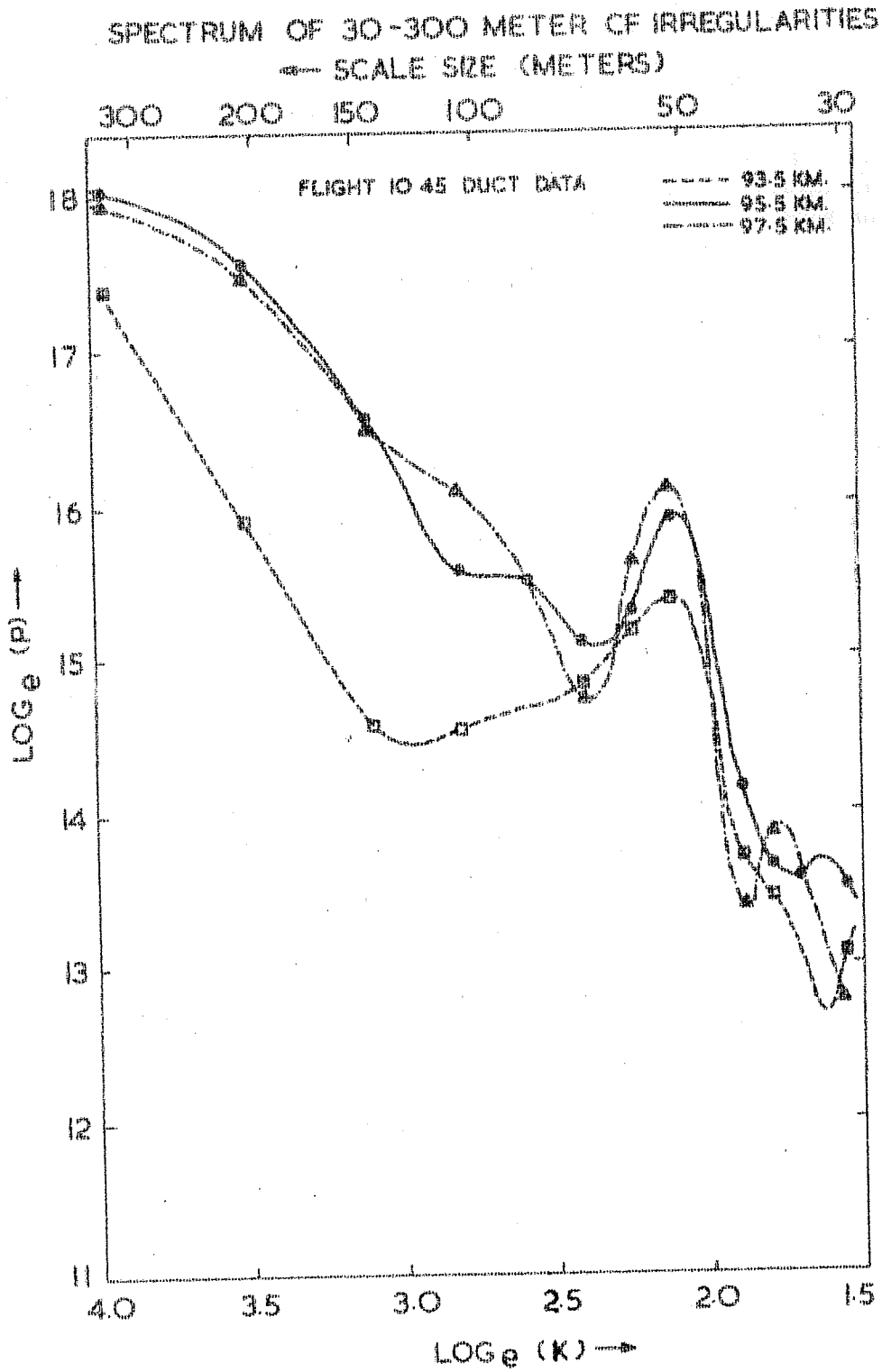

Fig. 4.19 Spectrum of the type Mc at three different altitudes obtained from the duct data of the flight 10.45.

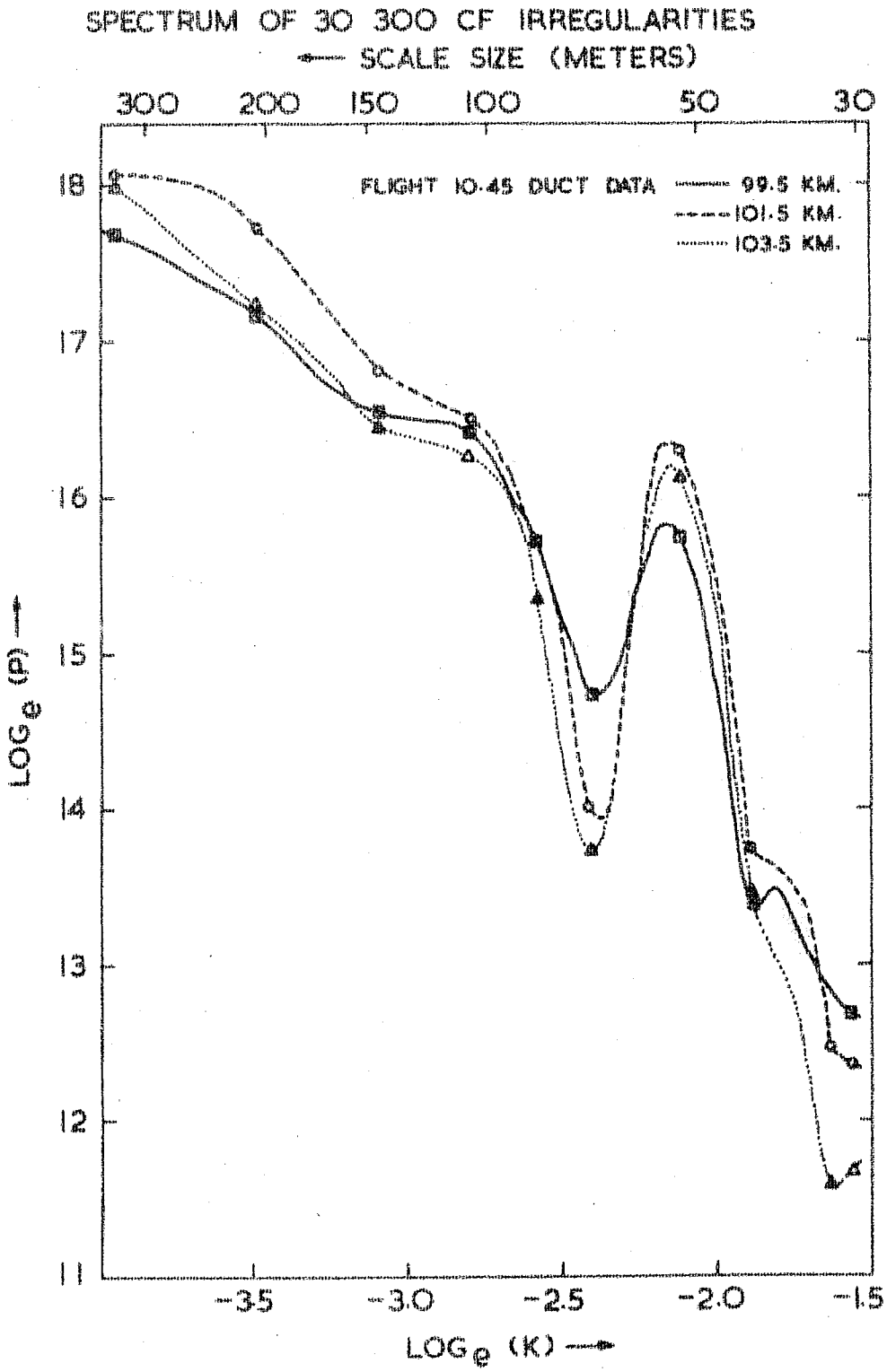

Fig. 4.20 Spectrum of type Mc at three different altitudes obtained from the duct data of flight 10.45.

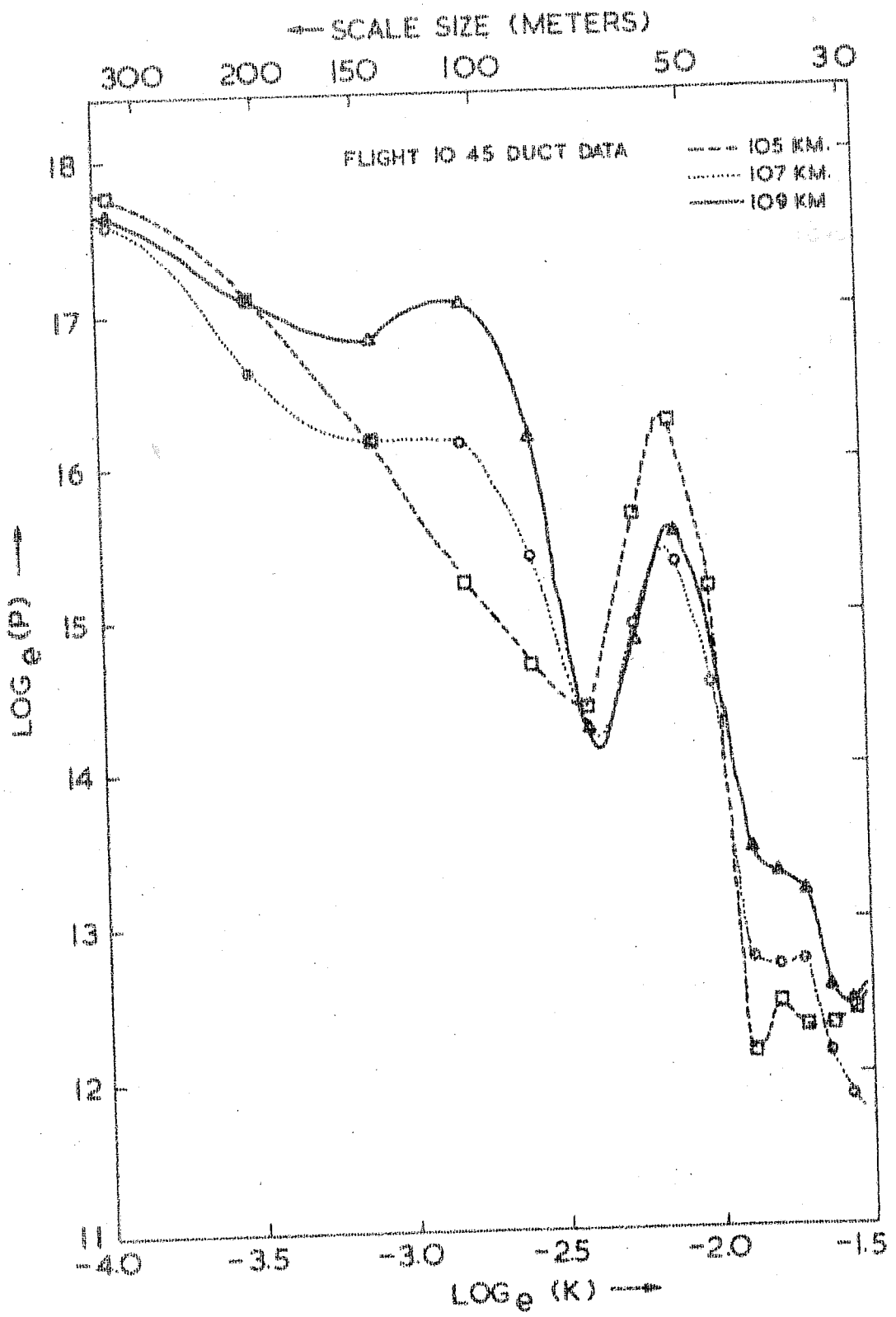

Fig. 4.21 Spectrum of type Mc at three different altitudes obtained from the duct data of flight 10.45.

It can be seen from fig. 4.19 that at 93.5 km the power drops down rapidly from 300 meters to about 150 meters below which there is a peak at 52.5 meters. Above 93.5 km the variation of power is nearly similar upto about 105 km beyond which there is a peak around 100 meters at altitude of 107 and 109 km. In all the figures 4.19 to 4.21 there is a distinct dip at 70 meters where smallest power is seen. The peak at 52.5 meters observed at 93.5 km goes on building till 105 km beyond which it starts becoming less prominent. The peak at 52.5 meters incidently corresponds to ion cyclotron frequency. The peaking at ion cyclotron frequency is seen prominently around those regions where electrojet currents peak.

d) Amplitude of Irregularities

In order to see the variation of percentage amplitude of a particular scalesize with altitude, the data for four arbitrarily chosen scalesizes namely 50, 75, 100 and 150 meters were analysed. The data of two daytime flights were chosen for such study. The RMS power at any desired wavelength is picked up from the spectrum analysis data and is converted into percentage amplitude.

Fig. 4.22 shows the variation of percentage amplitude of four scalesizes mentioned above. Beyond 97.5 km amplitudes were small and hence were not plotted. It can be clearly seen

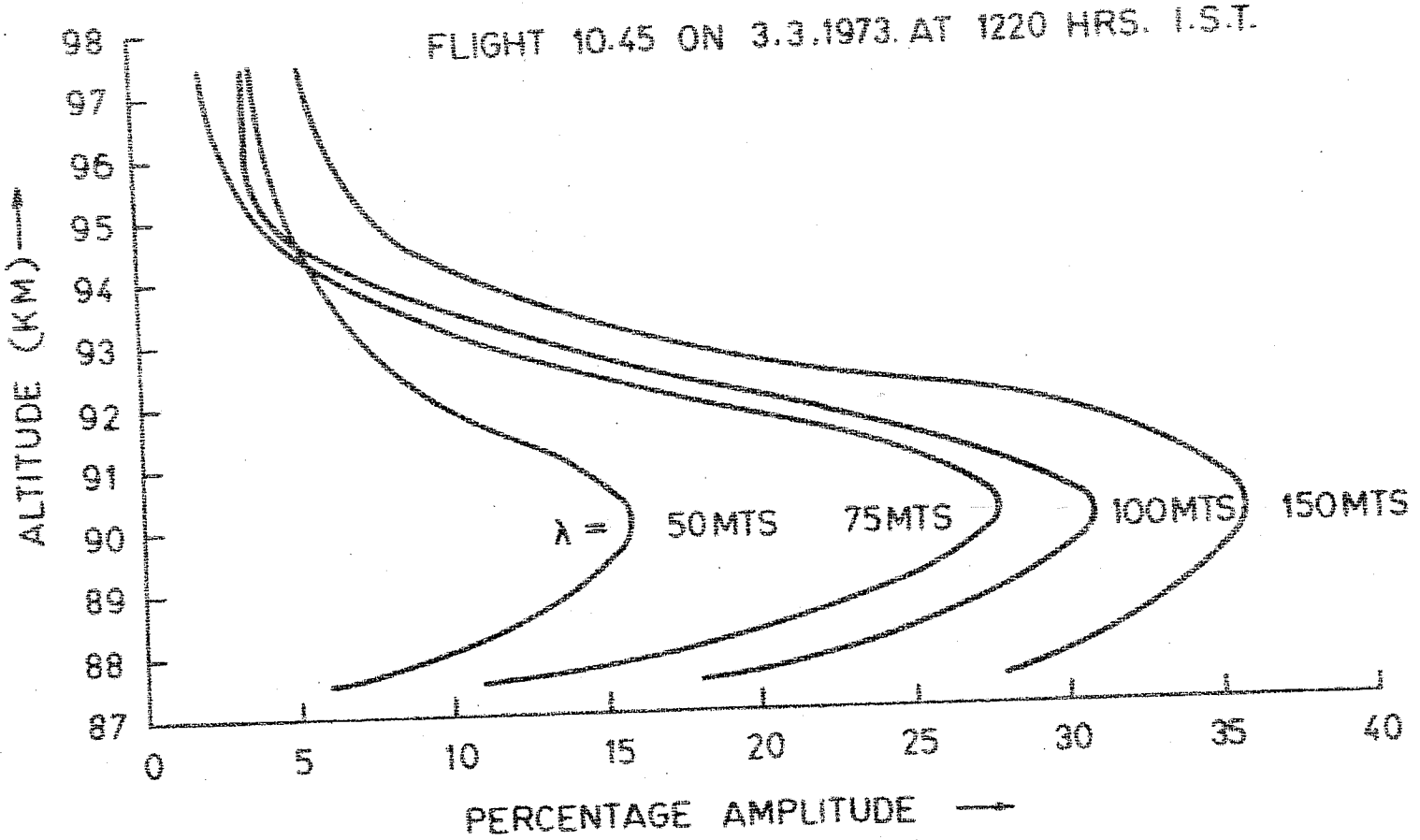

Fig. 4.22 Variation of percentage amplitude with altitude for four different scale sizes, produced by cross-field instability mechanism during flight 10.45.

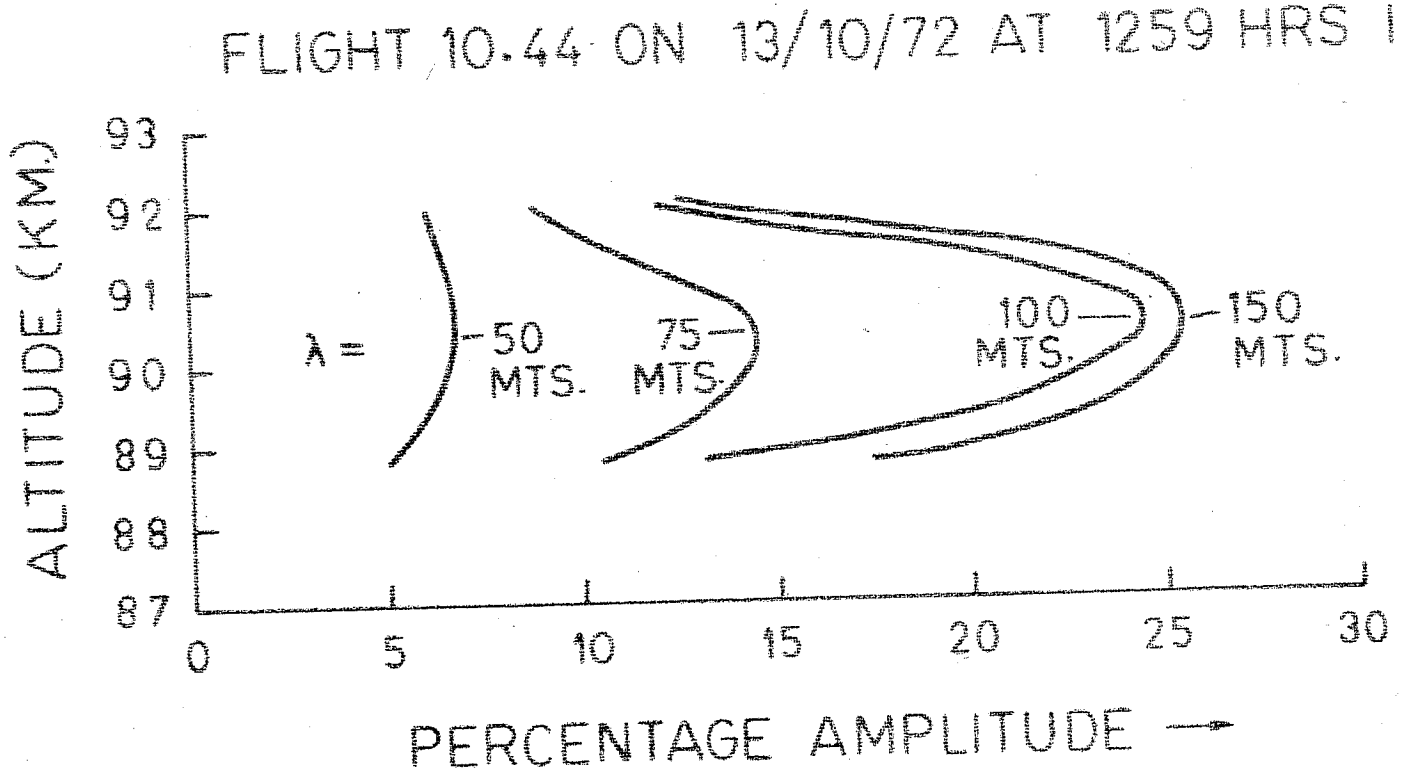

Fig. 4.23 Variation of percentage amplitude with altitude for four different scale sizes, produced by cross-field instability mechanism during flight 10.44

that all the four scalesizes behave in a similar fashion. Peak amplitude is observed around 90 km for all the scalesizes. Above 90 km the reduction in percentage amplitude is more pronounced for 75 and 100 meter scalesizes. Fig. 4.23 shows the similar plot for another daytime flight. Since this flight (10.44) did not have any duct amplifier onboard, the data beyond 92 km could not be obtained because of the smallness of the amplitudes above this height. It can be seen that the general behaviour of percentage amplitude is similar during both the flights. It may be noted here that in both the cases, the percentage amplitude peaks around 90 km for all the scalesizes.

e) Variation of Prominent Scalesize with Altitude

If one looks back at figs. 4.12 to 4.15 it can be ascertained at every given altitude region there is a most prominent scalesize. In order to see the variation of most prominent scalesize, mathematically, a simple zero crossings technique was employed. Since the technique is described in chapter III only the results are reported here. Table IV.3 shows the most prominent scalesizes at three different altitudes as observed on flight 10.45.

It can be seen from the above table that the most prominent scale is smallest at 90 km in all the three cases where moving averages are taken over 200, 250 and 300 meters. On an average the most prominent scalesizes at 87.5, 90 and 91.2 km are 189, 70 and 85 meters, respectively.

The evaluation of most prominent scalesize can also be made by using a simple visual method. On the telemetry chart one visually sees the combined effect of of frequency and the amplitude and hence a plot of A^2K versus K would give the visually prominent scalesize. Fig. 4.24 shows such plots at five different altitudes during flight 10.45. At 87.5 km the parameter A^2K peaks at a wavenumber which corresponds to 166 meter scalesize. At 90 km, 83 meters is the most prominent scalesize and 40 meters is the next prominent scalesize. At 91.2 km the most prominent scalesize is 130 meters.

Thus the results of zero crossings technique and visual method show that the most prominent scalesize is largest at 87.5 km, smallest at 90 km and is again large at 91.2 km. The irregularity data, of type M_c obtained on many other flights also suggest that the most prominent scalesize at 90 km altitude is smallest as compared to most prominent scalesizes in regions above and below this altitude.

4.3.2 Irregularities in 1-15 Meter Scalesize Range (Small scale Cross-field-type S_c)

a) Regions of Occurrence

These irregularities usually co-exist with type M_c. The regions of occurrence of type S_c as observed on seven rocket flights, which typically represent early morning, morning, noon, evening, and nighttime, are given in Table IV.4.

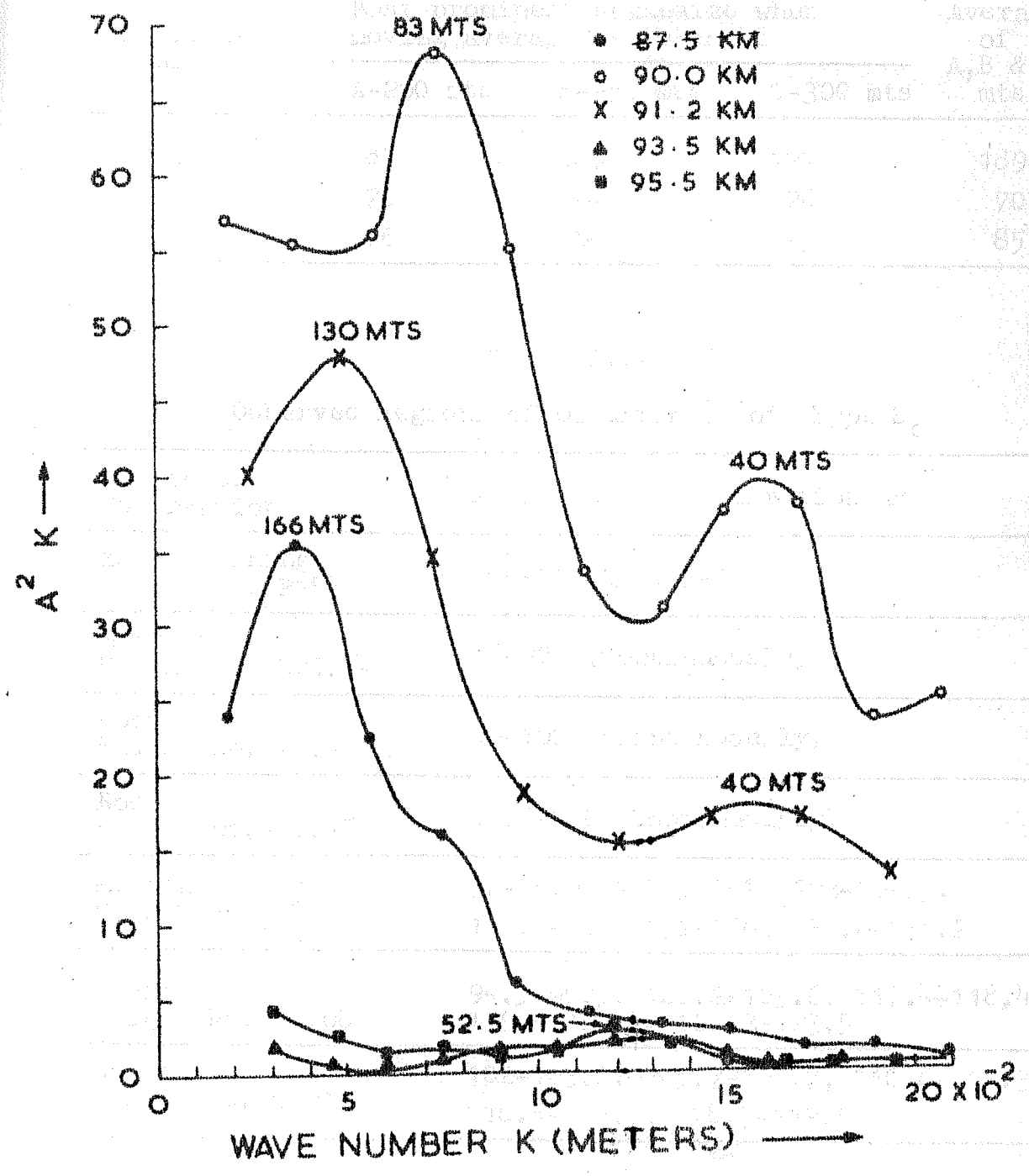

Fig. 4.24 Variation of visual index parameter A^2K versus K for flight No. 1045 at five different altitudes.

Table IV.3

Altitude Km.	Most prominent scalesize when moving average is taken at			Average of A,B & C mts
	A-200 mts	B-250 mts	C-300 mts	
87.5	185	185	197	189
90.0	70	64	76	70
91.2	76	84	95	85

Table IV.4

Observed Regions of Occurrence of Type S_c

Period of Observation	Altitudes of Observation Km.
Early morning Flight No. P158	110-112.2, 115-116
Morning Flight No. C05.14	86-97 (Continuously)
Noon Flight No. 10.44	90-100 (Continuously)
Noon Flight No. 10.45	90.8-100 (Continuously)
Evening Flight No. 10.13	97-98.8, 100.5-102, 103-104.5, 105.5-107, 132-134, 135.8-138.2
Night Flight No. 20.08	94.5-96.5, 102.2-103.6, 117.4-118.4 119.6-120.7, 122.3-123.5
Night Flight No. C-21	102-103.2, 105.7-107.7, 110.8-113.3 116.5-117.5, 118.5-119.5

It can be seen from the table IV.4 that like type M_c, type S_c are observed continuously between 86 to 100 km during morning and noon hours. At other times these irregularities are also

observed in isolated regions. The extent of these isolated regions varies from 110 to 116 km during early morning hours, and 100 to 120 km during nighttime. During evening time the irregularities are observed in isolated regions below 105 km and around 135 km.

While the amplitude of type M_c is as large as 35% the amplitude of type S_c is at best a few percent. Since these irregularities appear as high frequency fluctuation on the telemetry chart their shape could not be studied.

b) Spectrum of Irregularities

For studying the spectrum of these irregularities an eight channel spectrum analyser was used. The central frequency of the upper most channel (highest frequency), falls beyond the intelligence bandwidth of 70 KHz SCO channel and, therefore, the data from this channel was not used for estimating the value of spectral index 'n'. The procedure for arriving at the RMS power has been described earlier in chapter III. Fig. 4.25 and 4.26 show A.C. spectrum analyser outputs at eight different altitudes for a typical daytime flight No.10.44. Channel No.1, which is on the topside in both the figures, shows the composite signal whereas channels 2 to 8 show the output of seven filters in order of increasing centre frequency. It can be seen from fig. 4.25 that at 90 and 94.5 km there is hardly any signal in high frequency channels. Around 97.5 km

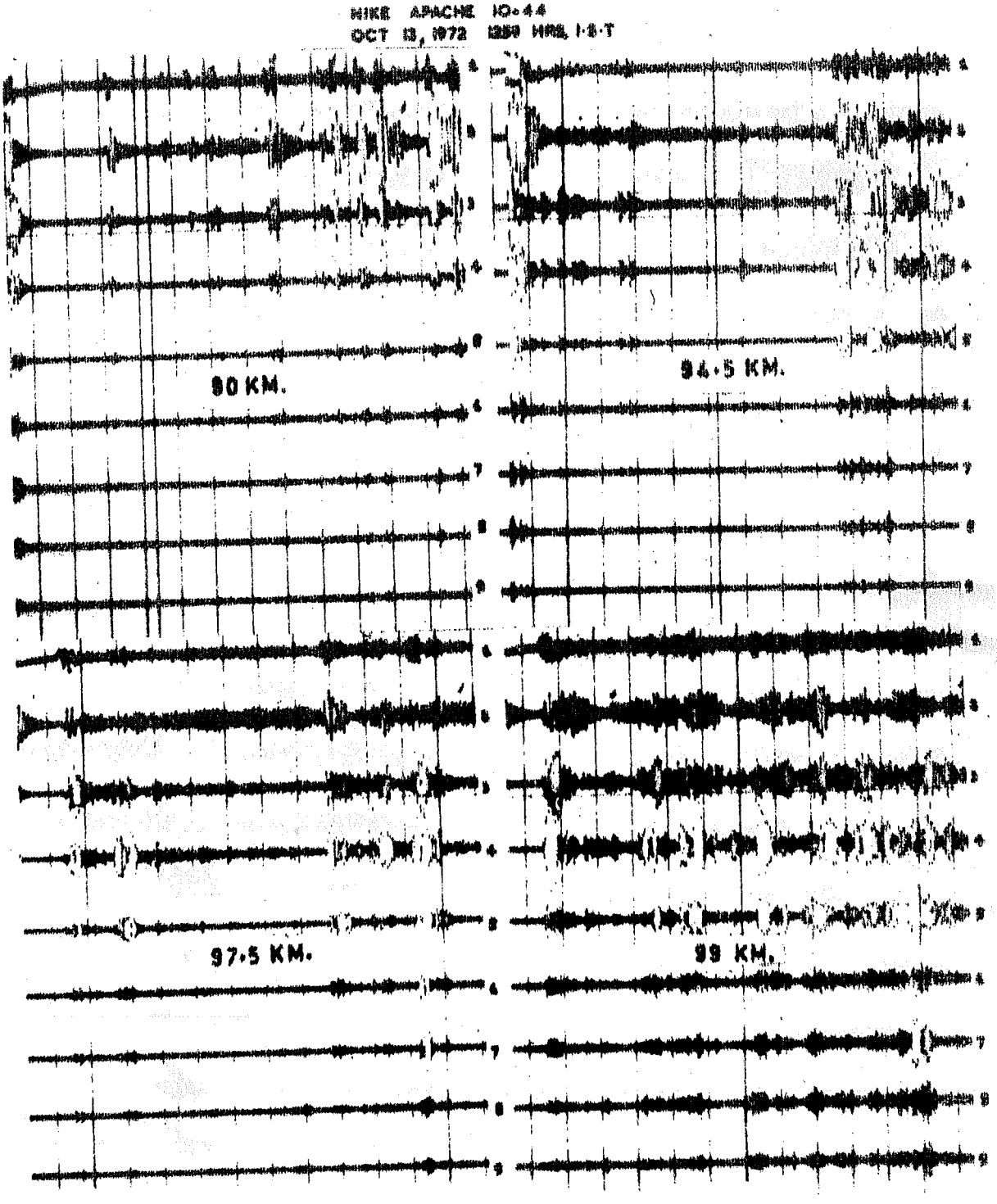

Fig. 4.25 Spectrum analyser records at 90, 94.5, 97.5 and 99 km for 1-15 meter irregularities produced through cross-field instability mechanism during flight 10.44.

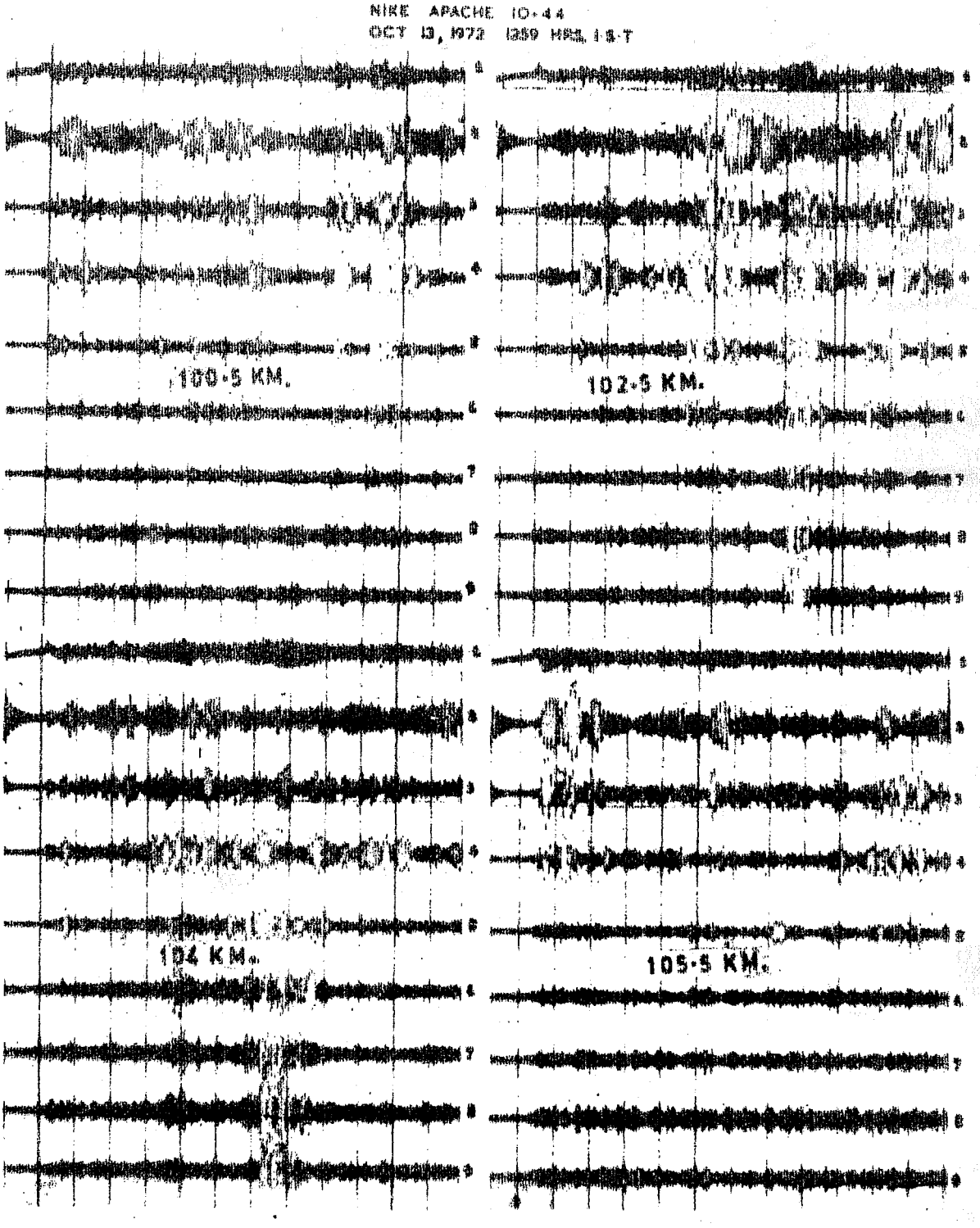

Fig. 4.25 Spectrum analyser records at 100.5, 102.5, 104 and 105.8 km for 1-15 meter irregularities produced through crossfield instability mechanism during flight 10.44.

the high frequency channels show up very weak signal and by the time altitude of 99 km is reached the signals in the high frequency channels have become substantially strong. Fig.4.26 shows the next four consecutive cycles. At 100.5 and 102.5 km although the signal in the high frequency channels is quite strong it is still less than the corresponding low frequency signal. Beyond 102.5 km the signal of S_c irregularities is mixed with the signal of another type of irregularity, characterized by type S_s, which is believed to be generated due to streaming of electrons (Prakash et al., 1973). Type S_s irregularities have maximum amplitude around 105 km, an altitude characterized by peaking of the electrojet currents. The properties and conditions of generation of type S_s irregularities have been discussed by Prakash et al. (1971c, 1973) and Rao (1976). Since the signal of type S_s is much stronger than that of type S_c at 105 km during daytime, type S_c cannot be studied in pure form around this altitude.

Fig. 4.27 shows the A.C. spectrum analyser output of S_c irregularities at 96 km during another daytime flight, No. 10.45. In this case also the topmost channel shows the composite signal and the next eight channels are the filter outputs. The last channel shows the main channel output also. In the main channel one can clearly see the zeromarker. The data near the zeromarker should be ignored for all channels. The total record length is nearly 2 km and the spacing between

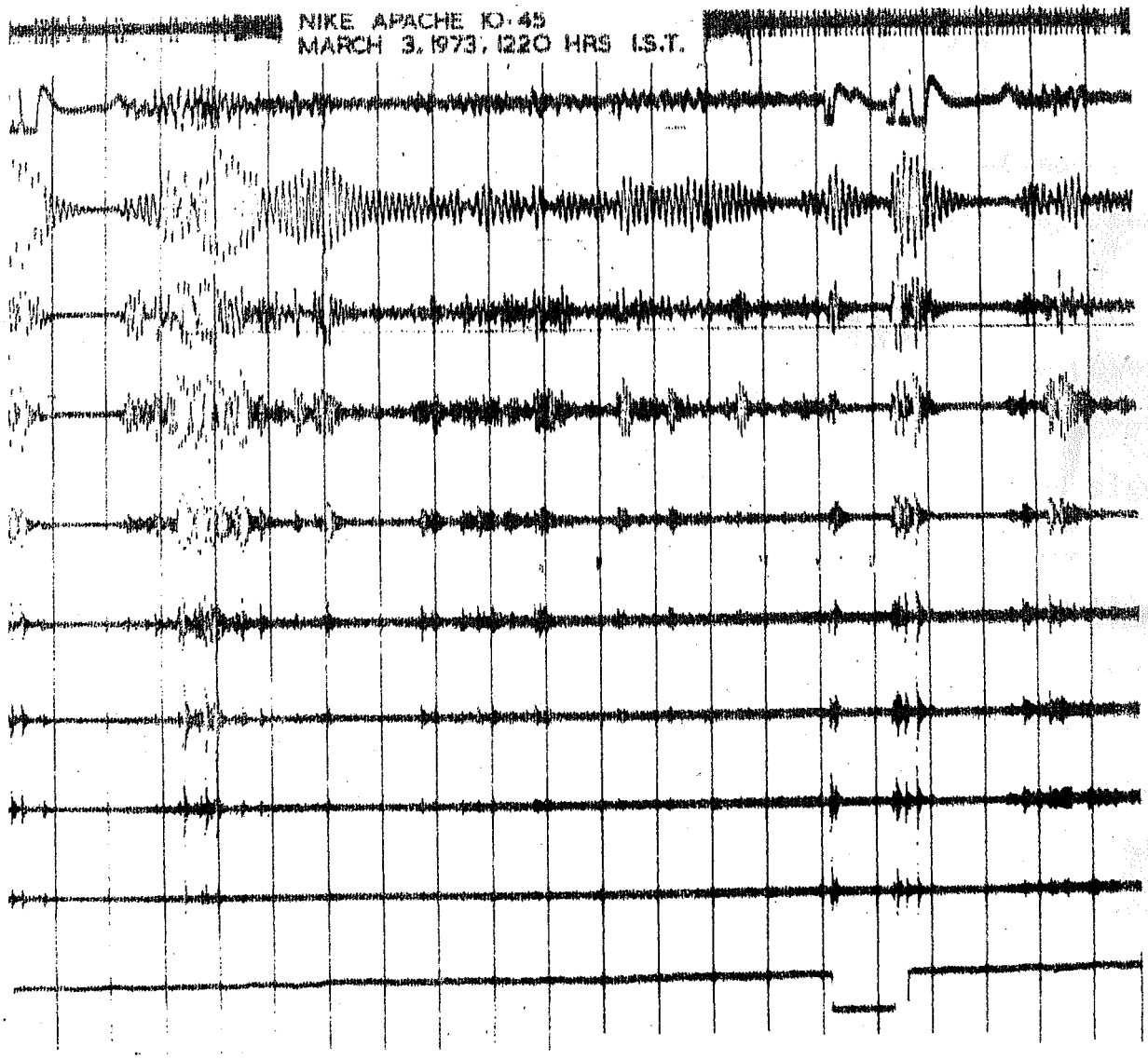

Fig. 4.27 Spectrum analyser record at 96 km for 1-15 meter irregularities produced through cross-field instability mechanism during flight 10.45.

two vertical lines is about 100 meters. The important point to note here is that the change of amplitude from low frequency channel to high frequency channel does not follow the same pattern for all irregularities. The nature of irregularities is highly variable and it is likely that these represent various phases of growth and decay of irregularities.

In order to get the quantitative estimate of the power associated with each wavenumber, the eight filter outputs were rectified with a time constant of 0.2 sec. The rectified signal was used to estimate the RMS power in arbitrary units. The details of the procedure adopted are given in chapter III. Since the output of only seven filters was usable and the centre frequency of lowest filter was slightly shifted to the lower side, the range of scalesizes which could be studied is 2 meters to 17 meters. Since this band of 2-17 meters also falls in the category of small scale irregularities this is discussed under the heading 1-15 meter irregularities.

Table IV.5 shows the RMS POWER at each wave number for eight different altitudes during flight 10.44. The power given in table IV.5 is plotted in figures 4.28 and 4.29. It can be seen from the table IV.5 and figs. 4.28 and 4.29 that at all the altitudes power is concentrated mainly in higher wavelengths and drops off rapidly towards smaller wavelengths. And also the spectra become flatter with increasing altitude.

Table IV.5

Power spectral density estimates for small scale CF irregularities
Type S_c

Flight No. 10.44 Date: 13.10.1972 Time of Flight - 1259 hrs IST

Wave Number METER^{-1}	Scale Size METERS	Power Spectral Density in Arbitrary Units at							
		90.5 KM	91.6 KM	92.8 KM	94.1 KM	95.4 KM	96.0 KM	97.9 KM	99.1 KM
0.3644	17.24	6877.2	3087.9	2889.3	878.8	1039.7	2154.0	3087.9	7384.7
0.5194	12.10	517.3	128.9	227.9	200.2	108.8	150.8	305.6	703.7
0.7330	8.57	117.9	31.5	74.3	87.4	46.5	117.9	258.7	309.9
1.0807	5.81	10.0	10.0	18.5	10.0	5.5	17.4	89.2	212.1
1.5080	4.17	3.9	1.6	3.9	3.1	1.1	4.8	18.0	67.1
2.1656	2.90	1.2	1.2	2.2	1.6	0.3	1.6	7.8	28.3
3.0830	2.04	0.8	0.8	1.1	0.6	0.3	0.3	4.2	21.2

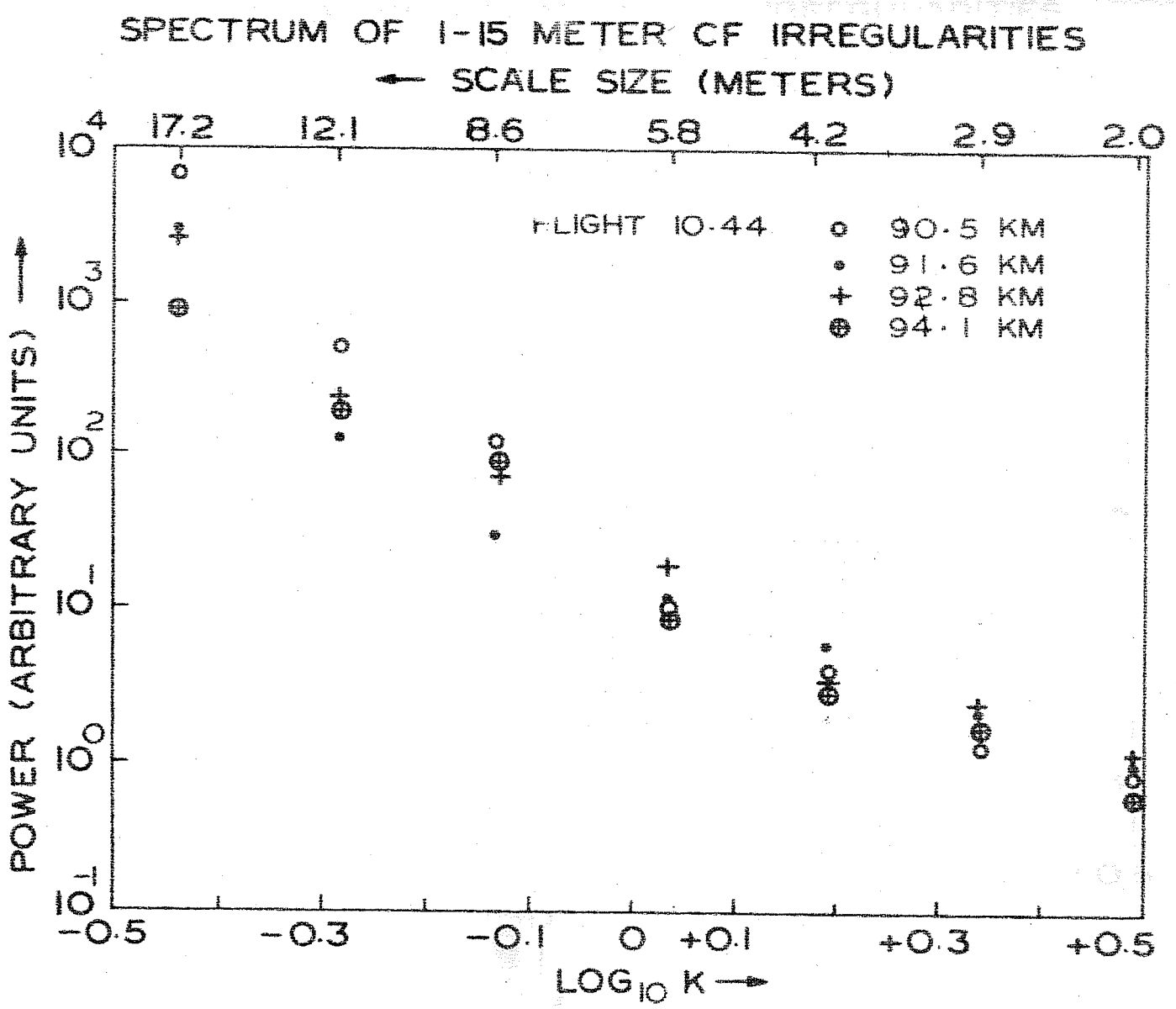

Fig. 4.28 Spectrum of type Sc at four different altitude obtained from the spectrum analyser data of flight 10.44.

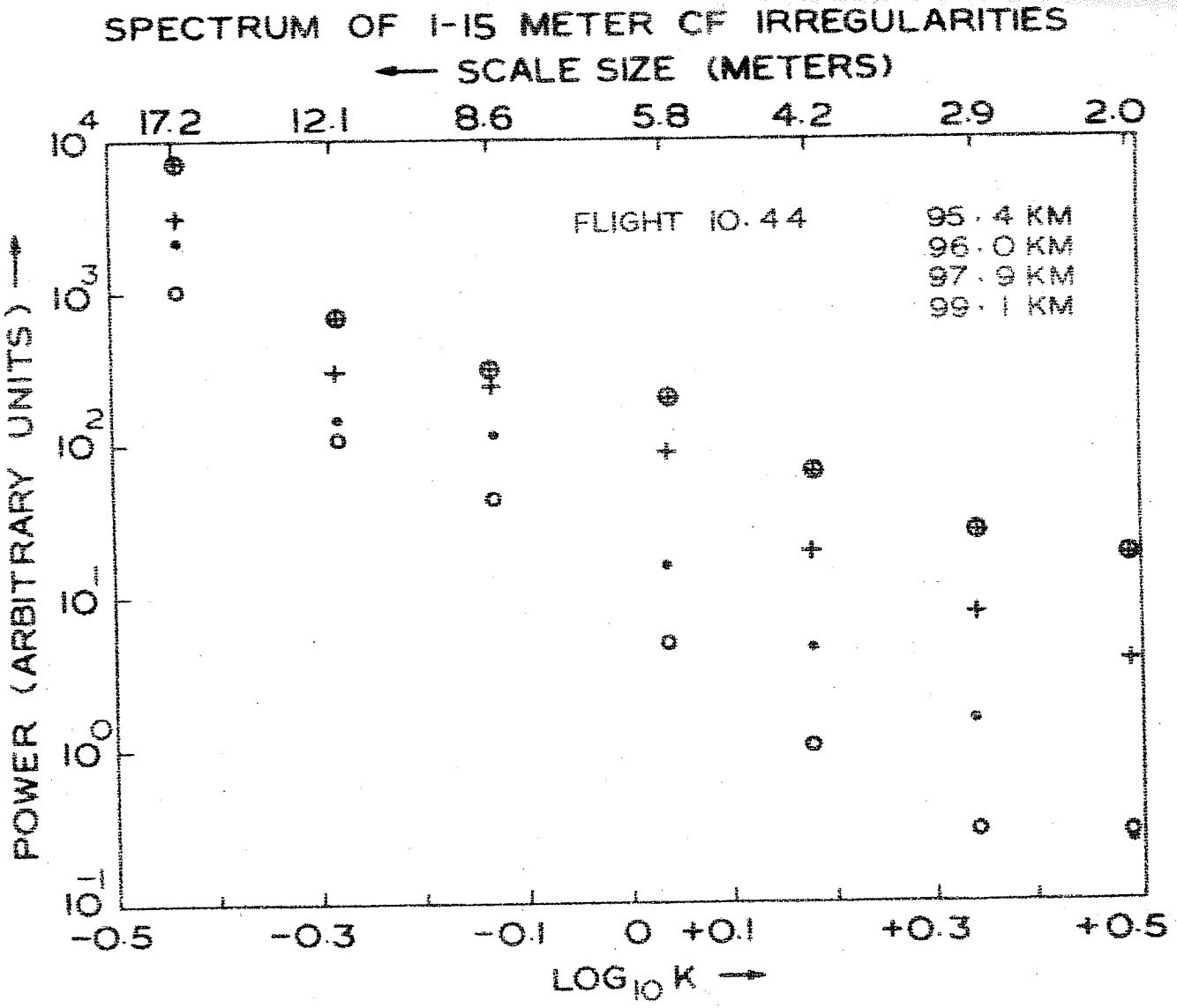

Fig. 4.29 Spectrum of type Sc at four different altitudes obtained from the spectrum analyser data of flight 10.44.

The flattening of spectrum of type S_c can be seen more clearly from table IV.6. Power spectral estimates for

Table IV.6

Flight 10.44 - Spectral Index of S_c

Altitude Km	Spectral Index 'n'	Altitude Km	Spectral Index 'n'
90.5	-4.3	95.4	-3.9
91.6	-3.7	96.0	-3.9
92.8	-3.6	97.9	-3.0
94.1	-3.5	99.1	-2.5

another daytime flight are given in table IV.7. During this flight the spectrum of type S_c was much steeper than that during flight 10.44 with the result that the signal in higher frequency channels was too small to be read accurately. In this case only four filter outputs were usable and hence the spectrum was evaluated by using only four scalesizes. The values given in table IV.7 are plotted in figs. 4.30 and 4.31. As seen in table IV.7 and IV.5 it might appear that the power is more in case of flight No. 10.45, especially at lower wavelengths, but one must remember that the power estimates are in arbitrary units and as such the data of both the

Table IV.7

Power Spectral Density Estimates for Small Scale CF Irregularities - Type S_c

Flight No. - 10.45 Date - 3.3.1973 Time of Flight - 1220 Hrs IST

Wave Number METERS^{-1}	Scale Size METERS	Power Spectral Density in Arbitrary Units at							
		90.8 KM	91.4 KM	92.3 KM	93.1 KM	94.2 KM	96.1 KM	96.6 KM	97.7 KM
0.3644	17.24	11591.7	6877.2	2222.9	14610.1	6315.7	3926.6	345.0	2889.3
0.5194	12.10	819.2	495.9	213.7	623.0	604.4	200.2	65.1	135.3
0.7330	8.57	244.7	231.0	74.3	471.5	192.1	231.0	68.3	273.1
1.0807	5.81	39.1	- *	- *	60.9	- *	18.5	3.7	34.8

* Data not clear.

flights cannot be compared. The general trend of the spectrum as seen from fig. 4.30 and 4.31 is similar to the trend shown during flight No. 10.44. The spectrum has a tendency to become flatter with altitude; this becomes more evident from the spectral index values listed in table IV.8.

Table IV.8

Flight No. 10.45 - Spectral Index of S_c

Altitude Km	Spectral Index 'n'	Altitude Km	Spectral Index
90.8	-5.1	94.2	-5.0
91.4	-4.9	96.1	-4.4
92.3	-4.9	96.6	-3.8
93.1	-4.9	97.7	-3.7

As seen from table IV.6 and IV.8 it appears that the spectral index for type S_c is best represented by a range of -4 ± 1.

4.4 Ionization Irregularities Produced Through Neutral Turbulence Mechanism

These irregularities were mostly observed in the region below 80 km. The observations of irregularities were again confined to 30-300 and 1-15 meters bands. The results of both these bands which represent medium and small scale

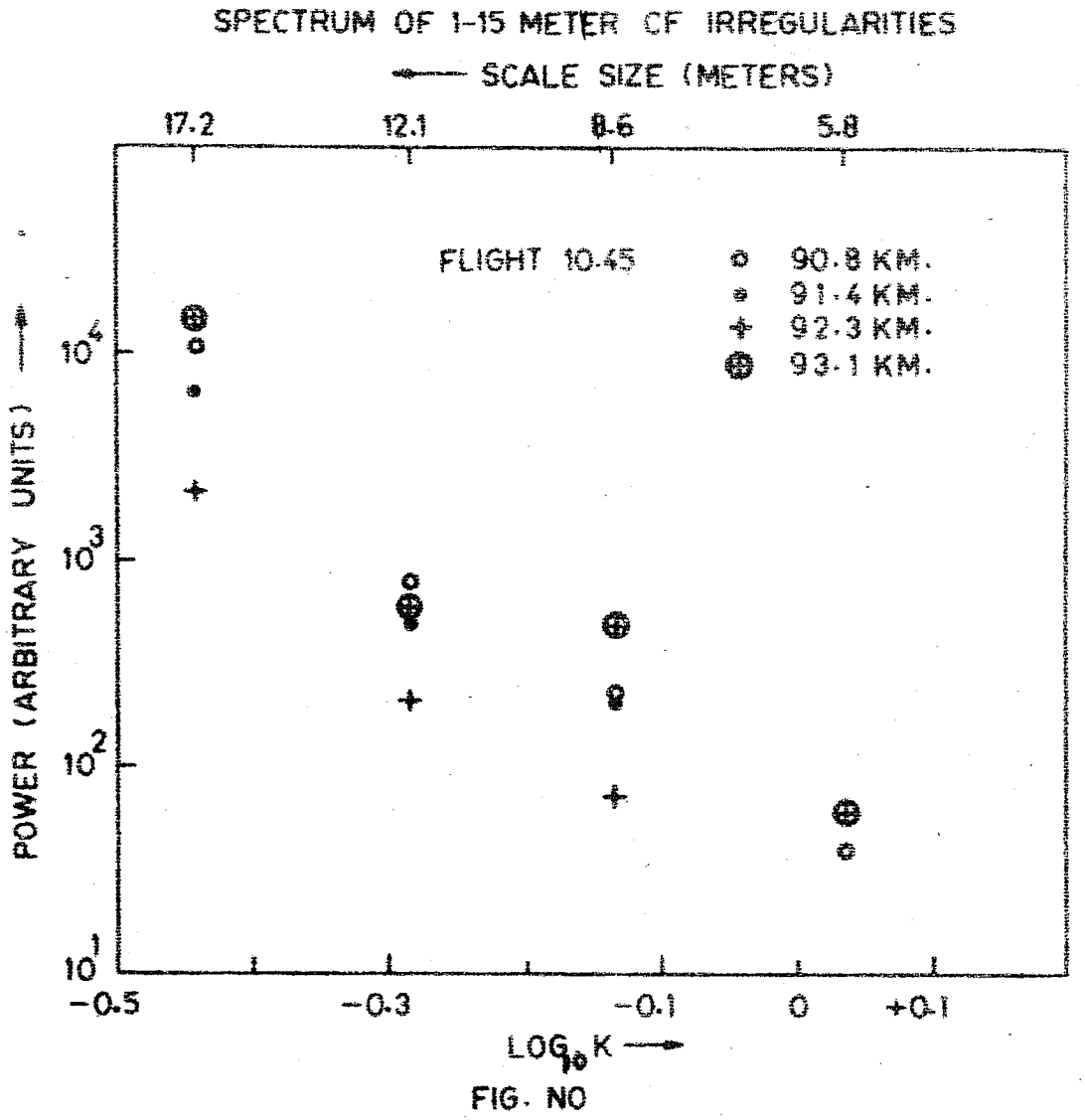

Fig. 4.30 Spectrum of type Sc at four different altitudes obtained from the spectrum analyser data of flight 10.45.

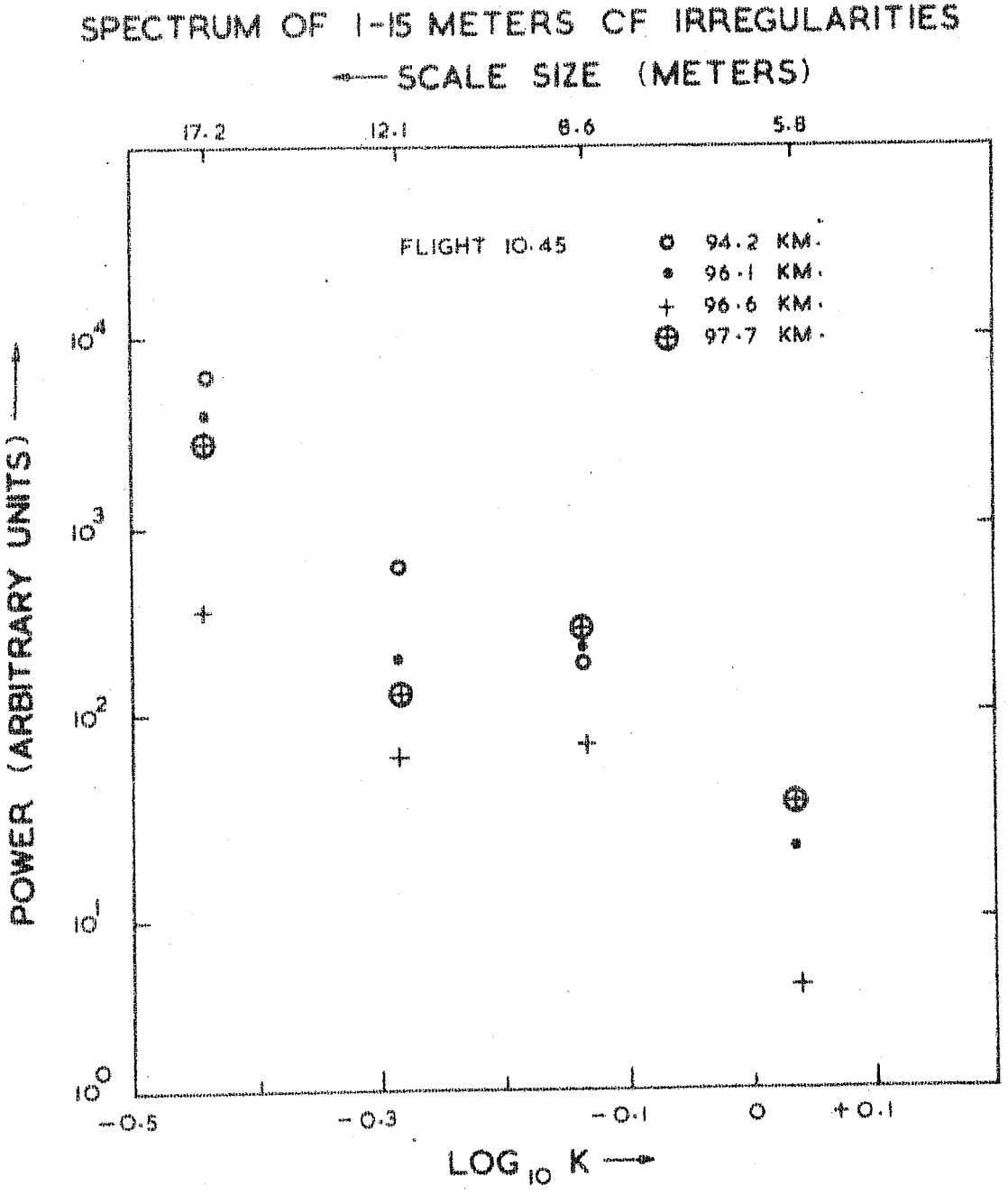

Fig. 4.31 Spectrum of type Sc at four different altitudes obtained from the spectrum analyser data of flight 10.45.

irregularities, believed to be generated through neutral turbulence mechanism, are reported here.

4.4.1 Irregularities in 30-300 Meter Scalesize Range (Medium Scalesize Neutral Turbulence - Type Mn)

These irregularities can be seen on the main channel of the L.P. output when their amplitude is applicable ($\geq$ 10%) and on duct amplifier channel when their amplitude is small. The amplitude of these irregularities is larger in the lower altitude region and is smaller in higher altitude region. Around 60-70 km the maximum amplitude varies between 10 to 15% whereas around 80 km region the amplitudes are about 4-7%.

These irregularities were always observed during daytime and were never observed on any of the evening or nighttime flights. Even during daytime these irregularities were not observed on all of the flights. The maximum vertical extent of these irregularities is about 4-5 km. Before the development of the duct amplifier an extent of a kilometer or so could only be observed because smaller amplitudes could not be seen on the main channel record.

Fig. 4.32 shows the main channel (1) the duct channel (2) and the composite noise channel (3) records at 77.2 Km during flight 10.45. Channel Nos. 1 and 2 refer to 30-300 meter irregularities and channel No.3 refers to 1-15 meters

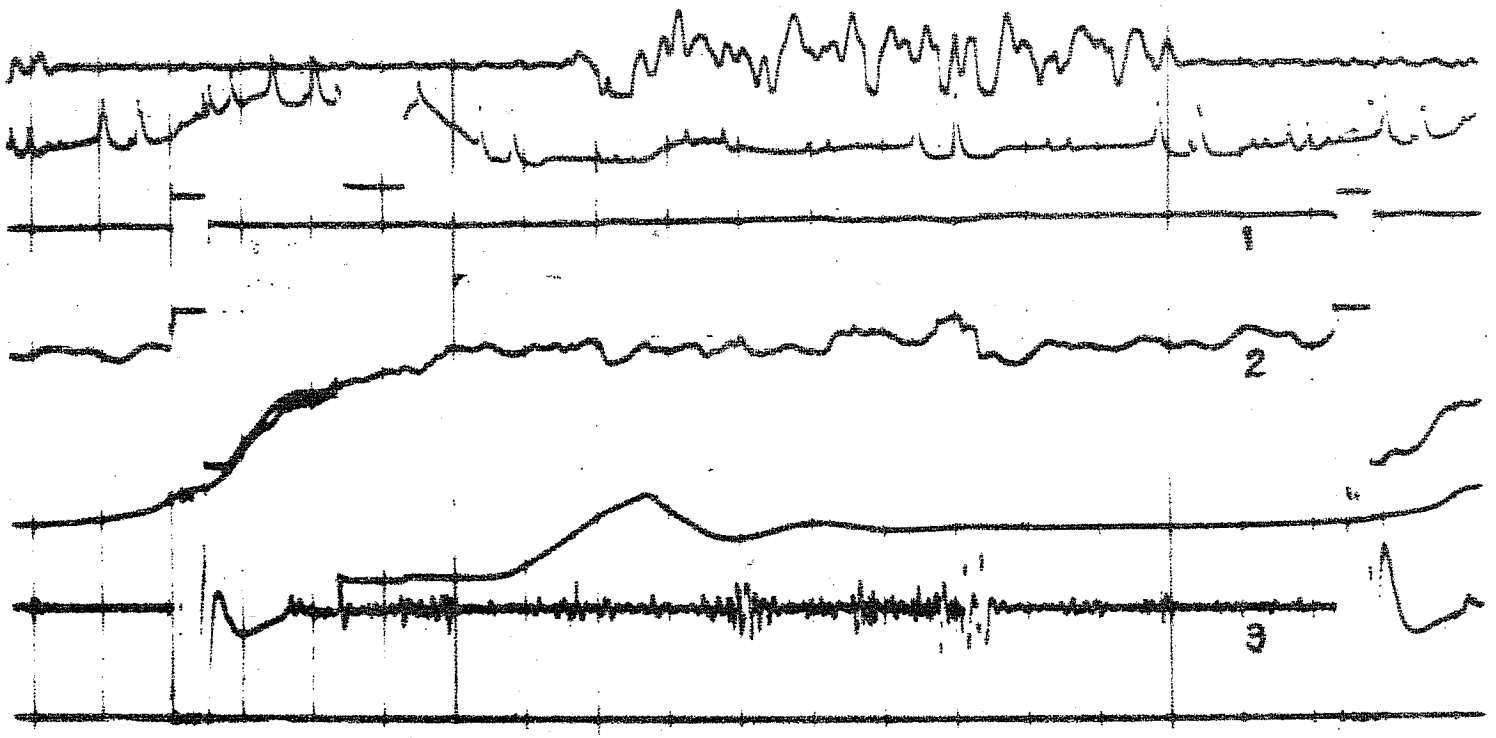

Fig. 4.32 Telemetry record showing the presence of irregularities of type Mn at 77.5 km during flight 10.45.

irregularities. The figure clearly shows that unlike type M_c these irregularities do not have any characteristic shape.

For computation of power spectrum, one case from main channel data of flight 10.37 and three cases from the duct data of flight 10.45 were chosen. The technique of Fourier transform used earlier to evaluate the power spectrum of

Table IV.9

Power spectral density and percentage amplitude for M_n irregularities

Flight No. 1037 Main Channel Data Altitude 70.5 Km.

Scale-size Meters	Wave Number PER METER	Power Spectral Density Var./Wave/METER	% Amplitude
300.0	0.0209	1500.0	13.20
150.0	0.0419	919.0	10.34
100.0	0.0628	341.0	6.29
75.0	0.0838	71.8	2.89
60.0	0.1047	29.8	1.86
50.0	0.1257	18.7	1.48
42.9	0.1465	21.2	1.57
37.5	0.1676	23.6	1.66
33.3	0.1887	20.0	1.53
30.0	0.2094	12.4	1.20

type M_c is used here also. Table IV.9 and IV.10 show the results of power spectral analysis. It is evident from table

Table IV. 10

Power Spectral Density and Percentage Amplitude for M_n Irregularities

Flight No. - 10.45 DUCT DATA

Scale Size METERS	Wave Number per METER	Power Spectral Density and Percentage Amplitude at					
		77.0 KM		79.5 KM		81.2 KM	
		RMS * Power	% Amplitude	RMS * Power	% Amplitude	RMS * Power	% Amplitude
330.0	0.0190	2800.0	5.13	6200.0	6.86	2600.0	4.43
210.0	0.0299	2540.0	4.88	3560.0	5.20	3010.0	4.81
140.0	0.0449	1180.0	3.33	1550.0	3.34	1600.0	3.51
105.0	0.0598	549.0	2.27	803.0	2.47	736.0	2.38
84.0	0.0748	261.0	1.57	380.0	1.70	306.0	1.53
70.0	0.0898	47.6	0.67	105.0	0.89	51.6	0.63
60.0	0.1047	36.2	0.58	64.8	0.70	49.1	0.61
52.5	0.1197	36.7	0.59	41.0	0.56	30.3	0.48
46.7	0.1345	32.0	0.55	34.1	0.51	21.0	0.40
42.0	0.1496	19.7	0.43	18.1	0.37	21.0	0.40
38.2	0.1645	17.5	0.41	27.1	0.45	16.4	0.36
35.0	0.1795	12.9	0.35	19.2	0.39	8.6	0.26
32.3	0.1945	13.0	0.35	14.1	0.33	5.4	0.20
30.0	0.2994	10.6	0.32	10.3	0.28	3.4	0.16

* Unit of RMS power is variance/wave/METERS.

IV.9 that around 70.5 Km the percentage amplitude is appreciable in the entire band and even for a scalesize of 30 meters the percentage amplitude is about 1.5%. The results of higher altitudes given in table IV.10 show that overall amplitudes are smaller in higher regions. Another important feature brought out from tables IV.9 and IV.10 is that at higher altitudes (77, 79.5 and 81.2 km) the smaller scalesizes have very little amplitude and only larger scalesizes have larger amplitudes.

Fig. 4.33 shows the spectrum at 70.5 km for flight 10.37. The power is maximum at 300 meters and falls off slowly upto 100 meters beyond which the fall is rapid. Using the power law described earlier the spectral index value turns out to be -2.32 for this altitude.

Fig. 4.34 shows the spectra at 77, 79.5 and 81.2 km for flight 10.45. Except at 79.5 km where the power associated with 300 meter scalesize is large the general nature of all the curves is same. The spectral index values for 77, 79.5 and 81.2 km altitudes turn out to be -2.72, -2.92 and -3.07, respectively. An important point to be noted here is that although the power at higher altitudes is more as compared to that at lower altitudes, the percentage amplitude at higher altitudes is less because of higher electron density prevailing there.

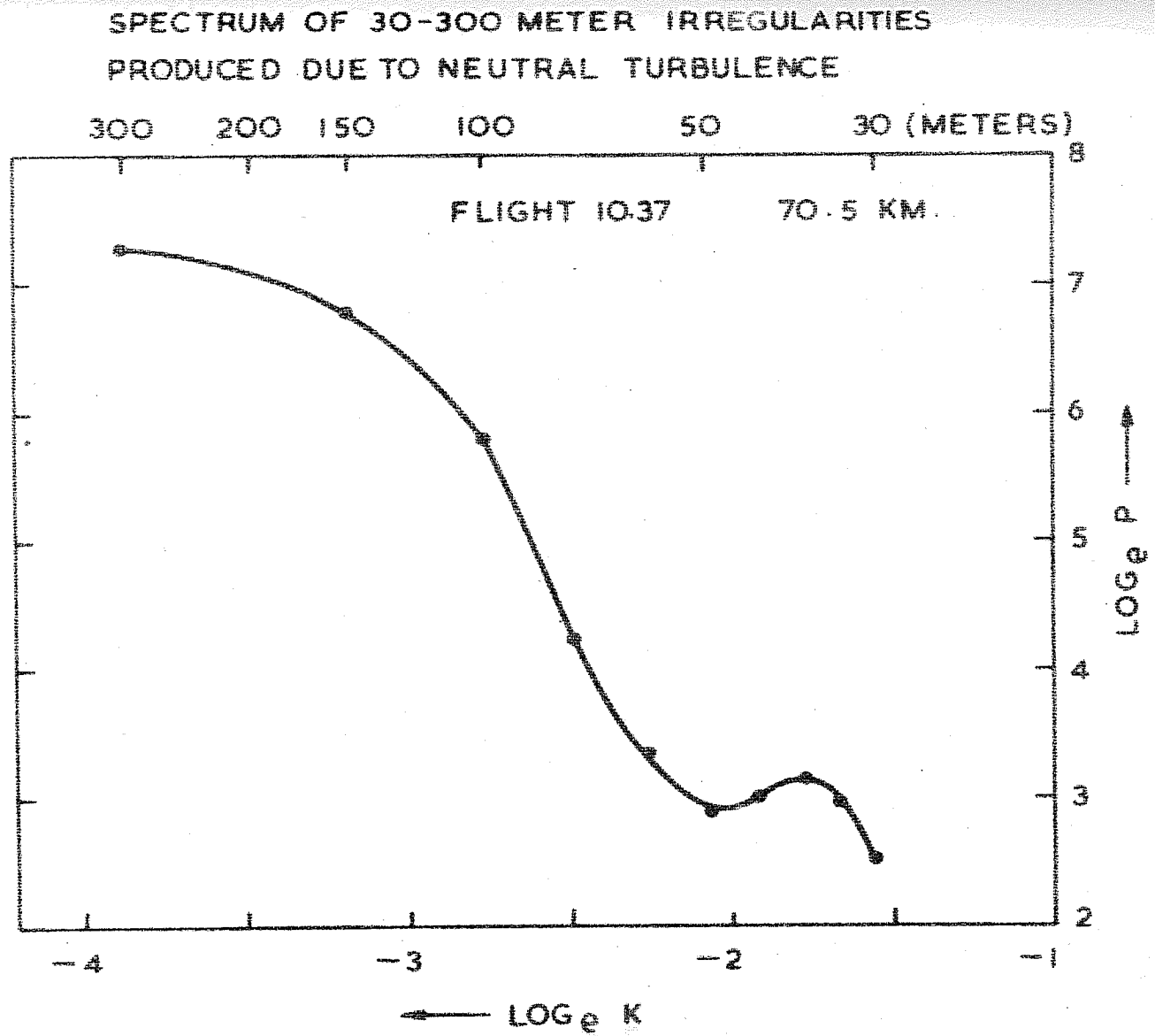

Fig. 4.33 Spectrum of type Mn at 70.5 km obtained from the main channel data of flight 10.37.

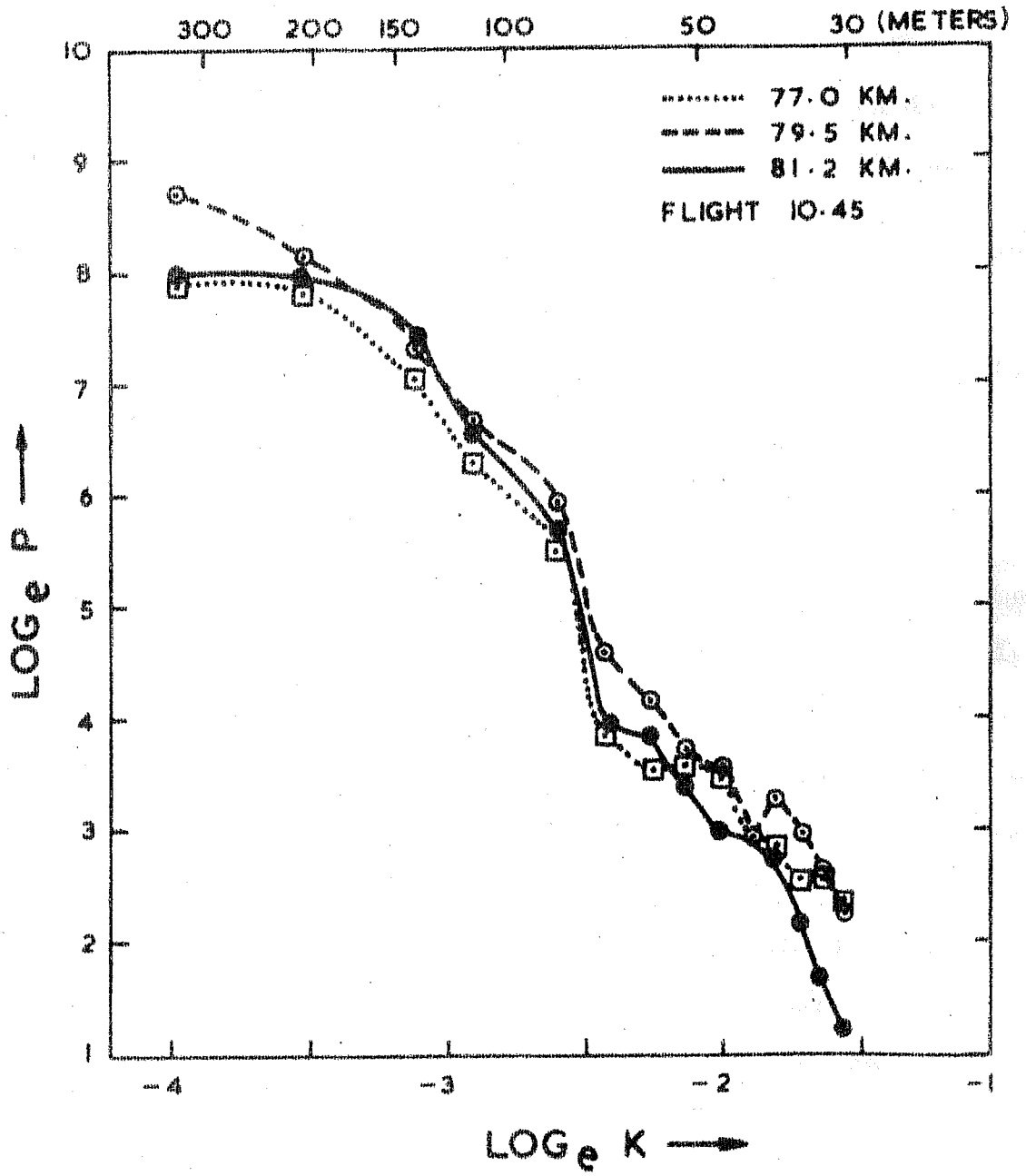

Fig. 4.34 Spectrum of type Mn at three different altitudes obtained from duct data of flight 10.45.

The average value of spectral index for all the four altitudes discussed above is -2.78.

4.4.2 Irregularities in 1-15 Meter Scalesize Range (Small Scalesize Neutral Turbulence - Type S_n)

The region of occurrence and time of observation of these irregularities is same as that of type M_n. The amplitude of these irregularities is much smaller than type M_n and is of the order of 1-2%. Fig. 4.35 shows the A.C. spectrum analyser output at 78.5 km. during flight 10.44. The topmost channel is the composite signal and the next seven channels are the filter outputs. It can be seen that the appearnce of the irregularities is very sudden as the signal appears abruptly in all the channels. Fig. 4.36 shows the spectrum for another daytime flight No. 10.45. In this case also the topmost channel is the composite signal, next eight channels are filter outputs and the last channel is the main channel of L.P. amplifier. The data near the zero markers, which are clearly seen on main as well as composite signal channels, should be ignored. The total record length is about 2 km and irregularities are observed only in about one km region. The appearance and disappearance of irregularities are equally abrupt.

For estimating the power spectrum of these irregularities the A.C. signal of each filter was rectified and

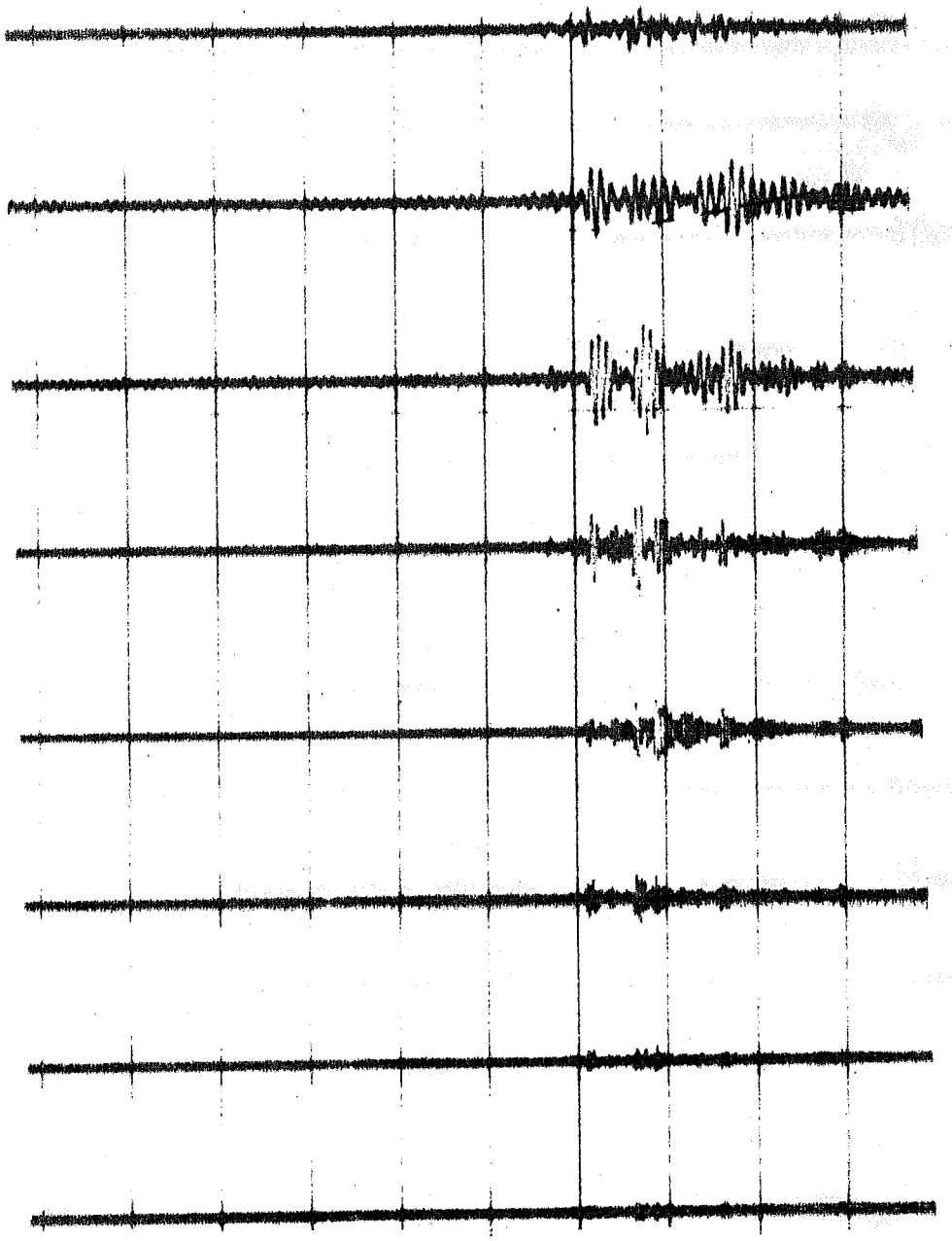

Fig. 4.35 Telemetry record showing the presence of irregularities of type Sn at 78.5 km during flight 10.44.

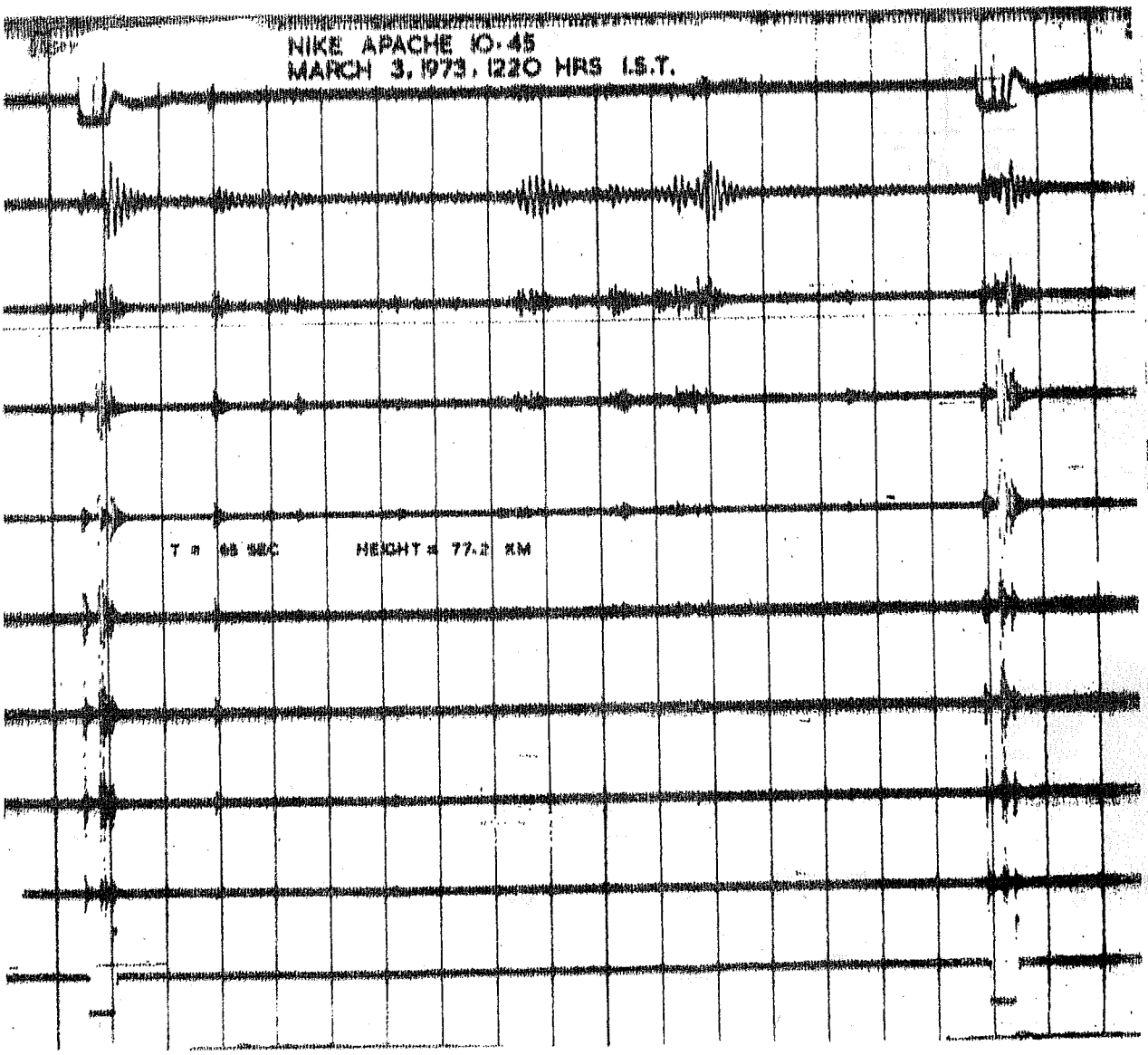

Fig. 4.36 Telemetry record showing the presence of irregularities of type Sn at 77.2 km during flight 10.45.

Table IV.11

Power spectral density estimates for small scale irregularities due to neutral turbulene - Type S_n

Wave Number METER^{-1}	Scale Size METERS	Power spectral density in arbitrary units								
		Flight No. G05.14 at 0745 Hrs IST				10.37 at 1040 Hrs IST			10.44 1259 HRS IST	10.45 1220 HRS IST
		61.9 KM	63.9 KM	66.2 KM	68.2 KM	61.4 KM	63.0 KM	70.3 KM	78.5 KM	77.0 KM
0.3644	17.24	1148.0	544.1	372.9	284.3	864.3	5309.2	1630.6	731.8	718.8
0.5194	12.10	204.0	138.9	111.3	85.0	222.3	1199.3	534.3	149.5	73.6
0.7330	8.57	170.0	100.1	85.1	62.1	225.8	1220.4	311.4	44.3	25.3
1.0807	5.81	88.7	69.1	70.4	33.6	150.4	478.8	108.1	14.6	4.6
1.5080	4.17	58.5	41.5	39.9	31.0	36.4	200.4	83.3	4.6	2.1
2.1656	2.90	27.3	23.9	25.3	20.0	9.3	45.8	18.3	0.9	0.8
3.0830	2.04	23.3	19.7	18.0	18.8	7.8	42.1	9.5	1.1	1.0

integrated for about 0.2 sec. The rectified data were used for estimating the power. Table IV.11 gives the rms power at scalesizes varying between 2.04 and 17.24 mts.for four different flights. We again note here that the power is in arbitrary units and hence a flight to flight comparison should not be made. During one flight the different power values may be compared.

Fig. 4.37 shows the variation of rms power with wavenumber at 78.5 km during flight No. 10.44 and at 77.0 km during flight No. 10.45. Since the power in both these cases is not comparable only spectral index will be reported. The value of spectral index during flight No. 10.44 at 78.5 km is -2.65 and during flight No. 10.45 at 77.0 km is -2.57.

Fig. 4.38 shows the variation of power with wavenumber for the morning time. Flight No. C05.14. The values of spectral index obtained at each altitude are listed in table IV.12.

Table IV. 12

Flight C05.14 Spectral Index of S_n

Altitude Km	Spectral Index 'n'	Altitude Km	Spectral Index 'n'
61.9	-1.4	66.2	-1.0
63.9	-1.1	68.2	-0.9

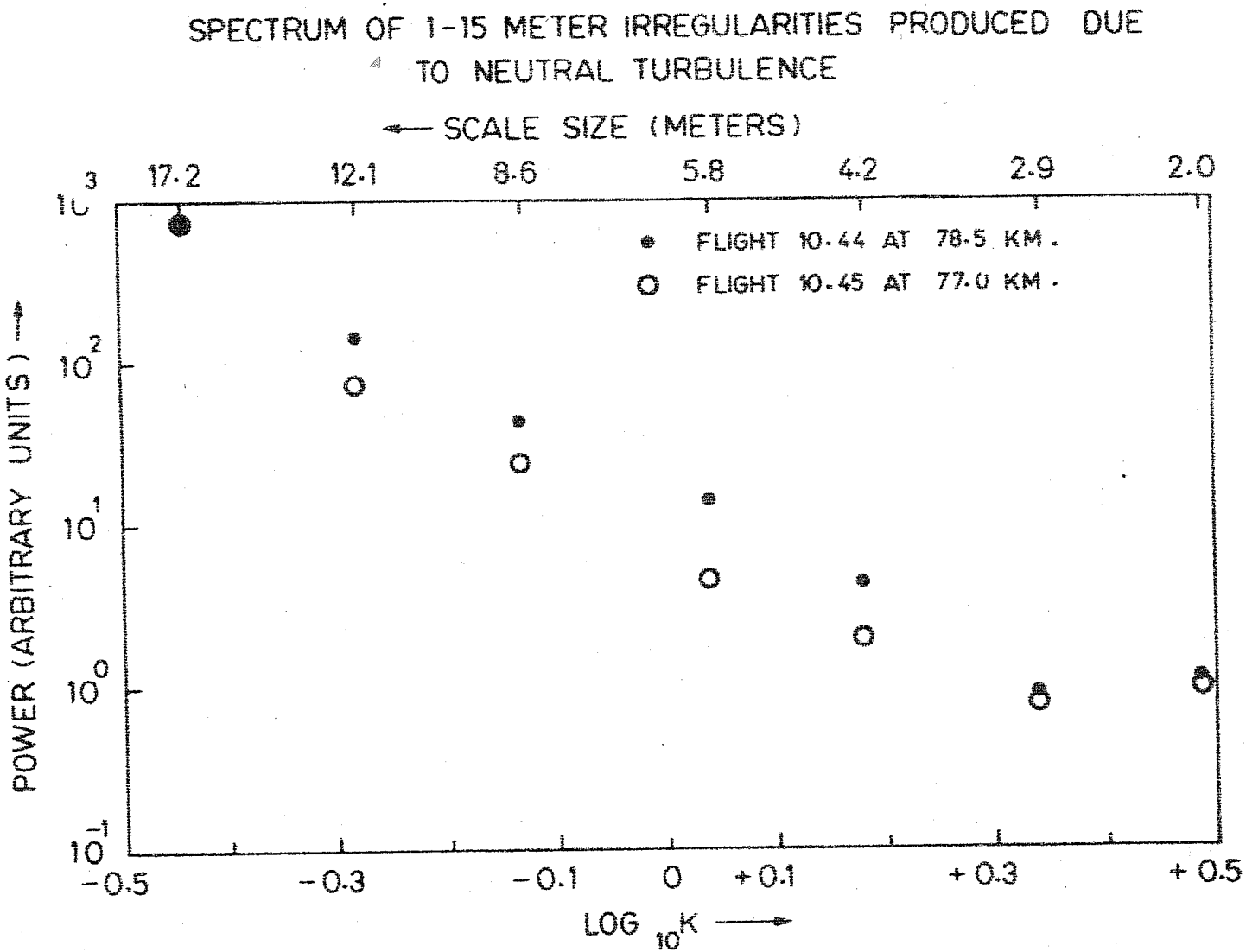

Fig. 4.37 Spectrum of type Sn during two daytime flights.

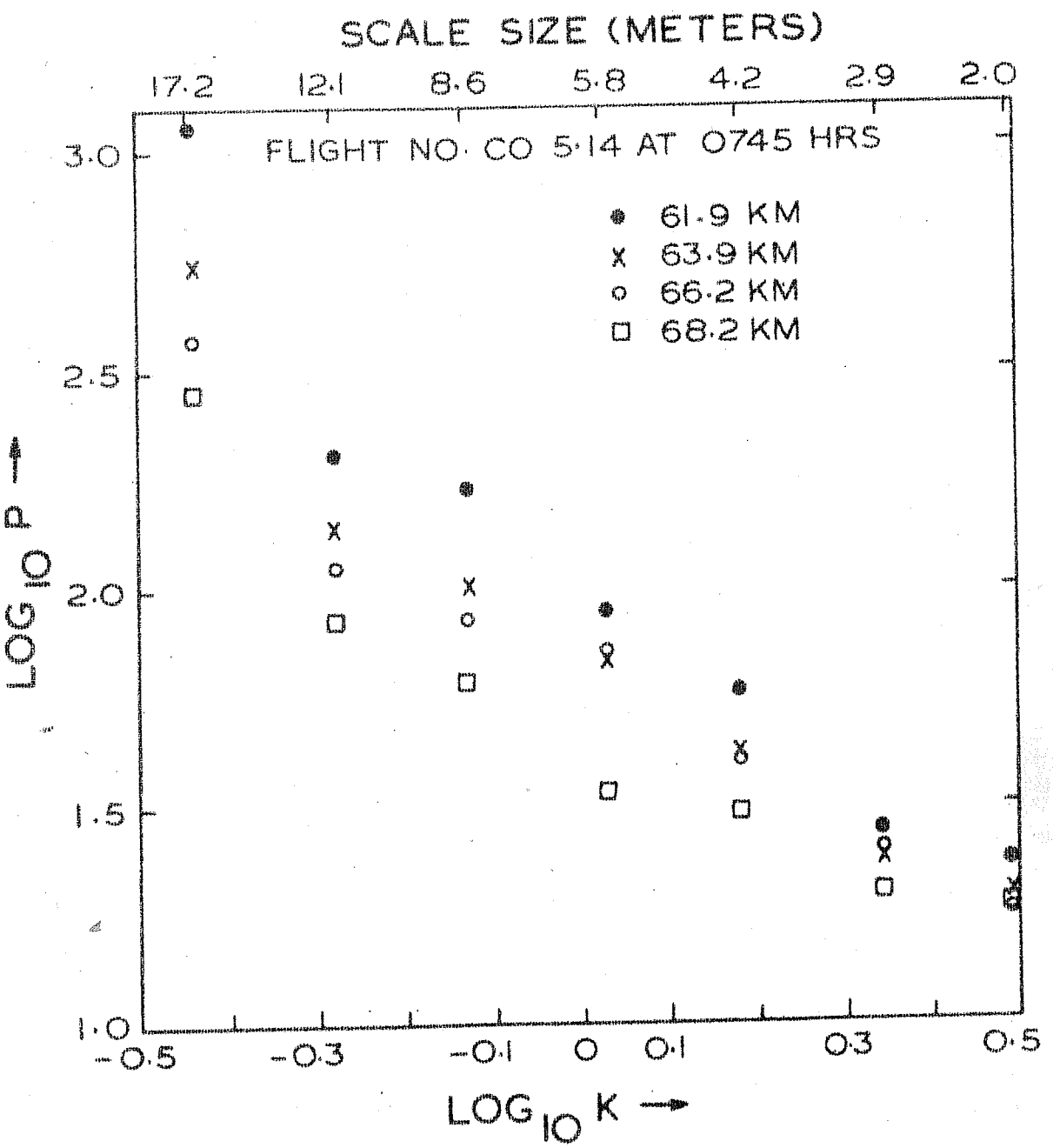

Fig. 4.38 Spectrum of type Sn at four different altitudes during a morning time flight CO 5.14.

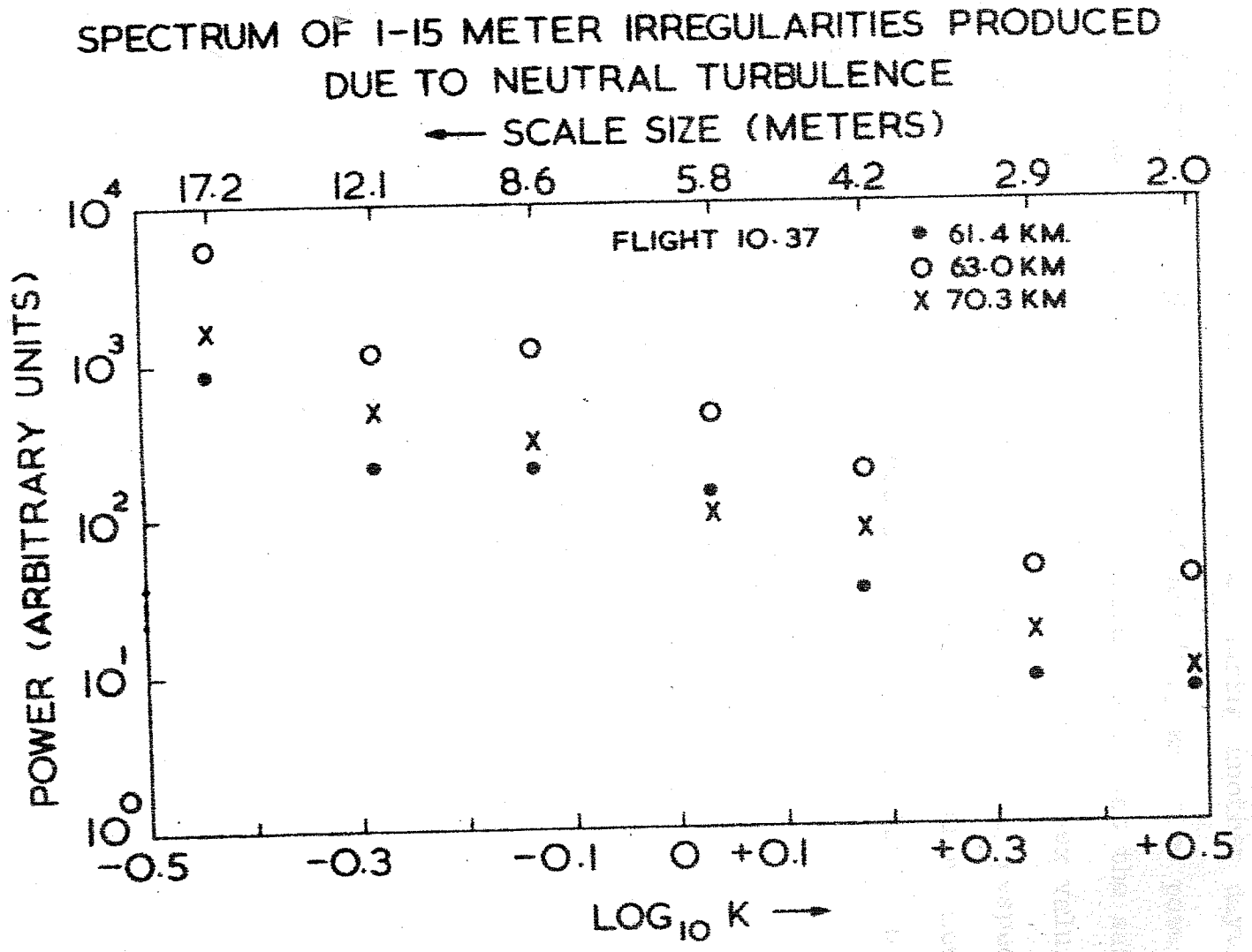

Fig. 4.39 Spectrum of type Sn at three different altitudes during daytime flight 10.37.

Fig. 4.39 shows the spectra of S_n during another daytime flight No. 10.37 at 61.4, 63.0 and 70.3 km. The power decreases with increasing wavenumber almost at the same rate in all the three cases. The spectral index values at 61.4, 63.0 and 70.3 km are -2.1, -2.1 and -2.2, respectively. The average spectral index value for all the above mentioned flights for all the heights considered turns out to be -1.77 for type S_n.

CHAPTER - V

RESULTS DURING PERIODS OF COUNTER ELECTROJET

5.1 Experimental Results During Counter Electrojet

Two Langmuir probe payloads were flown onboard Centaur rockets from Thumba during the periods of counter electrojet. The first rocket flight No. C05.16 was made on August 17, 1972 at 1532 Hrs I.S.T. and the second numbered as C-22 was made on April 21, 1975 at 1351 Hrs. I.S.T. In this section the ground based magnetometer and ionosonde records during the flight periods would be presented.

The magnetic field variations at Trivandrum ($0^{o}47'S$) and Alibagh ($24^{o}36'N$) have been studied. As suggested by Osborne (1964) and Kane (1973c), in order to restrict to ionospheric effects only, a station outside the influence of

electrojet has been chosen. Fig. 5.1 shows the variation of H_A, H_T and $H_T - H_A$ for 17th August 1972. The day was magnetically quiet day with an A_p index of 6. The H value at Alibagh gradually starts building up in the morning and attains a maximum around 1300 Hrs and then gradually drops down to nighttime base level. In case of Trivandrum the maximum occurs around 1000 Hrs and thereafter the field gradually decreases in steps upto 1300 Hrs after which the field suddenly drops down to nighttime base level. $H_T - H_A$ curve shows a maximum of 100 gamma above the baselevel at 1000 Hrs. The largest depression of magnetic field is about 35 gamma and incidently occurs around the time of rocket launch.

Thumba ionograms taken at the flight time showed that q-type of sporadic-E was absent and a strong blanketing - E_s was present upto 4.8 MHz. On the higher frequency side the sporadic-E trace looks to be degenerated into a transparent type extending upto 6.0 MHz. Fig. 5.2 shows two ionograms taken at 1502 and 1516 Hrs L.T. i.e. 16 and 30 minutes before the rocket flight. In these ionograms also a blanketing - E_s can be seen upto 4.2 MHz and a transparent type - E_s upto 5.8 MHz or so.

Fig. 5.3 shows the magnetic field variations for 21st April 1975 which is a slightly disturbed day with an A_p index of 23. In this case the largest depression in $H_T - H_A$ curve is around 1430 Hrs. At the time of rocket launch the $H_T - H_A$ curve is about 12 gamma below the base level.

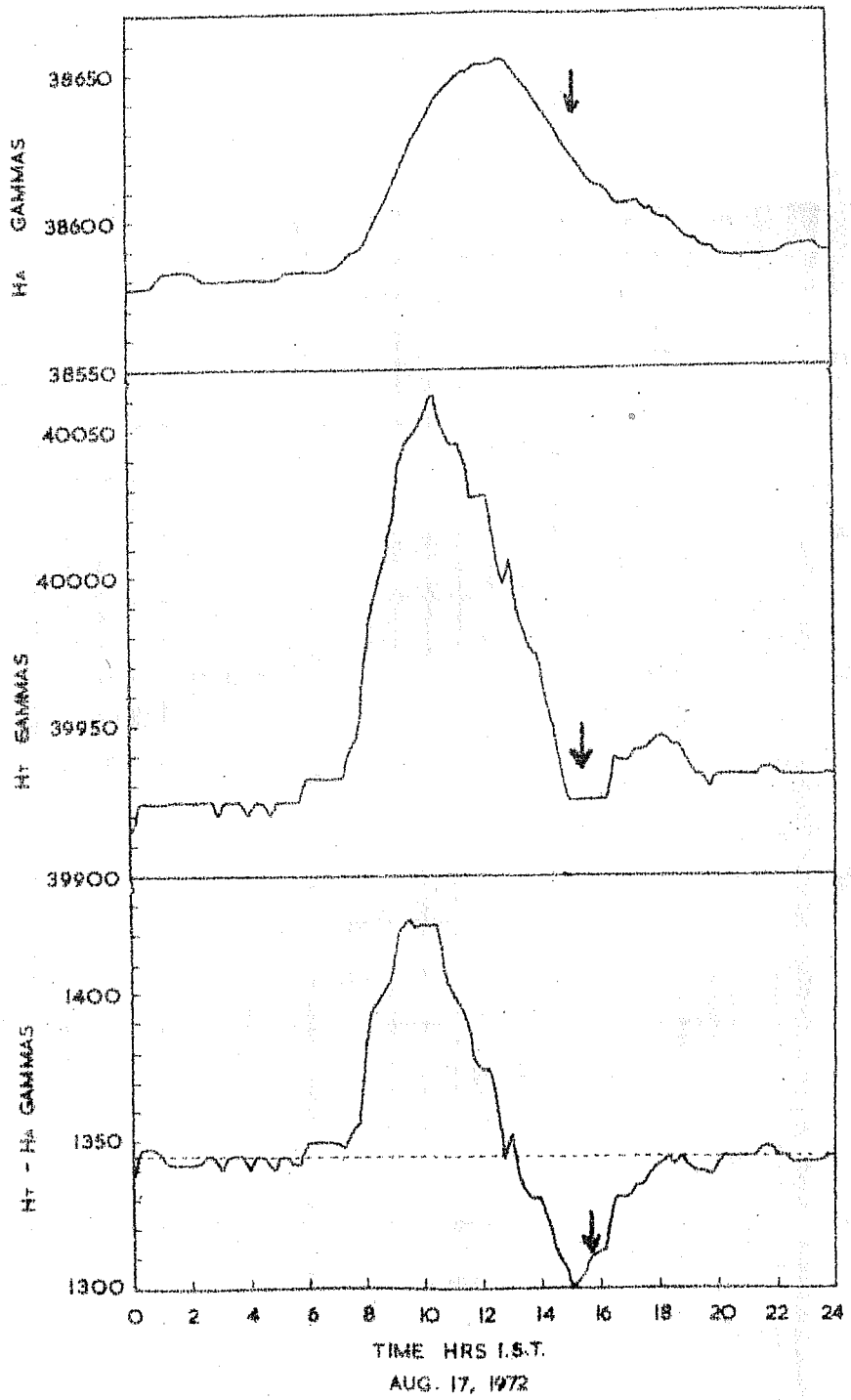

Fig. 5.1 Horizontal component of earth's magnetic field on 17th August, 1972 at Alibagh H_A (Top), at Trivandrum H_T (Middle) and the difference $H_T - H_A$ (bottom). The arrow indicates the time of rocket launching.

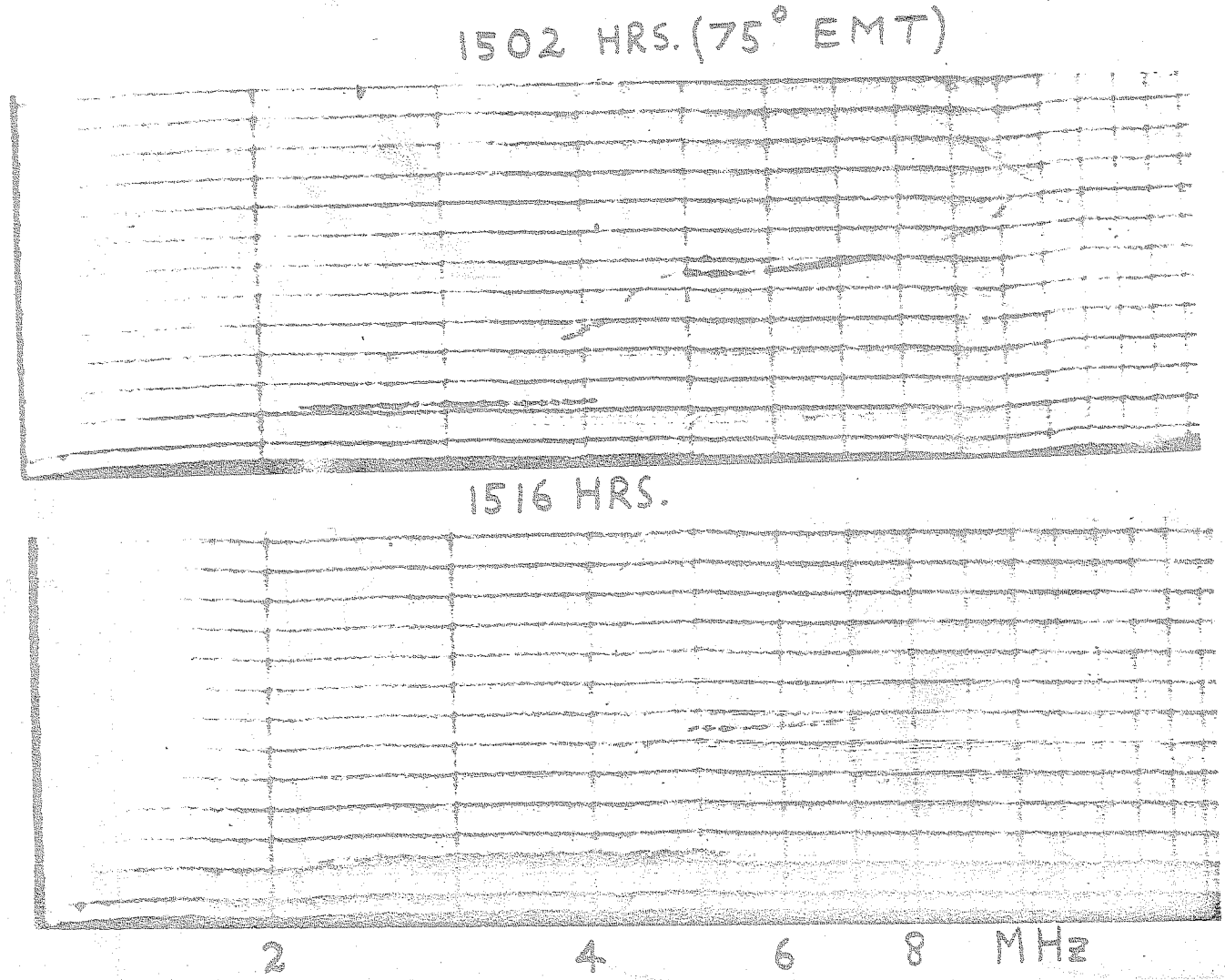

Fig.5.2 Ionograms of Thumba (dip 0.6°S) on 17th August, 1972 around afternoon showing the disappearance of Es-q followed by an appearance of blanketing sporadic-E.

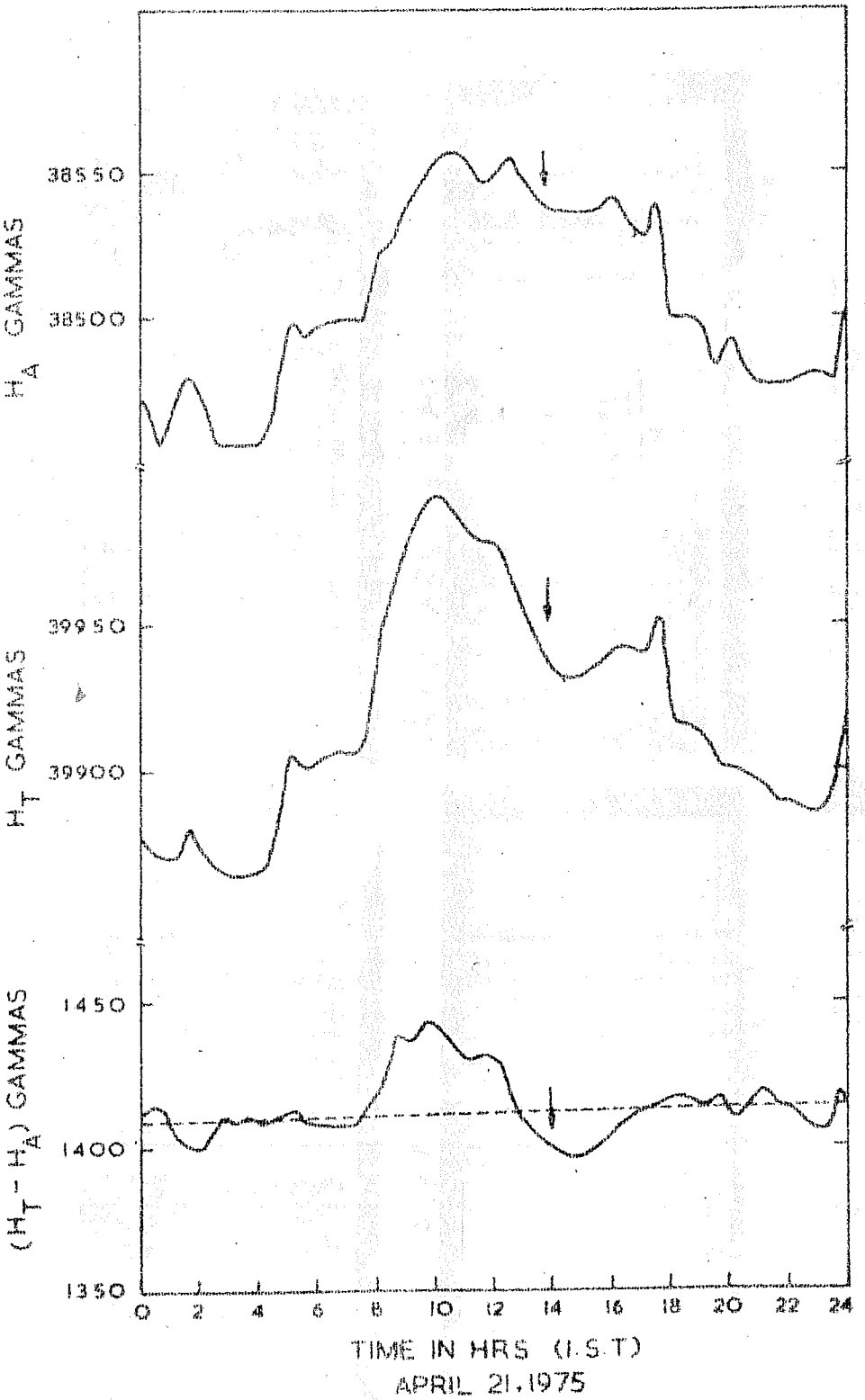

Fig. 5.3 Horizontal component of earth's magnetic field on 21st April, 1975 at Alibagh, H_A (Top), at Trivandrum, H_T (Centre) and the difference $H_T - H_A$ (bottom). The arrows indicate the time of the rocket launching.

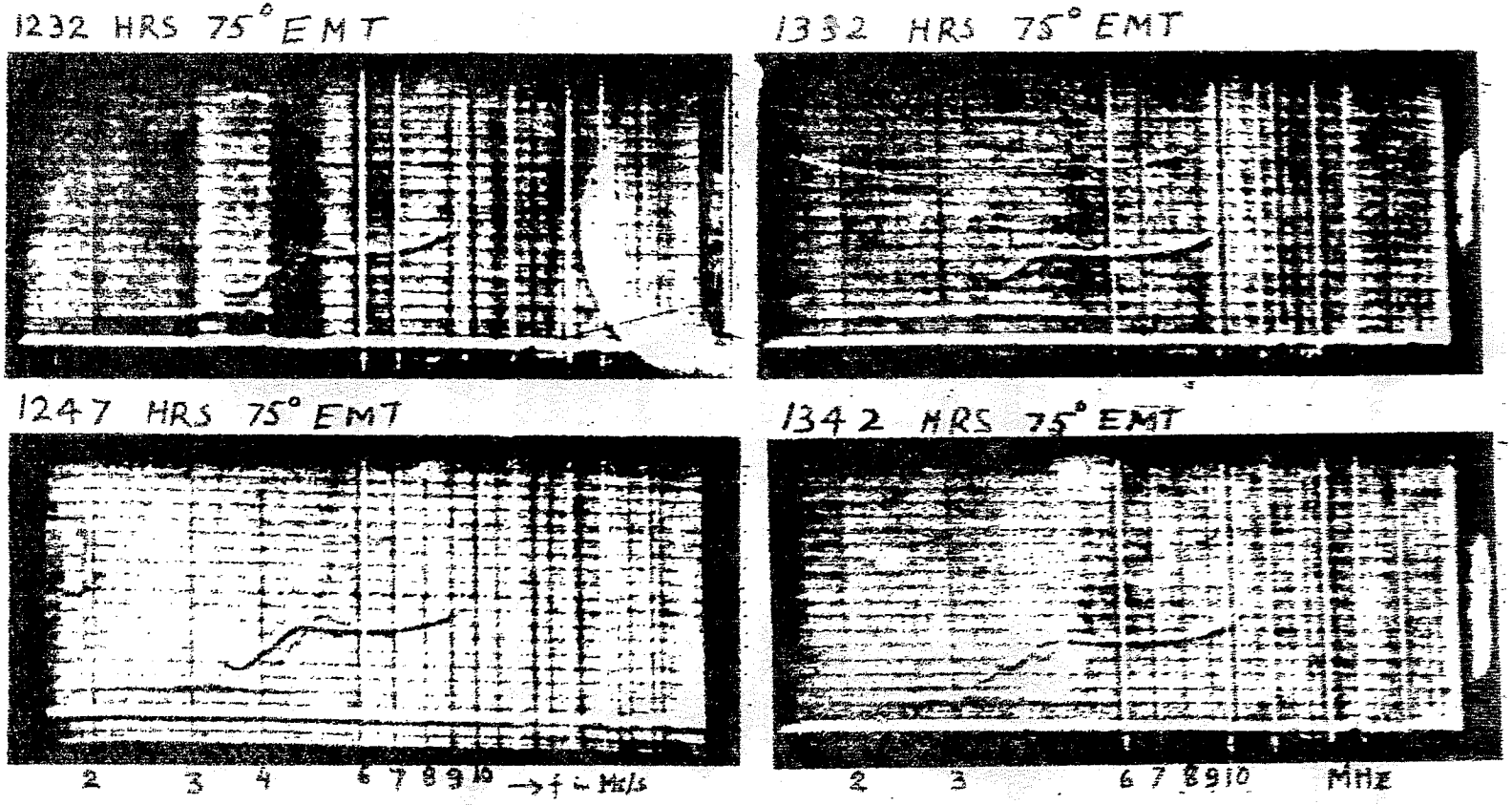

Fig.5.4 Ionograms of Thumba (dip 0.6°S) on 21st April 1975 around noon time showing the disappearance of E_{s-q} followed by an appearance of blanketing sporadic-E. Diffused echoes seen at 1342 hrs.(IST) which is nearest to the rocket flight time (1341 hrs.) are due to ionisation irregularities.

Fig. 5.4 shows four ionograms which were taken at Thumba at times close to depression in $H_T - H_A$ curve. The E_{s-q} is absent from all the four ionograms and instead a blanketing type of sporadic-E is present. In the ionogram taken at 1342 Hrs the trace is diffused.

5.1.1 Electron Density and Its Gradient

Electron density profiles derived from the Langmuir probe current are shown in fig. 5.5. In the case of flight No. C05.16 a sharp layer of ionization can be seen at about 94 km. It may be noted that during normal electrojet period no such layer was ever observed. The peak electron density in the layer is about 10^{-5} cm^{-3}. In case of flight No. C-22 also the sharp layer is present but its thickness is smaller than the one observed on C05.16. Although the shape of both the profiles is similar there appears a displacement of about 2 km. This is probably due to error in the trajectory data. Fig. 5.6 shows the nature of electron density gradients during both these flights. During the flight No. C05.16 there are positive gradients upto about 94 km. The strongest gradient is seen around 88 km where $(\frac{1}{L})$ becomes 1.53. Between 93 and 94 km there is a sharp increase in the positive density gradient. The region of positive gradient exists upto 95 km. Weak negative gradients are observed in the region lying between 95 and 98 km. Beyond 100 km the ambient density remains fairly constant.

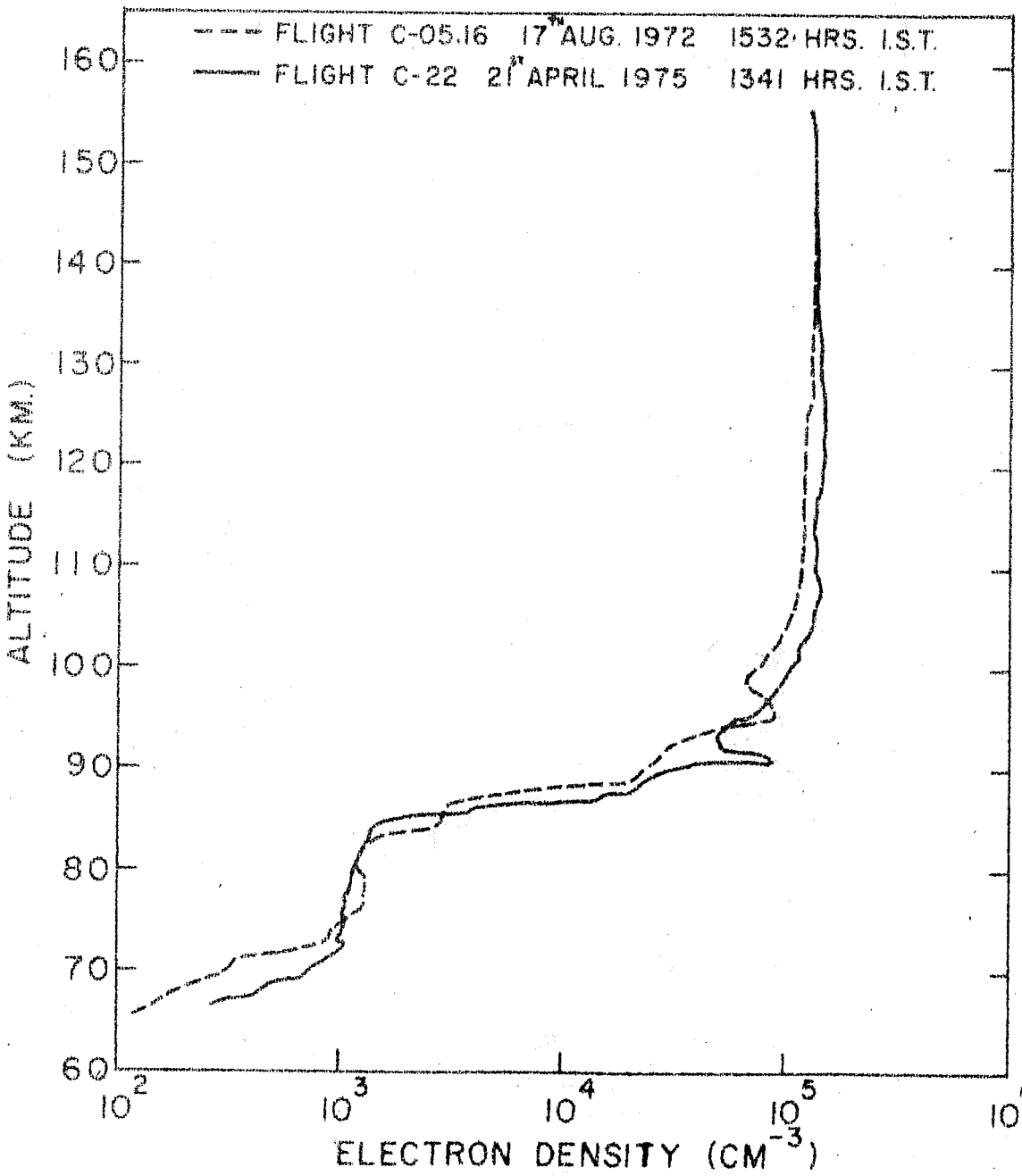

Fig. 5.5 : Electron density profiles as derived from the ascent data of two flights (CO 5.16 and C-22) which were carried out during the period of counter electrojet.

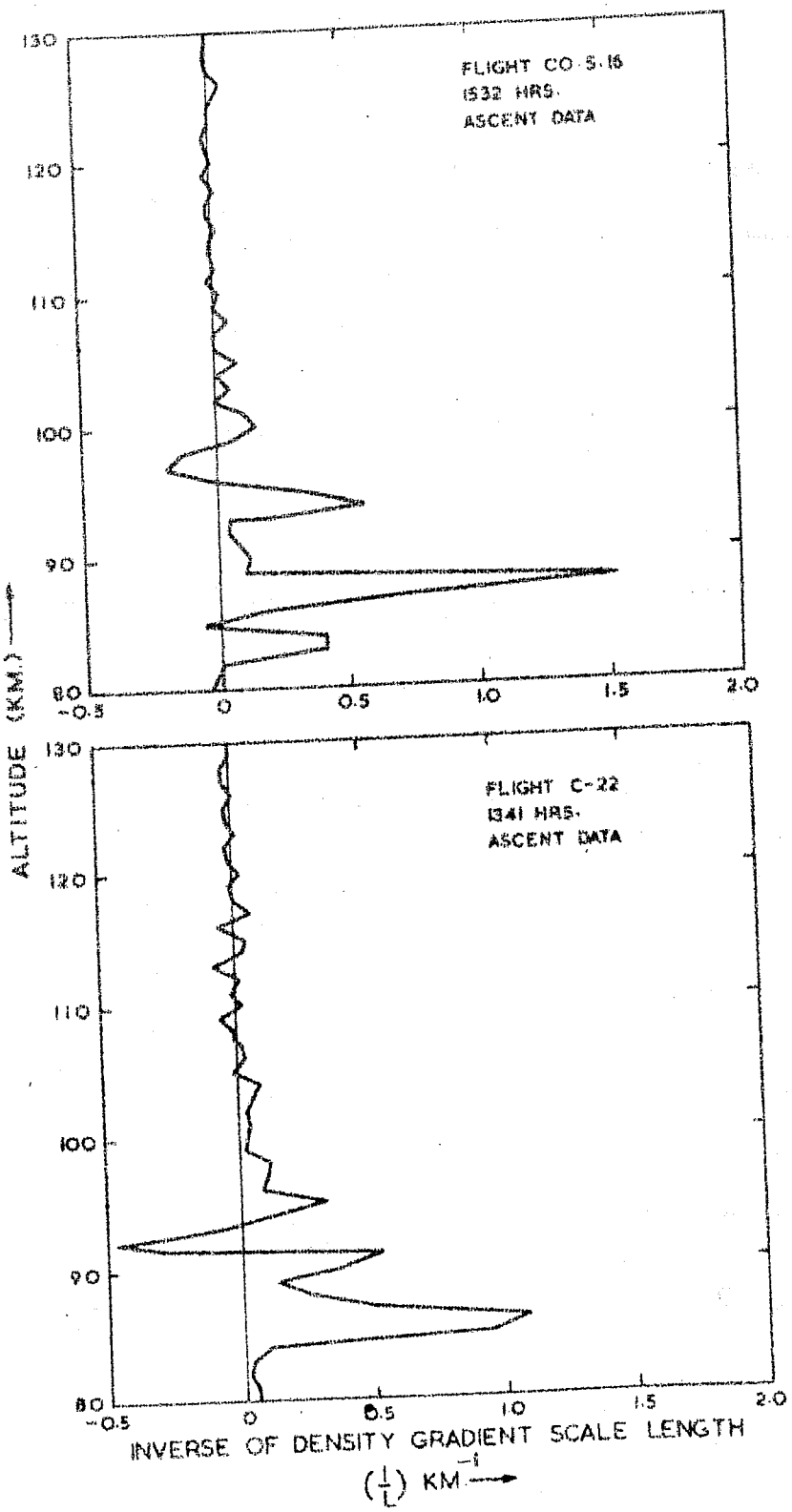

Fig. 5.6 Variation of electron density gradient with altitude for two flights conducted during periods of counter electrojet.

The lower curve in fig. 5.6 shows the nature of gradients during flight C-22. The positive gradients are very weak in 80-82 km region and increase rapidly upto 86 km where they become steepest. In the region of 91 km also the gradients are very steep and they give rise to a sharp layer on the density profile. The region of 92 to 93 km shows the presence of negative gradients. Beyond 93 km the gradient becomes positive exhibiting a minor peak at 95 km above which the ambient density remains fairly constant.

5.1.2 Irregularities due to Cross-field Instability Mechanism

As shown in chapter IV for normal electrojet the CF irregularities in 30-300 meter scalesize range have certain characteristic properties such as region of occurrence, relationship with gradient, shape and spectrum etc. On the basis of these properties the irregularities can be identified unambiguously. C F irregularities thus identified during the period of counter electrojet are described below.

Unlike the case of normal electrojet the CF irregularities were not observed in the region of positive density gradient. They were instead observed in the regions of negative density gradients on both the counter electrojet flights. Negative density gradient regions were observed around 97 and 92 km for flights C05.16 and C-22, respectively

(fig. 5.6). Fig. 5.7 shows the nature of CF irregularities observed in the regions of negative gradients on both these occasions. These irregularities have scalesizes of the order of many tens of meters which are typical scalesizes of CF irregularities. It has been shown in chapter IV and has also been reported earlier (Prakash et al. 1973) that CF irregularities in 30-300 meter range have typical sawtooth structures and the direction of steepening is such that as one moves along the density gradient the rise in electron density is much sharper than the fall. Fig. 5.7 shows the nature of steepening as observed on two counter electrojet flights. In fig. 5.7 (a) the density is increasing in positive y-direction whereas in 5.7 (b) the density is increasing in negative y-direction. The direction of density gradient is marked by an arrow in each case. It can be seen from both parts of fig. 5.7 that as one goes along the density gradient the rise in electron density is much sharper than the fall. In case of fig. 5.7 (a) the region of strongest negative gradient is encountered when voltage sweep was being applied to the sensor with the result that many switchings are seen on the record. Yet the steepening can hardly be missed.

5.1.3 Irregularities Due to Neutral Turbulence Mechanism

The ionisation irregularities generated due to neutral turbulence mechanism about which we have already discussed in chapters II and IV are found to be present during

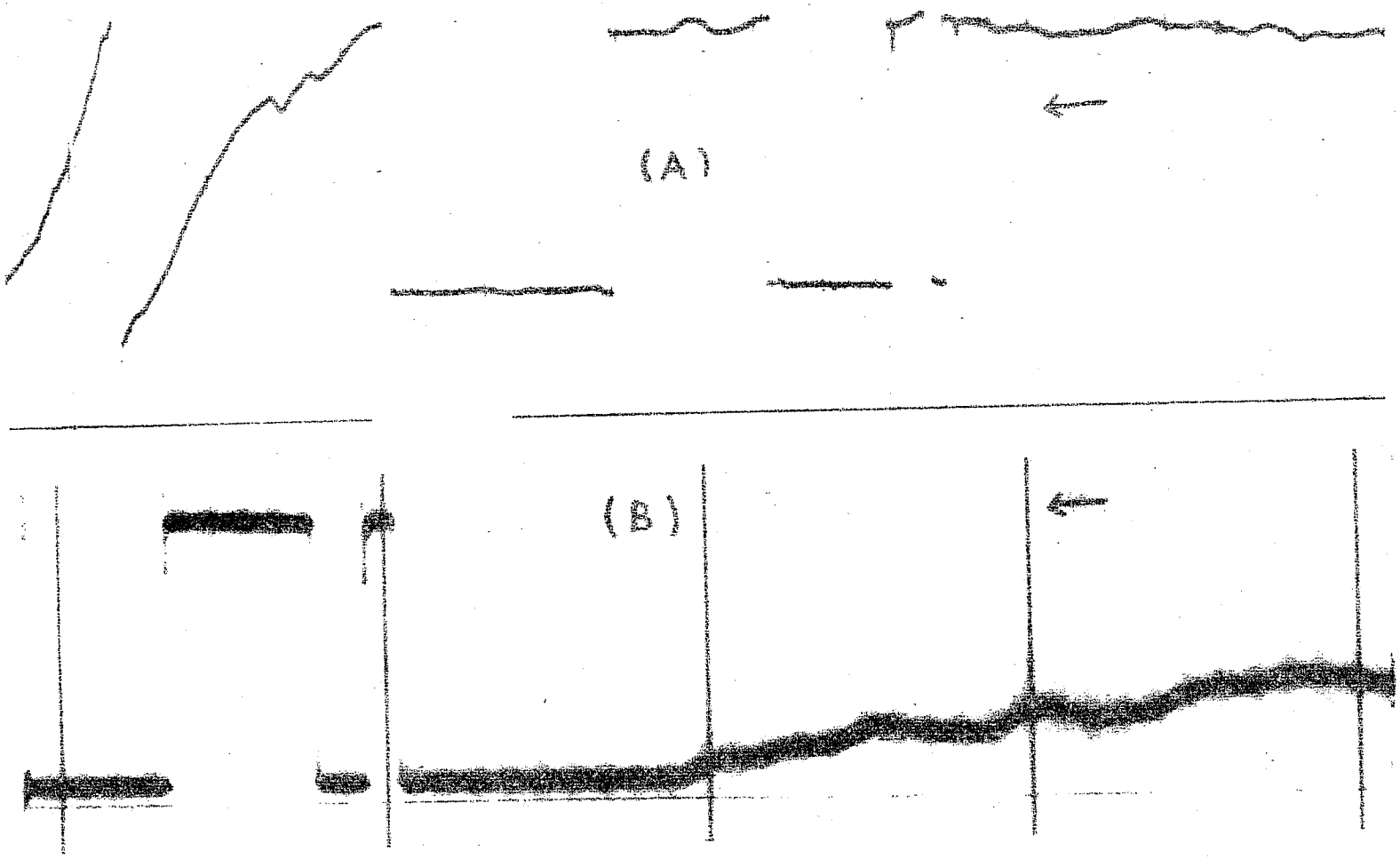

Fig. 5.7 Telemetry record of 30-300 meter cross-field irregularities during periods of counter electrojet. (A) at 97.7 km during C05.16 and (B) at 91.5 km during C-24.

periods of counter electrojet also. The region of occurrence of such irregularities is again confined to lower altitudes where collisional effects are dominant. These irregularities were observed both in medium as well as small scalesize ranges. Fig. 5.8(a) shows the main channel output of the Langmuir probe in 66.2 km. region for flight C05.16. It can be clearly seen from the figure that, unlike CF irregularities M_n irregularities (medium scalesize due to neutral turbulence) do not have any typical shape. Fig. 5.8(b) shows the M_n irregularities for the other flight viz. C-22. On this flight a duct amplifier was also flown and the output of the same is shown in the second channel. Since in case of C-22 the amplitude of M_n is small duct amplifier data could have been very useful. But unfortunately the deflection kept for duct amplifier channel was very small hence, as it is, duct amplifier output is not very much different from main channel output. After a rerecording this data can be used in analysis. Presentation of this data is only to show the existence of M_n irregularities during flight C-22.

Table V.1 shows the results of power spectral analysis of M_n irregularities observed at 66.2 km during flight C05.16. It can be seen from the table that amplitudes of M_n irregularities during counter electrojet are of the same order as the corresponding amplitudes during period of normal electrojet as seen in chapter IV.

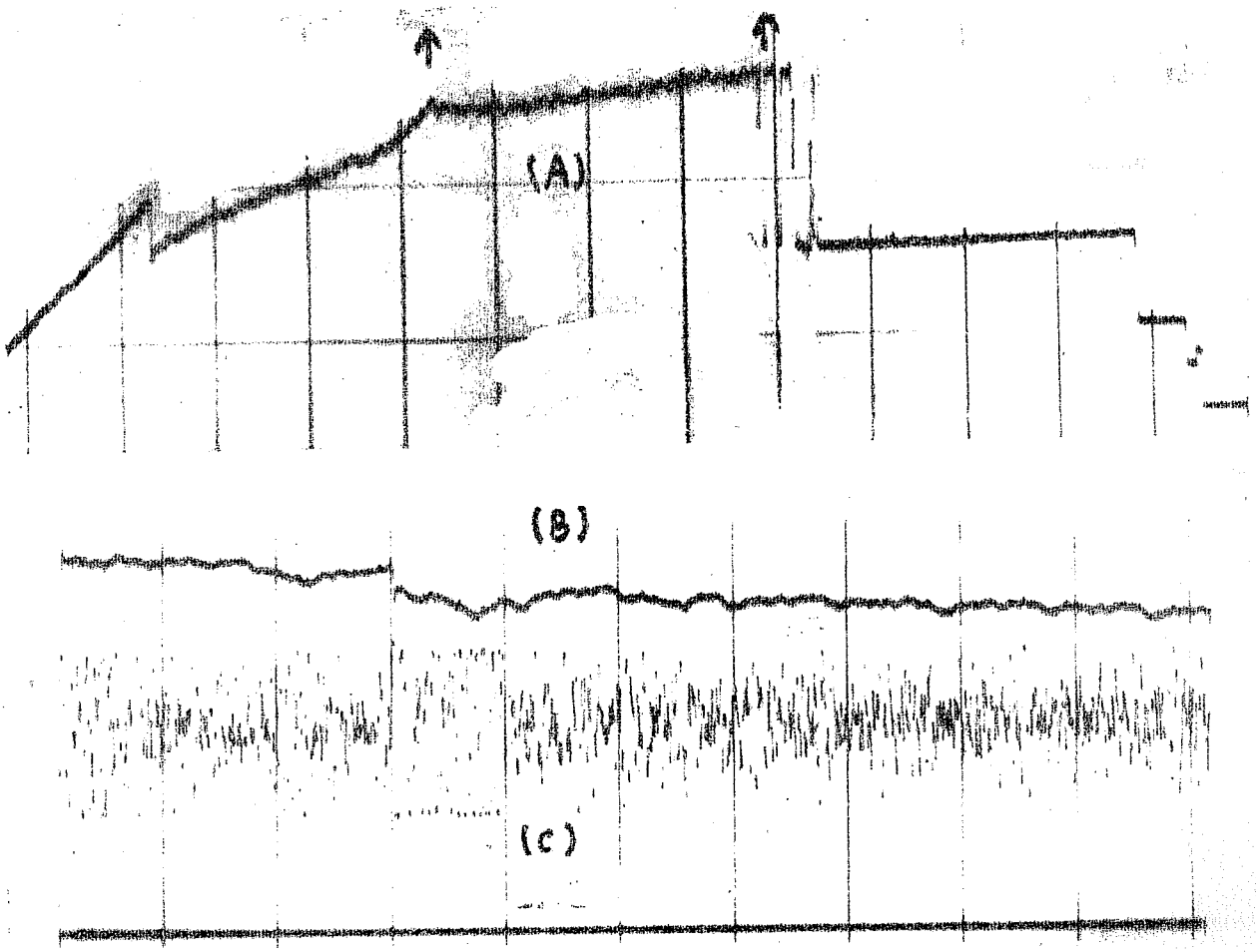

Fig. 5.8 : Telemetry record of irregularities due to Neutral turbulence mechanism, (A) shows Mn irregularities at 66.2 km during C05.16, (B) shows Mn irregularities at 67.8 km during C-22 and (C) shows Sn irregularities at 67.8 km during C-22.

Table V.1

Results of 30-300 Meter Irregularities Generated Through Neutral Turbulence Mechanism During the Period of Counter-electrojet

Flight No. - C05.16

Time - 1532 HRS. I.S.T.

Altitude - 66.2 km.

Wave No. per Meter	Scale Size METERS	Spectral Density Var/Wave/Meter	% Amplitude	Net Amplitude cm^{-3}
0.0524	120	73.4	5.45	8.6
0.1047	60	33.9	3.71	5.8
0.1571	40	19.1	2.79	4.4
0.2094	30	19.2	2.79	4.4

Average Ambient density at 66.2 km = 0.1571×10^3 cm^{-3}

Spectral Index = -1.04

Table V.1 shows the wavenumber, scalesize, spectral density, percentage amplitude and net (total) amplitude for M_n irregularities during counter electrojet. In this case also some sweep portion has contaminated the data which, therefore, has not been used in the analysis. If one refers back to fig 5.8 (a) the useful data can be spotted as the one lying between two vertical arrows; the data lying before the first

arrow contains sweep and hence has not been analysed. Since the useful data length was only 500 meters, scalesizes upto 120 meters only have been studied. As there was no duct amplifier onboard, information regarding amplitudes could not be obtained for higher altitudes. It can be seen from the table V.1 that the power is maximum in largest scalesize i.e. 120 meters and decreases steadily upto 30 meters. The value of spectral index turns out to be -1.04.

Fig. 5.9 shows three consecutive records of spectrum analyser output. In the first cycle which is the record at 59.9 km it can be seen that power is small in low frequency channels and gradually increases towards higher frequency channels. The next cycle shows that more power is getting accumulated in lower frequency channels. The beginning of the third cycle shows a marked increase in power in all channels with the result that the noise amplifier output is saturated during this portion of the cycle. No analysis of the saturated data was attempted. After a gap of 0.3 seconds or so the amplitudes came down to their normal values. In the last portion of the third cycle it can be seen that power is more in lower frequencies and in high frequency channels, only weak signal is present. Thus in a distance of 8 km or so the spectrum has changed from a flatter one to a steeper one. For estimating the power spectrum of irregularities each filter output was rectified and integrated for 0.2 sec. The results of spectrum

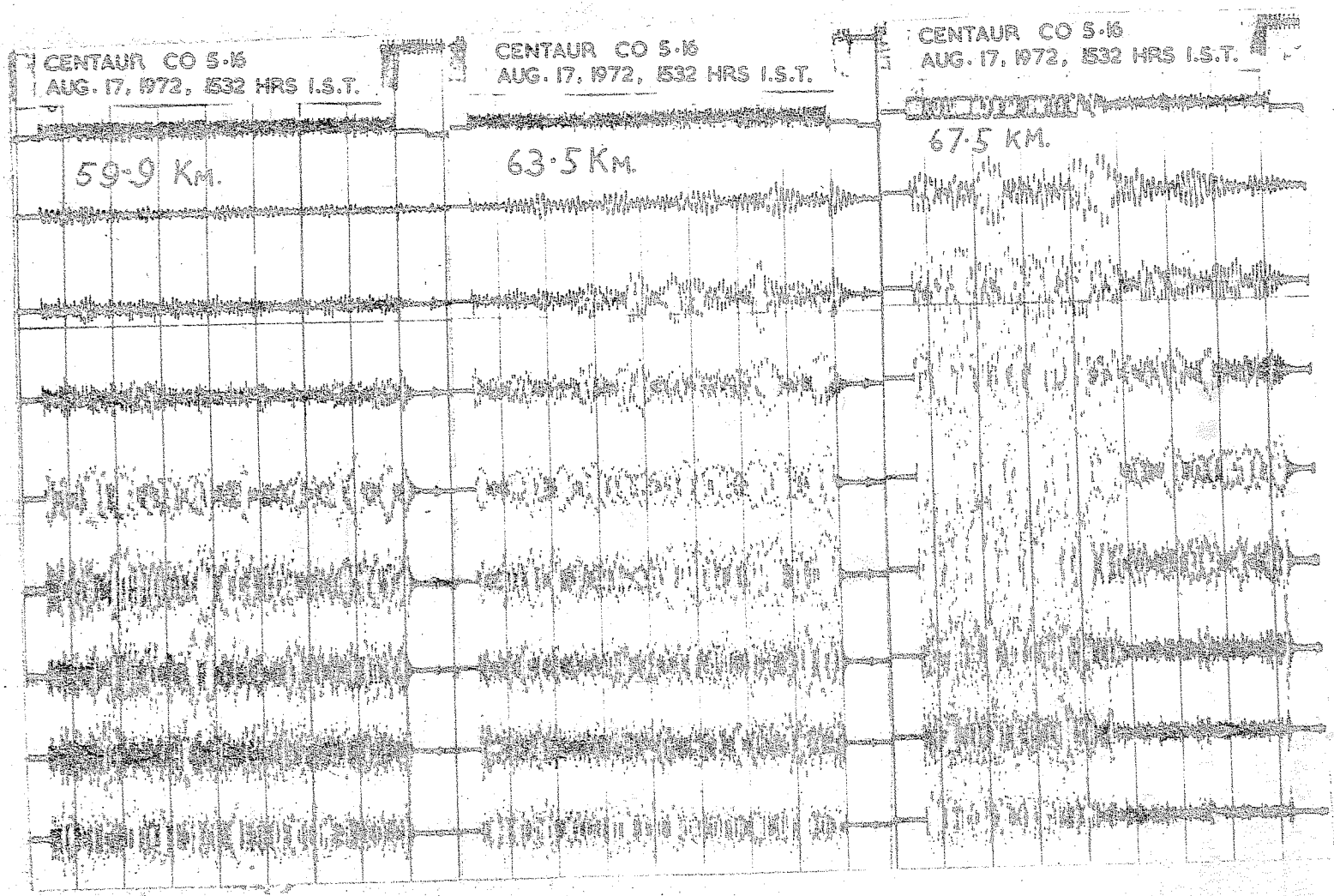

Fig. 5.9 : Spectrum analyser records at 59.9 km, 63.5 km and 67.5 km for 1-15 meter irregularities generated through neutral turbulence mechanism during the period of counter electrojet.

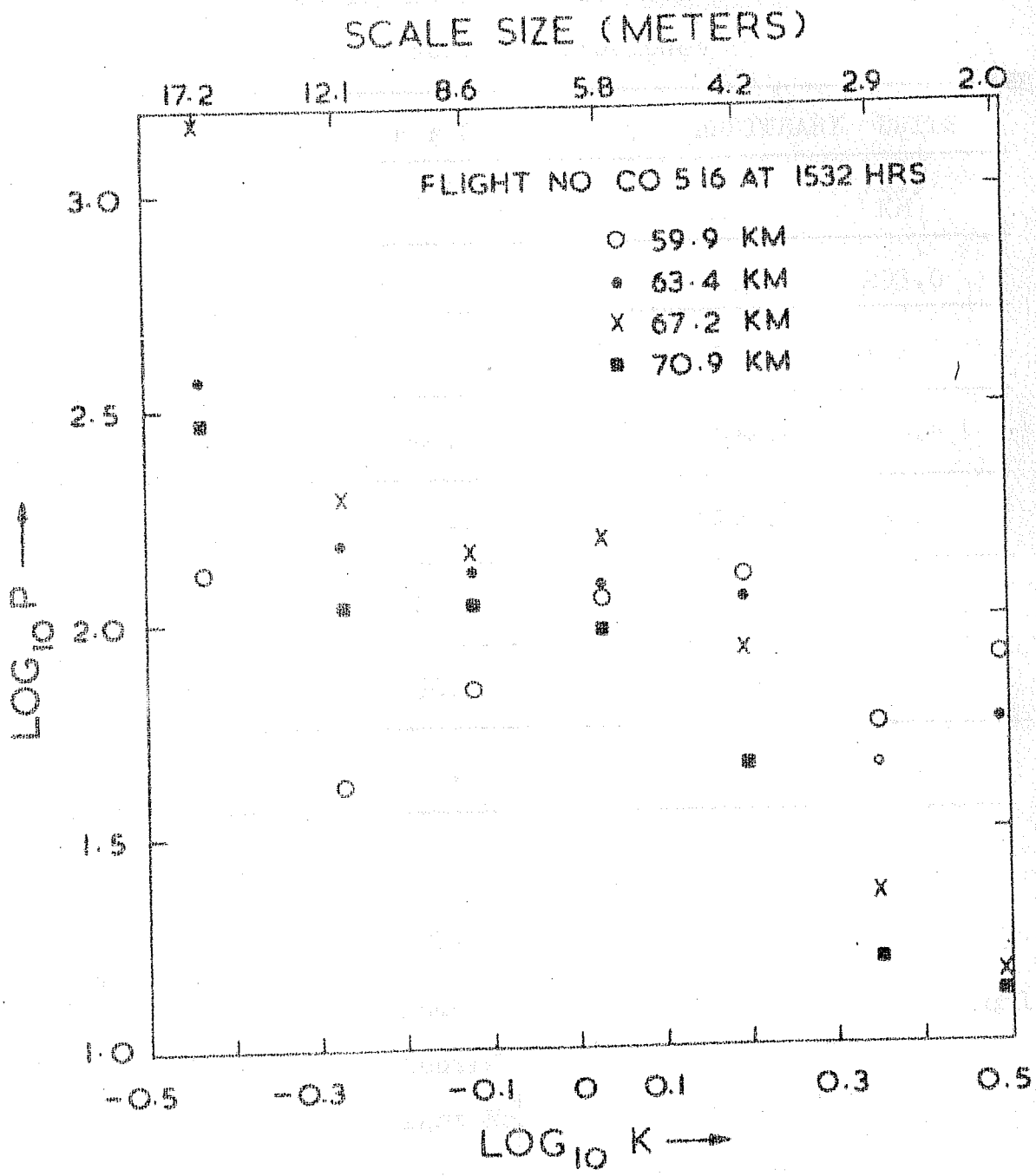

Fig. 5.10 : Spectrum of type Sn at four different altitudes during the period of counter electrojet.

Table V. 2

Power Spectral Density Estimates for Small Scale Irregularities Produced Due to Neutral Turbulence

Wave Number METER^{-1}	Scale Size METERS	R M S POWER IN ARBITRARY UNITS			
		59.9 KM	63.4 KM	67.5 KM	70.9 KM
0.3644	17.24	133.2	370.7	1505.6	293.0
0.5194	12.10	41.9	151.5	194.7	107.1
0.7330	8.57	69.0	132.6	148.4	110.4
1.0807	5.81	113.2	121.4	160.2	96.1
1.5080	4.17	127.1	113.0	85.2	45.8
2.1656	2.90	56.0	45.8	22.7	15.7
3.0830	2.04	81.6	57.2	14.9	13.1

Table V. 3

Variation of Spectral Index 'n' with Altitude for Smallscale Irregularities Due to Neutral Turbulence.

Flight No.CO 5.16

Altitude	Spectral Index 'n'
59.9 KM	-0.02
63.4 KM	-0.53
67.5 KM	-1.69
70.9 KM	-1.31

analysis of 1-15 meter irregularities are listed in table V.2 for four different altitudes. The lower three altitudes are the ones for which the A.C. spectrum analyser records have been shown in fig. 5.9. The RMS power which is expressed in arbitrary units in table V.2 is plotted in fig. 5.10. The spectra at 59.9 and 63.4 km are relatively flatter than the spectra at 67.2 and 70.9 km. The spectral index values for all the altitudes are listed in table V.3. The average value for all the heights is -0.88.

The small scale irregularities due to neutral turbulence mechanism were observed on flight No. C-22 also. The last channel of the lower diagrams of fig. 5.8 shows telemetry record of flight C-22. The presence of irregularities can be clearly seen there but as mentioned earlier no further analysis was possible at the time of preparation of this dissertation.

5.1.4 Irregularities due to Streaming Instability Mechanism

Irregularities due to streaming instabilities were observed in 106-112 km region during flight C05.16. These irregularities are similar in nature to type S_s observed by Prakash et al. (1973) during period of normal electrojet. The results of this type of irregularity will not be discussed here as they have been discussed by Rao (1976).

5.1.5 Irregularities Due to Unknown Mechanism

During flight No. C05.16 wavelike perturbations with wavelengths falling under medium scalesize range were observed around 94.2 km. The region of 94 km altitude is characterized by positive density gradients. The upper portion of fig. 5.11 shows these structures as seen on the main channel of the Langmuir probe output. The gradients in this region are very strong and especially so at an altitude which is marked by an arrow. Around the arrow the density increases so sharply that the amplifier goes into lower gain position. Unlike type M_c, these irregularities do not have any typical shape. The lower portion of fig. 5.11 shows the telemetry output of 70-1000 Hz channel. It can be seen that weak small scale irregularities are also present at 94 km altitude.

Table V.4 gives the RMS power spectral density, percentage amplitude and total amplitude for different wavenumbers. It can be seen from table V.4 that the power is maximum in larger scalesizes and decreases rapidly with scalesize. The steepness of the spectrum is characterized by the spectral index $n = -2.83$.

Some of the preliminary results of flight C05.16 were reported in an earlier communication by Prakash et al. (1976).

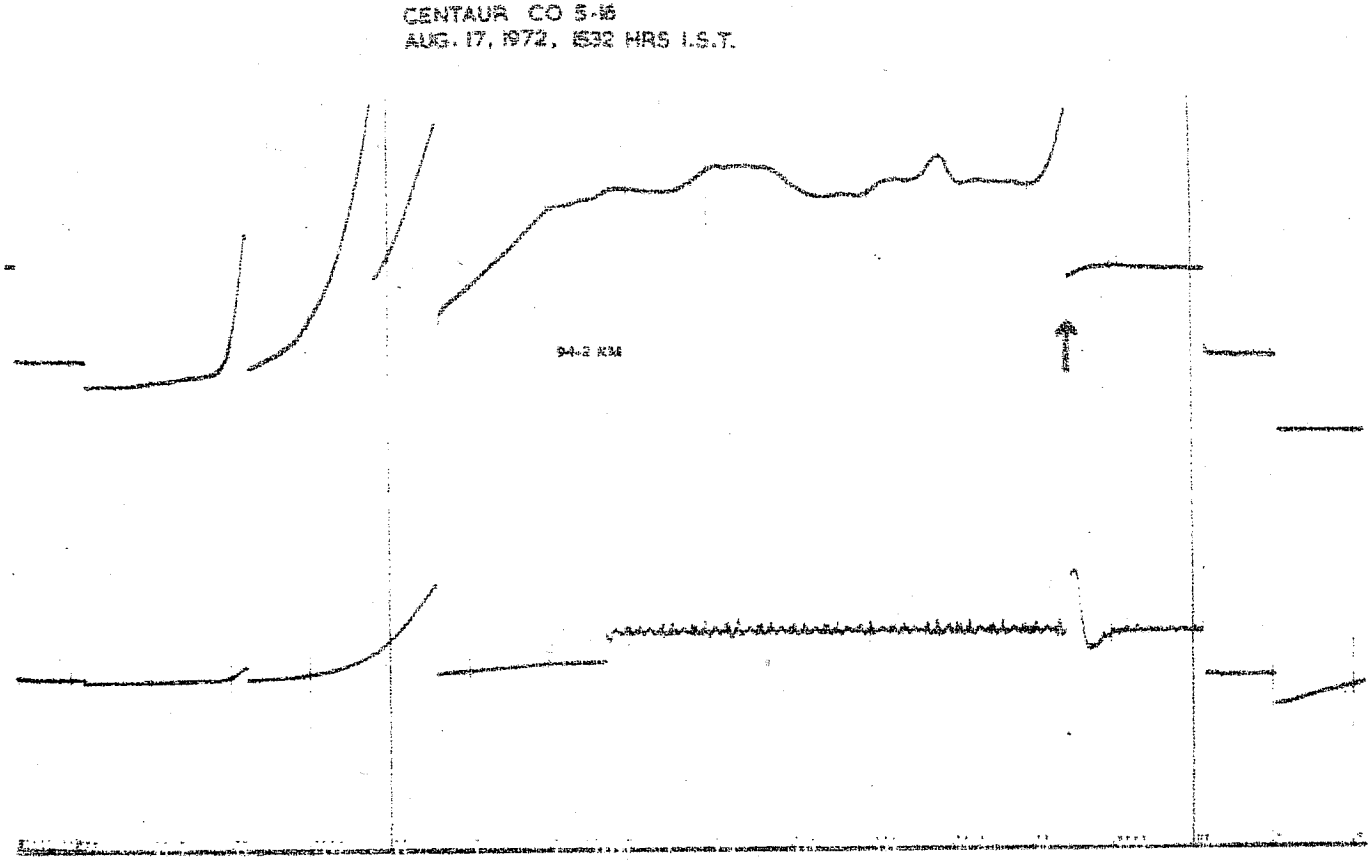

Fig. 5.11 Telemetry record of medium scale size irregularities produced through unknown mechanism of generation during period of counter electrojet. The arrow indicates the presence of very sharp gradient.

Table V. 4

Results of 30-300 Meter Irregularities Generated Due to Unknown Mechanism During Counter Electrojet

Flight - C05.16

Time - 1532 Hrs. I.S.T.

Altitude - 94.2 km

Wave No. Per Meter	Scale Size METERS	Spectral Density Var/Wave/METER	% Amplitude	Net Amplitude cm^{-3}
0.0349	180	0.532×10^{9}	39.9	0.230×10^{5}
0.0698	90	0.130×10^{9}	19.7	0.114×10^{5}
0.1047	60	0.363×10^{8}	10.4	0.602×10^{4}
0.1396	45	0.141×10^{8}	6.5	0.375×10^{4}
0.1745	36	0.633×10^{7}	4.3	0.252×10^{4}
0.2094	30	0.376×10^{7}	3.3	0.194×10^{4}

Average ambient density at 94.2 km = 0.5785×10^{5} cm^{-3}

CHAPTER - VII

DISCUSSION AND CONCLUSIONS

6.1 Irregularities Due to Cross-field Mechanism

6.1.1 30-300 Meter CF Irregularities During Normal Electrojet

It is well known that the excitation of cross-field instability takes place in a region where the electric field and the electron density gradients are in the same direction. The electric field in the case of electrojet is the vertical Hall polarization field and, in general, points vertically upwards during day and evening times and downwards during nighttime.

Our observations regarding the regions of occurrence of type M_c show that during morning and noonhours the

irregularities are continuously observed in a region between 87 and 110 km. During evening, night and early morning hours we observe irregularities in isolated regions of 86-100, 94-122 and 110-118.5 km respectively. Our observations regarding the electron density gradients show that during morning and noon hours positive gradients are present upto 100 km altitude. In the evening hours positive gradients are present below 100 km and at 133 and 137 km. During night time both positive and negative gradients are present between 85 and 130 km. During early morning hours also both types of gradients are present between 107 and 120 km altitude.

Now if one compares the regions of occurrence of type M_c and the nature of electron density gradient (Table IV.1 and fig. 4.7 - 4.11) it can be easily observed that irregularities are present in positive density gradient region during morning, noon and evening hours and, are present in negative density gradient regions during night and early morning hours. Again if one compares the direction of electron density gradient, in regions where irregularities are observed at a particular time, with the direction of Hall polarization field at that time it is found that both are always parallel. Since the direction of earth's magnetic field is N-S, our observations regarding the regions of occurrence strongly suggest that the observed irregularities are generated through cross-field instability mechanism.

Our observations have consistently shown that these irregularities have sawtooth type shape. Observations during daytime, eveningtime and nighttime, and during ascent as well as descent of the rocket show that as one moves along the direction of density gradient the rise in electron density is much sharper than the fall. We thus conclude that type M_c have sawtooth shapes in the vertical direction and the steepening is always in the direction of zero order density gradient.

Recently Rognlien and Weinstock (1974) have tried to explain these sawtooth structures observed by us by using a 2-dimensional non-linear theory of cross-field instability. The non-linear terms in the momentum transfer equations are the inertia and pressure terms. The non-linearity of inertia and pressure terms is small in linear regime and hence it was reasonably assumed by Rognlien and Weinstock (1974) that it would be small in non-linear regime also. The other non-linear terms are due to divergence of ion and electron flux in the continuity equation. A comparison of the electron and the ion term indicates that electron non-linearity is at least an order of magnitude larger than the ion non-linearity. Thus Rognlien and Weinstock identified $(\underset{\sim}{v}_{e1} \cdot \nabla n)$ as the strongest non-linearity. This term is vanishingly small for one dimensional case and hence was essentially ignored in some earlier analyses for one dimensional perturbations[Sato and Tsuda (1967) and

Rogister (1972)]. The important two dimensional non-linearity cascades down the energy to smaller scalesizes by mode coupling and in the final state a spectrum of density and potential fluctuations over a range of wavelengths is obtained which includes both linearly stable and unstable modes.

Based on the above theory Rognlien and Weinstock (1974) carried out numerical calculations for the nighttime electrojet over Thumba, India. The nighttime parameters at 105 km, which they used in their calculations seem to be quite reasonable. The theory of Rognlien and Weinstock (1974) qualitatively explains our nighttime observations of shape of CF irregularities. However, in their recent attempt to extend the theory to daytime Rognlien and Weinstock (1975) unfortunately carried out the numerical calculations for an altitude of 105 km during daytime also. It is clearly shown from our results that during daytime such sawtooth structures are observed only upto 92-93 km altitude and the most prominent ones are observed around 90 km. Beyond 94 km or so the amplitude of irregularities becomes so small that the shapes are not descernible. Even after giving the benefit of doubt regarding the shape of irregularities around 105 km, the saturation amplitudes of $\simeq$ 10% predicted by the theory cannot be reconciled by our observations which show that the amplitudes at that altitudes are much smaller than 1%. Thus during daytime our observed sawtooth shapes around 90 km cannot be explained by the theory as it is. Even for 105 km

the theory predicts saturation amplitudes which are an order of magnitudes more than observed by us. In view of large difference in parameters at 90 and 105 km. altitudes it is highly desirable to have the calculations redone for parameter values prevailing at 90 km altitude.

Our results about the spectrum of medium scale CF irregularities show that the average spectral index for these irregularities lies between -2.0 ± 0.7.

Tsuda and Sato (1968) made computer study of the evolution of cross-field instability in the E-region for a wavelength range of 5 to 100 meters, a range quite close to the one being discussed here. Tsuda and Sato (1968) found a spectral index of -3.0. Ott and Farley (1974) using the dimensional analysis showed that for cross-field instability the spectral index is -3.0 The experimental observations of cross-field instability in laboratory plasma yielded a value of -3.8 (Saxena and John, 1975). However, it may be pointed out that in the laboratory experiments the parameter regime was slightly different as compared to the ionospheric case. In laboratory plasma the regime is characterized by the condition $\lambda/L \gtrsim \Omega_i/\nu_i$ and the growth rate is of the order of real frequency because of which the excited modes are dispersive in nature. Whereas in the case of ionospheric plasma $\lambda/L \sim \nu_e/\Omega_e$ and the modes are non-dispersive in nature. Furthermore, the spectra observed

by Saxena and John (1975) is based on the observations of only few modes. The values of spectral index obtained by Tsuda and Sato (1968) and Ott and Farley (1974) are in excellent agreement with our observations.

Our observations of percentage amplitude of irregularities suggest that all the scalesizes in the band of 30 to 300 meters have maximum amplitude around 90-91 km.

The physical mechanisms responsible for amplitude saturation of cross-field instability are not very well understood as yet. It can however, be assumed that the saturation amplitudes depend on growth and decay processes of the irregularities. The linear dispersion relation given by Fejer et al. (1975) which is the modified form of earlier dispersion relations given by Rogister and D'Angelo (1970) and Sudan et al. (1973), has been used for the calculation of net growth rate. The growth rate Γ is given by

$$\Gamma = \frac{1}{1+\psi}\left[\frac{\psi}{\nu_i}\left\{\left(\frac{k V_d}{1+\psi}\right)^2 - k^2 C_s^2\right\} + \frac{\nu_i}{\Omega_i}\frac{1}{L}\frac{V_d}{(1+\psi)}\right] - 2\alpha N_0$$

where ν_e, ν_i are the electron and ion collision frequencies with neutrals

Ω_e, Ω_i are the electron ion gyrofrequencies.

k is the wavenumber

V_d is the electron drift velocity relative to ions

L is the density gradient scalelength

N_0 is the ambient electron density and

ψ is $\nu_e \nu_i / \Omega_e \Omega_i$

The first and third terms on the R.H.S. are the two-stream and cross-field driving terms; the second and fourth terms are the diffusion and recombination damping terms, respectively.

The net growth rate Γ was calculated at each kilometer between 88 and 108 km altitudes for four assumed values of primary electric field. The Chapman formula was used to calculate the collision frequencies, the neutral gas parameters were taken from atmospheric models of CIRA (1975) and Jacchia (1971). The gradient scalelength was estimated using the procedure already mentioned in section 4.2. For calculation of V_d, the electron drift velocity relative to ions, only electron drift velocity was calculated and the ion drift velocity, which is much smaller, was neglected. The ion-acoustic speed was taken as 360 m/s. The recombination coefficient was taken as 0.5×10^{-7} cm^3/sec [Rishbeth (1968)] . The magnetic field value over Thumba was taken as 0.378 Gauss.

Fig. 6.1 to 6.4 show the variation of net growth rate with altitude for two daytime flights namely 10.44 and 10.45 using CIRA (1975) and Jacchia (1971) models. It is found that the net growth rate is not significantly different for both the models. The increase in primary electric field value

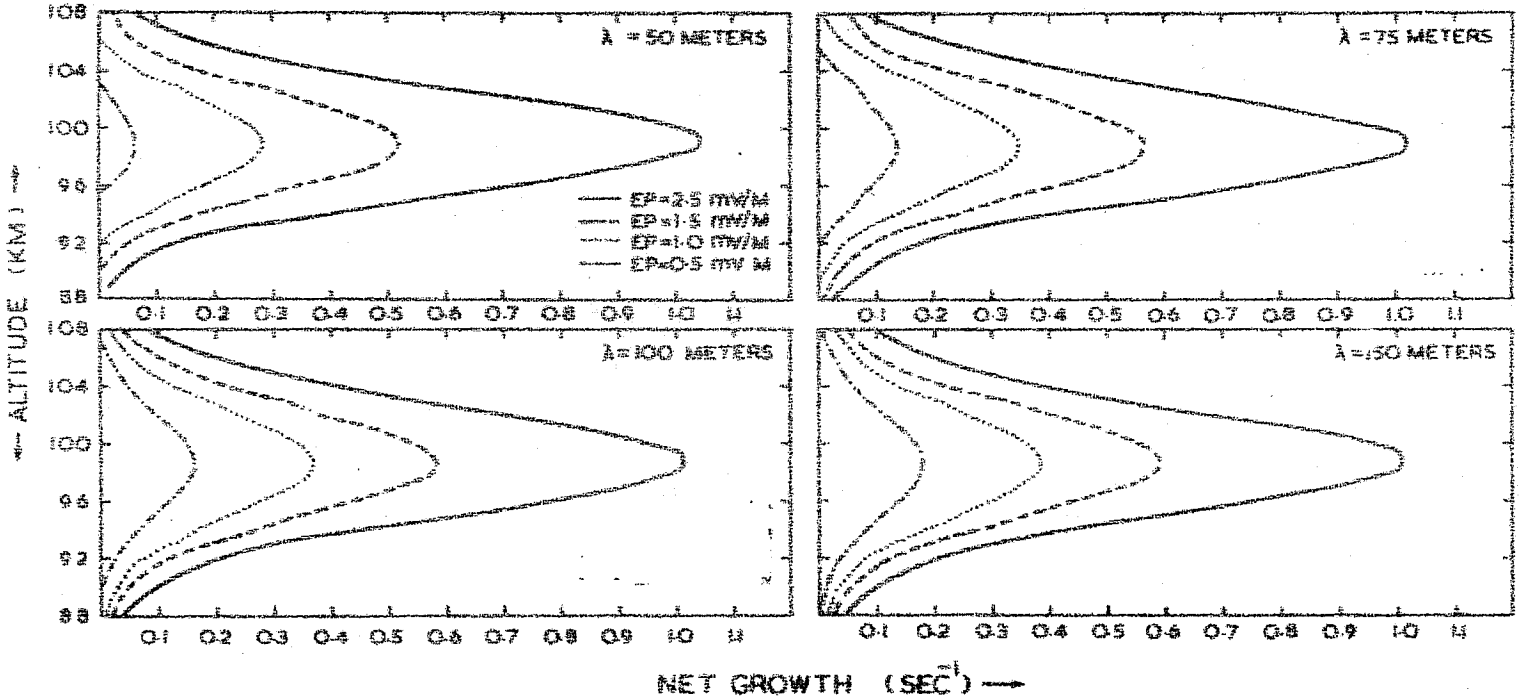

Fig. 6.1 Theoretical estimate of growth rate at different wavelengths for four different values of primary electric field EP for flight 10.44 using CIRA 1965 model.

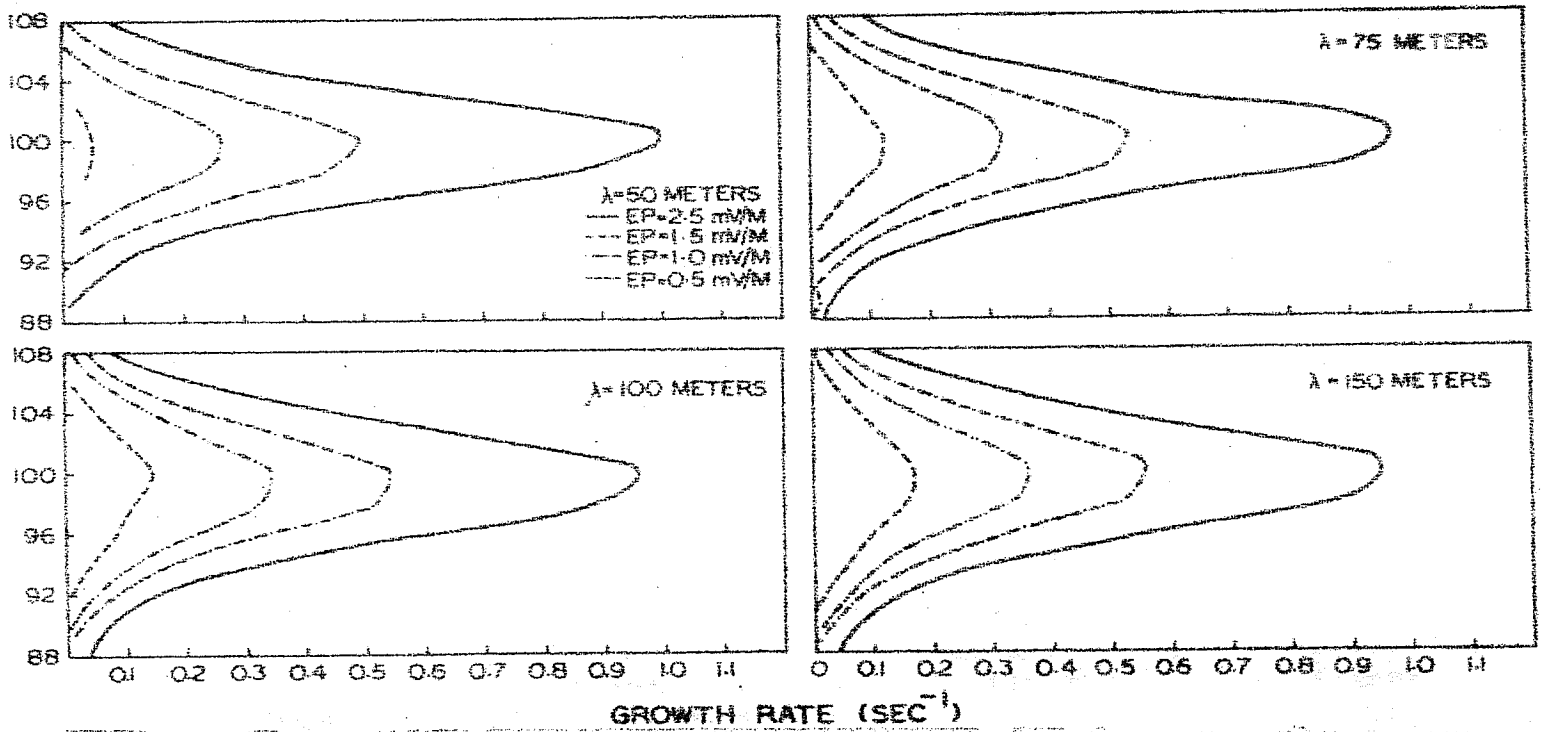

Fig. 6.2 Theoretical estimate of growth rate at different wavelengths for four different values of primary electric field EP for flight 10.44 using JACCHIA 1971 model.

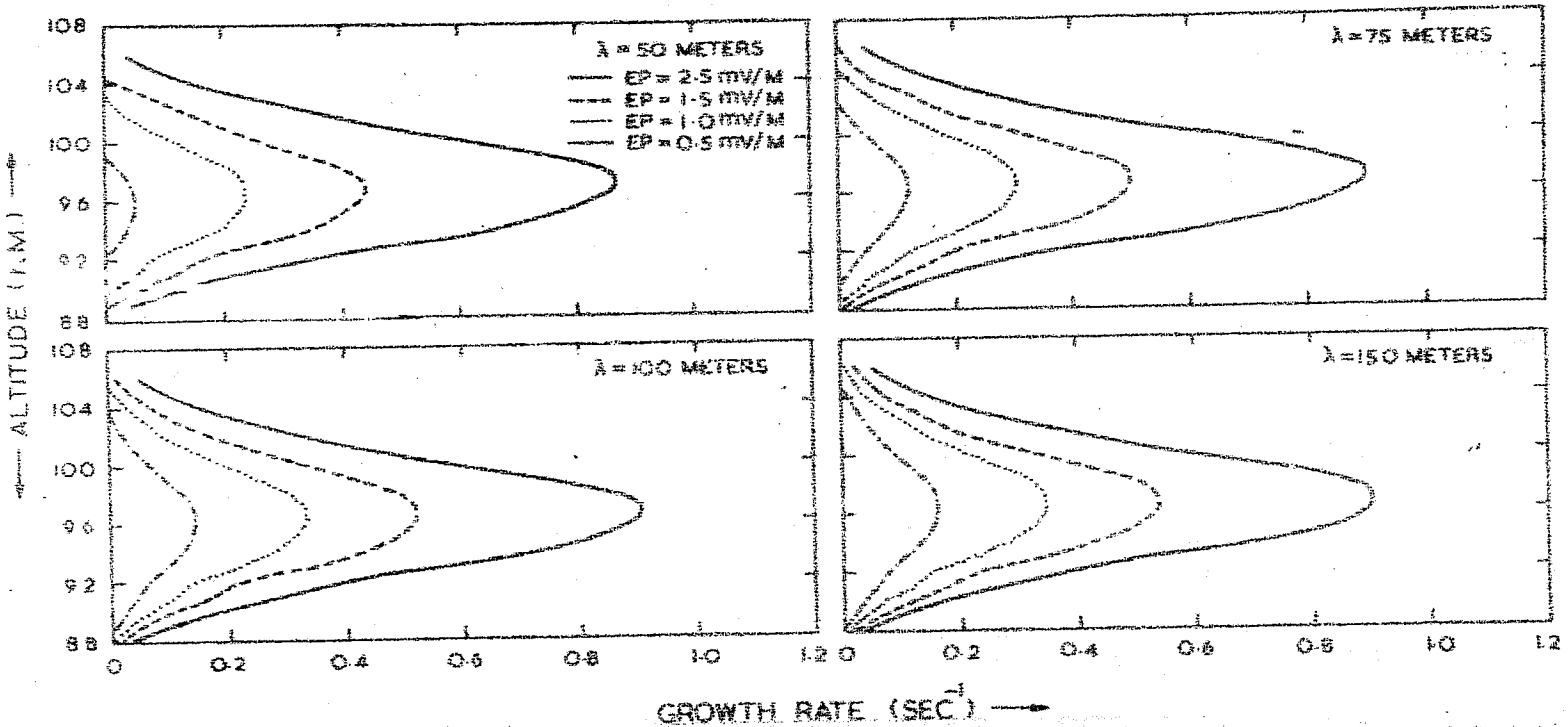

Fig. 6.3 Theoretical estimate of growth rate at different wavelengths for four different values of primary electric field EP for flight 10.45 using CIRA 1965 model.

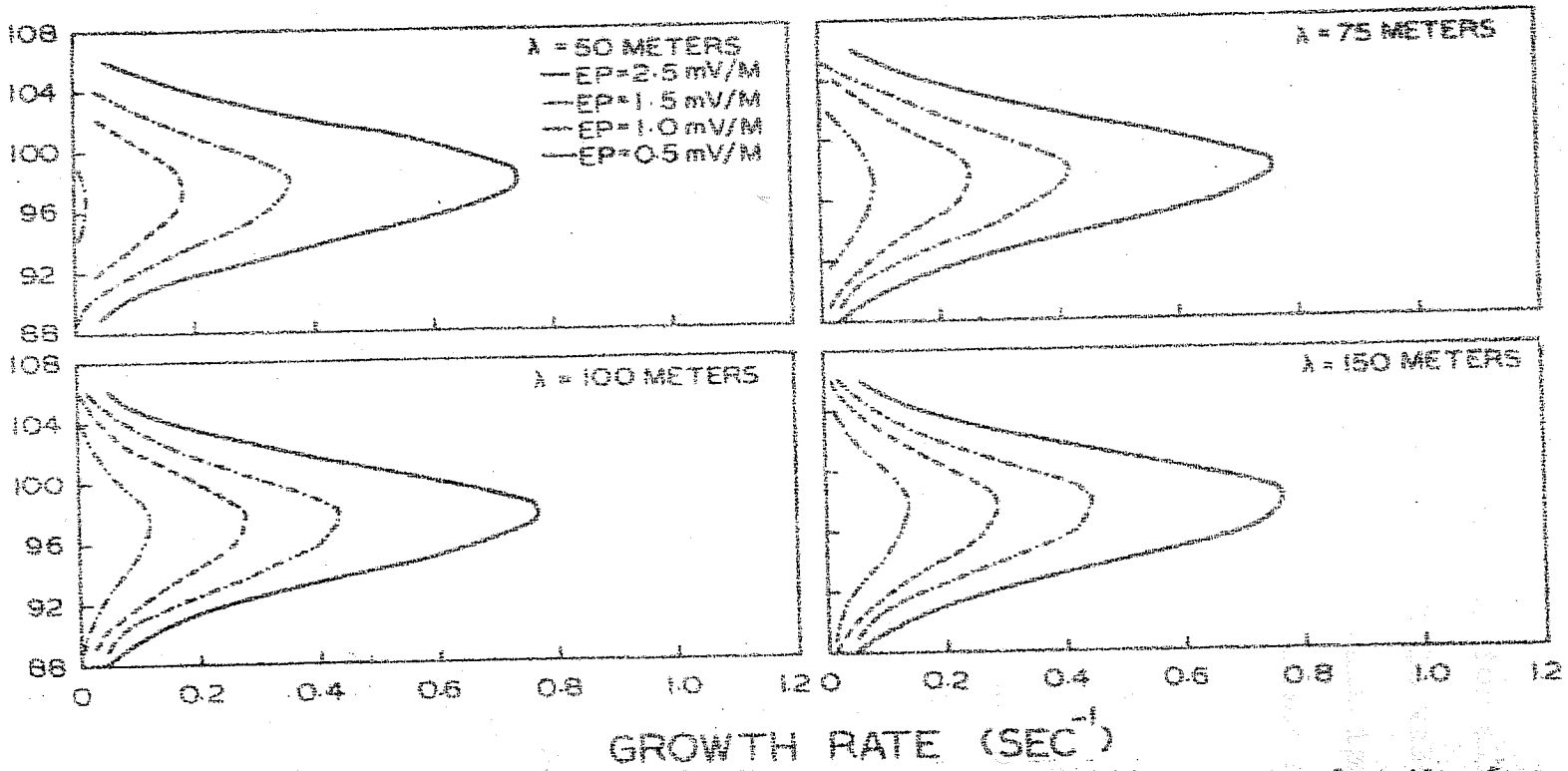

Fig. 6.4 Theoretical estimate of growth rate at different wavelengths for four different values of primary electric field EP for flight 10.45 using JACCHIA 1971 model.

increases the growth rate very rapidly for all the four scale-sizes. At a fixed primary electric field value the growth rate at any given altitude increases with scalesize, though the increase is very little. All the scalesizes have maximum growth rate at 97 km.

Now if one compares the growth rates with the actual observed amplitude variation with altitude (Fig. 5.1 - 5.4 and Fig. 4.22 - 4.23) it is found that both the peaks are separated by 6-7 km. Thus we see that even if the above argument that higher growth rate corresponds to higher saturation amplitude holds, the observed peaking does not coincide with theoretical estimates. The theoretically calculated growth rate peaks at an altitude of 97 km which is characterized by maximum of V_d. At 97 km the parameter ψ becomes unity and hence maximum V_d is obtained. Our experimentally observed amplitudes, on the other hand, maximize at an altitude of 90 km which is characterized by steepest gradients. Thus we feel that the role played by the density gradients is much more important than what is brought out by the theory.

Our observations regarding the variation of most prominent scalesize with altitude, show that around 90 km altitude the most prominent scalesize is smallest ($\simeq$ 70 meters). Above and below 90 km altitude the most prominent scalesize assumes larger values.

Since the generation of irregularities is basically governed by the electric fields, density gradients and collision frequencies etc. the altitude variation of these parameters would ultimately decide the most prominent scalesize at any altitude. But our analysis of most prominent scalesize and density gradients shows that the most prominent scalesize is best correlated with the parameter L, the density gradient scalelength.

6.1.2 30-300 Meter CF Irregularities During Counter Electrojet

Before discussing the nature of irregularities, during counter electrojet the phenomenon of counter electrojet would be briefly discussed.

a) Counter Electrojet

The observations of $H_T - H_A$ for both the flights namely, C05.16 and C-22 show a substantial depression below the baseline and especially so for the flight No. C05.16 which was conducted around the period of maximum depression (of about 35 gamma).

The ionosonde observations, taken around flight periods, at Thumba show that during both the flight the E_{s-q} was completely absent and instead a blanketing type of sporadic E was present.

The conditions of magnetic field during both the flights is same as observed by Gouin (1962) and Gouin and Mayaud (1967). The depressions during both the flights were observed in afternoon hours which as suggested by Rastogi (1974) is the most probable time of occurrence of counter electrojet.

The disappearance of E_{s-q} and appearance of E_{s-q} are also in agreement with the observations of Bhargava and Subrahmanyan (1964) and Cohen et al. (1962).

The observations of magnetic field and sporadic-E very strongly suggest that both the periods during which rockets were launched were counter electrojet periods.

Our observations of electron density and its gradient show that a sharp layer of ionization is present at about 94 km during flight No. CO 5.16. During the other flight also the presence of such layer was observed at 91 km. In addition, we have observed regions of negative density gradients during daytime at 95.7 - 98.8 km during flight No. CO 5.16 and at 91.3 - 93.5 km during flight No. C-22.

b) 30-300 Meter Irregularities Due to Cross-field Instability Mechanism During Counter Electrojet

As mentioned earlier in chapter V our studies during counter electrojet show that type M_c irregularities are

present in negative density gradient regions during both the flights. These irregularities are characterized by the saw-tooth structures with the steepening in the direction of zero order density gradient.

The irregularities of type M_c were not observed in the positive density gradient region during the period of counter electrojet. The regions of negative density gradients usually do not exist around noon hours on normal electrojet days. On the basis of occurrence of type M_c is negative gradient region and their absence in the positive gradient region, we conclude that the direction of Hall polarization field must have got reversed from vertically upwards to vertically downwards.

6.1.3 1-15 Meter CF Irregularities During Normal Electrojet

Rocket observations of 1-15 meter CF irregularities show that during different times of the day the irregularities are present in different altitude regions. The regions of occurrence of these irregularities are same as that of type M_c (tables IV.1 and IV.4) which are generated through cross-field instability mechanism. Thus we believe that the instability producing these irregularities (type S_c) must be basically driven by cross-field instability mechanism.

The regions of occurrence of type S_c which were found from rocket studies at Thumba (Prakash et al. 1973) were recently confirmed by Fejer et al. (1975). Using a VHF radar at 50 MHz with a modified range time intensity display, Fejer et al. (1975) observed that type II echoes are received from different height regions during different times of the day. Fig. 6.5 shows the intensity of VHF backscatter radar signal at Jicamarca, Peru, for 18-19 February 1971 during different times of the day. These are the backscattered signals from 3-meter type II irregularities.

Now the regions of occurrence of type S_c (table IV.4) would be compared with those of type II (Fig. 6.5) during different periods.

Noontime : Rocket results show that irregularities are continuously observed between 90 and 110 km altitudes. Radar results show that from 1230 Hrs upto 1700 Hrs irregularities are observed as one layer between 93 and 110 km.

Eveningtime: Rocket results show that irregularities are observed in isolated regions below 105 km and around 135 km. Radar results show that during evening and, sometimes, during afternoon hours more than one layer is observed. At 1730 Hrs and 1800 Hrs one can see two layers of ionization, a strong

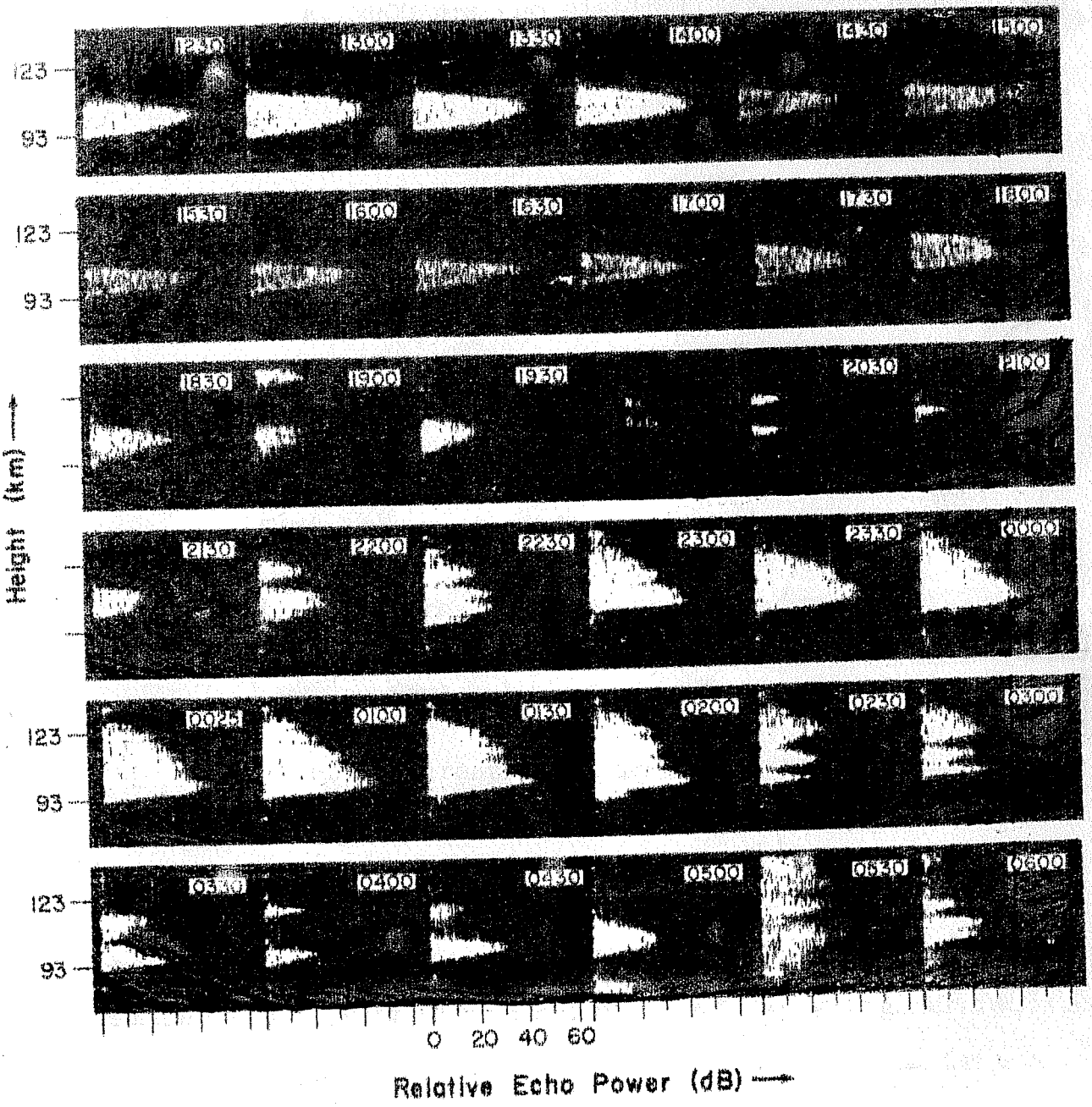

Fig.6.5 Backscattered power at 50 50 MHz from different regions of the electrojet. The times are local times (75°W or EST). Fejer et al (1975).

layer around 105 km and a weak one around 93 km. At 1900 Hrs two distinct layers can be seen one around 103 km and the other around 130 km.

Nighttime: Rocket results show that the irregularities are observed in many discrete regions between 94 and 120 km. Radar results show that during nighttime the region of irregularities is an extended one ranging from 93 km to 135 km. It can be seen from records at 2200, 2230, 0230 and 0300 Hrs (fig. 6.5) that during nighttime the type II signals come from discrete regions.

Early morning hours: Rocket results show that the irregularities are observed in three isolated regions around 0559 Hrs. Radar results at 0600 Hrs show that the irregularities are present in three prominent layers between 93 and 113 km.

The above observations support the findings of rocket borne studies that 3-meter type II irregularities are generated in the same region where CF irregularities are generated. This proves that the type II echoes are generated by CF irregularities as suggested earlier, by Prakash et al. (1971c).

The generation of scalesizes as small as few meters cannot be explained on the basis of linear theories of cross-field instability. Such small scalesizes get heavily damped by electron thermal diffusion across the geomagnetic field lines.

There appears to be no other linear instability which can explain the observations of such small scalesizes in the lower E-region where the drift velocity of electrons is smaller than the ion-acoustic velocity. One dimensional non-linear computer calculations were resorted to by Sato and Tsuda (1967). Later, Rogister (1972) did one dimensional non-linear analysis, analytically. In such non-linear analyses, energy is transferred from large wavelength linearly stable mode to small wavelengths. One dimensional analysis requires that long wavelengths should grow sufficiently ($\simeq$ 10%) to be able to transfer energy to small wavelengths. Sudan et al. (1973) showed that if a two dimensional mode coupling mechanism is invoked the energy can be transferred from long to small wavelengths even when the amplitude of the former is as small as a few percent. Sudan et al.'s theory involves the coupling between the vertical and horizontal wavenumbers, an effect which gets excluded when one dimensional analysis is performed.

Based on the theory of Sudan et al. (1973) the author has calculated the non-linear growth rate of small scalesizes in the vertical direction in an altitude range of 86 to 105 km. The calculation was intended to determine the smallest unstable scalesize for the conditions prevailing in the electrojet over Thumba. The collision frequencies which were used in the calculations were obtained by using Chapman's formula and Jacchia

(1971) model of neutral atmosphere. The drift velocities were taken from Prakash et al. (1971c) who carried out simultaneous experiments of Langmuir probe, Resonance probe and magnetometer. In this calculation one has to assume certain amplitude for large wavelength in horizontal E-W direction. We have performed the calculations with three different values of percentage amplitude for large wavelength of 100 meters. In the first calculation the actual amplitudes of 100 meter scalesize as observed by us at different altitudes (using main channel and duct data during flight 10.45) were substituted; this is reasonable since any perturbation in the ionosphere moves obliquely and has not both the components. In the second calculation a fixed 5% amplitude level for 100 meter scalesize was assumed. In the third calculation a fixed 10% amplitude for 100 meter scalesize was assumed. The results of the analysis show that if one uses actual observed amplitude for 100 meter scalesize, the smallest wavelength which can be generated is $\simeq$7 meters, when fixed 5 and 10% amplitudes are assumed the smallest wavelengths which can be generated are 6 and 3 meters respectively. Thus we conclude that with lot of stretching of arguments probably the small scalesizes may have a positive growth rate. But one does not know what sorts of amplitudes would be generated. Ideally speaking, one should take complete spectrum of large scale irregularities and consider their combined effect on one single small scalesize.

We have observed that 1-15 meter C F irregularities do not have a unique spectrum. The spectral index ranges between -4 ± 1 and increases with altitude.

As far as the spectra of type S_c are concerned it is found that they are much steeper than type M_c. Recently, McDonald et al.(1975) did a computer simulation experiment in which they observed large scalesizes degenerating into smaller scalesizes resulting into a kind of two dimensional turbulence. The spectral index obtained by McDonald et al. (1975) is incidently for the same scalesize range of 1-15 meters. They obtain a value of -3.5 which agrees very well with our observations.

As evident from the spectral index values listed in tables IV.5 and IV.6 the spectrum of type S_c becomes flatter at increasing altitudes. It has been pointed out by Prakash et al. (1973) that due to streaming of electrons one gets another type of irregularity which is termed as type S_s. Irregularities of type S_s are observed in 1-15 meter scalesize range at around 105 km which is the peak of the electrojet. The spectrum of type S_s is flat and is characterized by zero spectral index. Thus it appears that as one goes up in altitude one would see the combined effect of both the spectra (one due to type S_c and the other due to type S_s). Since the excitation of type S_s is very strong around 105 km the net

spectrum would be largely governed by the spectrum of type S_s which is flat. At lower altitudes (around 90 km) the excitation of type S_s is very weak and hence the net spectrum is largely governed by the spectrum of type S_a which is steep. In the intermediate region, therefore, one should see the flattening of the spectrum with increasing altitudes.

6.2 Irregularities Produced by Neutral Turbulence Mechanism

We have observed certain irregularities around and below 80 km altitude during the periods of normal as well as counter electrojet periods. Since the mechanisms of generation do not appear to be different for medium and small scalesizes the results of both the type would be discussed together.

These irregularities were observed on some of the daytime flights and could not be observed on any of the evening and nighttime flights. Usually these irregularities are observed from nearly 59 km to 70-75 km altitude but during flight 10.45 we found that irregularities were present even at 81.2 km altitude. The percentage amplitude of irregularities is much larger at lower altitudes (around 60 km) as compared to that at higher altitudes (around 75 km). These irregularities were found to be prominent during periods of counter electrojet.

These irregularities could not be observed during any of the evening and nighttime flights, and also below 59 km during daytime because during these periods the probe current is very small in lower altitudes and cannot be measured. The irregularities could not be observed above about 72 km altitude except during flight 10.45, where they were observed upto about 81 km. In higher regions ($>$ 84 km) irregularities due to cross-field instability are present, hence at these altitudes even if the irregularities due to neutral turbulence are present they would be masked. It may be reminded here that except for flight 10.45 on all other flights the study of irregularities is done through main channel of the Langmuir probe which can detect irregularities if their amplitudes are larger than 10% or so. Since the irregularities are not observed above about 75 km altitudes during all these flights, it is possible that either the irregularities do not exist above $\simeq$ 75 km or their amplitudes are smaller than 10%. The first possibility is unlikely because the use of duct amplifier (which can study amplitudes smaller than 10%) on flight 10.45 has clearly shown that irregularities are present above 75 km but their amplitudes are too small to be seen on the main channel.

In most of the regions where we observe these irregularities, both electrons and positive ions are unmagnetized and hence the excitation of cross-field instability is not

possible at these altitudes. There seems to be no other plasma instability mechanism which can produce ionization irregularities at such lower altitudes. As mentioned earlier in chapter II Gallet (1955) and Villars and Weisskopf (1955) have shown that in presence of background electron density gradient, neutral turbulence can produce ionization irregularities. The existence of neutral turbulence upto 100 km altitude was theoretically predicted as well as experimentally confirmed with vapour release experiments. Although the neutral turbulence is present upto 100 km it cannot efficiently generate irregularities beyond a critical altitude which is characterized by the following condition.

$$\nu_e > \Omega_e \quad \text{and} \quad \nu_i > \Omega_i$$

If one takes the collision frequency values given by Thrane and Piggott (1966) it can be readily seen that the above mentioned conditions are satisfied only upto 75 km altitude. Hence the region of occurrence of irregularities which we have observed coincides fairly well with the regions where neutral turbulence is expected to efficiently generate electron density irregularities. Hence we conclude that the above irregularities are generated by neutral turbulence mechanism.

During the normal electrojet periods the average spectral index for type M_n is -2.78 and for type S_n is -1.77.

During periods of coulter electrojet the average spectral index for type M_n is -1.04 and for type S_n is -0.88. The average spectral index of all the observationsturns out to be -1.62.

6.3 Irregularities Produced by Unknown Mechanism

We have observed wavelike perturbations in 94 km region during period of counter electrojet. The scalesize of perturbations is as large as 180 meters. The perturbations are observed in a region where strong positive density gradients prevail.

Since these irregularities do not have typical saw-tooth structure and also they are observed in a region where electric field and density gradients are antiparallel, the cross-field instability could not be their generating mechanism. The mechanism of production of these irregularities is not known. These irregularities have vertical scalesizes suitable for giving rise to scattering of radio waves and fading patterns at 2.7 MHz obtained with three spaced receivers' technique by Hulton and Oyinloye(1970) and Rastogi et al. (1971). It was also pointed out by these workers that the fading rate during the counter electrojet was much less than during normal electrojet. This could be due to the fact that during normal electrojet irregularities are generated through cross-field

instability mechanism which gives rise to scalesizes ranging from few meters to few tens of meters and hence have larger fading rates than the irregularities mentioned above which have very limited range of scalesizes. It has been pointed out earlier that a transparent type sporadic-E was observed on flight No. 005.16 ionograms in the frequency range of 4.8 MHz to at least 6.0 MHz. The CF irregularities at 97.7 km and unknown type at 94.2 km have scalesizes suitable for scattering of radiowaves in the above frequency range. Hence the transparent type sporadic E is mainly due to these types of irregularities.

6.4 Conclusions

The important results and conclusions of the thesis are following. The conclusions are listed under four headings which relate to the irregularities generated through cross-field instability, neutral-turbulence, unknown mechanism and the phenomenon of counter-electrojet.

CF Irregularities

1. The results of type M_c and S_c show that they usually coexist and are observed continuously between 86-100 km during morning and noon hours. At other times the irregularities are found to occur in isolated regions. The extent of these isolated regions varies

from 110 to 116 km during early morning hours and 94 to 120 km during nighttime. During evening hours the irregularities are observed in discrete regions below 100 km and around 135 km. The regions of occurrence of type II irregularities, as observed by backscatter radar, are same as those of CF irregularities observed by the rocket. This shows that type II echoes are generated through CF irregularities as suggested earlier by Prakash et al. (1971c).

2. The medium scalesize CF irregularities have typical sawtooth like shapes upto about 92-93 km during daytime on normal electrojet days. Above these altitudes the shapes of these irregularities cannot be ascertained due to the smallness of their amplitudes. However, during counter electrojet periods these irregularities were found to have sawtooth type shapes even at an altitude of 97.7 km. The direction of steepening of these structures is parallel to the direction of zero order density gradient. During nighttime such shapes are observed upto about 110 km or so. The observation of such shapes during nighttime has been explained by Rognlien and Weinstock (1974) but satisfactory explanation of daytime results apparently needs further theoretical investigation as pointed out in the discussion.

3. The spectral index of medium scalesize CF irregularities is in the range of -2.0 ± 0.7.

4. During normal electrojet periods in the daytime, the medium scale CF irregularities have maximum amplitude at 90-91 km altitude. It is observed that these are the altitudes where the density gradients are also sharpest. It is thus felt that observed saturation amplitudes of these irregularities correlate well with the ambient density gradients.

5. The most prominent scalesize is smallest at an altitude of 90 km. This feature is also well correlated with electron density gradient scalelength.

6. The generation mechanism of the small scalesize irregularities through cross-field instability mechanism is not very clear and the presently available theories need lot of stretching of arguments even for qualitative agreement.

7. The amplitude of small scalesize CF irregularities is of the order of a few per cent.

8. The spectrum of small scalesize CF irregularities has got a tendency to become flatter with altitude and is best represented by spectral index range of -4 ± 1. The flattening of spectrum is apparently because the

spectra of type S_c is mixed with the spectra of type S_s in the vicinity of 105 km altitude.

Neutral Turbulence Irregularities

1. The irregularities believed to be generated through neutral turbulence mechanism are observed in regions of 59 to 81 km during periods of normal as well as counter electrojet. Below 59 km the irregularities cannot be observed because of instrumental limitations and above 84 km or so even if the irregularities are present, they would be masked by dominant CF irregularities.

2. These irregularities could be observed only during daytime. The irregularities could not be studied during evening and nighttimes because the ambient electron density is too small to produce sufficient probe current during these periods.

3. The occurrence of these irregularities was very prominent during counter electrojet periods.

4. The percentage amplitude of irregularities is more in the lower altitude regions ($\simeq$60 km), and is less at higher altitude regions ($\simeq$ 75 km).

5. The spectral index of these irregularities is quite variable both for different ranges of scalesizes and

for different periods of observations. The spectral index ranges for type M_n and S_n are from -3 to -1 and -2.65 to -0.02 respectively. The average spectral index for both type M_n and S_n during normal as well as counter electrojet periods turns out to be -1.62.

Unknown Irregularities

1. Irregularities with predominant scalesizes of many tens of meters are generated in 94 km region during the counter electrojet period. These irregularities have scalesizes suitable for giving rise to fading patterns in the radio frequency signals relevant to three spaced receiver technique normally employed for studying the drift in the E-region.

Counter Electrojet

1. During two counter electrojet flights sharp layers of ionization were observed at 94 km (CO 5.16) and 91 km (C-22) altitude. These layers give rise to blanketing type of sporadic-E on C-4 ionograms.

2. Small regions of weak negative gradients have been observed in the daytime during the counter electrojet. The regions are from 95.7 to 98.8 km and 91.3 to 93.5 km during flights CO 5.16 and C-22 respectively.

3. On the basis of absence of CF irregularities in positive density gradient regions, presence in negative

density gradient region, characteristic shape and the direction of steepening, we conclude that during counter electrojet periods the direction of vertical Hall polarization field gets reversed.

4. During counter electrojet period a transparent type of sporadic-E is also observed on ionograms at frequency greater than 4.8 MHz. This is probably due to medium scale CF and unknown type irregularities observed at 97.7 and 94.2 km respectively.

Summary of the rocket results

No.	Type	Vertical Scale size	Regions of Occurrence (km)	Spectral indices S. I.	Maximum Amplitude	Time of occurrence	Mechanism of generation	Remarks
	*L	Few km.	85 - 120	-	25 times in few km.	Night (once a while)	Not known	E_{s-q} present. Horizontal scalesizes > 40 km.
	Mc	30 - 300 m	85 - 125	-2 ± 0.7	30%	All occasions	Cross-field instability	E_{s-q} present. Weak radar signals. Indicates the direction of E-field during counter electrojet.
	Sc	1 - 15 m	85 - 140	-4 ± 1	2%	All occasions	Cross-field instability	Coexists with type Mc, E_{s-q} present, weak radar signals. Occurrence and S. I. suggest similarity with type II.
	Mn	30 - 300 m	59 - 81	-3.0 to -1	20%	Daytime	Neutral Turbulence	Below 59 km probe current too small. Above 85 km those get masked by CF irregularities.
	Sn	1 - 15 m	59 - 81	-2.65 to -0.02	2%	Day time	Neutral Turbulence	Below 59 km probe current too small. Above 85 km those get masked by CF irregularities.
	*Ss	1 - 15 m	Always around 105	0	2%	Daytime during strong electrojet	Streaming of electrons	Strong E_{s-q} at higher frequencies, strong radar signals, occurrence and S.I. suggest similarity with type I.
	Mu	30 - 300 m	84	-2.83	30%	Observed only during counter electrojet periods.	Unknown	E_{s-b} present.
	*R	Few cm to 1 m	Near apogee	+ 2	1%	Night and Evening	Rocket motion	Electrostatic waves ($0.1\, f_{Ni} < f_{irr} < f_{Ni}$ observed only when $0.1\, f_{Ni} < \sqrt{\frac{I_B C_T}{V_R}}$ Because of telemetry limitations

I_B = Intelligence bandwidth, C_T = Ion acoustic speed, V_R = Rocket velocity and f_{Ni} = ion plasma frequency.

These have not been studied by the author.

REFERENCES

Allen J.E., R.L.F. Boyd and P. Reynolds (1957), Proc. Phys. Soc., 70, 297.

Aono Y., K. Hirao and S. Miyazaki (1963), Report of Radio. Res. Laboratories 9, 48.

Appleton, E.V. (1930), Proc. Roy. Soc. Ser A126, pp. 542.

Appleton E.V. and Barnett, M.A.F. (1925), Proc. Roy. Soc. London, A 109 pp. 621.

Bailey, D.K., Bateman, R., Berkener, L.V., Booker, H.G., Montgomery, G.F., Purcell, E.M., Salisbury, W.W. and Wiesner, J.B. (1952), Phys. Rev., 86, pp. 141.

Baker, W.G. and Martyn, D.F. (1953), Phil. Trans. Roy. Soc. 246, pp. 281.

Balsley B.B. (1967), Ph.D. thesis, Tech. Memorandum, IERTM, ESSA, USA, ITSA-89.

Balsley B.B. (1969), J. Geophys. Res., 74, pp. 2333.

Balsley B.B. and Farley D.T. (1971) J. Geophys. Res. 76, pp. 8341.

Balsley B.B., and R.F. Woodman (1971), WDC-A, Report UAG-17 October.

Bartels, J. and H.F. Johnston (1940),Terres. Mag. & Atmos. Electy. 48, pp. 269.

Batchelor, G.K. (1956), The Theory of Homogeneous Turbulence (Cambridge,England, Cambridge University Press 1956).

Bhargava B.N. and R.V. Subrahmanyan (1964), Proc. Ind. Acad. Sci. 60, pp. 271.

Blackman R.B. and J.W. Tukey (1959), The measurement of Power Spectra, Dover Pub. INC., New York.

Blamont J.E. and C. de Jager (1962), J. Geophys. Res. 67, 3113.

Booker, H.G. and Gordon, W.E. (1950), Proc. IRE, 38, pp. 401.

Bourdeau, R.E., J.L. Donley, G.P. Serbu and E.C. Whipple, Jr. (1961), J. of Astronautical Sciences, 8, 65.

Bowles, K. and R. Cohen (1957), NBS Equatorial Region VHF Scatter Research Program for the IGY, QST, 41, pp. 11.

Bowles K.L., R. Cohen, G.R. Ochs and B.B. Balsley (1960), J. Geophys. Res. Vol. 65, pp. 1853.

Bowles K.L., B.B. Balsley and R. Cohen (1963), J. Geophys. Res. 68, pp. 2485.

Briet, G. and Tuve M.A. (1925), Nature 116, pp. 357.

Briet G. and Tuve M.A. (1926), Phys. Rev. 28, pp. 554.

Cahill L.J., Jr. and Van Allen, J.A. (1956), J. Geophys. Res. 61, pp. 547.

Cain J.C. and Sweeney R.E. (1973), J. Atmos. Terr. Phys. 35, 1231.

Chapman S. (1951), Arch. Meteorol. Geophys. Bio Klimatol (Wein) A4.

Cicerone, R.J. and S.A. Bowhill (1967), Aeronomy Laboratory Report No. 21, University of Illinois.

Cohen I.M. (1963), Phys. Fluids, 6, 1492.

Cohen R. (1973), J. Geophys. Res. 78, pp. 2222.

Cohen R. and K.L. Bowles (1963), J. Res. N.B.S. See D, 47 pp. 459.

Cohen R., K.L. Bowles and W. Calvert (1962), J. Geophys. Res. 67, pp. 965.

Cowling, T.G. (1933), Mon. Not. R. Astr. Soc. 93, pp. 90.

Cowling T.G. and Borger R. (1948), Nature, London 162, pp. 142.

Crane R.K. (1970), Preprints 14th Radar Meteor. Conf. Tuscon Ariz., Amer. Meteor. Soc. pp. 101.

Cunnold, D.M. (1969), J. Geophys. Res. 74, 5709.

Davis T.N., Burrows K. and Stolarik J.D. (1967), J. Geophys. Res. 72, 7, pp. 1845.

Druyvesteyn, M.J. (1930), Z. Physik 64, 781.

Dungey J.W. (1959), J. Geophys. Res. 64, 2188.

Egan, R.D. (1960), J. Geophys. Res. 68, pp. 2343.

Egedal, J. (1947), Terr. Mag. Atmos. Elect. 52, pp. 449.

Egedal, J. (1948), Nature, 161, pp. 443.

Farley D.T. (1963), J. Geophys. Res. 68, pp. 6083.

Farley D.T. and Balsley B.B. (1973), J. Geophys, Res. 78, pp. 227.

Fejer, B.G., Farley D.T., Balsley B.B. and Woodman R.F. (1975), J. Geophys. Res. 80, 10, pp. 1313.

Finch, H.F. and Leaton B.R. (1957), Monthly Notices Roy. Astron. Soc. Geophys. Suppl. 7, pp. 314.

Gallet R.M. (1955), Proc. IRE 43B, pp. 1240.

Gouin P. (1962), Nature, 193, 1145.

Gouin P. and P.N. Mayand (1967), Ann. Geophys. 23,41.

(paper in French).

J.S. Greenhow and E.L. Neufeld (1959), J, Geophys. Res. 64, 2129.

Gupta S.P. (1970), Ph.D. Thesis submitted to Gujarat University, Ahmedabad.

Heikkila, W.J., Eaker, N., Fejer A.J., Tipple, K.R., Hugil J., Schneibel D.E. and Calvert W. (1968), J. Geophys. Res. 73, pp. 3511.

Hinteregger, H.E., K.R. Damon and L.A. Hall (1959), J. Geophys. Res. 64, 961.

Hoh F.C. (1963), Phys. Fluids 6, 1184.

Hok G., N.W. Spencer and W.G. Dow (1953), J. Geophys. Res. 58, 235.

Hooper E.B., Jr. (1970), Phys. Fluids, 13, 96.

Hutton R. and J.O. Oyinloye (1970), Ann. Geophys. 26, 921, "The Counter Electrojet in Nigeria'.

Jager, C. de (1952), I'Etude Optique de I'atmosphere Terrestre Liege Colloquium, 1951, pp. 223.

Johnson E.O and L. Malter (1950), Physical Review 80, 58.

Kane R.P. (1973a), J. Atmos. Terr. Phys. 35, 1249.

Kane R.P. (1973 b), Proc. Ind. Acad. Sci. 78A, 149.

Kato S. (1973), J. Geophys. Res., 78, 4, pp. 757.

Kim J.J. and A. Simon (1969), Phys. Fluids 12, 895.

Knox F.B. (1964), J. Atmos. & Terr. Phys. 26, 239.

Kolmogoroff A.N. (1941), C.R. Acad. Sci. URSS, 30, 301 and 32, 16.

Maeda K., T. Tsuda, and H. Maeda (1963), Rep. Ionos. Space. Res. Japan 17, 147.

Martyn D.E. (1948), Nature, London 162, pp. 142.

Matsushita S. (1957), J. Atmos. Terr. Phys. 10, 163.

Maynard N.C. and Cahill L.J. Jr. (1965a), J. Geophys. Res. 70, 23, pp. 5923.

Maynard N.C. and Cahill L.J., Jr. (1965b), J. Geophys. 70, 23, pp. 5975.

Maynard N.C. Cahill L.J. Jr. and Sastry T.S.G. (1965), J. Geophys. Res. 70, 5, pp. 1241.

McDonald B.E., T.P. Coffey, S. Ossakow and R.N. Sudan (1974), J. Geophys. Res. 74, 2551.

McDonald B.E., T.P. Coffey, S.L. Ossakow and R.N. Sudan (1975), J. Geophys. Res. 10, 247.

McNamara A.G. (1965), Aeronomy Report No. 10, Edited by Sechist Jr. C.F. and J.S. Shirke, University of Illinois, Urbana.

Mechtly, E.A., S.A. Bowhill, L.G. Smith and H.W. Knoebel (1967), J. Geophys. Res. 72, pp. 5239.

Morse D.L. (1965), Phys. Fluids 8, 1339.

Mottsmith H.M. and I. Langmuir (1926), Physical Review, 28, 727.

Muralikrishna P. (1975), Ph.D. Thesis Submitted to Gujarat University, Ahmedabad.

Ogawa, T. (1972), Ph.D. Thesis submitted to Deptt. of Electronics, Kyodo University, Kyoto, Japan.

Onwomechill A. (1964), J. Atmos. Terr. Phys. 26 pp. 729.

Osborne D.G. (1964), J. Atmos. Terr. Phys. 26, 1097.

Ott, E. and D.T. Farley (1974), J. Geophys. Res. 79, pp. 2469.

Packard, M. and Varian R. (1954), Phys. Rev. 93, pp. 941.

Pedersen P.O. (1927), 'Propagation of radio waves' Copenhagen, Denmark, Natur. Samf.

Prakash S. and B.H. Subbaraya (1967), Review of Sc. Inst. 38, 1132.

Prakash S., B.H. Subbaraya and S.P. Gupta (1968), J. Atmos. Terr. Phys. 30, 1193.

Prakash S., B.H. Subbaraya and S.P. Gupta (1969a), Space Res. IX, 237, Edited by Champion, K.S.W., P.A. Smith and R.L. Smith Rose, North Holland Pub. Co.

Prakash S., S.P. Gupta and B.H. Subbaraya (1969b), Rad. Sci. 4, 791.

Prakash S., S.P. Gupta and B.H. Subbaraya (1970), Planet. Space Sci. 18, pp. 1307.

Prakash S., S.P. Gupta and B.H. Subbaraya (1971a), Nature Phys. Sci. 230, pp. 170.

Prakash S., S.P. Gupta and B.H. Subbaraya (1971b), Space Res. XI - Academie - Verlag, Berlin, pp. 1139.

Prakash S., S.P. Gupta, B.H. Subbaraya and C.L. Jain (1971c), Nature Phys. Sci., 233, pp. 56.

Prakash S., Subbaraya B.H. and S.P. Gupta (1972), Ind. J. Rad. Spa. Phys. 1, pp. 72.

Prakash S., S.P. Gupta, B.H. Subbaraya, H.S.S. Sinha and C.L. Jain (1973), A Review of In-situ Measurements of E-region Irregularities presented at First Lloyd V. Berkner Symposium, AGU, Univ. Texas at Dallas, Dallas, May 14-17, 1973.

Prakash S., S.P. Gupta, H.S.S. Sinha and T.R. Rao (1976), Space Res. XVI, pp. 401.

Rao K.N., and K.S. Raja Rao (1963), Nature, 200 pp. 460.

Rao T.R. (1976), Ph.D. Thesis, Gujarat University, Ahmedabad.

Rastogi R.G. (1971), Planet. Space Sci. 19, 371.

Rastogi R.G. (1972), Ann. Geophys. 28, 717.

Rastogi R.G. (1973), J. Atmos. Terr. Phys., 35, 367.

Rastogi R.G. (1974), J. Geophys. Res. 79, 1503.

Rastogi R.G., H. Chandra and S.C. Chakravarty (1971), Proc. Ind. Acad. Sci. 74, 62.

Reid G.C. (1968), J. Geophys. Res. 73, pp. 1627.

Richmond A.D. (1973), Jour. Atmos. Terr. Phys. 35, pp. 1083.

Rogister A (1972), J. Geophys. Res. 77, 2975.

Rogister A. and N. D'Angelo (1970), J. Geophys. Res. 75, 3879.

Rognlien, T.D. and J. Weinstock (1974), J. Geophys. Res. 79, 4733.

Rognlien T.D. and J. Weinstock (1975), Rad. Sci. 10, 239.

Sagalyn, R.C. and M. Smiddy (1964), Space Research IV Edited by King Hale North Holland Publishing Company, 371.

Sastry T.S.G. (1968), J. Geophys. Res. 73, 5, pp. 1789.

Sastry T.S.G. (1970),Space, Res. X, pp. 778.

Sato T. (1971), Phys. Fluids 14, 2426.

Sato T. (1974), Phys. Fluids 17, 621.

Sato T. (1976), J. Geophys. Res. 81, 539.

Sato T. and T. Tsuda (1967), Phys. Fluids 10, 1262.

Sato T., T. Ogawa and Y. Matsuda (1972), Phys. Fluids 15, 1926.

Saxena Y.C. and P.I. John (1975), Geophys. Res. Letts. 2, pp. 492.

Schulz G.J. and S.C. Brown (1955), Physical Review, 98, 1642.

Schuster A. (1889), Phil. Trans. Roy. Soc. London A180, pp.467.

Schuster A. (1908), Phil. Trans. Roy. Soc. London A 208, pp.163

Serbu G.P. (1963), I.G.Y. Rocket Report No. 7, 162.

Simon A. (1963), Phys. Fluids 6, 382.

Singer S.F., E. Maple and W.A. Bowen (1951), J. Geophys. Res. 56, pp. 265.

Smith L.G. (1967), Revised version of Tech. Manual series COSPAR bulletin No. 117, Edited by K. Maeda.

Smith L.G. (1969), Small Rocket Instrumentation, North Holland Pub. Co., Edited by K. Maeda.

Sonin A.A. (1967), J. Geophys. Res. 72, pp. 4547.

Spencer N.W., L.H. Brace and G.R. Carignan (1962), J. Geophys. Res. 67, 157.

Steward, R.W. (1959), J. Geophys. Res. 64, pp. 2112.

Stewart (1882), "Terrestrial Magnetism", Encyclopaedia Britanica 9th Ed. Vol. 16, pp. 159.

Su C.H. and S.H. Lam (1963), Phys. Fluids, 6, 1479.

Subbaraya B.H. (1968), Ph.D. Thesis, submitted to Poona University, Poona, India.

Subbaraya B.H., Muralikrishna P., Sastry T.S.G. and Prakash S. (1972), Planet. Space Sci. 20, pp. 47-52.

*

Sudan R.N., J. Akinrimisi and D.T. Farley (1973), J. Geophys. Res. 78, 240.

Suguira M. and Cain J.C. (1966), J. Geophys. Res. 74, pp. 1869.

Suguira M. and Poros, D.J. (1969), J. Geophys. Res. 74, pp.4025.

Takayama, K., H. Ikegami and S. Miyazaki (1960), Phys. Rev. Lett. 5, 238.

Thrane E.V. and W.R. Piggott (1966), J. Atmos. and Terr. Phys. 28, 721.

Tsuda, T. and T. Sato (1968), Phys. Fluids, 11, 677.

Tsuda T., T. Sato and K. Maeda (1966), Radio Science 1, 212.

Tsuda T., T. Sato and S. Matsushita (1969), J. Geophys. Res., 74, 2923.

Untiedt J. (1967), J. Geophys. Res. 72, pp. 5799.

Villars, F. and V.F. Weisskopf (1955), Proc. I R F, 43, 1235.

Wesserstram, E., C.H. Su and R.F. Probstein (1965), Phys. Fluids, 8, 56.

Whitehead (1971), J. Geophys. Res. 76, 3116.

Woodman R.F. and Guillen A. (1974), J. Atmos. Sci. 31, 2, pp. 493.

* Subbaraya B.H., S. Prakash, S.P. Gupta and H.S.S. Sinha (1974) Planet. Space. Sci. 22, pp 180.